The role of stroma microenvironments in prostate cancer cell migration and metastasis

Matthew Antony Lakins

PhD

University of York

Biology

September 2012

Abstract

Terminal prostate cancer is the result of metastatic spread of the tumour from the prostate and is the 2nd leading cause of cancer deaths in men. Although *in vitro* assays have been developed to screen for inhibitors of prostate cancer metastasis and cell migration, they routinely utilise 2-Demensional (2-D) culture of prostate cancer cell lines. Current assays do not simulate complexity of the *in vivo* human tumour microenvironment which contains a mixture of normal and transformed epithelial cells and stromal cells. Therefore there is a requirement to develop novel 3-D models to recapitulate the *in vivo* tumour microenvironment to understand tumour stroma function. Utilising a 3-D co-culture spheroid model incorporating primary human tumour stroma with prostate cancer cells we have shown that the stroma has a key role in prostate cancer epithelial cell migration and motility. By utilising 4-D two-photon imaging and gene expression analysis we have analysed the molecular mechanisms of stromal cell mediated prostate cancer cell migration, identifying genes that regulate the migration process.

Analysis of human tumour stroma indicates a key role in the immune system in driving tumour stroma to express a lymphoid stromal phenotype that provides the microenvironment for active tumour cell migration. This offers an interesting dichotomy that the formation of lymphoid like stroma in aggressive tumours may paradoxically deliver help to drive the immune response to the tumour whilst simultaneously providing the microenvironment for tumour cell migration and metastasis.

The molecular mechanism of prostate cancer cell migration and metastasis and stroma-epithelial cell interactions involves a complex balance between the adhesion molecule VCAM-1 and two counter ligands VLA-4 and SPARC, also known as osteonectin or BM-40. The utilisation of shRNA knockdown, Fc chimeric proteins and blocking antibodies, indicates a key role for stromal-epithelia adhesion and detachment dependent cell migration mediated by VCAM-1, VLA-4 and SPARC.

Index

Table of Contents

List of Figures

List of Tables

Acknowledgements

Declaration

This thesis has not previously been accepted in substance for any degree and is not being concurrently submitted in candidature for any degree other than Doctor of Philosophy of the University of York. This thesis is the result of my own investigations, except where otherwise stated. Cell counts in figure 5.7(C) were collected by Amy Sawtell and imaging data for figure 5.10(A&B) was collected by Dr John Moore. Other sources are acknowledged by explicit references.

Signed   . . . . . *M. A. Calkins* . . . . . (candidate)

Date   . . . .

Chapter 1

Introduction

Prostate cancer is the most common cancer in men in the UK with 25% of all new cases of cancer diagnosed in men being prostate cancers. Now, more than 75% diagnosed are likely to survive their disease beyond five years compared to just 30% in the 1970s (Mayor 2012) (Cancer Research UK).

1.1 The Prostate and Prostatic Disease

1.1.1 The Prostate Gland

The human prostate is a small exocrine gland, functioning primarily to secrete the bulk component of the fluid that makes up seminal fluid. This fluid is strongly alkali to modify the acidic environment of the vagina to ensure sperm survival post ejaculation. The prostate sits at the base of the bladder surrounding the urethra where it also performs a secondary, muscular function to control the flow of urine (Maitland 2008). A common diagnostic observation of prostatic disease is often the malfunction of this muscular function (Sharma et al. 2009). While females do not have a prostate, the female Skene's gland or the female paraurethral gland shares some common characteristics including secretory function and anatomical positioning to the prostate and is indistinguishable from the male prostate at very early stages of development (Thomson 2008). Although extremely rare, adenocarcinoma of Skene's gland closely resembles prostatic adenocarcinoma (Pongtippan et al. 2004).

Whilst the normal adult human prostate does not exhibit distinct lobes as seen in many other mammals (Timms & Hofkamp 2011) it can be divided in to three discreet zones. The peripheral zone (PZ) which surrounds the urethra at the posterior of the gland constitutes 70% of the total volume, and is the origin of the majority of prostate cancer. The central zone (CZ) surrounds the ejaculatory ducts, and accounts for approximately a quarter of

the prostate while the transition zone (TZ) surrounds the urethra and accounts for 5% of the gland (McNeal et al. 1988).

In humans, prostate development is dependent on male androgens (K. Xu et al. 2009) and stromal-epithelial interactions between epithelial cells and the prostatic mesenchyme (Thomson 2008; Timms 2008). During early human embryo development, in the 10th week of gestation, androgen receptor (AR) expression on the local mesenchyme results in the development of a secretory structure (Shannon & Cunha 1983). Androgen signaling through this AR results in smooth muscle patterning in the mesenchyme, a key component of the prostate secondary muscular function (Maitland 2008). During the third trimester, testosterone levels in the embryo then drop, prostate development ceases, and a quiescent state of the gland is entered. The organ remains quiescent until a dramatic change, brought about by high pubescent levels of testosterone, leads to a doubling in size of the prostate gland, resulting in a mature gland with full secretory function.

The secretory ducts of the prostate contain a bilayer of prostatic epithelial cells (Figure 1.1). The first layer on the lumen side of the duct consists of prostate specific antigen (PSA) secreting, terminally differentiated, luminal cells which express cytokeratins 8 and 18 (Lawson et al. 2010). In between these luminal cells, sporadically situated, resides a rare and less well studied cell type, the neuroendocrine (NE) cells. They are thought to regulate prostate growth and development (Taylor et al. 2010) and interestingly also make up a small population (usually <1% of all tumour cells) in all prostatic adenocarcinomas (Tai et al. 2011; Sun et al. 2009). Beneath the PSA secreting luminal and NE cells lay intermediate or transit-amplifying cells and basal cells. This second layer is highly proliferative and undifferentiated epithelium, where a very small population of prostate stem cells that can give rise to all epithelial cells in the prostate (0.1%) are located (Mackenzie 2008; Maitland & Collins 2005). Prostate epithelial stem cells express cytokeratins 5 and 14 (Lawson et al. 2010) and the epithelial stem cell marker CD133 (Promini-1) (Signoretti & Loda 2007) and can, when isolated, successfully form fully differentiated prostatic acini in mice (Richardson et al. 2004).

Stem cells are defined by their potential both to self-renew and to differentiate into different effector cell populations (Evans & Kaufman 1981; Takahashi et al. 2007). In normal tissues stem cells have a key role in tissue homeostasis (Potten & Loeffler 1990). Prostate epithelial stem cells are protected from signals that would otherwise lead to their differentiation through their location in a protective microenvironment known as the stem cell niche (Slack 2000; Xie & Li 2007). Stem cells in their specialised niche remain stem-like and only differentiate once they have left the niche, undergoing rapid proliferation and differentiation into basal, transit-amplifying or luminal epithelial cells. The niche is maintained by complex stromal signals which have a key role in controlling the prostate stem cell environment as well as additional signals from differentiated epithelial cells in the immediate vicinity of the stem cell which actively inhibit stem cell differentiation (Cunha 1994). The stromal component of the gland has a key role in both the development and upkeep of the prostate and secretes a complex array of signaling molecules and growth factors (Kooistra et al. 1995; Lang et al. 2000; Tuxhorn et al. 2002; Mueller & Fusenig 2004; Kooistra et al. 1995).

1.1.2 Prostatic Disease

Prostatitis, Benign Prostate Hyperplasia (BPH) and Prostate Cancer are three of the most common prostatic pathologies.

Prostatitis: This condition results from inflammation caused most commonly by bacterial infection or physical trauma resulting in epithelial disruption (De Marzo et al. 1999; De Marzo et al. 1999). Incidence of prostatitis depends on geographical location, criteria of evaluation and the physician carrying out the diagnosis, but is reported to be anywhere between 2% and 16% of men tested (Krieger et al. 2002). Prostatic inflammation is directly associated with the presence of BPH, but prostatitis patients are not predisposed to cancer (Delongchamps et al. 2008).

Benign Prostatic Hyperplasia: BPH is non-malignant prostate hypertrophy. Both the fibromuscular stromal and glandular epithelial cells undergo hyperplasia but the etiopathogenesis of BPH is still largely unresolved (J. Tang & J. Yang 2009). Prevalence correlates with age with 8% of younger men (ages 31-40) exhibiting BPH. This increases to an incidence of over 80%

in men aged 80 and above (Guess et al. 1990). BPH was first described as a stromal disease nearly 150 years ago from one of the first histological observations of BPH (Timms & Hofkamp 2011). It is now understood that paracrine signaling between the stroma and epithelium is essential for normal development and disruption of normal paracrine signaling impacts on prostate development, leading to prostatic pathologies. This has been hypothesised to be a factor in the etiology of BPH involving pathways required for normal development becoming disregulated, leading to inflammation (Kramer et al. 2007). T cells, B cells and macrophages are all chronically activated in BPH and are responsible for producing an array of inflammatory cytokines and signaling molecules including the cellular growth and differentiation factor, transforming growth factor-β (TGF-β) (Kramer et al. 2002), which in turn, induces growth of the fibromuscular compartment in BPH.

The presence of androgens and an increase in age are factors linked to BPH, but the fundamental etiology remains unknown. A correlation has been observed between the onset of BPH and the presence of lower urinary tract infection leading to localised inflammation. Additionally, changes in interactions between stromal and epithelial cells have been observed during the development of BPH in the transition zone of the human prostate (Shapiro et al. 1992). Changes in gene expression and stroma-epithelial interactions in a murine BPH model may not be that informative of the etiology leading to the human pathology due to differences in prostate anatomy. The discreet zones within a human prostate is not well represented by the clear rodent prostate lobular structure. Prostate specific overexpression of prolactin induces a BPH like disease in mice, resulting in down-regulation of apoptosis-associated genes in prostatic epithelial cells. This was coupled with reduced apoptosis and increased proliferation in the stromal cells with many of the differentially expressed genes being directly associated with the stroma and ECM including secreted proteins such as fibronectin, laminin and collagens (Dillner et al. 2003). Gain of function in the Notch signaling pathway in both prostate epithelium and the adjacent stroma induced a prostatic disease with histological characteristics of human BPH. Upregulated Notch caused the inhibition of phosphatase and tensin homolog (PTEN) and the activation of the Akt cell survival pathway leading to epithelial and stromal expansion (Wu et al. 2011). However, whilst there is

no evidence that notch mutations are involved in BPH, and is unlikely to be the causative agent in human disease, this demonstrates that paracrine signaling in the prostate can alter the epithelial-stromal interactions contributing to hyperplasia and other pathological conditions (Timms & Hofkamp 2011).

The androgens testosterone and dihydrotestosterone (DHT) have been shown to have a role in BPH. Castration results in incomplete prostate development, and in men who naturally have low or zero levels of DHT, there is a reduced incidence of BPH (Ho & Habib 2011). Removal of androgens in the mouse through castration results in prostatic involution, which can be rescued by the exogenous delivery of androgens (Colombel & Buttyan 1995). Estrogens also have a role in prostate growth and pathology but their role in BPH is less clear. The receptors for estrogens; estrogen receptor-alpha (ERα) and estrogen receptor-beta (ERβ) work in opposition during BPH (Bonkhoff & Berges 2009), with an increase in ERα, leading to hyperproliferation in both the stromal and epithelial prostatic compartment, while the apoptosis regulator ERβ is lost in the stroma but highly expressed in the epithelial cells (Royuela et al. 2001). This results in an increase in the stromal cell volume in the prostate.

Prostate Cancer: Prostate cancer exhibits the six traditional hallmarks of cancer. Namely; the evasion of apoptosis, self-sufficiency for growth signals, insensitivity to anti-growth signals, invasion of tissues and metastasis, unlimited replicative potential, and sustained angiogenesis (Hanahan & Weinberg 2000). This was updated a decade later to include two emerging hallmarks in the deregulating of cellular energetics and the evasion of immune destruction, as well as the enabling characteristics which are tumour-promoting inflammation and genome instability with mutations (Hanahan & Weinberg 2011). Sustained cell proliferation in prostate cancer is mediated by many events. Cells of the prostate respond to androgens via the AR, and a key regulator of AR expression is Paxillin. Paxillin is a cytoplasmic adaptor protein that regulates both extra- and intranuclear AR as well as extracellular signal-regulated kinass (ERK) signaling in prostate cancer cells (Sen et al. 2010). Elevated in human prostate cancer microarrays, Paxillin mediates AR regulated transcription, resulting in cell proliferation (Sen et al.

2012). Atypical cell proliferation is also induced via AR through aberrant Wnt/β-catenin signaling that regulates the processes of cell differentiation, epithelial mesenchymal transition (EMT) and prostate epithelial cell hyper-proliferation. Although overexpression of Wnt proteins as observed in prostate cancer have not been conclusively shown as being solely responsible for the stimulation of the Wnt/β-catenin signaling, it is clear that Wnt overexpression promotes proliferation - a hallmark of both prostate cancer and BPH (Kypta & Waxman 2012).

PTEN regulates many different cellular processes in the prostate including proliferation through control of the cell cycle. Usually an attenuator of proliferation, PTEN can be mutated resulting in a deregulation of its function. Platelet-derived growth factor (PDGF) is a known regulator of cell proliferation, particularly in the bone. In the prostate, stromal cell proliferation is induced by PDGF which is secreted by both epithelial and fibroblastic cells (Kaminski et al. 2006). Deletion of PTEN *in vitro* in normal mouse prostate epithelium resulted in an expression pattern of PDGF similar to that previously shown in human prostate cancer cells as well as tumour biopsies (Conley-LaComb et al. 2012). It was concluded that PTEN, through PDGF and PDGF receptors (PDGFR), can promote and drive prostate cancer through sustained cell proliferation and has influence upon other cellular processes such as enhanced cell migration, differentiation and phenotypic transformation (Conley-LaComb et al. 2012). PTEN is classed as a growth suppressor and so too is TP53. Evading growth suppressors and resisting cell death are other hallmarks of cancer and in approximately 70% and 25% of all human prostate cancers either PTEN or TP53 respectively is lost (Martin et al. 2011). Loss of both suppressors in mouse models results in rapid development of prostate cancer and an increase in the development of invasive adenocarcinoma. TP53 in its absence is no longer able to promote apoptosis as is its normal role during cellular stress (Z. Chen et al. 2005).

In order for tumours to grow continually, cancer cells need to acquire replicative immortality (Hanahan & Weinberg 2011). Telomeres are regions at the terminal of chromosomes containing a nucleotide repeat and over time telomeres become shortened resulting from chromosome replication. Telomerase is a reverse transcriptase that uses its own RNA template to extend telomeres post chromosome replication. Telomerase is constitutively

active in prostate cancer cells (Keith et al. 2007) and can be expressed up to 200-fold in putative prostate cancer stem cells compared to tumour cells from the same tissue (T. Xu et al. 2011). This over activity of telomerase effectively renders prostate cancer cells immortal allowing them to grow beyond the limits of normal cell division.

For cells to sustain a high rate of proliferation and elevated levels of growth, tumours need a ready supply of nutrients and oxygen. This is achieved by increasing the blood supply via angiogenesis which is essential for progression of the disease (Weidner et al. 1993). Vascular endothelial growth factor (VEGF) a factor that promotes endothelial cell proliferation and the formation of new blood vessels, is up-regulated within prostate tumours and increased in the serum of patients with prostate cancer with metastatic and castration resistant disease (Tomić et al. 2012). In fact, VEGF levels can be used as a diagnostic marker of advanced disease. Thrombospondin-1 (TSP-1) acts as a potent angiogenic inhibitor by regulating VEGF through a receptor complex comprising CD36, VEG-F receptor 2 (VEGFR2) and β1 integrin in a complex cascade of events involving the phosphorylation of VEGFR2 (Zhang et al. 2009). In prostate cancer, TSP-1 expression correlates with disease severity and is significantly lower in high grade disease. Thus VEGF function is significantly higher in tumour tissue compared to BPH tissue. Expression was also higher once again for VEGF and lower for TSP-1 in metastatic disease as opposed to localised prostate cancer (Kwak et al. 2002).

The loss of E-cadherin promotes cancer cell invasion, and along with metastasis, this represents the sixth and final hallmark of cancer (Hanahan & Weinberg 2000; Cao et al. 2008). One of the ways E-cadherin-mediated motility and invasion can be regulated is through β-catenin. The interaction of Protein Kinase D1 (PKD1) with E-cadherin affects cell motility in prostate cancer (Jaggi et al. 2005), and is mediated by β-catenin (Syed et al. 2008). Using siRNA against PKD1 and E-cadherin resulted in increased proliferation and invasion as well as cell migration in the DU-145 prostate cancer cell line. This phenotype can be reversed by the addition of β-catenin suggesting an important role for this pathway in metastasis (Syed et al. 2008).

1.1.3 Prostate Cancer Pathology: Gleason Grade

Dr Donald F Gleason developed the Gleason grading system for classifying adenocarcinoma of the prostate in the 1960s. The Gleason grading system is based entirely on histologic and architectural growth patterns of the arrangement of carcinoma cells in hematoxylin and eosin (H&E) stained prostatic tissue sections (Humphrey 2004; Gleason 1966). The Nine original patterns of adenocarcinoma histology (1, 2, 3A, 3B, 3C, 4A, 4B, 5A and 5B) are now consolidated into five grades from Gleason grade 1 to 5. Even after this simplification around 50% of all tumours contained more than one histologic grade. After much debate it was decided that the two grades should be averaged by adding the two scores together but not dividing. Thus a prostate exhibiting both grades 3 and 4 is classified as being Gleason grade 7 (Gleason 1992) (Figure 1.2).

1.2 Prostate Cancer Models

1.2.1 Stochastic versus Stem Cell Model

Despite intensive investigation, relatively little is known about the fundamental causes of prostate cancer. Prostate cancer most commonly arises from the peripheral zone (70%) (Berry et al. 2008) and there are at two main proposed models of prostate cancer initiation; the stochastic model and the stem cell model. The stochastic model states that the tumour is homogeneous in that there is no cellular hierarchal structure or function of epithelial cells with each cell having the same potential to induce tumour formation. Phenotypic heterogeneity often observed in tumours results from accumulated epigenetic changes in the expanding clonal population of epithelium. Thus the cancer is initiated by and resulting from random mutations and subsequent clonal selection and expansion (Wicha et al. 2006). The stem cell model for prostate cancer states that the tumour is not simply a homogeneous population of inappropriately growing cells and instead has hierarchal differentiation. This includes the existence of prostate cancer stem cells (CSC). The CSCs are proposed to be a small subset of cells (less than 0.1%) which are the only cells capable of initiating tumourigenesis. The gold standard for identifying cancer stem cells is the ability of these cells to recapitulate a tumour in a new host, for example, the transplantation of putative human CSCs to a mouse host resulting in the growth of a tumour (Mackenzie 2008).

Gene expression in CSCs in prostate cancer has been characterised based upon cells exhibiting a CD44$^+$/α2β1^{hi}/CD133$^+$ phenotype which have been shown to have stem cell capacity. These cells generate phenotypically mixed and differentiated cell types expressing different cell products in line with their proposed function. For example, the production of PSA by terminally differentiated luminal cells (Collins et al. 2005). The proposed stem cell model for tumour persistence post-treatment states that the CD44$^+$/α$_2$β$_1$^{hi}/CD133$^+$ tumour cells are AR deficient. This is important when considering the efficacy of hormone treatment. Treatments aimed at killing rapidly dividing cells (chemotherapy, radiation), to which CSCs would be relatively unresponsive are also ineffective and CSCs maintain the ability to recapitulate the tumour in full post-treatment (Figure 1.3) (Maitland & Collins 2008).

Whilst the exact origin of the initiation of a tumour is unknown, it has been proposed that CSCs or cancer initiating cells (CICs) could arise from normal stem cells or indeed from more differentiated progenitor cells that have regained the ability to self-renew (Vassilopoulos et al. 2008). Stem cells are unique in their ability to both maintain their niche via self-renewal and also asymmetrically divide to give rise to daughter cells that will differentiate down a certain lineage (Knoblich 2008). The longevity of stem cells makes them more susceptible to the accumulation of multiple consecutive genetic mutations, potentially increasing the risk of transition to CSCs. Of the 581 genes found to be significantly different in prostate CD133$^+$/α$_2$β$_1$^{hi} CSCs compared to their differentiated normal counterparts (CD133$^-$/α$_2$β$_1$^{low}), the JAK-STAT pathway, focal adhesion signaling and extracellular matrix genes were identified as key processes in the biology of CSCs (Birnie et al. 2008). Genetic changes can also occur at the chromosome level in the form of gene fusions. The most common genetic rearrangement in human prostate cancer is the TMPRSS2-ETS fusion (Mosquera et al. 2007) a byproduct of DNA double strand break (DSB) repair gone wrong. One model proposes that DSBs occur via androgen stimulation which in rare cases leads to a TMPRSS2-ERG fusion (Tomlins et al. 2005; Bartek et al. 2010) commonly found in human prostate cancers (Maitland et al. 2011).

1.2.2 Non-murine Models of Prostate Cancer

The past 40 years has seen the establishment of approximately 30 putative immortalised human prostate cancer cell lines (van Bokhoven et al. 2003). Three classical cell lines are predominantly used in prostate cancer studies. In order of establishment the cell lines are DU 145 (1977) (Stone et al. 1978), PC-3 (1978) (Kaighn et al. 1979) and LNCaP (1980) (Horoszewicz et al. 1980) which originate from brain, bone and lymph node metastases respectively. These cell lines have been used in countless studies and have contributed vastly to our understanding of many processes involved in prostate cancer and tumour formation in general. PC-3 cells carry significant genetic abnormalities including aneuploidy which changes over time in culture and affects the majority of chromosomes which always results in the loss of chromosome 2 and 3 (Ohnuki et al. 1980).

Many other cell lines have been derived from human cancers from as early as 1948 including the fibrosarcoma derived cancer cell line HT-1080. This cell line was first described in 1974 and originates from a biopsy of a fibrosarcoma with multiple metastases from a 35-year old male. This cell line survived cell culture conditions and has been thoroughly characterised (Rasheed et al. 1974). HT-1080 cells were immortal in culture, tumour initiating in mice, and contained several chromosome abnormalities exhibiting pseudodiploidy (Rasheed et al. 1974). Since then, this cell line has been used to analyse cell migration and invasion both *in vitro* and *in vivo* (Roomi et al. 2006; Armstrong et al. 1982; Mishima et al. 1998). Due to this cell line's spontaneous and random nature of migration in culture, HT-1080s were used in this thesis to develop the 3-D model of cancer cell migration and used as a positive control for single cell migration.

However, as with all cell line models of disease these systems have their limitations. In particular cell lines do not represent the myriad of heterogeneity involved in the disease and experiments are often carried out in a 2-D environment with no thought to, or representation of, the 3-D microenvironment experienced in whole tissues. Furthermore, long-term culture of such cell lines leads to the alteration of biological, genetic and phenotypic properties. Cancer cells are mutated by definition within the primary tumour, but adaptations to culture conditions means that cancer cell lines can become mutated beyond what is observed in the original disease.

These problems, in part, can be addressed by culturing primary malignant prostatic cells and normal epithelial prostatic cells (Peehl 2005).

Methods have been described for culturing cells from many different sources; radical prostatectomy, needle biopsies, and bone marrow aspirates among others. The primary cultures were established and subsequently maintained in conditions similar to those used to culture normal cells. This has been successful for all grades of prostate cancer from well-differentiated Gleason grade 3 cancers, to poorly differentiated Gleason grade 5 cancers. These cells can then be used in experiments similar to those designed for use with cell lines only now using a more physiologically relevant cell type.

Alternative non-murine animal models exist in the form of dogs and some strains of rat (Rosol et al. 2003; Rosol et al. 2004). Human prostate cancer is most closely mirrored by the disease exhibited in dogs, being age dependent and showing bone metastasis in a quarter of cases (Winter et al. 2003). However, there are obvious limitations with such animal models, particularly the dog. There is a long disease latency, a high upkeep cost, long gestation periods and little or no room for genetic manipulation. In rats, the disease is sporadic, highly variable and rarely exhibits metastases.

1.2.3   Murine Models of Prostate Cancer

The four main mouse models used to model the human disease discussed here are human tumour xenografts, transgenic mice expressing oncogenes under the control of prostate specific genes, mice with germline deficiency in tumour suppressor genes and prostate specific conditional gene knockout mice.

Xenograft models were first described in 1980 when human prostate cancer tissue was transplanted into athymic nude BALB/c mice which lack T cells and so have limited capacity to reject implanted tissue (Hoehn et al. 1980; Valkenburg & B. O. Williams 2011). The xenograft model has been improved through the development of more complete immunodeficient mice. Severe combined immunodeficiency (SCID) mice have very limited numbers of T and B cells and thus allow more efficient engraftment of the xenografts. This was further improved by crossing the SCID mice with nonobese diabetic (NOD) mice that have functional deficiencies in antigen-presenting cells

(APCs) and natural killer (NK) cells. However, although xenografts were accepted at a higher rate, there was still considerable rejection, and it wasn't until the development of the most severe immunodeficient mouse, the NSG (NOD/SCID/Gamma chain deficient mice) and GcRag (Common Gamma chain, Rag deficient mice) mouse models that completely lack NK cells, that a significant success rate was observed with xenograft implantation (Shultz et al. 2005).

Despite the leap forward in complexity of xenograft models this system has its limitations. The lack of a competent immune system, which allows the success of the implantation of foreign tissue, could have a direct effect on the growth, development and progression of the tumour. In the case of cancer, it is clear that the immune system has a critical role in tumour formation *in vivo* (Rakhra et al. 2010; Kundu & Surh 2008; Grivennikov et al. 2010; Tan et al. 2011; Bollrath & Greten 2009). Additionally, by definition xenograft models fail to model the early stages of tumour initiation as these are negated by implantation of a mature piece of foreign cancerous material.

It is possible to dissect the early events of disease formation by using the transgenic models of prostate cancer. This technique was first used in the 1980s to investigate brain (Brinster et al. 1984) and lymphoid (Adams et al. 1985) malignancies. An ideal transgenic mouse model needs to fulfill three main criteria. First, to allow a better understanding of the complexities of cancer tumour biology in the context of an intact immune system. Second, to allow short term studies without comprising on genetic and/or epigenetic changes. Third, to allow preclinical evaluation of novel therapies against prostate cancer which are accurate and relevant (Jeet et al. 2010).

The best characterised mouse model of prostate cancer is the transgenic adenocarcinoma of the mouse prostate (TRAMP) model. The TRAMP model utilises the prostate-specific rat probasin promoter to drive expression of the Simian Vacuolating Virus 40 (SV40) large and small t antigen (Tag). Overexpression of the large T antigen, a proto-oncogene originated from SV40, down modulates expression of p53 and retinoblastoma tumour suppressors and this, coupled with the effect of the small t antigen effects promotes epithelial cell growth and survival, leading to the subsequent development of aggressive tumours (Greenberg et al. 1994; Greenberg et al.

1995; Gingrich et al. 1996; Gingrich et al. 1997). Metastasis occurs in ~100% of TRAMP cases to the lymph nodes and lungs and is rarely found to target the bone, kidney and adrenal glands (Gingrich et al. 1999).

A less aggressive variety of the TRAMP model, the LADY mouse model spontaneously develops metastases (Venkateswaran et al. 2004) but to a lesser extent reaching only the lymph node, liver and lung in two thirds of cases. Similar to the TRAMP model, LADY transgenic mice have SV40 driven expression of the large T antigen specifically targeted by the rat probosin promoter, but lack the expression of the oncogenic small t antigen leading to a less aggressive disease phenotype (Valkenburg & B. O. Williams 2011).

There are many further examples of transgenic prostate cancer mouse models most of which act to cause prostate cancer via the expression of SV40 driven T antigen (Ahuja et al. 2005). However these are less representative of human prostate cancer in that SV40 T antigen is not normally expressed in the human disease and transformation likely does not normally occur in terminally differentiated cells. Rather than being the result of a prostate specific oncogenic event, the transgenic mouse models of the disease, such as TRAMP and LADY, is a result of tissue specific loss of the tumour suppressor genes p53 and retinoblastoma.

Gene knockout mice are generated through homologous recombination in embryonic stem cells leading to the production of mice that do not express the targeted gene due to either deletion of critical exon(s) or insertion of a transcriptional or translational stop. However, using germline deficient mice it very difficult to determine organ-specific roles for genes due to their role in other developmental systems. This is particularly true of genes like the retinoblastoma protein that has essential roles in embryo development. Unexpected roles for proteins in prostate development and disease have been deduced based on observations made from gene knockouts including the retinoic acid receptor gamma (RARγ) knockout mouse where 100% of male mice exhibited problems in prostate development (Lohnes et al. 1993). RARs are transcription factors that mediate retinoid effects and deregulation of such factors have been linked to many malignancies (Richter et al. 2002). The presence of multiple RARs has been shown from day zero in the mouse prostate which suggests that they are important for development (Aboseif et

al. 1997). This is compounded by the RAR knockout mouse in which 100% male mice develop squamous cell metaplasia in the prostate as well as having perturbed prostate developmental. However no carcinoma was ever detected (Valkenburg & B. O. Williams 2011).

No germline mouse knockout has been developed that accurately models prostate cancer. Many are either embryonic lethal, have developmental defects or develop tumours in multiple tissue types. In PTEN$^{-/-}$ Nkx3.1$^{-/-}$ mouse (H. Gao et al. 2006) loss of the classic tumour suppressor PTEN combined with the loss of the putative tumour suppressor Nkx3.1 leads to prostate cancer that can exhibit lymph node metastases (Bethel & Bieberich 2007). The loss of Nkx3.1 expression in human prostate cancers correlates with tumor progression (Bowen et al. 2000). However, it is difficult to conclude prostate specific origins for tumours in these mice.

The application of the Cre-loxP recombination system has led to the development of prostate-specific gene knockouts. This permits the study of genes that would otherwise be embryonic lethal or have developmental abnormalities. Briefly, the recombinase protein Cre can be expressed by specific tissues using either transgenic mice with Cre under the control of tissue specific promoter or knock-in of Cre into tissue specific gene loci. Once Cre is expressed, it acts on a pair of 34 base-pair LoxP sites which flank the gene of interest leading to recombination and removal of the intervening segment of DNA. Cre fused to the estrogen domain has been developed permitting induction of cre activity under the control of exogenous tamoxifen thereby allowing both tissue and temporal-specific gene targeting in the mouse (Metzger & Chambon 2001).

The Cre-lox technology has been used extensively to study gene function in development, immune responses and cancer. In the prostate, PTEN, retinoblastoma (Rb) and Nkx3.1 have been targeted using prostate specific cre leading to a wide and varied range of disease phenotypes. The tumour suppressor PTEN, when conditionally knocked-out using the probasin Cre transgenic mouse line, causes a full range of low-grade and high-grade intraepithelial neoplasia, invasive carcinoma and metastasis, with metastasis homing to the lungs and lymph nodes within 12 weeks (S. Wang et al. 2003; Kasper 2005). In comparison loss of the putative tumour suppressor Nkx3.1

leads to a more benign phenotype only reaching low-grade intraepithelial neoplasia with no high-grade intraepithelial neoplasia, invasive carcinoma or metastasis (Abdulkadir et al. 2002). Conditional loss of Rb in the prostate epithelium increased prostate cell hyperplasia as early as 12 weeks due to an Rb-mediated loss of cell cycle control which lead to prostatic disease reflective of human prostate cancer (Nagy 2000) (Maddison et al. 2004).

No current mouse model fully represents and recapitulates human prostate cancer, in part due to structural differences between human and mouse prostate. However, the development of more advanced inducible gene knockouts has, and will continue to provide insights into the mechanisms of human disease in the context of a fully functional immune system.

1.3   Stroma

The normal prostate stroma is critical for the correct development and maintenance of epithelia (Berry et al. 2008). Correspondingly prostate stroma has a key role in BPH and prostate cancer and is implicated in each and every stage of prostate carcinogenesis and metastatic disease (Hall et al. 2002). Tumour stroma has been shown to contribute to the malignant characteristics of many other epithelial tumours including mammary tumours (Trimboli et al. 2009). For example, loss of the tumour suppressor gene PTEN in the stroma results in an acceleration of the initiation, progression and malignancy of mammary tumours in mice (Trimboli et al. 2009).

Stroma is an umbrella term in biology for a wide range of cell types that can either be activated *in situ* and/or recruited to the local tumour environment. These include fibroblasts, immune cells and vascular and lymphatic endothelial cells, smooth muscle cells and pericytes. Many of these cells interact with the extracellular matrix (ECM) components deposited by stroma, as well as interacting with the 'normal' and transformed cancerous cells which all together regulate many aspects of tumourigenicity in a tumour microenvironment (Mueller & Fusenig 2004; Tlsty & Hein 2001; Tlsty 2001; Bissell & Radisky 2001). The complex nature of the three-dimensional architecture of the ECM and the numerous cell types that make up the tumour microenvironment makes it challenging to dissect. In culture,

fibroblasts rapidly outgrow and outcompete other cell types and after only one or two passages the primary cultures become morphologically homogeneous (Kopantzev et al. 2010). Thus *in vitro* generated microenvironments will differ to those found *in vivo*.

The crosstalk between epithelia tumour cells and stromal cells during disease progression is a burgeoning field of research. Specifically in prostate cancer, there are two pathways by which this communication occurs; the efferent and the afferent pathway (De Wever & Mareel 2003). Typically at the early stages of disease the efferent pathway is thought to control changes to the stroma, with transformed epithelial cells releasing soluble factors such as transforming growth factor (TGF)-β and platelet derived growth factor (PDGF) which can transform fibroblasts into myofibroblasts (Skobe & Fusenig 1998; Sieweke et al. 1990) and induces epithelial-mesenchymal transition (EMT) as characterised by high levels of Vimentin expression. At later stages of disease, the afferent pathway, driven by the now changed stroma, acts as the tumour becomes more invasive. The roles are reversed and cancer cells now respond to the modified, "reactive" cancer stroma. This reactive stroma releases soluble factors and ECM components which can induce migration and invasion of the cancer cells in to the local stromal environment (Y.-N. Niu & Xia 2009).

Stromal cells in many cancers have been shown to be activated in a way that is different to normal conditions. This includes the over-secretion of growth factors and pro-migratory ECM components, upregulation of matrix metalloproteinases (MMPs) and the induction of inflammation via chemokine secretion (Mueller & Fusenig 2004). The fibroblasts in cancer stroma have been found to have an influence on the development and progression of cancer leading to the potential of stromal-targeted therapeutics (Bhowmick et al. 2004). A change in the stroma environment throughout the progression of prostate cancer creates an ever changing, functionally different microenvironment with the reactive stroma becoming enriched for myofibroblasts and fibroblasts, whilst smooth muscle content decreases (Tuxhorn et al. 2002). TGFβ and PDGF are two common growth factors secreted by a range of cells in the tumour (De Wever & Mareel 2003). However, the role of TGFβ is uncertain with contradictory outcomes being seen in terms of tumour progression whether it is inhibited or overexpressed

(Bhowmick et al. 2004; Weeks et al. 2001). PDGF has a clearer role in the induction of myofibroblast proliferation and differentiation (Shao et al. 2000).

More recently it has been shown that via the secretion by tumour cells of the C-C chemokine CCL21 (Shields et al. 2007), a lymphoid-like reticular stromal network was induced around melanoma tumours, which shifted the host immune response from immunogenic to tolerogenic (Shields et al. 2010). This facilitates and enhances tumour progression in a stroma dependent way and has furthered the case for therapeutic strategies to target the tumour stroma and immune infiltrate in future treatments. CCL21 is a ligand for the C-C chemokine receptor CCR7 which is expressed by DCs. Upon activation, CCR7 expression is upregulated in DCs allowing them to follow a CCL21 and CCL19 chemotactic gradient set up by chemokine secreting lymphatics and lymph nodes (Randolph et al. 2005). In 3-D, DCs have an enhanced response to CCL21 over CCL19 (Haessler et al. 2011). CCR7 is also expressed on T cells and has a vital role in the trafficking of such lymphocytes to the lymph nodes (Mashino et al. 2002). By secreting CCL21, tumour cells are setting up a tumour specific chemokine gradient to which stromal cells and immune cells important for tumour progression can home to (Mashino et al. 2002).

1.4   Microenvironment and ECM

Although *in vitro* assays, often using a proteomic approach, have been developed to screen for inhibitors at the different stages of metastatic prostate cancer, they often utilise cell lines and crucially do not simulate the *in vivo* tumour microenvironment. Aspects of such microenvironments include direct focal adhesions between different cell types, the presence of multiple cell types including the vascular system, the mix of stromal cell types, the collagen architecture and other ECM components.

There are also other features attributed to tumour growth and survival which the microenvironment supports such as acidic pH, limited nutrient levels, higher interstitial fluid pressure and significant oxygen level fluctuation which is thought to directly relate to the abnormal vascular network that exists in tumours (Lunt et al. 2009). Not only does the ECM act as a support, it can also act as a physical barrier and is one of the first barriers

encountered by a cancer cell going through metastasis both on leaving the primary tumour and entering the secondary site. The tumour microenvironment can undergo significant remodeling during tumour growth and metastasis and has a key role in determining therapeutic efficacy (Kumar & Weaver 2009).

The ECM is a complex mixture of different proteins including proteoglycans and fibres such as collagen, elastin, fibronectin and laminin. Cells interact with the ECM through membrane bound receptors such as integrins linking the ECM microenvironment to cellular function including changes to cytoskeletal organisation (Davis & Senger 2005). Integrins consist of α- and β-chains which combine to make an array of heterodimers that interact with cell surface receptors such as inter cell adhesion molecule (ICAM)-1, vascular cell adhesion molecule (VCAM)-1, CD44, N- and E-cadherin mediating the adhesive process (Humphries et al. 2006; Schmidt & Friedl 2010). Many cell types contribute to the makeup of the ECM, particularly fibroblasts, a large constituent of stroma, which lay down many components of the ECM architecture. There are two basic forms of the ECM; the basement membrane and the interstitial matrix (Sorokin 2010).

1.4.1 Basement Membrane

The basement membrane (BM) underlies all epithelia and endothelia tissue. Composed of dense ECM it is highly cross-linked and forms a sheet-like structure in direct contact with the basal cells of the organ or tissue it surrounds (Kalluri 2003). The BM creates a barrier between the cells and the interstitial, loose matrix, whilst simultaneously connecting the two entities (Timpl & J. C. Brown 1996). During normal processes and events such as periods of development, the BM has to be breached and crossed by specific cells. During neural crest cell migration from the pharyngeal pouches to produce peripheral neurons and the cardiac outflow, neural crest cells have to migrate in to and through the BM which was since successfully replicated *in vitro* (Bilozur & Hay 1988). This is particularly important taking in to account that cell invasion is key to the pathology of metastatic cancer (Kusuma et al. 2012; Yu & Machesky 2012), and indeed many other human diseases. Termed one of the hallmarks of cancer, the activation of invasion through the BM is one of the first barriers a metastasising cancer cell or group of cells has to concur (Hanahan & Weinberg 2011).

The BM is not simply a static divide or connective entity between two different environments. Cell adhesion, migration, polarity and spreading can all be regulated by the BM and this directly modulates the cellular cytoskeleton arrangement through signaling from integrins and receptors that bind to ECM proteins (Hamill et al. 2009). Laminin is a key component of the BM and is known to be key to BM function. Laminin is formed as subunits and it is now understood that in humans there are genes that encode for five α-, three β- and three γ-subunits. These assemble in to at least 16 familiar heterotrimeric functional laminin proteins (Aumailley et al. 2005) which makes determining the role of individual laminin proteins difficult. The different laminin forms are thought to have differential functions in many biological processes.

The BM is also composed of collagens, fibrillin, perlecan and nidogens. The collagen component of most BMs is predominantly collagen IV which provides much of the mechanical strength acting as a scaffold and is essential for overall BM stability (Pöschl et al. 2004). Collagen is an excellent substrate with which cells can bind to. Typically these interactions occur via integrins such as $\alpha_2\beta_1$ as well as non-integrin receptors, including the basal cell marker CD44 (Khoshnoodi et al. 2008). Cell adhesion to the BM is critical for cell polarity as well as structural organisation of the tissue itself.

The other main components of the BM are perlecan, a heparan sulphate proteoglycan, and nidogens. Figure 1.4 shows how these two proteins interact with specific sites in the laminin protein leading to cross linkage with collagen IV thus creating an ordered protein network (Sorokin 2010). Both perlecan and nidogen have the ability to further crosslink the matrix by being able to bind collagen IV, fibulin, fibronectin and elastin as well being able to bind to each other to form a highly tensile ECM (Aszódi et al. 2006).

The BM has a key role in the maintenance of the stem cell niche. Most stem cell microenvironments contain a BM which is in contact with stem cells, the interactions between the BM and the stem cells is thought to be important in the upkeep and regulation of stem cell function (Solozobova et al. 2012).

BM complexity allows for extremely tissue specific and site specific differences. The BM is a major barrier for cells going through extravasation either as a result of development, immune infiltration or metastasis. Electron microscopy and ultra-structural studies of BM from different organs is consistent with extravasation being site specific. Clear differences in BM electron density was seen between BMs in different organs such as the lung, kidney and liver, which equate to attachment points that may contain adhesion molecules (Paku et al. 2000).

1.4.2   Interstitial Matrix

The interstitial matrix (IM) along with the BM collectively makes up the ECM. The IM is distinctly different in composition to the BM containing a vast array of collagens, fibronectins, and proteoglycans (Laurila & Leivo 1993). Often termed a loose fibrillar network, this is the second component after the BM that an extravasating cell encounters. Although adjacent to each other, the BM and IM are completely separate structures and no crossover of materials, or of mixed matrices, have been reported in normal tissue (Leivo 1983a; Leivo 1983b).

The difference in the composition of the two matrices is mirrored by the different mechanisms that cells employ when transmigrating the ECM. Taking leukocytes as an example, it has been shown that the cells take on an amoeboid shape aligning with collagen fibres whilst using the fibres as tracks (Korpos et al. 2010) which is independent of matrix degradation (Wolf et al. 2003). This process of moving through the IM has also been shown to be possible in an integrin-independent manner by knocking out the major integrins in dendritic cells (DCs). Integrin deficient DCs migrated in an identical manner to wildtype DCs and further dynamic imaging revealed a role for actomyosin contraction in leukocyte locomotion along a chemokine gradient (Lämmermann et al. 2008). This shows that cells have adapted to migrate through the ECM by different mechanisms depending on the constituency of the matrix, and the varying secondary structures within.

Cancer cells also use tracks created by the fibrillar components of the IM (Madsen & Sahai 2010). The mechanisms by which cancer cells extravagate and subsequently invade secondary sites are varied and depend upon the ECM microenvironment of the tissue. During tumour metastasis, when a

cancer cell first encounters a secondary tissue site, integrin and non-integrin cell surface receptors engage with the local ECM facilitating tissue entry (Gritsenko et al. 2012). By utilising different combinations of cell surface receptors and integrins, cells can be selective for different components of the ECM thereby creating a signature for specific tissue-type ECMs.

1.5   Cell Migration

Cell migration involves a complex set of events. These events are dependent on the immediate ECM and cellular microenvironment, the signals driving the migration process, if cells are migrating as single cells, or a collective cell manner. The migration process is key for tissue remodeling during embryonic morphogenesis, organ development, immune surveillance, wound repair and indeed cancer cell invasion (Friedl & Gilmour 2009). Single cell migration has a key role in the function of the immune system, higher order collective cell migration is an important process during embryonic development but has little role in normal tissue homeostasis.

Collective migration is defined by the cohesive movement of a group of cells (Rørth 2009). During collective cell migration, cells migrate in tight groups as sheets, sprouts, branches, streams and free groups. An extreme example of collective migration is eye migration in flounder and other flat fish (Hildahl et al. 2008). Extreme collective cell migration is also observed during fetal thymus development where the thymus migrates from its site of origin in the 3rd pharyngeal pouch to the thoracic cavity, an active process involving neural crest cells. This process is dependent on Eph/Ephrin interactions between neural crest derived mesenchyme (Foster et al. 2010). The same processes observed during development and tissue morphogenesis have been observed in invasive carcinoma where groups of cancer cells invade surrounding tissues, ECM and vasculature (Friedl 2004; Friedl & Alexander 2011).

The mechanisms of single cell migration have been extensively studied *in vitro*. Often termed as mesenchymal or amoeboid cell migration this can be confusing as multiple different cell types including but not limited to mesenchyme can undergo single cell migration. Single cell migration can be characterised by five or more steps; protrusion, adhesion, leading edge

stabilisation, cell body translocation and detachment of the rear of the cell (Ridley et al. 2003) in an integrin dependent process. Whilst exerting forces on the ECM, this process usually involves a degree of ECM degradation in order to create paths through which the cell can migrate. Tumour fibroblasts exhibit this degradation dependent movement, the tracks which they create being utilised by following carcinoma cells (Gaggioli et al. 2007; Scott et al. 2010). The mechanism by which other cell types migrate as single cells is markedly different. Leukocytes employ an amoeboid migration tactic which is fast and can be up to 30μm/min. This rapid motility means there is insufficient time to create strong adhesive interactions rather they form very transient interactions and only forming stable interactions during cellular activation. Leukocytes do not degrade ECM and thereby do not remodel the cellular microenvironment (Shulman & Alon 2012). In contrast fibroblasts migrate at velocities of 1μm/min with strong ECM interactions and adhesion, utilising a key function of matrix metalloproteinases (MMPs) that can lead to ECM degradation (Wolf et al. 2003; Wolf et al. 2007).

Typically, a migratory cancer cell, potentially capable of metastasis, is thought to follow a mesenchymal route of migration. This happens through the expression of a mesenchymal gene profile potentially through the process of EMT. In mesenchymal cells and migrating cancer cells lamellipodia and filopodia form a meshwork of branched actin filaments (Chhabra & Higgs 2007; Small 2010). The force of actin polymerisation toward the leading edge of a cell induces the edge to push forward into the area in front of the cell driving the cell forward. Active and yet unengaged integrins and receptors are continually recycled to and from the leading edge, sampling the ECM and cellular microenvironment in front of the cell to determine changes in migration direction depending on local environmental cues (Galbraith et al. 2007).

The process of cellular migration not only requires the actin polymerisation and integrin recycling but also the rear edge of the cell has to detach in a controlled manner enabling a push from behind. During detachment, retracting fibres are formed at the rear of the cell which assist in the detachment process. However, this can lead to a loss of membrane with a major fraction of integrin-containing membranous material is left behind. This action creates migration tracks left by the cell which marks the route it

has taken that have been observed both on glass and on matrix substratum (Kirfel et al. 2004). The membranous deposit left behind is rich in β_1 integrins and results from a membrane ripping process (Palecek et al. 1996; Lauffenburger & Horwitz 1996). Tracks laid down by cells, and in particular by fibroblasts migrating through the ECM, have been shown to be used by cancer cells as routes upon which they can migrate (Scott et al. 2010; Gaggioli et al. 2007). Without such routes, some cancer cells may be unable to migrate through ECM, thus this particular process of fibroblast lead collective invasion could potentially be a molecular target that could be utilised in therapeutic intervention.

1.6   Metastasis

Metastasis is defined as the ability of tumour cells in a primary tumour to invade other tissues and to spread throughout the body (Selivanova & Ivaska 2009). Terminal prostate cancer is the result of metastatic spread of the tumour from the prostate to peripheral sites primarily the bone and lymph nodes. The process involves the migration of the primary tumour cells, circulation, homing, invasion and growth of a new tumour (Welch & Rinker-Schaeffer 1999).

Although the exact molecular pathways required for this process are unknown, studies have shown that loss of function of specific genes interfere with the metastatic process (Yoshida et al. 2000; X. Yang et al. 1997). Classically, metastasis is thought to be preceded by EMT whereby the highly polarised and ordered epithelial cells change morphologically in to a mesenchymal state losing polarity and gaining migratory capacity (Thiery 2002). This process involves the down regulation of epithelial proteins such as E-cadherin and the upregulation of mesenchymal associated proteins such as vimentin (Jechlinger et al. 2003). Briefly, this enables them to breach the basement membrane, migrate out in to the ECM and infiltrate either the lymphatics or blood vasculature. The disseminated cells have to then establish at a secondary anatomical site where outgrowth of the secondary tumour occurs (Geiger & Peeper 2009).

Prostate cancer has an extremely high propensity to metastasise to the bone (Carducci & Jimeno 2006). There are many features of the bone marrow

which make it an attractive place for tumours to seed and grow. These features include growth factors such as vascular endothelial growth factor (VEGF), high levels of CXCL12 expression, physical features such as hypoxia which can stimulate the tumour cells to in turn stimulate osteoclast function in a viscous cycle promoting tumour growth in bone (Kingsley et al. 2007). Osteonectin, a glycoprotein important in bone formation, has also been found to enhance the invasion of prostate cancer cells in to bone through a mechanism that remains unclear (N. Chen et al. 2007).

Osteonectin, also known as Secreted Protein Acidic and Rich in Cysteine (SPARC) has been linked to cell proliferation, morphology and the binding of collagen (H. Sage, Decker, et al. 1989a; H. Sage, Vernon, et al. 1989b). Along with being a principal component of the bone microenvironment, SPARC expression is increasingly being linked to cancer cells in a variety of cancers. In prostate cancer models, SPARC has been shown to induce PC-3 cell migration (Jacob et al. 1999), and the expression of SPARC has also been linked, and correlates with, the progression of the disease (R. Thomas et al. 2000).

1.7   Cellular function in 2-D versus 3-D cell culture systems

A key difference between 2-D cell culture and culture involving a more complex environment including the ECM and different cell types, is the different physiological 3-D context. Cells employ different techniques, signaling pathways, morphology and changes in proliferation when exposed to a 2-D flat surface that is often plastic or glass, as opposed to a 3-D environment consisting of collagen and other ECM components. Typically this 3-D environment will also include other cells which becomes critically important when trying to recreate *in vivo* scenarios *in vitro*. Most cells *in vivo* inhabit a complex 3-D environment and studies comparing cell-matrix adhesions and cytoskeletal organisation have shown important differences (Rhee et al. 2007). There are, however, important similarities too. Analysis of the cytoskeleton and force measurement via traction force microscopy show that, despite the differences in many cell behaviours in 3-D compared to 2-D environments, the forces generated within either culture system are remarkably similar (Kraning-Rush et al. 2011).

Signaling pathways employed in 3-D environments can differ significantly or not feature at all when considering migration in 2-D. One such pathway is the MEK-cofilin signaling pathway in human T cells which exclusively mediates migration in 3-D, but not in 2-D. During T cell migration Ras localised in the lamellipodium activates MEK which in turns inhibits LIM kinase 1. This allows the dephosphorylation of cofilin – a protein that remodels f-actin during T lymphocyte migration (Klemke et al. 2010). This work was carried out in human T cells, but work carried out on tumour and tumour-associated stromal cells showed that the same LIM kinases were required for invasive path generation by fibroblasts in tumour cell migration in 3-D independent of MEK-mediated regulation (Scott et al. 2010).

Analysis of mesenchymal migration using mouse embryonic fibroblasts (MEFs), has shown that the movement of MEFs depends on focal adhesion formation and disassembly (Friedl 2004). The focal adhesion protein NEDD9 has been shown to localise to focal adhesions and has now been shown to have a key role in focal adhesion disassembly specifically. MEFs null for NEDD9 move faster on 2-D surfaces but significantly slower in 3-D collagen matrices (Zhong et al. 2012). Having previously been reported as a pro-metastatic protein (O'Neill et al. 2007) this is now being considered as a potential therapeutic target.

The 2-D approach to cell migration assays continues to be commonly used, particularly in high-throughput experiments. This could bias the experimental outcomes when investigating, particular when considering growth factor-induced cancer cell migration. Whilst the migration properties of breast cancer cells in 2-D do not correlate with their behaviour in 3-D, there is a robust relationship between membrane protrusions elicited by growth factor stimuli and subsequent enhanced migration in 3-D (Meyer et al. 2012). Using a panel of seven growth factors and serum, it was shown that the acute lamellipodial protrusion dynamics of the breast cancer cells can predict motility within 3-D collagen I matrices. By characterising this process it is possible to use a 2-D assay, in some instances, to predicts outcomes of 3-D assays without the need to carry them out (Meyer et al. 2012). The reason for the continued use of 2-D assays as opposed to 3-D assays is mainly due to technical difficulty. The known differences in cell movement between 2-D and 3-D calls in to question whether anti-migratory drugs should be

screened *in vitro*, in 3-D (Zaman et al. 2006; Fraley et al. 2010). A comprehensive review concluded that no single *in vitro* 2-D assay is sufficient to analyse migration and that 3-D assays offer a far more complex and physiologically relevant model, but there has to be standardisation in order to produce efficient quantitative analysis of cell migration in 3-D drug screening (Decaestecker et al. 2007).

1.8   Two-photon Imaging Technologies

Two-photon excitation fluorescence microscopy or multi-photon laser scanning microscopy (MP-LSM) has been widely used for imaging cells and tissues (Denk et al. 1990). It has many advantages over single photon confocal microscopy such as higher depth penetration, less phototoxicity and second harmonic generation (SHG). SHG is a second-order nonlinear optical process that has symmetry constraints confining signal to regions lacking a centre of symmetry (Campagnola et al. 2002). SHG results from secondary structures detected in samples when light is reflected back at exactly half the excitation wavelength and is collected in a non-descanned detector (NDD). This process does not involve the use of fluorescent proteins or fluorophores. Collagen I SHG is frequently used in the intravital imaging of tissues (Georgiou 2000; Theodossiou et al. 2006).

Two-photon imaging relies on extremely short pulses (in the order of femto-seconds) of longer wavelength (near infrared) light. A fluorophore is only excited when two or more photons are absorbed at twice the normal excitation wavelength compared to single photon excitation. As such, half the energy is used, thereby lowering the levels of energy the sample experiences hence lower phototoxicity (Provenzano et al. 2009). Also, the excitation field volume is lowered due to the fact that excitation remains strictly within the focal volume thereby further decreasing phototoxicity (Squirrell et al. 1999).

The development of two-photon microscopy has greatly enhanced the imaging of living tissues and *in vitro* cell culture models and provides a powerful platform for studying single cell behaviour in ever more complex microenvironments both *in vitro* and *in vivo*. Using two-photon imaging, fluorescence lifetime imaging microscopy (FLIM) can be used to monitor

metastasis in the context of the tumour microenvironment. Through FLIM, a detailed understanding of single cell behaviour within a multi-cellular and ECM rich microenvironment has been achieved and has provided key insights into the process of tumour metastasis (Provenzano et al. 2009). FLIM takes advantage of the intrinsic differential excited state lifetimes of fluorophores, both endogenous and exogenous, and can be used to create a map of the environment. This phenomenon has been used to study molecular parameters, local environment changes, metabolic states of cells (Bird et al. 2005) and protein-protein interactions (Becker 2012). This technique can utilise the endogenous fluorescence of cellular metabolites.

Intravital imaging using two-photon microscopy has been key to understanding how the immune system functions *in vivo* (Germain et al. 2012). More recently this approach has been used to study mechanisms of bacterial and parasitic infection (Beattie et al. 2010; Beattie et al. 2011; Germain et al. 2012; Tam et al. 2011; Chtanova et al. 2008; Junt et al. 2007), and to tracking cellular migration and cell fate in 4-dimensions in developing mouse embryos (Liu et al. 2011).

Two-photon microscopy has had a significant impact on understanding mechanisms of tumour metastasis. Initial studies of GFP expressing breast cancer cells in primary tumours *in situ* with two-photon microscopy allowed visualisation of single cancer cell behavior (W. Wang et al. 2002). This study allowed for the first time, the correlation between gene array data and *in vivo* observations within the primary tumour (W. Wang et al. 2002). The capability of FLIM in cancer studies has been used to study the process of tumour cell invasion in a 3-D collagen matrix, which was used to study drug uptake and toxicity through its capacity to detect 3-D topography, cellular kinetics and biological outputs (Bakker et al. 2012).

By utilising two-photon imaging of *in vitro* organotypic culture models, the role of tumour fibroblasts in remodeling the ECM was analysed in cultures where carcinoma cells retained their epithelial phenotype (Gaggioli et al. 2007). These tumour cells had not undergone EMT which had previously been thought to be a prerequisite of epithelial cells to take on a more mesenchymal phenotype in order to migrate, invade, and metastasise (Thiery 2002). Two-photon imaging of fluorescently labeled fibroblasts

mixed with squamous cell carcinoma (SCC) cells allowed deep imaging in to the matrix, over time, revealing a leading role for the fibroblasts. The fibroblasts were seen to lead a group of migratory SCC cells in to the matrix, whereas in the absence of fibroblasts, no invasion was seen despite the continued motility of SCC cells being evident (Gaggioli et al. 2007). Later, using a similar technique the LIM kinases were shown to have an essential role in this process of path generation by leading fibroblast cells during collective cancer cell invasion (Scott et al. 2010).

More recently two-photon laser scanning microscopy has also been developed as a tool for the diagnosis of superficial skin cancers. Through employing the unique properties of such imaging it is possible to visualise human skin at the bedside using endogenous flouresecent proteins and metabolites including NADH, keratin, melanin and collagen (Paoli et al. 2009).

The use of two-photon microscopy in using *in vitro* 3-D models and *in vivo* intravital models is an extremely powerful tool in cancer research. In this thesis I have utilised two-photon confocal microscopy to carry out high-resolution, long term 3-D imaging of human prostate cancer cells to investigate the mechanisms of human prostate cancer cell migration.

1.9   Summary and Aims

The underlying mechanisms leading to the induction of human prostate cancer remains unknown. Significant advances have been made in the field identifying key signaling pathways and the roles of different cell types and proteins in disease progression. Potential targets for drug discovery continue to be identified, but to date, there is no vaccine or successful treatments for high grade human prostate cancer. Current *in vitro* models of prostate cancer do not recreate the complex microenvironment found *in vivo* including the incorporation of primary human stroma. Whilst mouse models and 2-D studies on tumour cells have developed molecular insights into prostate cancer formation many questions remain unanswered, particularly in regard to the mechanisms driving tumour metastasis which is the source of lethality in humans.

The role of prostate stroma in cancer cell migration, development and metastasis is largely unknown. The molecular mechanism of stroma mediated cancer cell migration is an emerging area of cancer biology research. The initiating event(s) which leads to prostate cancer becoming an invasive metastatic disease is also largely unknown therefore it is important to generate and utilise advanced 3-D co-culture methods, to study cell migration, invasion and metastasis.

The role of CSCs in tumour metastasis are unknown. It has been shown that the putative CSCs in prostate cancer can recapitulate the full complement of disease both *in vitro* and *in vivo* but the relative capacity of CSCs to migrate is unclear. The role of cancer stem cells in the metastasis process may lead to new insights into how tumours metastasise and form secondary tumours.

Therefore, the aims of this thesis are to develop an advanced 3-D model of cell migration in the context of prostate cancer and utilise this model to address a number of questions focused around cancer cell migration. The objectives of this thesis are:

1) To develop and validate a 3-D *in vitro* model of stroma-epithelial cell migration within a suitable ECM.
2) To investigate the role of stroma in cancer cell migration.
3) To characterise the properties of CSCs within the 3-D model.
4) To address the molecular mechanism of stroma mediated prostate cancer cell migration.
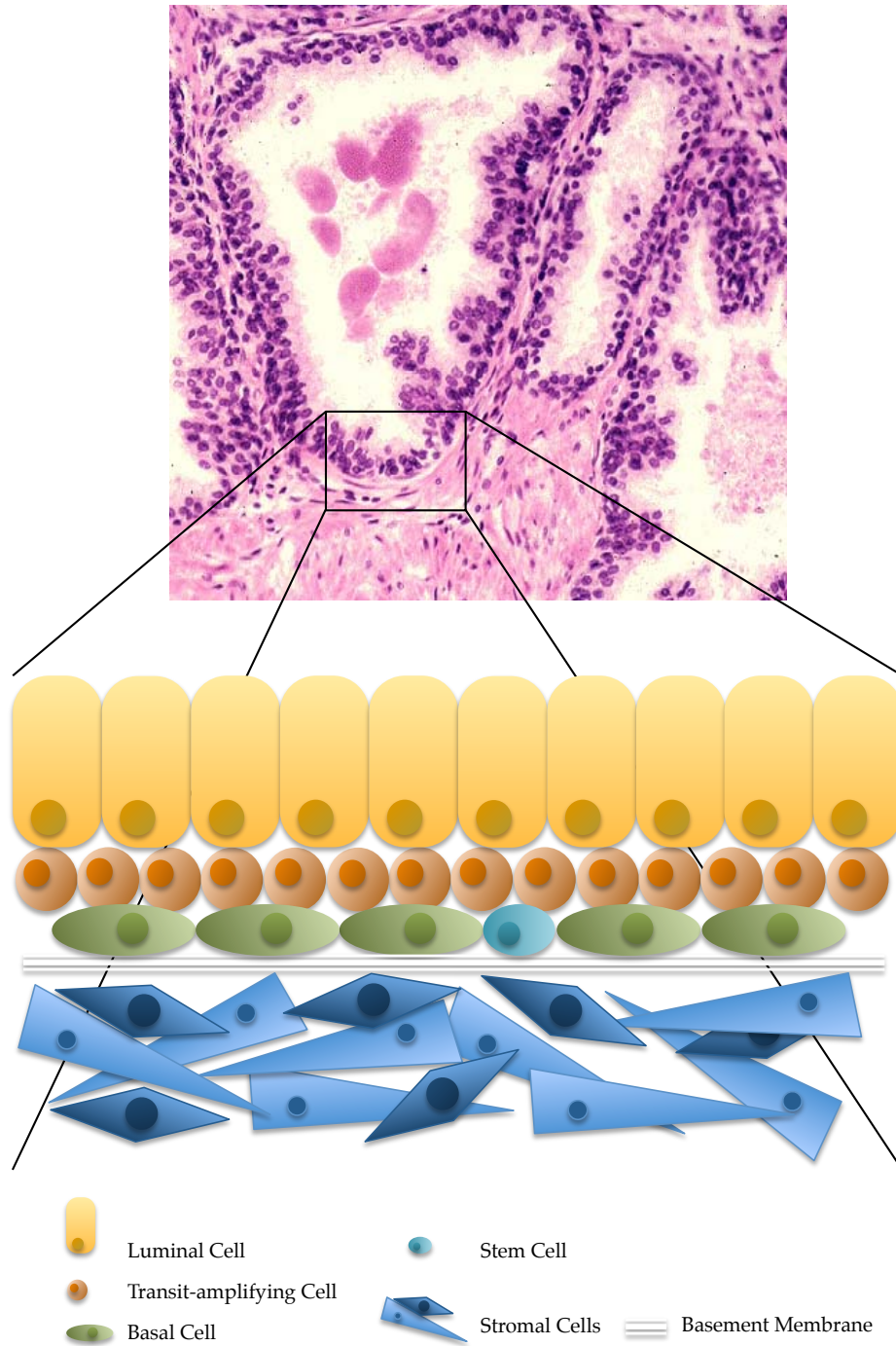
Figure 1.1 Above: H&E stained section of normal human prostate tissue showing secretory glands consisting of columnar epithelial cells surrounded by the stroma (John Hopkins University School of Medicine). Below: Graphical representation of the bilayer of epithelial cells consisting of the luminal cells (yellow) and the intermediate and basal cells (orange and green). The stroma (dark blue) is separated from the epithelium by a basement membrane (white horizontal line). Adapted from Maitland & Collins 2008.
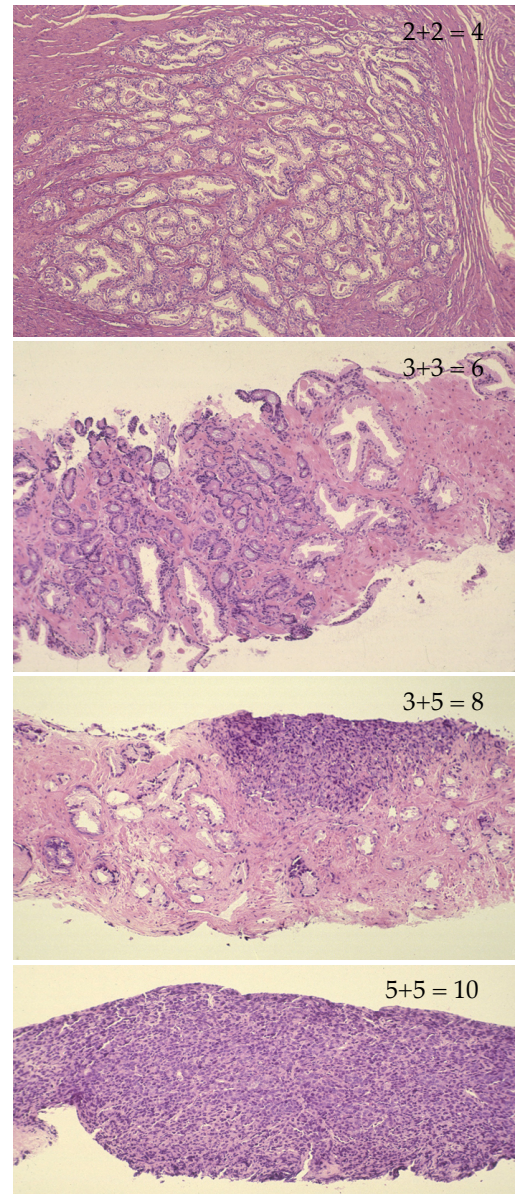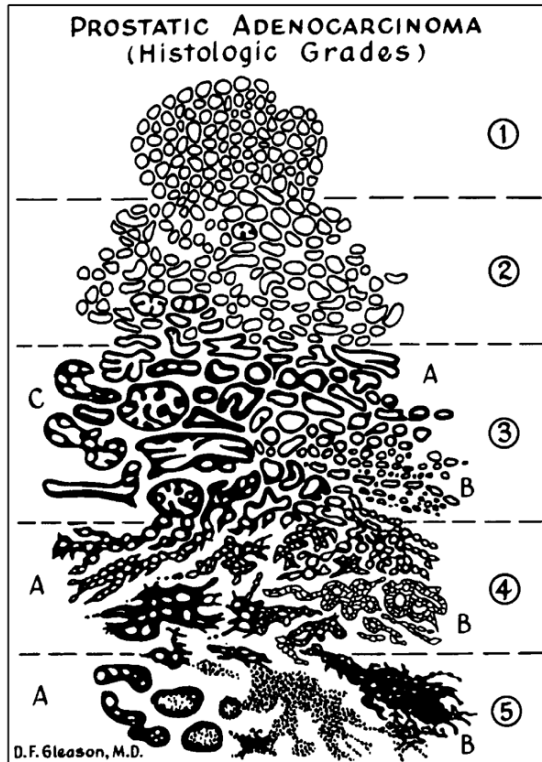
Figure 1.2 Histologic Grading of Prostate Cancer, then and now. The left panel depicts the original histologic patterns for standardising the grading system by Donald Gleason himself (Gleason DF, 1966) adapted from Gleason DF, 1992. The panels on the right depict H&E stained tissue sections of modern day pathology scoring of human prostate cancer. The system grades the primary and secondary patterns in the section, which are added together to give a final Gleason score (Humphrey et al, 2004)

Radiotherapy, chemotherapy, immunotherapy & gene therapy can eradicate the bulk of the tumour. However, the PCS cells, which make up less than 0.1% of the tumour, may persist.

Tumour re-growth is now possible from the few PCS cells remaining. The mature tumour cells express differentiation markers such as Androgen Receptor (AR) and Prostate-specific Antigen (PSA).

Isolated PCS cell in new environment

Figure 1.3 The stem cell model for the persistence of prostate cancer post therapy. The model states that the tumour consists of a hierarchy of differentiated cells containing a small population of stem cells, typically 0.1% of the tumour. After therapy these cancer stem cells persist and can establish a new tumour. Adapted from Maitland et al 2005.
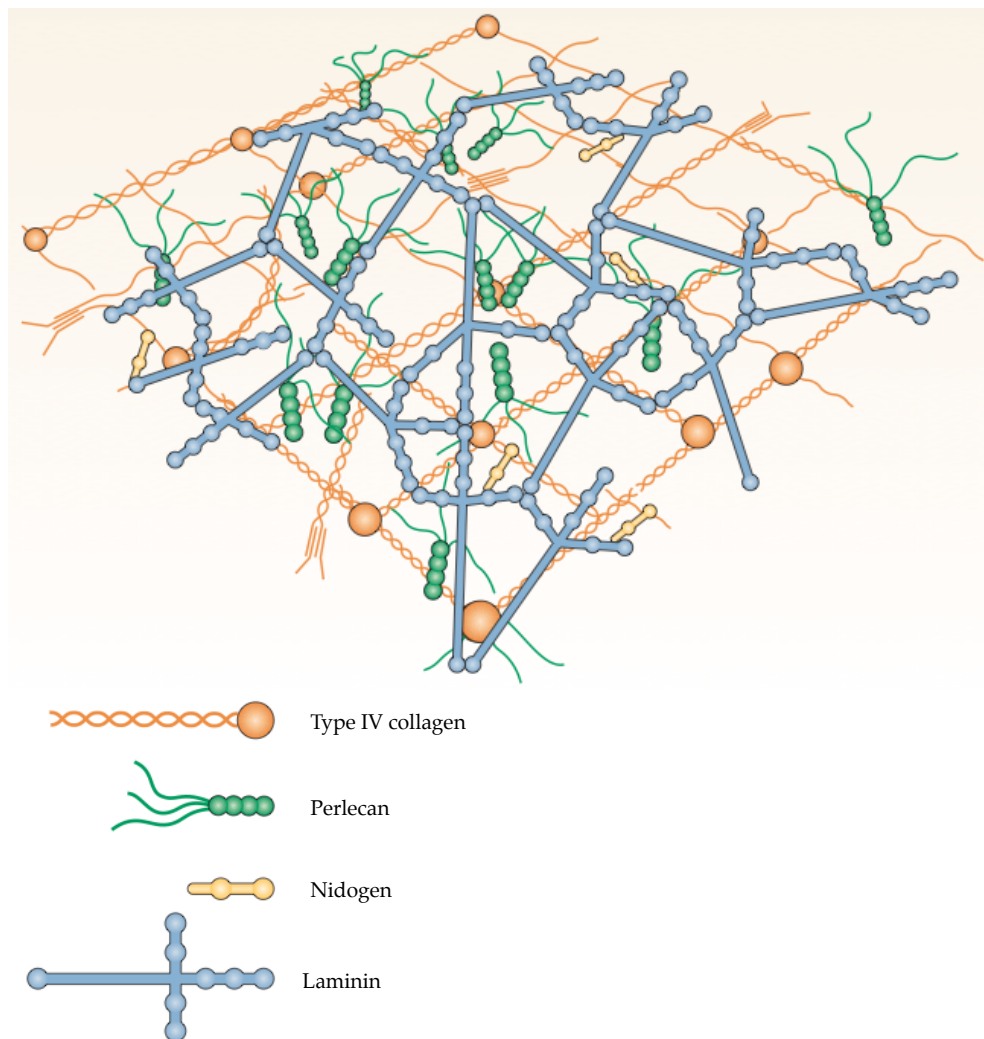
Figure 1.4 Basement membranes are thin (50-100nm) consisting of collagen IV, laminin, nidogens, perlecan and several minor glycoproteins (not shown). All four proteins become crosslinked creating a highly ordered and robust protein network. Adapted from (Sorokin 2010).

Chapter 2

Materials and Methods

2.1 Cell culture

2.1.1 Human prostate cancer cell lines

PC-3 and PC-3M prostate cancer cell lines were cultured in Hams Nutrient Mixture F12 (HAMS-F12) (Lonza) supplemented with 2mM L-glutamine (Invitrogen) and 7% Foetal Calf Serum (FCS) (Hyclone). Both cell lines were sourced from ATCC via Yorkshire Cancer Research (YCR) and were fingerprint matched by STR analysis (Promega) to original ATCC stocks routinely.

2.1.2 Human fibrosarcoma cell line

The human fibrosarcoma cell line HT1080 was cultured in Dulbecco's Modified Eagle Medium (DMEM) (Sigma-Aldrich) supplemented with 2mM L-glutamine and 10% FCS.

2.1.3 Primary prostate stromal cells

Primary stromal cells isolated from prostate tumour biopsies were cultured in Roswell Park Memorial Institute formulation 1640 (RPMI-1640) medium (Sigma-Aldrich) supplemented with 2mM L-glutamine and 10% FCS.

2.1.4 Human foreskin fibroblasts

Human foreskin fibroblasts (HFF) were cultured in Minimal Essential Medium (MEM) with Earle's salts and without L-glutamine (Sigma-Aldrich) supplemented with 10% FCS, 2mM L-glutamine, 0.1mM non-essential amino acids (Invitrogen) and 1mM sodium pyruvate (Sigma-Aldrich).

All cells and cell lines were cultured at 37°C with 5% CO_2.

2.1.5 Cell passage

Once cells had reached between 70-90% confluence, culture medium was removed by aspiration and discarded. Cells were then rinsed twice with Dulbecco's phosphate buffered saline (D-PBS) containing no $CaCl_2$ and no $MgCl_2$ (PAA) to remove all traces of serum. Typically, 1ml 1XTrypsin-ethylenediaminetetraacetic acid (EDTA) (Gibco) was added per $75cm^2$ tissue culture flask (Corning) and cell/Trypsin mixture was incubated at 37°C with 5% CO2 for no more than 5 min. Cells were periodically observed under an inverted light microscope until cells became rounded and detached from the surface. Cells that remained attached were detached from the surface by gentle tapping. Complete growth medium containing FCS was then added and cells were removed by gentle aspiration, spun at 300 g for 5 min and resuspended in complete growth medium. T25, T75 or T125 tissue culture flasks (Corning) were used depending on experimental requirements.

2.1.6 Cryopreservation

Cells were cryopreserved at a density of 0.5×10^6 cells/ml in a 50:50 mix of cell-specific culture medium and freezing medium (FCS containing 20% dimethyl sulfoxide (DMSO) (Sigma-Aldrich)). The cells were aliquoted in to 2ml cryovials (Corning), placed in a 'Mr Frosty' freezing container (Nalgene) which was then allowed to freeze overnight at -80°C. Cells were stored long-term in liquid nitrogen (LN_2).

Recovery of frozen cells was carried out by thawing in a water bath set at 37°C until ~90% of the ice had melted. 1ml of complete culture medium, prewarmed to 37°C, was then added to the 1ml of cells in freeze medium. The cells were removed from the cryovial, spun at 300 g for 5 min and resuspended in 5ml complete culture medium, prewarmed to 37°C. Once resuspended the cells were added to a tissue culture flask and incubated at 37°C with 5% CO_2.

2.2 Primary culture of human prostate cells

2.2.1 Separation of stromal cells from epithelium

Tissue was sourced from Hull and East Yorkshire Hospitals NHS Trust in accordance with an agreement between YCR at the University of York and the Trust and ethical permission (ref: R0609 – 07/H1304/121). Fresh tissue

was rinsed in PBS and sliced. A section was set aside for embedding in optimal cutting temperature (OCT) compound for histology, with the remainder of the tissue diced in to small pieces. Up to 1g of tissue was then digested in 7.5ml of collagenase I solution (5ml RPMI containing 10% FCS, 2.5ml basal containing 1.35mg collagenase I) and then incubated at 37°C overnight on an orbital shaker, shaking gently. The mixture was then spun at 300 g for 10 min to pellet the cells and the supernatant was discarded. The cells were resuspended in 10ml PBS and spun at 300 g for 10 min twice more. The final cell pellet was resuspended in 10ml RPMI containing 10% FCS and the cells were allowed to settle for 15 min at room temperature. Epithelial cells will settle and the supernatant will contain fibroblasts and stroma (including haematopoietic cells). The suspended cells were collected with a Pasteur pipette and the process of spinning, resuspending and settling was repeated twice more or until no more epithelial cells settled out. The remaining supernatant contains the fibroblast stromal compartment.

2.2.2   Primary stromal cell culture

The supernatant from section 2.2.1 was spun at 300 g from 15 min, the supernatant discarded and cells resuspended in 15ml RPMI containing 10% FCS, 2mM L-glutamine and 1% penicillin/streptomycin. The cells were added to a T75 tissue culture flask and allowed to settle for at least 2 days at 37°C with 5% CO_2. This incubation is necessary in order to remove immune cells, cell debris and erythrocytes from the culture. After 2 days the media was aspirated off and 10ml PBS was added to the flask. Gentle agitation was applied by hand to loosen any debris and remove any remaining erythrocytes. The PBS was aspirated off and replaced with complete RPMI media and cells were allowed to grow until ~90% confluence.

2.2.3   CD133^{+} selection of epithelial stem cells

Epithelial cells collected in section 2.2.1 were resuspended in 5ml 1x trypsin and incubated at 37°C for 30 min whilst shaking in an orbital shaker at 80rpm. 10ml complete RPMI containing 10% FCS was then added to halt trypsinisation and the mix was spun at 300 g for 10 min. The cell pellet was resuspended in 5ml complete RPMI containing 10% FCS and warmed to 37°C.

A Biocoat collagen I plate (BD Biosciences) was blocked for 1 hour at 37°C with 0.3% BSA in PBS. The prewarmed cell mixture was plated out on the blocked Biocoat collagen I plate (3ml per plate) and incubated at 37°C for 20 min. The media was collected from the plate and retained. The plate was then rinsed with 1X PBS and was also retained with the media. The cells were spun at 250 g for 10 min. This pellet contains the $\alpha_2\beta_1^{low}$ fraction (luminal and transit-amplifying cells).

Adhered cells ($\alpha_2\beta_1^{high}$) were collected by incubation with 10x trypsin at 37°C for 15 min. Cells were collected in complete RPMI containing 10% FCS and the process repeated until all cells were collected. Cells were then spun at 250 g for 10 min and the pellet resuspended in 300μl MACS buffer (PBS/2mM EDTA with 0.5% FCS) plus 100μl FcR blocking reagent and 100μl CD133 beads (Miltenyi Biotec), mixed well, and incubated at 4°C for 30 min on a MACS roller. 3ml of MACS buffer was then added to the mix which was then centrifuged at 300 g for 10 min. The supernatant was removed and the cell pellet was resuspended in 500μl MACS buffer.

A MACS column was saturated with 500μl MACS buffer and allowed to run through. The cells were then added to the column to allow magnetic separation. The column was then washed three times with 500μl MACS buffer with the flow through containing the CD133⁻ population of cells being collected.

To obtain the CD133⁺ population, the column was removed from the magnetic clamp and 1ml of MACS buffer was added to the column. This was firmly flushed through with a plunger. The cells were then washed once with 500μl MACS buffer and spun at 300 g for 10 min. Once the supernatant was discarded the cell pellet was resuspended in keratinocyte serum-free medium (KSFM).

2.3 Cell transfection

2.3.1 Fluorescent protein vector transfection

Prostate cancer cell lines PC-3 and PC-3M were each transfected with pCMV-GFP and pCMV-tdTomato using Lipofectamine® 2000 Transfection Reagent (Invitrogen). 24 hours before transfection, 0.5 x 10⁵ cells were added to a 24-

well tissue culture treated plate (Corning) in 500µl culture medium without antibiotics. 0.8µg plasmid DNA was diluted in 50µl Opti-MEM® Reduced Serum Medium (Invitrogen) without serum. 2µl Lipofectamine® 2000 Transfection Reagent was diluted in 50µl Opti-MEM® Reduced Serum Medium without serum. The diluted DNA and diluted Lipofectamine® were combined, mixed and incubated for 20 min at room temperature. 100µl of the DNA/Lipofectamine® mix was then added to the well containing the cells and the plate was mixed by gentle rocking. Cells were incubated at 37°C with 5% CO_2 overnight. Stable cell lines were created by passaging the cells 1:10 into fresh growth medium 24 hours after transfection with the medium changed a further 24 hours later to selective medium containing 200ng/ml G418 (Sigma-Aldrich). After 14 days, the highly fluorescent cell populations were sorted on a Beckman MoFlo XDP Cell Sorter. The sorted cells were maintained in culture as in section 2.1.1.

2.3.2 Inducible shRNA vector transfection

Bacterial glycerol stocks containing shRNA constructs (Sigma-Aldrich) were streaked for single colonies on to LB-Agar plates containing 100µg/ml ampicillin and incubated for 24 hours at 37°C. To obtain plasmid DNA, single colonies were picked and grown overnight in Luria Broth (LB) containing 100µg/ml ampicillin at 37°C whilst shaking. A Plasmid Midi Kit (Qiagen) was used to purify plasmid DNA to a high concentration and purity. Plasmid DNA was run on a 1% agarose gel via gel electrophoresis and purity was assessed by a NanoDrop (Thermo Scientific). Plasmid DNA was transfected in to PC-3 cells using a Neon® Transfection System (Invitrogen) using the following electroporation parameters; pulse voltage: 1250v, pulse width: 30ms, pulse number: 1, cell density: 0.5 x 10^6 cells/ml, tip type: 10µl. Transfected cells were selected for in the presence of 200ng/ml neomycin 72 hours after transfection. The cells remaining were treated as a bulk culture. Single cell clones were obtained by plating transfected cells in to a 96-well tissue culture plate at a density of 0.5 cells/well. Each well was checked for the presence of a single cell 24 hours later and marked. Cell culture medium was changed every 3 days and once cells were ~80% confluent, they were passaged in to larger culture vessels from a 96-well plate, to a 48-well plate, etc. until there were enough cells to seed a T75 75cm² tissue culture flask. Single cell clones were kept under 200ng/ml neomycin selection thereafter. The shRNA construct was induced by adding dioxin-free

Isopropyl β-D-1-thiogalactopyranoside (IPTG) (Sigma-Aldrich), reconstituted in sterile water, to a final concentration of 100mM in normal complete HAMS-F12 media for 3 days. Wildtype PC-3 cells which had not been transfected with shRNA were used as experiment controls.

2.4 Collagen

2.4.1 Collagen preparation

Type I Collagen was prepared from adolescent rat tails following a protocol adapted by myself and Roger Leigh (Coles Group) based on published methods (B. R. Williams et al. 1978). Preparation took place under sterile conditions with all solutions and equipment 0.2μm filter sterilised and/or autoclaved where applicable. Rat tails from juvenile male rats were skinned and the proximal and distal ends removed. Each joint was then in turn snapped and pulled away from the main body of the tail using a hæmostat clamped on either end. The dislocated joint was pulled drawing out the tendons through the tail. Tendons were then cut from the dislocated joint and placed in sterile water and washed briefly in 95% ethanol before being briefly dried and then weighed. Tendons were then dissolved in 50ml 0.5M acetic acid per 1g of tendon at 4°C for no longer than 36 hours and tendon/acetic acid was then centrifuged for 60 min at 20,000 g at 4°C. The supernatant was retained and stored in aliquots at 4°C. In order to reduce acidity, dialysis or lyophilisation was used.

Collagen in 0.5M acetic acid was dialysed against a great excess of 0.1X DMEM in 0.02M acetic acid at 4°C using high retention seamless cellulose tubing (Sigma-Aldrich). The buffer was replaced twice over 3 days and the final dialysed collagen was stored in aliquots at 4°C. Collagen concentration was determined using a Bradford assay and adjusted to 3.33mg/ml.

Alternatively, collagen in 0.5M acetic acid was also lyophilised in a bench top Lyotrap lyophiliser (LTE) and reconstituted in 0.02M acetic acid at a known concentration of 3.33mg/ml.

2.4.2 Collagen gels

Collagen gels were prepared on ice by adding cooled 10X DMEM containing phenol red to collagen prepared as in section 2.4.1 to achieve a final DMEM

concentration of 1X and a final collagen concentration of 3mg/ml. The collagen/DMEM mixture was then neutralised to pH7.0-pH7.5 using cooled 1M NaOH. The pH was monitored using the phenol red colour change and the final pH was confirmed using pH indicator strips (VWR). For single cells suspended in collagen, pelleted cells were resuspended in neutralised collagen once the growth medium had been removed by aspiration. The collagen gel/cell mix was then added to a cooled PEI treated 3.5cm Glass Bottom Dish (MatTek) and allowed to set at 15°C for 1hr. Alternatively, 30μl collagen alone was added to the centre of a PEI-treated stainless steal washer support (internal diameter 6mm) previously adhered to the glass surface of a PEI treated 3.5cm Glass Bottom Dish by vacuum grease, all kept on ice. Spheroids, as prepared in section 2.13 were then introduced in to the gel by pipetting. Once enough spheroids had been added to the gel, the whole dish was incubated at 15°C for 1hr to allow collagen gel to set. Enough complete growth medium was then added to the dish to cover the gel taking care to wet the collagen gel first by adding the medium slowly to prevent mechanical disruption of the gel. The dish containing the cells/spheroids in collagen was then incubated at 37°C with 5% CO_2 before imaging.

2.5   Poly(ethylenimine) surface treatment

Collagen does not adhere to most surfaces effectively and so to counteract this a protocol was developed to surface treat the glass and metal surfaces with poly(ethylenimine) (PEI) (Sigma-Aldrich). Glass surfaces and metal supports used in the formation of collagen gels were washed once with 95% ethanol and allowed to dry. All surfaces to come in to contact with collagen were treated with 1% PEI for 10 min and then washed once with 95% ethanol. Once dry, the PEI coated surfaces and/or supports were functionalised with 1% glutaraldehyde for 30 min followed by washing six times with sterile water. All items were then air dried thoroughly before use.

2.6   Matrigel

Frozen aliquots of Matrigel™ were thawed on ice. All materials to come in to contact were kept cool on ice, including pipette tips which had been stored at -20°C until use. Once thawed, Matrigel™ was added to the base of a 3.5cm glass bottom dish and allowed to set at 37°C for 30 min before the addition of 2.5ml pre-warmed complete media containing cells. The dish was then

returned to the incubator in 37°C with 5% CO_2 typically overnight. For gels containing cells, the appropriate number of cells were pelleted by centrifugation at 300 g for 5 min. Media was removed by aspiration and the tube and pellet were cooled on ice for at least 5 min. Cell pellets were resuspended in Matrigel™ gently but quickly before being swiftly added to a 3.5cm glass bottom dish. The gel was set at 37°C for 30 min before the addition of 2.5ml complete media pre-warmed to 37°C. The dish was then returned to the incubator at 37°C with 5% CO_2 typically overnight.

2.7   CFSE labeling of prostate stroma

Stromal cells were collected from culture flasks via trypsinisation as in section 2.1.5. The cells were then washed via centrifugation in serum-free RPMI media warmed to 37°C. The cells were then resuspended in warm serum-free RPMI media containing 5μM carboxyfluorescein diacetate, succinimidyl ester (CFSE) (Invitrogen) (1:2000 dilution from a 10mM stock) and incubated for 8 min. After flooding immediately with excess cold RPMI media supplemented with 10% FCS, cells were washed once with complete RPMI media and twice in serum-free RPMI media at which point they were ready to be counted and utilised.

2.8   Cell tracker staining

CellTracker™ Green (CMFDA) (Invitrogen) at a stock concentration of 10mM was used to make a dye mixture containing a final concentration of 5μM (1:2000 dilution) in serum free media. After warming to 37°C, 5ml of the dye mixture was added to cells that had previously been trypsinised from the culture flask and pelleted by centrifugation at 300 g for 5 min. The cell/dye mix was gently mixed by pipetting and incubated at 37°C for 30 min. Cells were pelleted by centrifugation at 300 g for 5 min and the dye mixture removed by aspiration. Normal media containing 10% serum was added and the cells resuspended by gentle pipetting and the mix incubated at 37°C for a further 30 min. Labeled cells were then ready to use. CellTracker™ Red (CMTPX) (Invitrogen) was also used as described for CMFDA in this section, however prior to making the initial 5μM dye mixture, undiluted CMTPX was mixed 1:1 with Pluronic F-127 (Invitrogen) to facilitate dissolving.

2.9   Cytospins and Giemsa staining

Cells were collected via trypsinisation as in section 2.1.5. 2.0×10^5 and cells were spun at 300 g for 5 min, the supernatant aspirated and discarded and cells were resuspended in 200µl PBS. 2.0×10^5 cells in 200µl PBS were spun on to polysine slides (VWR) using a cytospin centrifuge at 1800 rpm for 3 min. Cells were then fixed in 100% methanol and allowed to air dry. Fresh Geimsa reagent (3.6ml Sorenson A (9.5g Na_2HPO_4/L dH_2O) + 1.4ml Sorenson B (9.07g KH_2PO_4/L dH_2O) + 45ml dH_2O + 5.55ml Giemsa stain) was prepared and used in which to incubate the slides at room temperature for 20 min. Slides were then thoroughly rinsed in running water and allowed to air dry before coverslips were mounted using DEPEX mounting medium (Sigma-Aldrich) and visualised using phase contrast microscopy.

2.10   Immunocytochemistry of prostate stromal cells in 3-D

Prostate stromal cells in 30µl collagen gels were fixed for 1 hour in 4% paraformaldehyde (PFA) at room temperature. Gels were washed three times over a total of 30 min in PBS containing 0.5% Triton™ X-100 (Sigma-Aldrich). Gels were then incubated in PBS containing 0.5% Triton™ X-100 for 30 min in order to render cells permeable. The f-actin stain Phalloidin Alexa 647 (Fluka) and the nuclear stain YO-PRO (Invitrogen) were mixed together at a dilution of 1:1000 in PBS. Gels were incubated overnight in the dye solution at 4°C whilst slowly shaking. The next day, gels were washed three times in PBS containing 0.5% Triton™ X-100 over the course of 8 hours before being fixed in 4% PFA for 30 min. The PFA was replaced with PBS and the gels were imaged on a Zeiss 710 confocal microscope.

2.11   Quantitative Real-Time Reverse Transcriptase PCR

2.11.1 RNA isolation

Cells were spun at 300 g for 5 min. The supernatant was aspirated and the cell pellet was disrupted by resuspension and agitation in 350µl of RLT buffer (Qiagen). RNA was isolated using QIAshredders and RNeasy spin columns according to the manufacturer's (Qiagen) instructions. The eluted RNA was quantified for concentration and analysed for purity on a NanoDrop (Thermo Scientific).

2.11.2 cDNA synthesis

cDNA synthesis from previously isolated RNA as in section 2.11.1 was carried out using an EZ-First Strand cDNA Synthesis Kit For RT-PCR (Geneflow). Briefly, 1µg of RNA was added to a primer mixture containing 1µl 40µM oligo(dT)20 primer and DEPC-Treated water up to a final volume of 10µl in a 0.2ml thin-walled PCR micro-centrifuge tube. This was mixed gently and incubated at 70°C for 10 min and then rapidly placed on ice. To the RNA/Primer mix, 8µl of Reaction Mix (2.5X) and 2µl of 100mM DTT was added and mixed gently. The reaction mix was then incubated at 42°C for 60 min and the synthesis reaction terminated by incubating at 70°C for 15 min. The cDNA synthesised was then stored at -20°C or used immediately in RT-PCR experiments.

2.11.3 Primer design

Gene specific primers were designed using Gene and Primer-BLAST (NCBI). All primers spanned an exon-exon boundary to rule out binding to any genomic DNA contamination. Primers were ideally 18-22 base pairs in length, resulting in a PCR product of between 75 – 120 base pairs in length, with a T_m of 60°C ± 1°C. Primers used for RT-PCR are detailed in Table 2.1.

2.11.4 RT-PCR

cDNA generated as in section 2.11.2 was diluted to a final volume of 100µl by adding 80µl of DEPC-treated water. An RT-PCR mix was made up consisting of 12.5µl of SYBR Green (Applied Biosystems), 8.5µl of dH_2O, 1µl of forward primer (1µM) and 1µl of reverse primer (1µM). The resulting mix was added, in triplicate, to the appropriate wells of a MicroAmp Optical 96-well reaction plate and 5µl of cDNA was added to the RT-PCR mix. After being sealed the plate was loaded on to an ABI Prism 7000 RT-PCR machine. The RT-PCR was carried out using the following thermal cycling program: 50°C for 2 min, 95°C for 10 min, 40 cycles of 95°C for 15 sec + 62°C for 30 sec + 72°C for 30 sec, then 72°C for 5 min. The plate was then cooled to 4°C until the machine was shut down and data was analysed using the 7000 system SDS software. Primers for the housekeeping gene GAPDH were used as a housekeeping control to which the expression of target genes was normalised to.

Table 2.1 Primers for RT-PCR

Gene	Direction	Sequence	Reference
C-MET (HGFR)	Fwd	CAGAGGGTCGCTTCATGCAGGTTG	NM_001127500.1
	Rev	GGAGACACTGGATGGGAGTCCAGG	
CD45	Fwd	AGGCATGGTTTCCACATTCGAGCA	NM_002838.3
	Rev	CTGGGGCACCAAGTGGATTAACACA	
COL4A1	FWD	ATCTGTTGATCACGGCTTCC	NM_001845.4
	REV	TCATTGCCTTGCACGTAGAG	
COL1A1	Fwd	CACACGTCTCGGTCATGGTA	NM_000088.3
	Rev	AAGAGGAAGGCCAAGTCGAG	
DES	Fwd	GCGGACGTGGATGCAGCTACT	NM_001927.3
	Rev	GCAACTCACGGATCTCCTCTTCATGCA	
CDH1 (E-Cadherin)	Fwd	AGGCGGAGAAGAGGACCAGGACT	NM_004360.3
	Rev	TGGCAGGGCGGGGAAGATACC	
FSCN1	Fwd	CATCGAGTGGCGTGACCGGC	NM_003088.3
	Rev	GCTCTGAGTCCCCTGCTGTCTCC	
FN1	Fwd	GGTGGAATAGAGCTCCCAGG	NM_212482.1
	Rev	GCAGCCTGCATCTGAGTACA	
GAPDH	Fwd	AAGGTGAAGGTCGGAGTCAA	NM_002046.3
	Rev	AATGAAGGGGTCATTGATGG	
ICAM1	Fwd	GACCGCAGAGGACGAGGGCA	NM_000201.2
	Rev	GTTGGGCGCCGGAAAGCTGTA	
LAMA1	Fwd	TTGGTGCTGATGTGAGCATT	NM_005559.3
	Rev	CCTGGTCTTGCTGCTGTGT	
MAdCAM-1	Fwd	GGAGGTGGTGTCGGGAG	NM_130760.2
	Rev	CTACTGCCAGGCCACGAT	
MMP1	FWD	GGGAGATCATCGGGACAACTC	NM_001145938.1
	REV	GGGCCTGGTTGAAAAGCAT	
MMP14	FWD	CGCTACGCCATCCAGGGTCTCAAA	NM_004995.2
	REV	CGGTCATCATCGGGCAGCACAAAA	
MMP2	FWD	TGATCTTGACCAGAATACCATCGA	NM_004530.4
	REV	GGCTTGCGAGGGAAGAAGTT	

Table 2.1 Primers for RT-PCR, continued

Gene	Direction	Sequence	Reference
MMP3	FWD	TGGCATTCAGTCCCTCTATGG	NM_002422.3
	REV	AGGACAAAGCAGGATCACAGTT	
MMP7	FWD	GTGGTCACCTACAGGATCGTA	NM_002423.3
	REV	CTGAAGTTTCTATTTCTTTCTTGA	
MMP8	FWD	TGGACCAACACCTCCGCAAATTACA	NM_002424.2
	REV	TCAAGGCACCAGGGTCAGAGGA	
MMP9	FWD	TGGGGGGCAACTCGGC	NM_004994.2
	REV	GGAATGATCTAAGCCCAG	
CDH2 (N-Cadherin)	Fwd	CCACCTTAAAATCTGCAGGC	NM_001792.3
	Rev	GTGCATGAAGGACAGCCTCT	
NETO2	FWD	TGGGCAGATGAAGGTAGTCGGC	NM_018092.4
	REV	TGCAGGGAGGCTCCACAAAGGA	
P63	FWD	CCTGACCCTTACATCCAGCGTTTCG	NM_003722.4
	REV	GCTCTGGGACATGGTGGATCGG	
HSPG2 (Perlecan)	Fwd	GGCAGCGTCTACATCGGCGG	NM_005529.5
	Rev	TGCTGCAGGTCCAGGGGCT	
PDPN	Fwd	GGGAAGGTACTCGCCCTAAAGAGC	NM_006474.4
	Rev	TGGGCCAGGCAAGTGTTCCA	
α-SMA	Fwd	TGCCTATCCCCGGGACTAAGACGGG	NM_001141945.1
	Rev	CCCCAGCAAAGCCGGCCTTACA	
SPARC	FWD	GGAGGTGGTGGCGGAAAATCCC	NM_003118.3
	REV	GGGTCCTGGCACACGCACAT	
TGFB1	Fwd	CACGCAGTACAGCAAGGTCCTGG	NM_000660.4
	Rev	GGCTTGCGGCCCACGTAGTAC	
TRANCE	Fwd	TCAGAGCAGAGAAAGCGATGGTGGA	NM_003701.3
	Rev	TGGCCCAACCCCGATCATGGT	
VCAM-1	Fwd	GTCTCCAATCTGAGCAGCAA	NM_003478.3
	Rev	TGGGAAAAACAGAAAAGAGGTG	
VLA-4	Fwd	ACAGGAAGCATACAGGTGTCCAGCA	NM_002211.3
	Rev	TGTCCCGCACATCTTTCCGCA	

2.12   Methyl cellulose preparation

6mg of methyl cellulose (Sigma-Aldrich) was autoclaved and dissolved in 250ml DMEM or HAMS-F12 medium pre-heated to 60°C. A further 250ml room temperature media was added and mixed at 4°C for 2 hours and the total 500ml was centrifuged at 2500 g for 1 hour. The clear supernatant was retained as a 2.4% (w/v) stock and stored at 4°C in aliquots.

2.13   Spheroid formation

All spheroids were formed in 0.3% (w/v) methyl cellulose in either DMEM or HAMS-F12 media depending on cell type, using a hanging drop culture method. This protocol was adapted from Laib et al (Laib et al. 2009). Typically, cells (starting number varied between experiments) were spun at 300 g for 5 min in a Universal tube. The supernatant was aspirated and the cell pellet was resuspended in 0.3% (w/v) methyl cellulose to a final cell density of 1 x 10^5/ml. The cell/methyl cellulose mix was then pipetted on to the base of a petri dish in discreet aliquots of 25μl to give 2.5 x 10^3 cells/droplet. The base of the petri dish was then inverted to create the hanging drop culture and incubated overnight at 37°C with 5% CO_2. Sterile water was added to the petri dish to maintain humidity and prevent evaporation of the methyl cellulose. Spheroids which had formed overnight were gently washed from the plate with PBS containing 10% FCS prewarmed to 37°C and spheroids were then ready to be implanted in to collagen gels by pipetting.

2.14   Imaging

2.14.1 2-photon microscopy

2-photon imaging was carried out both on a Zeiss LSM 510 Meta NLO microscope and a Zeiss LSM 780 Meta NLO microscope. Typically, images were acquired using a C-Apochromat 40x/1.1W Corr UV-VIS-IR objective and 3 non-descanned detectors (NDD, LSM 510) or 1 NDD and 2 GaAsP detectors (LSM 780). The sample was excited using a Chameleon XR Ti:sapphire laser (Coherent) tuned to 870nm. GFP emission was collected via a 500-550nm band pass emission filter in NDD2 (LSM510) or GaAsP1 (LSM780). Td-tomato emission was collected via a 575-640nm band pass emission filter in NDD3 (LSM510) or GaAsP2 (LSM780). Second Harmonic Generation (SHG) emission of collagen was collected via a 415-435nm band

pass emission filter in NDD1 (LSM510 and LSM780). The microscope stage was maintained at 37°C by a blackout environmental chamber (Solent Scientific, UK).

2.14.2 Confocal microscopy

All immunohistochemistry and immunocytochemistry experiments were imaged using a LSM 710 laser scanning confocal microscope on an Observer.Z1 inverted base (Zeiss) using 0.5 and 1.4 numerical aperture (NA) 20X and 40X objectives (Zeiss). Multiple microscope, filter and laser line configurations specific to each experiment were used. For comparative imaging and subsequent analysis between samples, laser power and detector gain voltage and offset were kept constant. Routinely, multi-track imaging was used to minimise bleedthrough.

2.14.3 Stereo microscopy

Whole tumours resulting from PC-3-tdTomato cells were visualised for red fluorescence using a SteReo Lumar stereo microscope (Zeiss) with a BDO100 mercury lamp. Images were collected with an AxioCam digital CCD camera (Zeiss). This set up was also used to look for metastases resulting from PC-3-tdTomato metastasis from the main tumour.

2.14.4 Bright-field live cell imaging

Cells were seeded in to 3.5cm glass bottom dishes and allowed to attach overnight at 37°C with 5% CO_2. Cells were imaged in a live cell imaging chamber on an Andor Revolution CD spinning disk microscope scope using a 0.5NA 20X objective (Zeiss). The live cell imaging chamber was kept at a constant 37°C with a gas supply containing 5% CO_2 in air. Images were acquired over 6 hour periods at intervals of 5 min unless otherwise stated. Analysis was carried out using the imaging analysis software package ImageJ.

2.14.5 Transmission electron microscopy

Whole collagen gels containing HT-1080 cells were prepared by fixation in transmission electron microscopy (TEM) fixative composed of 5ml 200mM phosphate buffer (pH 7.2), 2.5ml 16% PFA, 1ml 25% glutaraldehyde (Sigma) and 1.5ml dH_2O to give a final concentration of 4% PFA and 2.5% glutaraldehyde in 100mM phosphate buffer.

Samples were fixed at 4°C overnight and then washed three times in phosphate buffer. Samples were then stored in phosphate buffer at 4°C. Fixed samples were stained with 1% (w/v) osmium tetroxide followed by dehydration using an acetone series before being embedded in Spurr's resin. Ultrathin sections (approximately 80nm) were transferred to TEM grids and were stained with uranyl acetate and Reynold's lead citrate prior to imaging.

Imaging was carried out using a TECNAI G2 TEM (FEI, Hillsboro, Oregon, USA) with a MegaView III CCD (Olympus, Münster, Germany).

2.15   Migration assays

Migration assays were carried out using 8μm pore size PET trans-well inserts for 24-well plates (VWR) in a 24-well plate (VWR). According to the manufacturer's instructions and published techniques (Xue et al. 2009) 800µl media was added to the lower well and a defined number of cells were seeded on top of the insert in 300µl media at a density equivalent to 80% confluence as a proportion of a T75 culture flask, thus, PC-3 cells were seeded at 2.8 $x10^4$ cells/cm^2. At set time points inserts were removed and fixed in 4% PFA for 10 min before cells on the upper surface were removed by scraping. The membrane was removed from the insert and mounted on a glass slide under a coverslip and imaged using an LSM 710 inverted confocal microscope.

2.16   Tissue digestion

Mice were sacrificed and the tumour(s) excised. As much hair, skin and fat was removed as possible and all tumours were measured using calipers (dimensions X, Y and Z) and weighed to the nearest mg. A small piece (approximately 5mm^3) of tumour was excised from the main bulk of the tissue and cut in to several smaller pieces (approximately 0.5mm^3). The pieces were placed in digestion buffer 1 (1.5ml RPMI containing 2% FCS + 37µl Collagenase.D + 2.5µl DNAse I) allowed to digest at 37°C in a heat block with vigorous shaking at 900rpm. At intervals of 15 min the tissue pieces were mechanically disrupted by pipetting before being returned to the heat block. After 60 min the sample was further disrupted mechanically by pipetting 5-6 times and spun down at 1400rpm for 5 min. The supernatant

was then discarded and 1.5ml digestion buffer 2 (1.5ml RPMI containing 2% FCS + 37μl Collagenase.Dispase + 2.5μl DNAse I) was added. The mix was then incubated at 37°C for 30 min whilst shaking at 900rpm, with mechanical disruption by pipetting performed half way through. After 30 min of incubation, 15μl 0.5M EDTA was added and the mix was resuspended by vortexing briefly. Cells were then filtered through a 40μm cell strainer (Corning) into a 50ml Falcon tube (Corning) containing 8.5ml RPMI containing 2% FCS. The filter was rinsed with 10ml RPMI containing 2% FCS and cells were spun down at 300 g for 10 min. Cells were resuspended in 10ml RPMI containing 2% FCS and counted. Typically 1 x 10^5 cells were spun down and resuspended in FACS buffer (PBS containing 0.05% bovine serum albumin (BSA)) for analysis by flow cytometry.

2.17 Flow cytometry analysis of cell surface marks

2.17.1 Antibody staining

1 x 10^5 cells were aliquoted into 15ml centrifuge tubes and spun at 300 g for 5 min and resuspended in 500μl FACS buffer (PBS + 0.05% BSA) and incubated on ice for 10 min. Cells were the spun at 300 g for 5 min, resuspended in 500μl FACS buffer and spun at 300 g for a further 5 min. Cells were then resuspended in 100μl FACS buffer containing specific fluorescent or unlabeled primary antibodies or appropriate isotype controls at concentrations specified in Table 2.2 and Table 2.3. The cell/antibody mix was incubated for 30 min on ice in the dark. 400μl of FACS buffer was added to the cells and the cells were spun at 300 g for 5 min. Cells were washed by resuspending in 500μl FACS buffer and spinning at 300 g for 5 min twice more. Cells were then immediately run on a CyAn ADP flow cytometer (Beckman Coulter). For larger sample numbers (≥12) a U bottom 96-well microtitre plate (Sterilin) was used and volumes adjusted accordingly.

Where possible, 5μl 7-Amino-Actinomycin D (7-AAD) (BD Pharmingen™) was added 10 min prior to flow cytometry acquisition to exclude nonviable cells. Cells positive for 7-AAD in FL3 (PE-Texas Red) were deemed nonviable and negated in further analysis.

2.17.2 Flow cytometry data acquisition and analysis

Cells labeled with fluorescent antibodies as in section 2.17.1 were run and on a CyAn ADP flow cytometer (Beckman Coulter) controlled by the Summit software (Beckman Coulter). Isotype control labeled samples, or unlabeled samples only where no isotype control antibodies were available, were used to set voltages and typically the threshold was set to 1.0%. Offline analysis of acquired flow cytometry data was carried out using the Summit software package (Beckman Coulter) and FlowJo.

2.18 Frozen sections

2.18.1 Frozen tissue sections

Human tissue was collected from the Yorkshire Cancer Research laboratories already frozen in Optimal Cutting Temperature (OCT) compound (Tissue-Tek). Mouse tissue from PC-3 tumours, LL/2 tumours and xenografts were removed from mice and a small piece of tissue, typically with a 2-D surface of approximately $5mm^2$, was removed using a scalpel and tweezers and placed in a disposable vinyl specimen mold (Cryomold, Tissue-Tek). The tissue sample was then completely covered with OCT compound and the Cryomold placed directly on dry ice until the OCT turned white indicating the sample was frozen. Frozen tissue samples in OCT were stored at -80°C until use. A cryostat (Leica Microsystems) was used to cut 10μm thick sections which were transferred to a polysine slide (VWR). The sections attached to polysine slides were allowed to air dry overnight and were stored at -20°C in a sealed slide box containing silica gel beads (Sigma-Aldrich) to absorb residual moisture.

2.18.2 Frozen collagen gel sections

Collagen gels and tissue containing GFP+ cells were fixed in 4% PFA for 30 min at room temperature. After rinsing in PBS, samples were placed in 15% sucrose solution in PBS at 4°C overnight. This was changed to a 30% sucrose solution for 4 hours after which the samples were embedded in OCT and placed on dry ice to freeze. Frozen sections of typically 10μm were cut immediately as in section 2.18.1 or samples embedded in OCT were stored at -80°C.

2.19 Immunohistochemistry of frozen tissue sections

Slides were prepared as in section 2.18. Slides were defrosted at room temperature for 30 min and tissue sections were fixed in ice cold acetone for 10 min. After being allowed to air dry the frozen sections were encircled using a hydrophobic Immedge pen (Fisher) and allowed to air dry again. Sections were rehydrated in PBS containing 0.05% BSA in slide baths for 15 min. Sections were then blocked in PBS containing 5% goat serum for 30 min at room temperature. Subsequently, sections were washed in PBS containing 0.05% BSA for 5 min. Primary antibodies were diluted in PBS containing 5% goat serum and added to the relevant sections and incubated at room temperature for 45 min in the dark. Sections were washed once quickly with PBS containing 0.05% BSA and then a further 3 times for 10 min each. If a secondary antibody step was required, secondary antibody was diluted to a suitable concentration in PBS containing 5% goat serum, added to the sections and incubated at room temperature for 30 min in the dark. Sections were then washed three times with PBS containing 0.05% BSA for 10 min each before a final wash in PBS only. Excess PBS was blotted away and slides were mounted using ProLong® Gold antifade reagent with DAPI (Molecular Probes) and a 22x50mm #1.5 coverslip (VWR). Slides were kept overnight at 4°C before being sealed with nail varnish. Frozen tissue sections labeled with fluorescent antibodies were imaged using a Zeiss LSM 710 inverted confocal microscope. A complete list of all primary and secondary antibodies used in this study is shown in table 2.2.

Table 2.2 Primary Antibodies

Specificity	Fluor	Clone	Company	Use
αCytokeratin, Pan	Pur	PCK-26	Sigma-Aldrich	IHC
αCytokeratin, Pan	488	AE1/AE3	eBioscience	IHC
αHu c-Met (HGFR)	FITC	eBioclone 97	eBioscience	FC
αHu CD106 (VCAM-1)	Biotin	1G11B1	AbCAM	FC, IHC
αHu CD106 (VCAM-1)	Pur	STA	eBioscience	FC, IHC
αHu CD133/1	Pur	AC133	Miltenyo Biotec	FC
αHu CD31	488	M89D3	BD Pharmingen	FC, IHC
αHu CD45	Pur	H130	eBioscience	FC, IHC
αHu CD54 (ICAM-1)	PE	HA58	eBioscience	FC, IHC
αHu CD54 (ICAM-1)	Pur.	HA58	eBioscience	FC, IHC
αHu Collagen I	Pur	721240	AbCAM	IHC, ICC
αHu Desmin	Pur	GR20599-1	AbCAM	IHC, ICC
αHu Fascin	Pur	609505	AbCAM	IHC, ICC
αHu Fibronectin	Pur	743700	AbCAM	IHC, ICC
αHu Integrin α5	488	eBioSAM-1	eBioscience	FC
αHu Laminin	Pur	047k4763	Sigma-Aldrich	FC, IHC
αHu SMA	Cy3	1A4	Sigma-Aldrich	FC, IHC
αHu SPARC	Pur	443481	AbCAM	FC, IHC, ICC
αMs CD106 (VCAM-1)	647	429	eBioscience	FC, IHC
αMs CD11c	Pur	N418	eBioscience	FC
αMs CD11c	APC	N418	BioLegend	FC
αMs CD3	FITC	390	eBioscience	FC
αMs CD45	APC	30-F11	eBioscience	FC, IHC
αMs CD45	Biotin	30-F11	eBioscience	FC
αMs CD45	APC	H130	eBioscience	FC
αMs CD54 (ICAM-1)	Pur	YN1/1.7.4	eBioscience	FC, IHC
αMs CD54 (ICAM-1)	647	YN1/1.7.4	BioLegend	FC, IHC
αMs EpCAM	PE-Cy7	G8.8	eBioscience	FC
αMs F4/80	647	BM8	BioLegend	FC
αMs GR1	PE	RB6-8C5	eBioscience	FC
αMs Podoplanin	488	eBio8.1.1	eBioscience	FC, IHC, ICC
αMs TCR-β	PE	H57-597	eBioscience	FC

Table 2.3 Secondary Antibodies

Specificity	Fluor	Company
GtαMs IgG H+L	488	Invitrogen
GtαMs IgG H+L	594	Invitrogen
GtαMs IgG H+L	647	Invitrogen
GtαRb IgG H+L	488	Invitrogen
GtαRb IgG H+L	594	Invitrogen
GtαRb IgG H+L	647	Invitrogen
GtαRt IgG H+L	488	Invitrogen
GtαRt IgG H+L	561	Invitrogen
GtαRt IgG H+L	594	Invitrogen
GtαRt IgG H+L	647	Invitrogen
Strepavidin	594	Invitrogen
Strepavidin	647	Invitrogen
Strepavidin	eFluor 450	eBioscience
Strepavidin	PB	Invitrogen
Strepavidin	PE-Cy7	eBioscience

2.20 Cell Cycle Analysis (DAPI)

Cells were collected via trypsinisation as in section 2.1.5 and were washed once in PBS and spun at 300 g for 5 min. 1×10^6 cells were resuspended in 150µl PBS and placed on ice. 400µl ice cold ethanol was then added whilst vortexing at low speed to ensure thorough mixing. Cells were spun at 200 g for 3 min in a microfuge and the ethanol/PBS removed. Cell pellets were resuspended in 500µl PBS containing 0.15% Triton-X-100 and 1µg/ml DAPI. Cells were kept on ice until being run on the flow cytometer. Cell cycle analysis was carried out offline using the Cell Cycle Analysis protocol within FlowJo.

2.21 Absolute cell counts by flow cytometry

A known number of cells were typically seeded in to 6-well plates in triplicate wells. At specific time points, cells were trypsinised, washed one with 1X PBS via centrifugation at 300 g for 5 min before being resuspended in 100µl PBS supplemented with 0.05% BSA. AccuCheck Counting Beads (Invitrogen) were thoroughly resuspended before 100µl of beads was added to the cell suspension. The mix was then analysed by flow cytometry. According to manufacturers instructions, a minimum of 1,000 bead events was required to obtain reliable values. For all experiments, a minimum of 30,000 bead events was collected.

Offline analysis was carried out and beads were gated upon according to size and their fluorescence in FL2 (PE channel). The two populations of beads (one fluorescent, one not) were confirmed as being at the correct ratio of 1:1 and the number of cell events was determined by gating on cell events according to FSC vs SSC plot. The absolute number of cells was determined by following the formula:

$$\frac{Number\ of\ cells\ counted}{Number\ of\ beads\ counted} \times Number\ of\ beads\ per\ \mu l$$

2.22 Agilent microarray

RNA was extracted from 8 stromal cell cultures as in section 2.11.1. RNA quality was assessed on an 2100 Bioanalyzer (Agilent) which produces an electropherogram to assess degradation. An RNA Integrity Number (RIN), based on the ratio between human ribosomal peaks, of 7-10 was deemed of

sufficient quality to be used in the microarray. RNA was amplified, Cy3 labeled and hybridised with an Agilent Sure Print G3 Hmn GE 8x60k Microarry chip (Agilent Technologies, cat no G4851A) according to manufacturers instructions. Raw data was generated by running the .tif files generated through Agilent's Feature Extraction software. Further analysis was carried out using Microsoft Excel, R or TreeView (Java).

2.23 Mice

C57BL/6, *Rag*$^{-/-}$, *Rag*$^{-/-}$*Gc*$^{-/-}$, *RORγt*$^{-/-}$, *Wnt1-Cre; R26R*^{YFP} and IL-4-GFP reporter mice were obtained from the Biological Services Facility (BSF) at University of York (UoY). All mice were maintained under specified pathogen free conditions at the UoY. All animal care and experimental procedures were carried out in accordance with United Kingdom Home Office requirements and performed with local ethical approval.

2.24 Statistics

All data were tested for normality using a Kolmogorov-Smirnov test. Percentage datasets were arcsine transformed for use in analyses. Paired or unpaired *t* tests were carried out on data fitting Gaussian distributions and Mann-Whitney on non-Gaussian distributed data, where comparisons were being made between 2 datasets. For multiple datasets of 3 or more, ANOVA was used followed by a Tukey's post-hoc text. Data was analysed in Graphpad Prism and SPSS.

Chapter 3

The Role of Tumour Stroma in PC-3

Migration *in vitro* in 3-D

3.1 Introduction

3.1.1 PC-3 Human Prostate Cancer Cell Line

The human prostatic carcinoma cell line PC-3 has been used extensively in cancer research for nearly 40 years. It originates from a human prostatic adenocarcinoma metastasis to the bone which, when cultured, showed anchorage-independent growth and had the capacity to generate subcutaneous tumours in nude mice (Kaighn et al. 1979). The three most commonly used human cell lines in prostate cancer research are PC-3, DU-145 and LNCaP.

These human prostatic cell lines have been functionally and phenotypically well characterised. PC-3s, along with all other human prostate cancer cell lines with the exception of LNCaP, were initially thought not to express androgen receptor (AR) and therefore to be non-responsive to androgens (Mitchell et al. 2000). Androgen irresponsive PC-3 cells have been used as negative control for AR (Chlenski et al. 2001) and were only responsive to Androgens when transfected with a full length functional AR, restoring AR expression to the level of LNCaP cells (Marchiani et al. 2010; Bonaccorsi et al. 2000). However, other groups have shown that PC-3 cells do express a low level of AR and therefore has implications on function and regulation within the cell in *in vitro* and *in vivo* assays (Alimirah et al. 2006). Whether PC-3s are responsive to androgens remains unclear, it is quite possible that there are multiple different PC-3 cells lines in existence, it is not uncommon for cell lines to become contaminated with other lines due to their rapid growth capacities. The PC-3 cell line was used in this study due to its basal

phenotype, putative stem-like compartment and the ability of PC-3 cells to form subcutaneous tumours in mice (S.-N. Tang et al. 2010).

3.1.2 Prostate Stroma and Tumour Stroma

Prostate stroma has an essential role in the development of the prostate gland. Communication between the epithelium and the stroma is multifactorial involving diverse factors including ECM deposition and remodeling, soluble cytokines, chemokines and growth factors all regulating the local microenvironment (Cunha 1994). Androgen signaling has a key role in the normal development and maintenance of the prostate throughout an individuals lifetime (Cunha et al. 1987). In the prostate; epithelial, endothelial and stromal cells, all express AR and are responsive to androgens (Y. Niu et al. 2008). One surprising exception are normal prostate stem cells and prostate cancer stem cells, which are defined by the expression of the β_1 integrin, CD133 and CD44 and are AR negative, thereby providing a pool of cancer cells driving castration-resistant (androgen independent) disease (Heer et al. 2007; Oldridge et al. 2011).

More recently the role of stroma in tumour progression has lead to a better understanding of the role of the larger tumour microenvironment in cancer progression leading to the idea of the tumour-stroma environment. To further understand the function of stroma in the prostate gene expression analysis of cancer-associated fibroblasts (CAFs) and normal prostate fibroblasts has been performed. Numerous proteins were identified that are differentially expressed in either source of fibroblast. Asporin (ASPN) and osteonectin (SPARC) were both associated with high expression throughout the stroma of tumours. Caveolin-1 (CAV-1) however was depleted in prostate CAFs, having previously been described in breast CAFs (Finak et al. 2008; Di Vizio et al. 2009), and predicts early tumour recurrence and poor outcome (Orr et al. 2011).

The tissue architecture of the prostate strongly suggests an interplay between the stromal compartment and the epithelium, with just a thin basement membrane separating the two cell populations (Maitland 2008). The epithelium is constantly exposed to strong signals from the stroma, including basic fibroblast growth factors (bFGF), transforming growth factor beta

(TGFβ) and other growth factors such as insulin-like growth factor (IGF), platelet derived growth factor (PDGF) and epidermal growth factor (EGF) (Slater et al. 2000). This is not a one directional relationship, epithelial cells have a key role in shaping their own environment by signaling to stroma. In cancer the cell-stroma crosstalk is highly interactive (De Wever & Mareel 2003). These pathways can drive the differentiation of fibroblasts to myofibroblasts or lead to the induction of EMT (Tuxhorn et al. 2002). Tumour associated stroma, often termed reactive stroma, can now release soluble factors, secrete ECM components and importantly increase motility and invasion of the cancer cells (Y.-N. Niu & Xia 2009). This was seen experimentally whereby CAFs were combined with non-tumourigenic epithelial cells which stimulated progression of tumourigenesis *in vivo* (Olumi et al. 1999).

Physiologically, stromal cells have been shown to have a key role in the very first step in the tumour metastasis process when the cancer cell escapes the local tissue microenvironment and invades the surrounding tissue. Invasive path generation by CAFs has been analysed which showed that LIM kinases are required for invasive path formation in matrigel through stimulating the ECM degradation by stromal cells (Scott et al. 2010). The paths created by the stromal fibroblasts in the matrigel form a track of minimal resistance which can then be utilised by following stroma and cancer cells in order to invade neighbouring tissues. This movement is collective and there is only one direction the cells can migrate which is the path of least resistance. This process might have some similarities to *in vivo* metastasis, however it is unclear whether this same process is functionally important.

In high Gleason grade tumours the basement membrane surrounding the epithelium is already disrupted and the stroma and epithelial cells occupy the same environmental space. Metastasis in prostate cancer is strongly associated with high grade aggressive tumours. This makes a strong case to include stromal cells as well as epithelial cells in an *in vitro* model when modeling the process of tumour cell migration. Thus models analysing molecular mechanisms of tumour cell behaviour in the absence of stroma will likely identify very different mechanisms to those that occur in the presence of stroma.

3.1.3 HT-1080 Fibrosarcoma Cell Line

The HT-1080 fibrosarcoma cell line was first isolated in 1974 (Rasheed et al. 1974). Since then, HT-1080s have been used as a model cell line to investigate tumour cell migration (Wolf et al. 2007), invasion (Armstrong et al. 1982), cell metabolism (Roomi et al. 2006), proliferation (Péterfia et al. 2012), tumour development (Yamauchi et al. 2012), and tumour metastasis (Mishima et al. 1998). Because HT-1080s can spontaneously migrate through 3-D collagen rich matrices, this cell line was used to set up the 3-D migration model in this thesis.

3.1.4 Extracellular Matrix

Whilst the ECM comprises many different components including fibronectin, elastin and laminin, is the most abundant structural protein is collagen. Collagens are the most abundant proteins found in animals with collagen I being the most abundant protein in the human (Di Lullo et al. 2002). The molecules that make up the ECM interact by various different mechanisms. This could be as simple entanglement or more substantial cross-linking and charge-dependent interactions (Wight & Potter-Perigo 2011). These now bioactive polymers can, in part, regulate the biomechanical properties of the tissue. The influence of the ECM on cell behaviour ranges from adhesion and survival, to proliferation and, most importantly for this chapter, cellular migration (McCarthy & Hay 1991).

Collagen comes in over 20 different types of fibrils with Type I, II and III being the most common. Stromal cells, and in particular myofibroblasts in reactive stroma, synthesize collagen I in high quantities (Lagacé et al. 1985) and collagen I is well studied as having a role specifically in cellular migration (Friedl et al. 1995; Sorokin 2010; McCarthy & Hay 1991; Wight & Potter-Perigo 2011; Gunzer et al. 2000). Collagen I has been used extensively as a 3-D matrix for *in vitro* studies due to it's physiological relevance and biophysical properties that permits formation of high tensile hydrogels (Friedl et al. 1998; Friedl et al. 1995; Ma et al. 1997; B. R. Williams et al. 1978). In this study, collagen I extracted from rat has been used as an *in vitro* ECM component to produce 3-D hydrogels. Telopeptides, the amino acid sequences at the N and C termini of the collagen polypeptide chain, were not confirmed to be present in these gels. However, the lack of pepsin digestion throughout the extraction protocol and the use of acetic acid to dissociate

collagen fibrils rather than digest them, would in all probability leave them intact. Telopeptides are needed to form higher-order collagen fibres from individual fibrils via the lysyl oxidase cross-linking of adjacent molecules (Woodley et al. 1991).

3.1.5 *In vitro* models of tumour metastasis

Many *in vitro* tumour models do not recapitulate the immediate cellular tumour microenvironment in 3-D. Migration assays are routinely carried out using invasion chambers during which a cell is counted as migratory based on its ability to cross an artificial porous membrane typically across a serum or chemotactic gradient. Not only does this not take in to account the inherent 2-D nature of the initial seeding, but the role of the ECM is difficult to model. In essence this type model system does not represent mechanisms guiding tumour cell migration within the complexity of the tumour microenvironment.

Matrigel™ is a commercial gelatinous protein mixture secreted by Engelbreth-Holm-Swam (EHS) mouse sarcoma cells, the exact constituency differs from batch to batch. Matrigel is rich in laminin, collagen IV, heparin sulfate proteoglycans and numerous growth factors, it crucially lacks a high collagen I content. To mimic the basement membrane in tumours a layer of Matrigel™ is put on top of the membrane in a similar chamber as described above. This assay has been used as an assay of invasive tumour potential, although it is a matter of debate the applicability of this model. One potential model is that cells settle and the migration through the membrane results from enzymatic digestion of the matrigel rather than an active migratory process. To improve the matrigel assay an inverse migration assay has been developed. Here cells settle on top of the matrigel and then through inverting the matrigel the cells begin at the bottom and have to actively invade from the bottom up (Scott et al. 2010). It is possible to mix collagen with Matrigel™ to create a scaffold that more accurately recreates the microenvironment seen by cells *in vivo* and thus enables enhanced cell survival and invasion (Dewitt et al. 2009). Fibrous collagen structures have been shown in these mixes through SEM imaging (Hooper et al. 2006).

3.1.6 Imaging

Multi-photon confocal microscopy permits long-term deep florescence imaging in 3-D environments with highly reduced phototoxicity permitting analysis of highly photosensitive specimens including developing mammalian embryos (Squirrell et al. 1999). Using 2-photon microscopy it is possible to image cells, at high-resolution, using fluorescent proteins and labels, additionally it is possible to image endogenous structural proteins through second-harmonic signal generation both *in vitro* and *in vivo* (Campagnola et al. 2002; Sahai et al. 2005). Collagen can be visualised via SHG and is a critical ECM component involved in many cellular processes. For particular interest to this thesis it is the reorganisation of collagen I at the tumour-stromal interface which can facilitate local invasion (Provenzano et al. 2006).

By using a 2-photon confocal microscope configured with a blacked out, temperature and gas controlled imaging chamber, it is possible to image cellular behaviour over long periods of time. This allows the tracking and quantification of single cell (tumour and stroma) movement, migration, morphology and interactions.

3.2   Summary and Aims of this chapter

3-D cell culture models more closely model the *in vivo* tumour environment than 2-D cell culture models. Whilst cell lines have been, and continue to be, a valued source of research data, it is important to factor in multiple different cell types and ECM found *in vivo*. Two-photon confocal imaging permits long term time lapse imaging of 3-D tumour models minimising cellular damage. By using the PC-3 cell line, coupled with primary human prostate tumour stroma, in a 3-D collagen rich matrix, this chapter aims to investigate the migration of PC-3 cells in the context of stromal cells. The specific role and influence of stroma in prostate cancer cell migration and metastasis is completely unknown. Therefore, the specific aims of this chapter are:

1)   To develop and utilise an *in vitro* 3-D model of the *in vivo* prostate tumour microenvironment.

2)   To investigate and determine the role of tumour stroma in prostate cancer cell migration in 3-D.

3)   To develop a high through put system for the screening of factors on 3-D cultures of stromal-epithelial cell spheroids.

3.3   Results

3.3.1   3-D *in vitro* model of *in vivo* type I collagen

Collagen I was extracted from rat's tail as in section 2.4.1 and the monomeric collagen concentration was ascertained by Bradford Assay and was found to be 6.5mg/ml. Dilutions using 0.02M acetic acid were made in the order of 90% (5.85mg/ml), 80% (5.2mg/ml), 70% (4.55mg/ml), 60% (3.9mg/ml), 50% (3.25mg/ml) and 40% (2.6mg/ml). HT-1080 GFP and HT-1080 tdTomato cells were combined in a 50:50 ratio and were seeded in to collagen at a density of 1.5×10^5 cells/ml. Once gelled at 15°C, the collagen was carefully overlaid with complete media and incubated at 37°C with 5% CO_2 overnight. The following day gels were imaged using 2-photon confocal microscopy as described in section 2.4.2.

Prior to imaging, the collagen gels at higher concentrations were much stiffer and more robust. Collagen gels at 5.85mg/ml were visually opaque and was much drier than the gels containing less collagen. The gel containing just 2.6mg/ml collagen was far more translucent, but had still gelled and remained intact after the addition of tissue culture media. Imaging of the gels (Figure 3.1) show in detail collagen fibres using second harmonic fluorescence of the collagen fibres. In the gels containing the higher concentrations of collagen (Figure 3.1 A,B) there was little to no evidence of significant collagen fibril formation. At collagen concentrations just either side of 4mg/ml (Figure 3.1 C,D) the gel consists of short thin fibrils with spaces opening up between the fibrils. At the lower concentrations of 3.25 and 2.6mg/ml (Figure 3.1 E,F) the collagen fibrils are distinct and relatively long with what appear to be large gaps between them. In Figure 3.1 (F) a cell in the centre of the image is shown protruding under a bundle of fibrils and through one of these spaces more reminiscent of what is observed *in vivo* (Weigelin et al. 2012). At higher magnification and with higher resolution imaging it is possible to observe the individual fibrils of the collagen gel revealing the highly complex heterogeneous interconnecting web of fibres (Figure 3.2 A). High magnification scanning electron microscopy (SEM) (Figure 3.2 B) shows how the individual fibres are in fact interconnecting and branching off from one another.

To model prostate cancer PC-3 cells were transfected with green fluorescent protein (GFP) and were seeded at 1.5 x 10^5 cells/ml into 3mg/ml collagen gels. After gelation at 15°C, the addition of complete HAMS-F12 media containing 7% FCS and an overnight incubation at 37°C with 5% CO_2 the gels were imaged by 2-photon confocal microscopy. PC-3 cells survive in the *in vitro* collagen environment and are observed spreading out in to the collagen matrix (Figure 3.2 C,D).

3.3.2   HT-1080 cells use the collagen fibrils as tracks on which to migrate

HT-1080 cells were introduced in to the optimised collagen gels (section 3.3.1). The gels were imaged every 20 minutes for 18 hours using 2-photon microscopy visualising the cells via GFP fluorescence and the collagen by SHG. Initial results from the time lapse imaging and observations of cell movement showed that HT-1080 cells spontaneously migrate through the collagen matrix. Using high resolution imaging and digital magnification of the image, it was possible to observe single cells attaching to, and then migrating along, single collagen fibrils (Figure 3.3 A-D). The same collagen gels containing HT-1080 cells that were imaged were then fixed and processed for transmission electron microscopy (TEM). Analysis of the images show that the collagen fibrils that make up the collagen gel at high magnification (Figure 3.3 E-G) including a single HT-1080 cell interacting with the matrix (Figure 3.3 F). It is possible to observe interactions between the cell membrane and the collagen fibrils in the ECM, perhaps specifying points of integrin interactions with the fibres.

Two-photon confocal imaging of HT-1080 containing collagen gels was performed in standard growth media and the velocity and displacement of individual cells was tracked using the software package Volocity (Improvision). A MMP inhibitor GM6001 which inhibits collagenase, was subsequently added to the growth media surrounding the collagen gels at a final concentration of 10μM and cells velocity and displacement quantified using 2-photon confocal microscopy. HT-1080 cells in the presence of the MMP inhibitor moved significantly further and faster than those in the control gels ($p<0.001$) (Figure3.3 H) consistent with MMPs having a complex role in the tumour environment as their activity inhibits tumour cell migration whilst having a role in breakdown of the basement membrane.

3.3.3 PC-3 cells do not migrate through *in vitro* collagen gels as single cells

PC-3 GFP and PC-3 tdTomato cells were seeded at a density of 1.5×10^5 cells/ml in 3mg/ml collagen and imaged using 2-photon confocal microscopy. Images were acquired across a 100µm Z depth every 30 min over 2 consecutive days. Cell tracking confirmed that PC-3 cells, unlike control HT-1080 cells did not migrate through collagen spontaneously (Figure 3.3). PC-3 cell filopodia are observed to extend into the matrix but not interact. PC-3 cells remained active and alive throughout the two days of imaging. To determine if this failure to migrate was a result of no chemotactic signal, PC-3 cells were seeded into collagen gels containing a gradient of FCS from 7% to 20%. Analysis showed no increase in cell migration as compared to cells with no FCS gradient (Figure 3.3 C).

Previously we have shown that the addition of the broad range MMP inhibitor, GM6001, increased the migration of HT-1080s through an *in vitro* collagen matrix. Therefore, a 3mg/ml collagen gel containing 1.5×10^5 PC-3 cells/ml was overlaid with complete HAMS-F12 media containing 7% FCS and 10µM GM6001. The addition of GM6001 had no effect inducing PC-3 cell migration or behaviour (Figure 3.3 C).

3.3.4 PC-3 cells form a network of interconnecting cells in matrigel

Matrigel™ contains many of the components that make up the ECM, but does not contain collagen I but is a commonly used ECM substrate in cancer research. Thus the effect of Matrigel™ on the migration of HT-1080 and PC-3 cells was determined. Cells transfected with either td-Tomato or GFP were mixed 50:50 and either seeded within a 1.5ml Matrigel™ gel or seeded on top of an already set layer of Matrigel™. Strikingly, both HT-1080s and PC-3s create ordered networks of interconnecting cells when seeded on top of Matrigel™ (Figure 3.4 A,C). At 16 hours after seeding, no evidence of invasion down in to the matrix is observed in the lateral views in (Figure 3.4 B,D). When seeded within the 3-D Matrigel™ matrix, cells appeared rounded with possible evidence of small apoptotic blebs throughout the gel (Figure 3.4 E). HT-1080 cells showed significant invasion down in to the matrix in the Z dimension after 6 days in culture on Matrigel (Figure 3.4 F). Invasion is seen as single cellular strands reaching up to 400µm down in to the matrix

perhaps as a result of leading cells digesting the matrix creating a path of least resistance for others to follow behind.

3.3.5 Co-culture of PC-3 Cells with tumour stroma reveals stromal cell migration and matrix destruction and remodeling

A significant component of the prostate gland, and prostatic disease including BPH and cancer, are stromal cells. Stroma isolated from biopsies of patients with different Gleason grade prostate cancers and BPH were cultured. To observe stromal cell behaviour and interactions with epithelial cells *in vitro*, tumour stromal cells were labeled with Cell Tracker green dye and mixed 50:50 with PC-3-tdTomato cells at a density of 1.5×10^5 cells/ml in a 3mg/ml collagen gel. Stromal cells actively migrate through the collagen matrix (Figure 3.5). Single cell tracking showed a significant difference between the migratory behaviour of the stromal cells and the static PC-3 cells in the same gel. Although difficult to quantify in static images, matrix destruction occurs, not through enzymatic degradation, but through the physical forces applied by the stromal cells attaching to the matrix and ripping it apart. What was a stable matrix that contained PC-3 or HT-1080 cells at the beginning of the time course becomes extremely dynamic, going through constant physical remodeling as a result of stromal cell migration. Stromal cells were observed to be attached to the collagen matrix to which they remain adhered as they move through the matrix thereby pulling and ripping the fibres from one another. Some PC-3 cell movement is observed at later time points, however this does not appear to be an active migratory process rather PC-3 cells are observed being pulled when attached to a moving fibre or stromal cell. Single cell tracking shows a degree of stromal cell displacement significantly higher than that of PC-3 cells as shown in Figure 3.5 (C).

3.3.6 PC-3 cells form tumour spheroids only when co-cultured with stroma

PC-3 cells alone do not form cohesive spheroids. The cells aggregate and form loose sheets at the base of the methylcellulose droplet. When handled carefully the cell aggregate can be transferred into collagen gels but when imaged using confocal microscopy gaps between cells were observed with a distinct lack of cell-cell contact (Figure 3.6 A). In contrast the same number of stromal cells form tight compact spheroids (Figure 3.6 B). PC-3 cells and

stromal cells were mixed at a ratio of 50:50 prior to resuspension in methylcellulose and subsequent spheroid formation. The result of mixing the two cell types together was the formation of spherical 3-D structures with an even distribution of each cell type (Figure 3.6 C). These spheroids were robust enough to be washed from the surface of the petri dish with PBS containing 10% FCS prewarmed to 37°C, were able to be handled and seeded singularly in to collagen gels by pipetting. Analysis of the spheroids by confocal microscopy showed no gaps between the different cell types (Figure 3.6 C).

3.3.7 PC-3 cells only migrate through collagen from spheroids when co-cultured with tumour stroma

We have previously found no evidence that PC-3 cells can migrate through a collagen matrix *in vitro* either as single cells, or as part of a multi-cell aggregate. Therefore, PC-3-tdTomato and PC-3-GFP cells were mixed 50:50 with tumour stromal cells (unlabeled) and formed in to spheroids. Once implanted in to collagen gels, the spheroids were cultured for 48 hours prior to imaging for a further 18hrs. Analysis of PC-3 only spheroids show a tight boundary between the cellular aggregate and the surrounding collagen matrix (Figure 3.7 A) with no evidence of PC-3 cell migration into the matrix, in contrast to spheroids with 50% tumour stromal cells (unlabeled) where there was clear migration of PC-3 cells in to the surrounding collagen matrix as shown in Figure 3.7 (B). To visualise stromal cells, CellTracker dyes (Invitrogen) were used to directly label primary tumour stromal cells (Figure 3.7 C,D) in green. Imaging stromal cells in stroma-epithelial spheroid revealed interactions between the green stromal cells and the collagen matrix as highlighted by the white arrows. These interactions take the form of adhesion and contraction bringing the collagen fibres into the centre of the spheroid. By 8 hours PC-3 cells (yellow arrow) and tumour stromal cells (blue arrow) are observed to enter the surrounding collagen matrix between the two spheroids. At the beginning of the imaging window, stromal and epithelial cells are evenly dispersed. Throughout the course of the experiment stromal cells rapidly occupied the centre of the spheroid with the effect of excluding PC-3 cells to the periphery. Stromal cells may have a strong preference to adhere to one another than PC-3 cells with the effect being spheroid contraction and possible epithelial cell exclusion from the spheroid's centre.

3.3.8 Development of a 24-well plate high throughput assay of stroma-PC-3 spheroids

To develop an assay that can be used for higher throughput experiments a 24-well format of the spheroid assay was developed. PEI coated collagen support rings were placed in the centre of the wells of a tissue culture treated 24-well plate (Corning) secured in place with a thin layer of vacuum grease. The plate was then cooled on ice for a minimum of 30 min. Monomeric collagen was neutralised on ice and 30µl was added to the centre of each ring within each of the 24-wells of the plate. Initial tests showed that the neutralised collagen in the ring remained liquid for at least 2 hours whilst the plate was kept on ice providing ample time to prepare and implant up to 48 spheroids (2 per well).

Spheroids were prepared and isolated by pipetting using a Gilson P2 PIPETMAN Classic fitted with a 10µl tip. Spheroids were then carefully implanted in to the centre of each gel. A second spheroid was then implanted close to the first leaving a gap of less than 1mm between the two. Once all 48 spheroids had been implanted in to the 24 collagen gels, the 24-well plate was placed at 15°C for a minimum of 1 hour or until the collagen gels had set. Each gel was overlaid with 1ml complete RPMI media supplemented with 10% FCS and placed at 37°C with 5% CO_2 for 2 hours. Each spheroid pair was imaged via epifluorescence and care was taken to note the position of each spheroid pair for each well to allow subsequent imaging at later time points. Typically images were retaken at 24 hours and 48 hours post implantation (Figure 3.8 A,B). The image analysis software package Fiji was used to quantify to the size of each spheroid, the circumference and the centroid position of each spheroid in X and Y. The 2-D extended focus fluorescent images were first converted to a binary image before quantification was carried out (Figure 3.8 C,D). Using these parameters it was possible to not only follow the growth of the spheroid in relation to an increasing area measurement, but also by using the position of the centroid it was possible to measure the movement of spheroid toward each other (Figure 3.8 E-G). Measurements revealed no centroid movement for spheroids containing solely PC-3 spheroids or for those containing PC-3 cells mixed with BPH stroma. Significant centroid movement was measured between spheroids containing tumour stroma with PC-3 cells indicating that tumour stroma is required in this model for cell migration (Figure 3.8 G).

3.4   Discussion

To understand the molecular mechanisms driving tumour metastasis we have developed a 3-D spheroid model that permits dissection of the role of stroma and epithelium in prostate cancer cell migration. To do this we have utilised collagen, a natural ECM protein, that we polymerised to form *in vitro* collagen matrices in which cells and spheroids were implanted. We selected collagen over the more commonly utilised Matrigel because of its links to physiological cell migration, its location in normal prostatic tissue and the tumour microenvironment. In contrast Matrigel is derived from mouse tumour cells, is not found in normal tissues, is difficult to manipulate due to its temperature sensitivity and has little secondary structure, thus no second harmonic signal generation (SHG) is observed for collagen fibres using 2-photon confocal microscopy. Collagen fibre SHG could not be observed when collagen I was mixed into Matrigel, thus there was no added value to using mixed gels.

Surprisingly, *in vitro* the metastatic PC-3 prostate tumour cell line did not migrate as single cells in collagen gels, even with the addition of an FCS gradient or a stromal cell monolayer beneath the matrix. Very rarely are cells found as single cells in mammalian biology thus cellular migration *in vivo* likely involves either clusters of cells or multiple cell types. In the context of tissues cells are in direct contact with one or more other cells of the same, or different, type as well as the surrounding ECM. Surprisingly the fibroscarcoma cell line HT-1080 did display single cell migration in a 3-D collagen matrix *in vitro*. This may result from the mesenchymal origins of this tumour type as mesenchymal cells show high capacity to migrate. There have been reports of stromal conditioned media inciting PC-3 migration, but this was done using the method of trans-well migration assays (Jacob et al. 1999). This is whereby cells are placed on to a membrane, sometimes coated with collagen, Matrigel or some other ECM component, beneath which is a chemo-attractant of some variety. Migration is deemed positive in these cases if the cell can pass through the pores and attach the opposite side of the membrane. In essence, going from being exposed to a 2-D environment, squeezing through a ~7μm pore and ending up on a second 2-D surface upside down. Some reports have shown migration of PC-3 cells in 3-D, however, on closer inspection of the methods the cells are layered in a

sandwich collagen gel. Cells are seeded on to a 2-D flat collagen gel and allowed to adhere before the addition of a second gel on top of the first (Packard et al. 2009). This exposes the cells to two 2-D surfaces rather than a true 3-D environment as in the model reported here.

Although initial work involved analysing cells distributed throughout collagen gels this is highly un-physiological. In the absence of cellular interactions single cells often go through apoptosis due to the lack of key survival factors from near neighbours through the active secretion of vascular endothelial growth factor (VEG-F) and fibroblast growth factor (FGF) (Korff & Augustin 1998). Some cells, such as the HT-1080 cell line, no longer depend on exogenous survival factors and can survive, grow and migrate within 3-D collagen environments (section 3.3.2.). HT-1080s not only migrate in the collagen gels but also lead to matrix degradation and manipulation. This behaviour is very similar to that observed for primary human tumour stromal cells, perhaps characteristic of fibroblastic cells. Although stroma will migrate in gels through interacting with the ECM, the addition of stromal cells was insufficient to induce the migration of PC-3s. This experiment is consistent with experiments using a stromal cell monolayer beneath the gel or stroma conditioned media, both of which failed to promote PC-3 migration. In combination these results would indicate that the presence of stromal cells in the vicinity of PC-3s, or components they may secrete, is not sufficient for PC-3 cell migration rather it must require direct cell-cell interactions between the epithelium and stroma as is observed in higher grade tumours *in vivo*.

PC-3 cells alone failed to form 3-D spheroids when seeded in methylcellulose, which is not unusual for epithelial cells unlike mesenchymal and endothelial cells, but they will form spheroidal structures over time when single cells are embedded in Matrigel (Härmä et al. 2010; Lang et al. 2001). This process takes 7-10 days with evidence of cell-cell contacts and tight junction formation, with the centre of the spheroid being necrotic containing cellular debris (Lang et al. 2001). Time-lapse imaging of PC-3 cell aggregates (the result of attempting to form spheroids in methylcellulose in this study) showed that cell-cell contact of PC-3 on PC-3 cells had no affect on the ability of the cells to migrate. Whilst the cells remain intact with no

signs of cell death and no sign of a necrotic core, there was no evidence of cell migration.

In contrast when PC-3 cells formed in to spheroids in conjunction with tumour stromal cells, PC-3 cells became migratory. Morphologically, mixed spheroids become highly compacted with tight cell-cell contacts. Time-lapse imaging of these spheroids showed that both cell types, the tumour stromal cells and the PC-3 cells, underwent active migration. This activity took the form of movement of the cells both within the spheroid and also invasion out in to the surrounding collagen matrix. By using SHG imaging of the collagen fibrils the interaction between stroma and surrounding matrix and the physical displacement of collagen are inconsistent with MMPs or matrix destruction having a role in prostate cancer cell migration.

PC-3 cells, when seeded as single cells in Matrigel, formed spheroids within seven to ten days. They then often underwent a spontaneous transformation towards an invasive phenotype after two weeks in culture (Härmä et al. 2010). This invasive morphology consisted of the extension of filopodia in to the surrounding matrix which we believe is inconsistent with migration and displacement and is dependent on an MMP dependent process. This is contrary to what we have observed whereby PC-3 cell migration is induced immediately upon co-culturing with primary human tumour stroma in 3-D spheroids. Thus we would speculate that MMP inhibitors might actually lead to stronger metastasis potential through enhancing the collagen network upon which stroma and epithelial cells in close contact can migrate, perhaps consistent with clinical failures of MMP inhibitors for the therapeutic treatment of cancer (Coussens et al. 2002; Pavlaki & Zucker 2003).

The difference in behaviour of PC-3 cells in Matrigel compared to collagen, mirrors that of HT-1080s. This albeit interesting and beautiful network of cells created on top of Matrigel is probably the result of Matrigel expulsion, and occurs when many different cell types are placed on top of matrigel including endothelial cells. Cells prefer to exclude Matrigel, the formation of hexagonal structures is the most thermodynamically stable conformation of cell networks. This would suggest that the material itself affects the cells similarly whereas before we have seen the two cell types behave differently in collagen. Due to the nature of handling Matrigel, the aims of this project

and the broad affect of Matrigel on different cell types, Matrigel was not used when characterising the molecular mechanisms of prostate cancer metastasis.

Through developing a 24-well plate assay we developed a higher content assay that we could use to screen for genes and signaling pathways that regulate tumour cell growth and migration in 3-D by using small molecule inhibitors and shRNAs. Using this setup will permit rapid analysis of stromal cell types, from genetically diverse individuals, different Gleason grades of the same tumour type, or stromal cells from a range of different types of tumours including breast, pancreas and melanoma. The technology also permits the assessment of different prostate cancer lines including LNCaP and DU145.

The application of 4-D 2-photon imaging has provided very high rich data sets on the behavior of different cell types. Although imaging using epifluorescence does not give the level of detail of 2-photon or confocal microscopy, using multiple times points allows the tracking of spheroid growth and some cell migration, and differences were beginning to emerge between spheroids containing different stroma. Further development is required to bring this technology to a commercially viable system, in particular standardising the distance between the tumour spheroids. This could be done utilising a number of methodologies, in particular forming collagen gels containing pits at regular intervals may lead to selective control of spheroid placement. The spheroids should settle out in these indentations and a second collagen gel could be overlaid on the first. Proper standardisation would then need to be carried out and experimental reproducibility confirmed.

3.5   Conclusions

PC-3 cells do not migrate as single cells through collagen, but do migrate once formed into spheroids when co-cultured with tumour stroma. This is consistent with prostate cancer cell migration being stroma dependent, mimicking the tumour environment found *in vivo*. Thus by analysing the gene expression of stroma and tumour epithelium may provide insight into the mechanisms regulating cancer cell migration.

Primary prostate stromal cells like the HT-1080 fibrosarcoma cells attach to and mechanically disrupt the collagen matrix. This was observed both when stromal cells were seeded singularly within the collagen gel and when in PC-3 tumour spheroids. Thus adhesion molecules, particularly integrins and associated signaling pathways are likely to have a key role in regulating stromal cell function and interactions between the ECM and cancerous epithelium.

Through setting up a growth, migration, and invasion assays *in vitro* using spheroids implanted into collagen I hydrogels we have provided a platform to investigate the properties and influences of stroma on cancer cell migration. Using this method, it is possible to generate 4-D analyses of the migration process utilising two-photon time-lapse imaging and subsequent single-cell tracking of individual cells. Through developing a high throughput system, generation of a genetic screen for pathways regulating the 3-D migration of prostate cancer cells has been permitted.
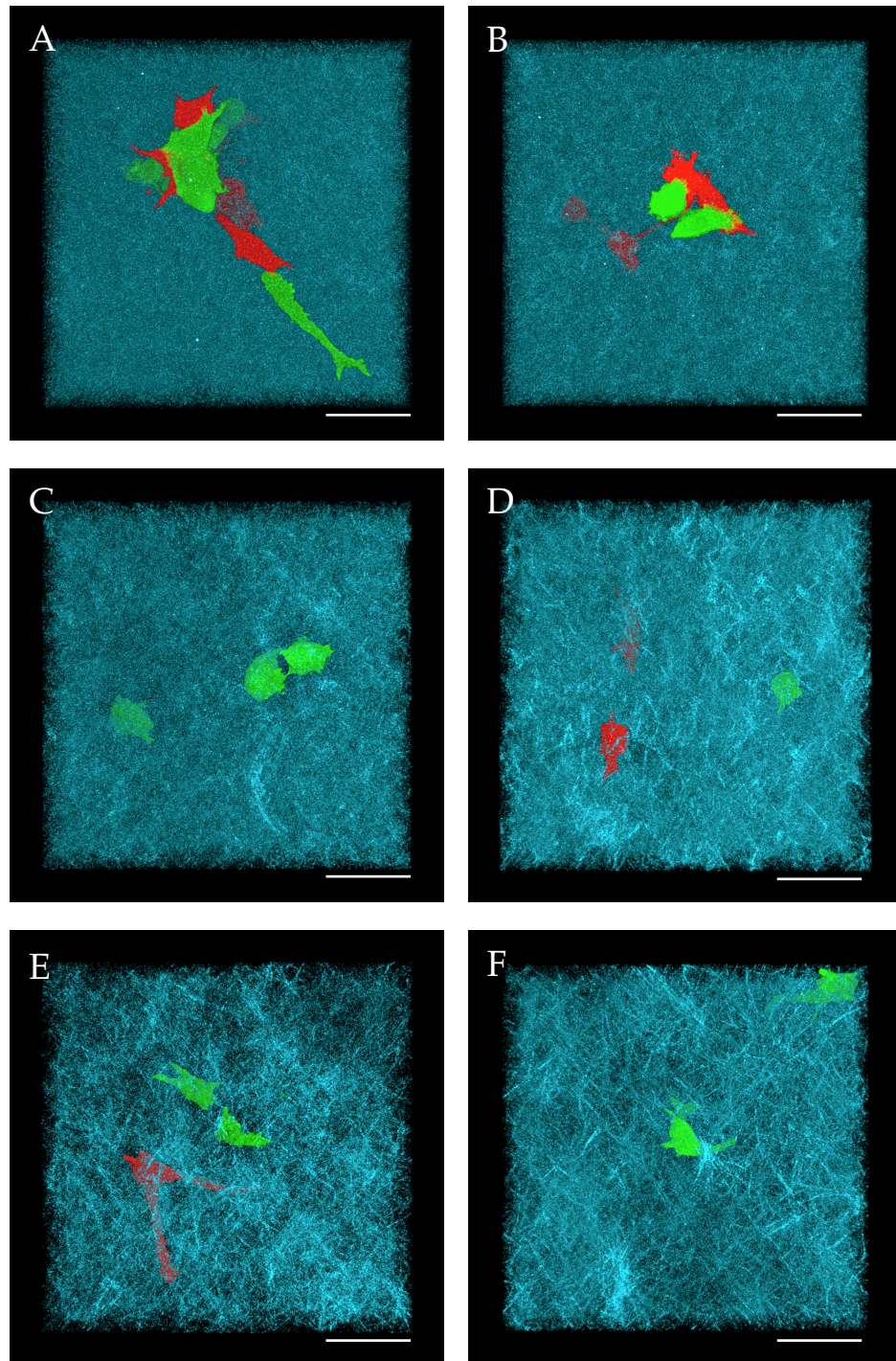
Figure 3.1 3-D reconstructions of HT-1080 GFP (green) and HT-1080 td-Tomato (red) cells cultured in 3-D collagen gels (blue) *in vitro*. From a stock concentration of 6.5mg/ml 6 gels of decreasing collagen concentration were made (A) 90%, 5.85mg/ml (B) 80%, 5.2mg/ml (C) 70%, 4.55mg/ml (D) 60%, 3.9mg/ml (E) 50%, 3.25mg/ml (F) 40%, 2.6mg/ml Bar: 20μm.
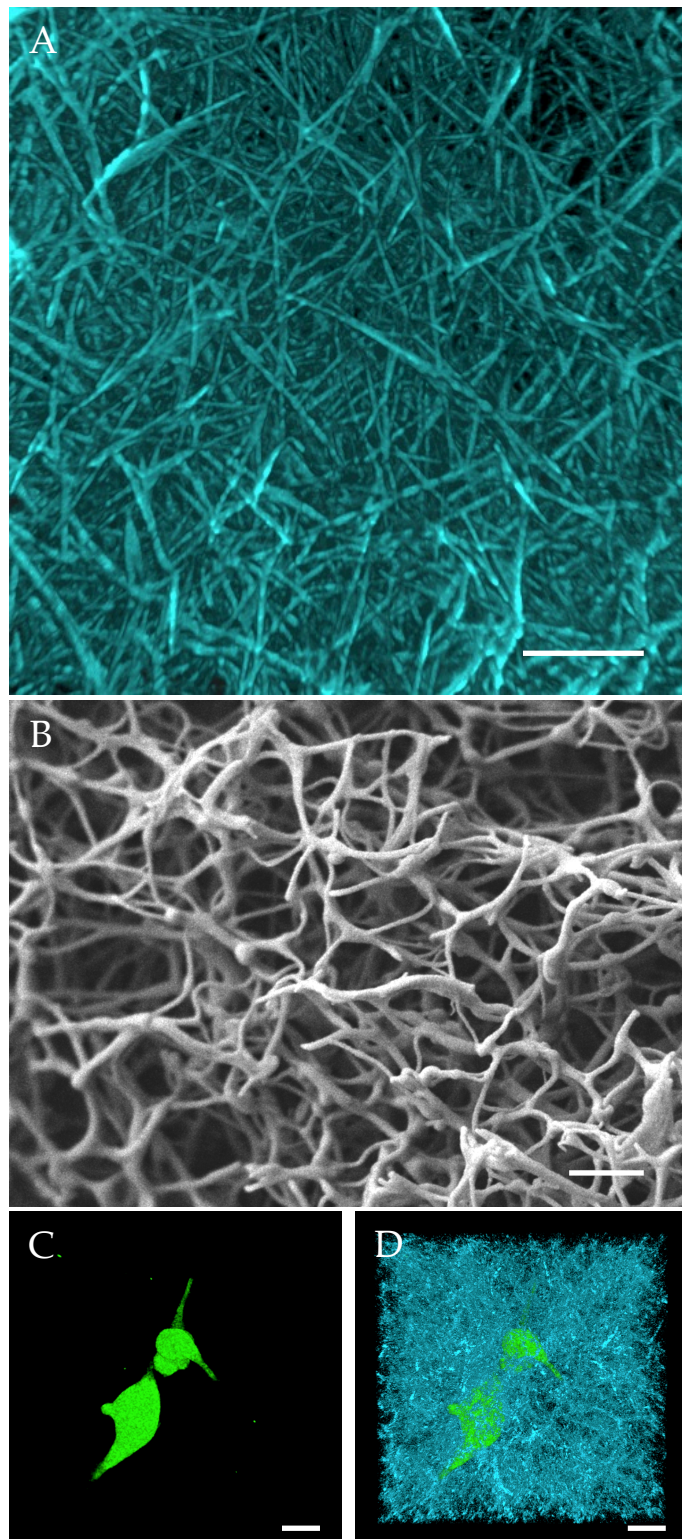
Figure 3.2 PC-3 cells survive in collagen. 3-D reconstruction of (A) 3mg/ml collagen alone set at 15°C and visualised at high-resolution by second harmonic generation of 2-photon microscopy. Collagen is false coloured cyan. Bar: 10μm (B) Fine collagen fibres as seen by scanning electron microscopy within a collagen gel set at 37°C. Bar: 2μm. Image courtesy of Amanda Barnes, Coles lab. (C) PC-3 cells expressing GFP spreading out in the same collagen gelled under the same gelling conditions as (A) 24 hours after cells were implanted with the collagen signal removed and (D) present (cyan). Bar: 10μm.
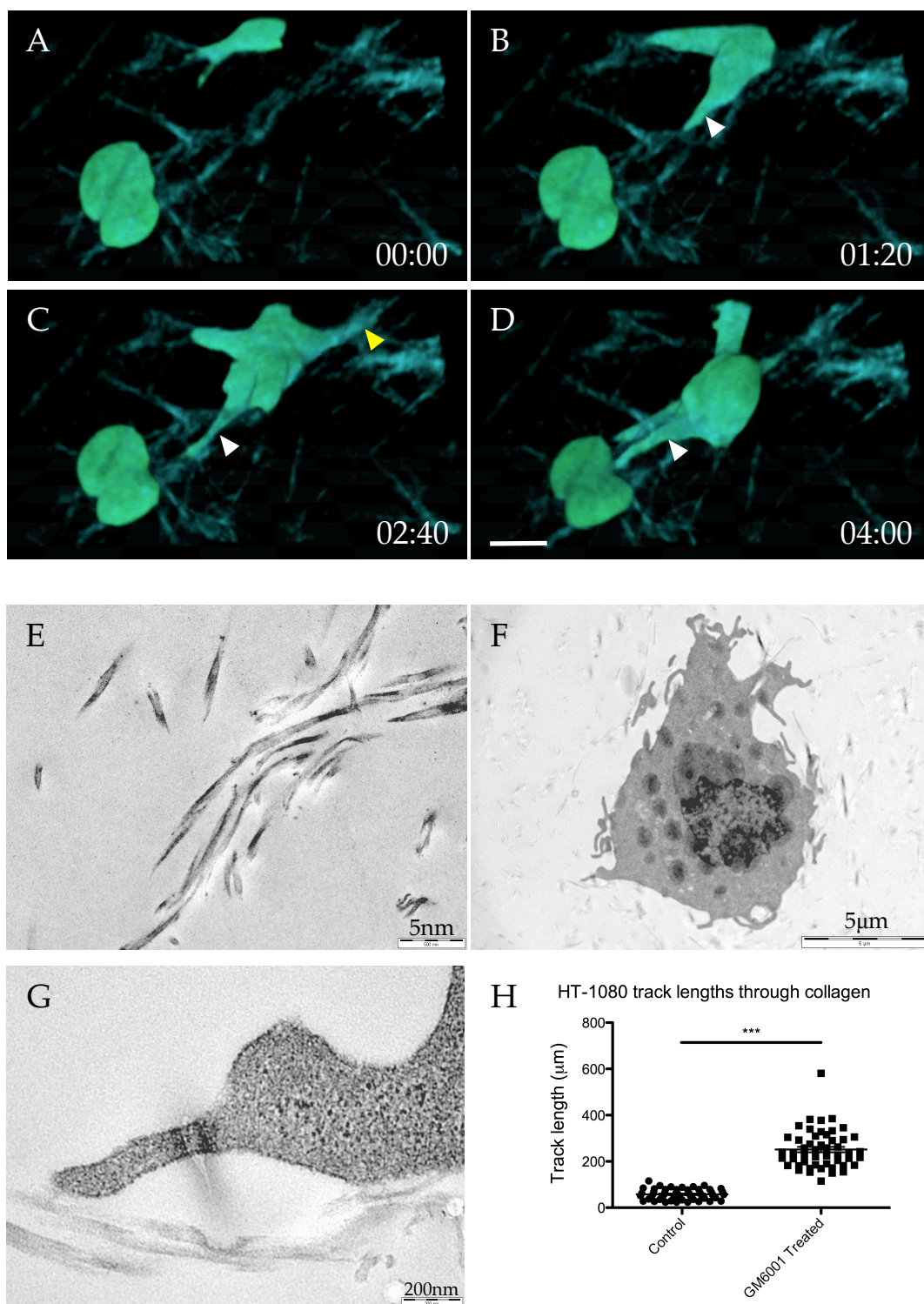
Figure 3.3 HT-1080s use collagen fibrils as tracks to migrate through the matrix. (A-D) still frames from time-lapse imaging showing a single HT-1080 cell (green) using a collagen fibril (cyan) to migrate along. The leading point of the cell (white arrow in B-D) attaches to the fibril, and drags itself along leaving a trailing point of the cell behind it (yellow arrow in C). (E-F) TEM images showing (E) collagen fibrils within the collagen gel, (F) a single HT-1080 cell embedded in the matrix and (G) a close-up of possible cell-collagen interactions on the cell periphery. (H) tracking of single HT-1080 cells showed that after the addition of a broad range MMP inhibitor GM6001, the cells migrated further. Bar represents mean±SEM, ***$p<0.0001$ (t test) (A-D) number represents time in hours (h) and minutes (m) (hh:mm) Scale bar in (D): 10μm
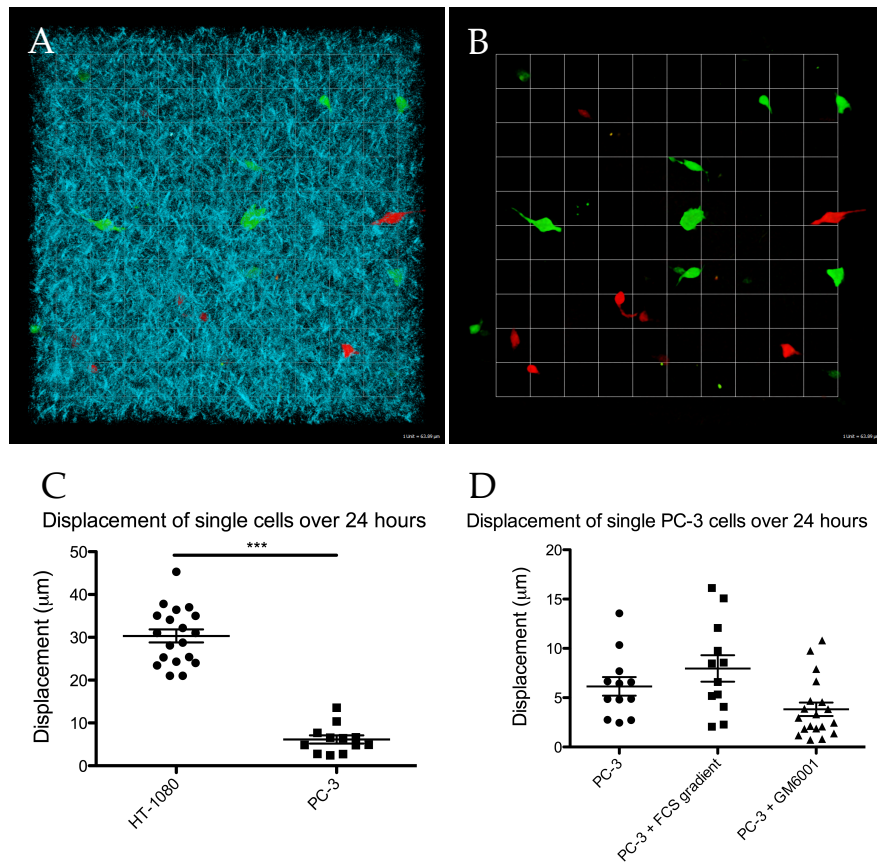
Figure 3.3 PC-3 cells do not migrate through *in vitro* collagen as single cells. (A) 2-photon microscopy image revealing the collagen gel fibres (cyan) and the even distribution of PC-3 GFP (green) and PC-3 tdTomato (red) cells throughout the gel. (B) The same image as (A) but the SHG signal of the collagen fibres has been removed. Both (A) and (B) are images at the start of a 48hour time-lapse. Scale unit: 63μm. (C) Quantification of single cell tracking displacement over 48 hours in collagen of migratory HT-1080 cells compared to PC-3 cells alone. Bar represents mean±SEM, ***p<0.0001 (t test) (D) tracking of PC-3 cells alone, PC-3 cells exposed to an FCS gradient, and PC-3 cells in the presence of the broad range MMP inhibitor GM6001. Bar represents mean±SEM, data not significantly different (two-way ANOVA)
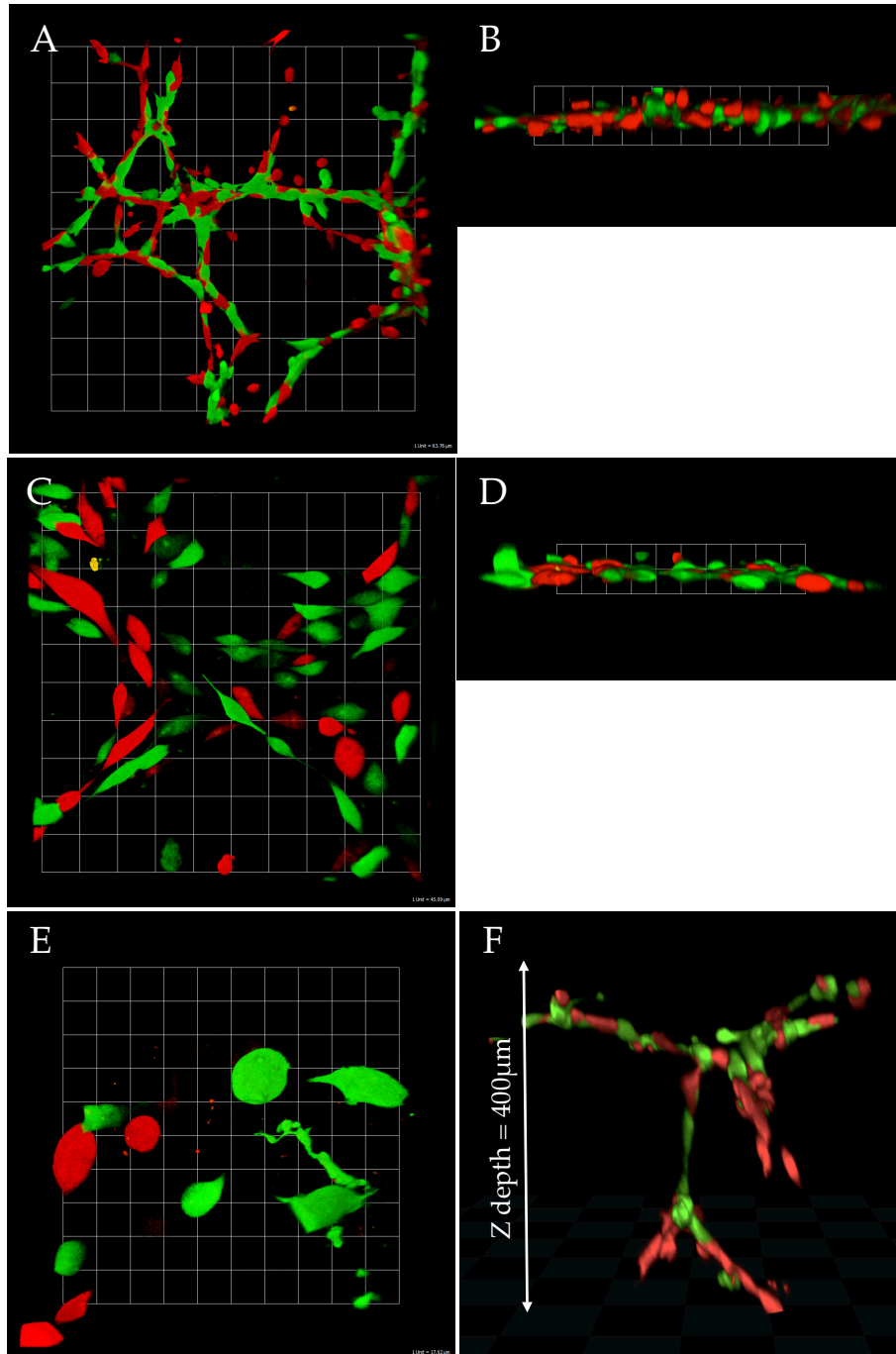
Figure 3.4 PC-3 cells form an interconnecting network of cells when seeded on top of Matrigel but round up in 3-D. (A) The fibrosarcoma cell line HT-1080 forms a highly organised interconnecting web of cells when seeded on top of Matrigel in 2-D. (B) At 24 hours there is no evidence of invasion as seen in this side-on view. (C&D) The same is true for PC-3 cells. (E) When seeded within Matrigel, PC-3 are observed as round, non-migratory cells. (F) Lateral view of HT-1080s invading in to the Z dimension up to 400μm after 6 days in culture. Scale units: (A&B) 83μm, (C&D) 45μm, (E) 18μm.
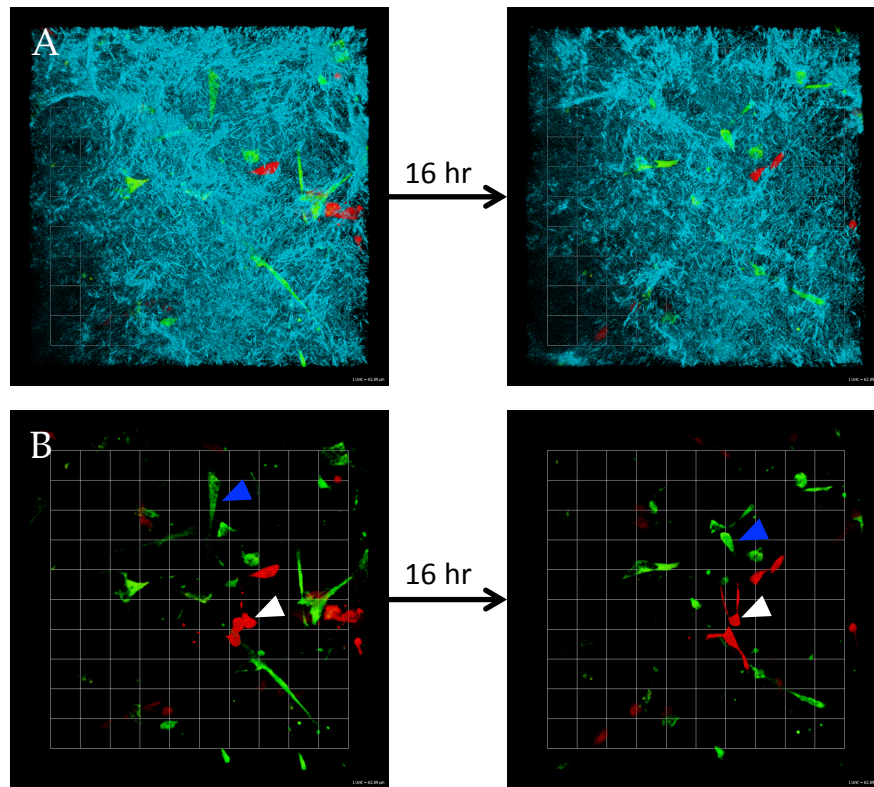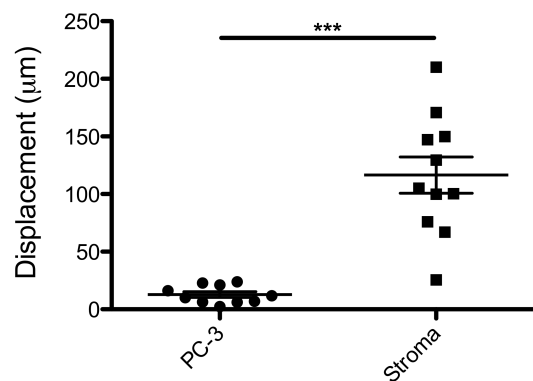
Figure 3.5 Tumour stromal cells interact with and migrate through the collagen matrix whereas PC-3 cell do not to the same extent. (A) Tumour stromal cells (green) and PC-3 tdTomato cells (red) were seeded as single cells in to a collagen gel and imaged over time. Scale unit: 63μm. (B) With the SHG signal of the collagen signal removed it is revealed that the green stromal cells are migrating through the matrix (blue arrow) whereas the red PC-3 cells are not (white arrow). Scale unit: 63μm. (C) Quantification of single cell tracking of both cell types. Bar represents mean±SEM, ***p<0.0001 (t test).
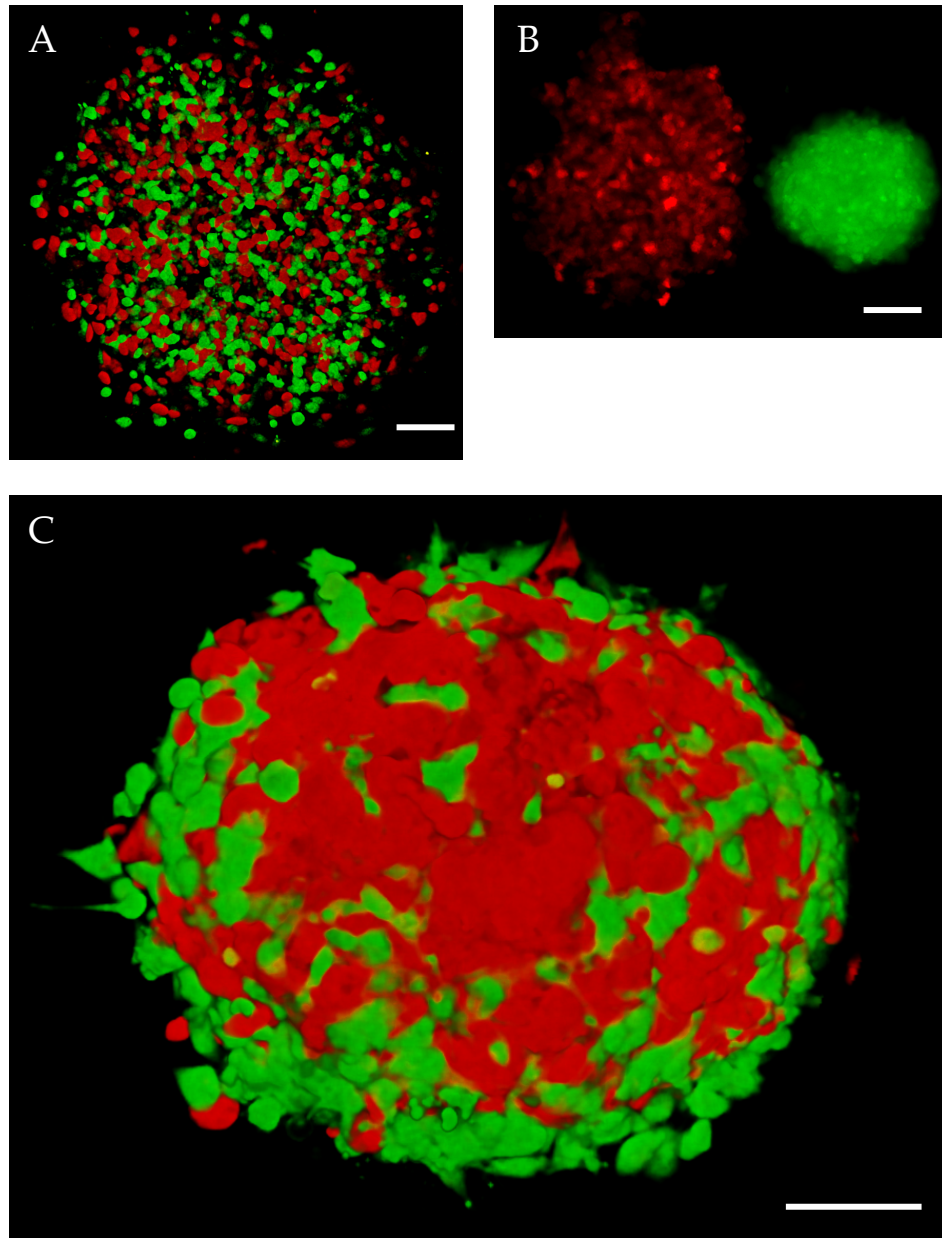
Figure 3.6 PC-3 cells form loose spheroids compared to spheroids formed by stromal cells alone or a 50:50 mix. (A) The result of an attempt to form spheroids from solely PC-3 cells. PC-3 GFP (green) and PC-3 tdTomato (red) form loose aggregates of cells as seen here by confocal microscopy. Bar: 150μm (B) Epifluorescence image of a PC-3 tdTomato only spheroid (red, left) in close proximity to a tumour stroma only spheroid (green, right) Bar: 100μm. (C) A compact spheroid consisting of PC-3 cells (green) mixed 50:50 with tumour stromal cells (red) approximately 2 hours after being implanted in to a collagen gel. Bar: 120μm
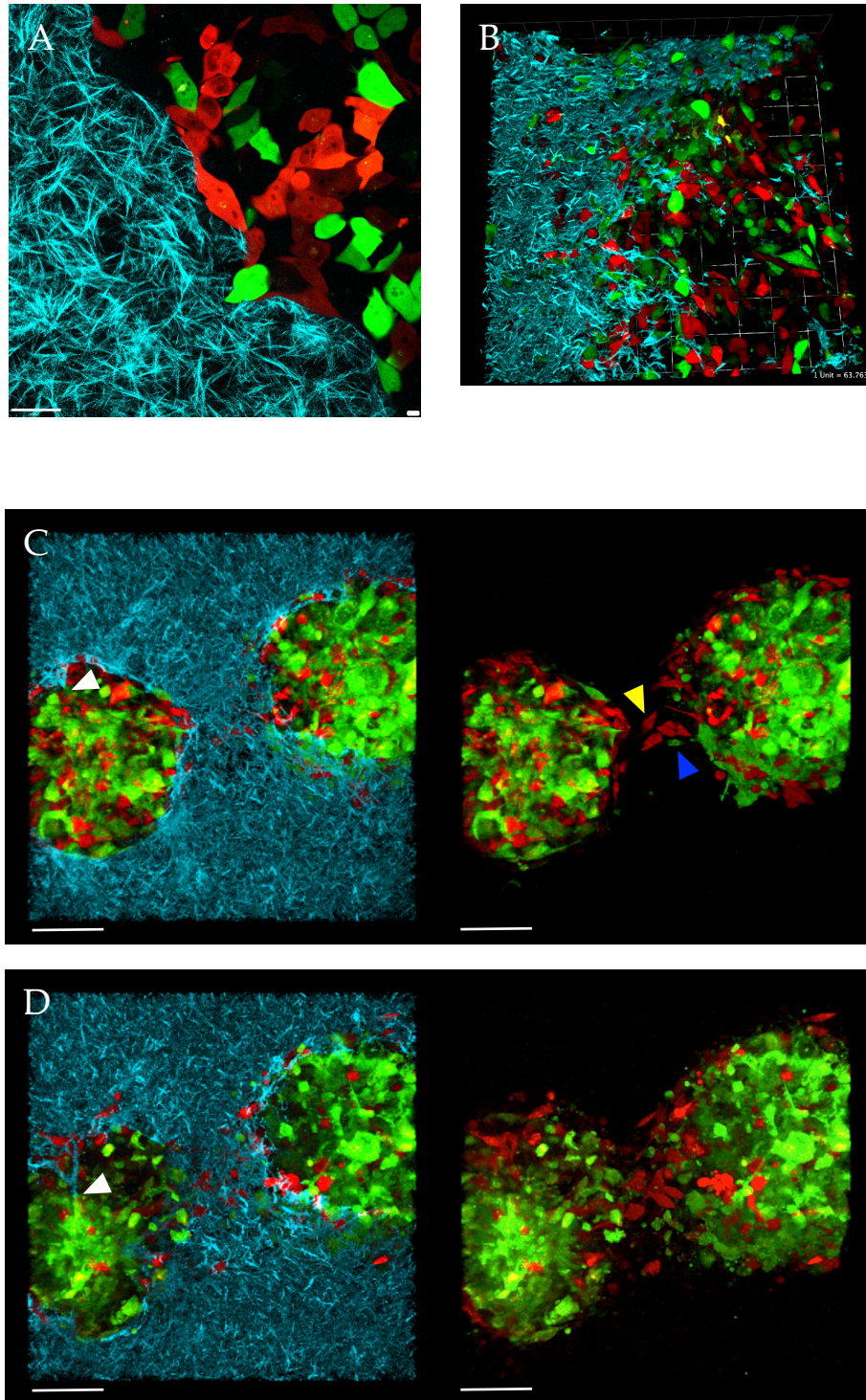
Figure 3.7 PC-3 cells only invade the collagen matrix in the presence of stroma. (A) A single Z-slice through the centre of a PC-3 only (red & green) spheroid showing the unbroken boundary between the cells and the collagen matrix. Bar:15μm (B) The same PC-3 cells (red & green) in spheroids with tumour stromal cell (unlabeled) clearly invading the matrix. Scale unit: 64μm. (C) Spheroids made from a 50:50 mix of PC-3 (red) and tumour stromal cells (green) promote cell migration between two spheroids and invasion in to the collagen matrix. Both PC-3 (yellow arrow) and stromal cells (blue arrow) exhibit this behaviour. Bar:100μm. (D) The same spheroid pair after 48 hours of time-lapse imaging reveals the extent of migration and interaction with the collagen fibrils in the matrix (white arrow). Bar:100μm.
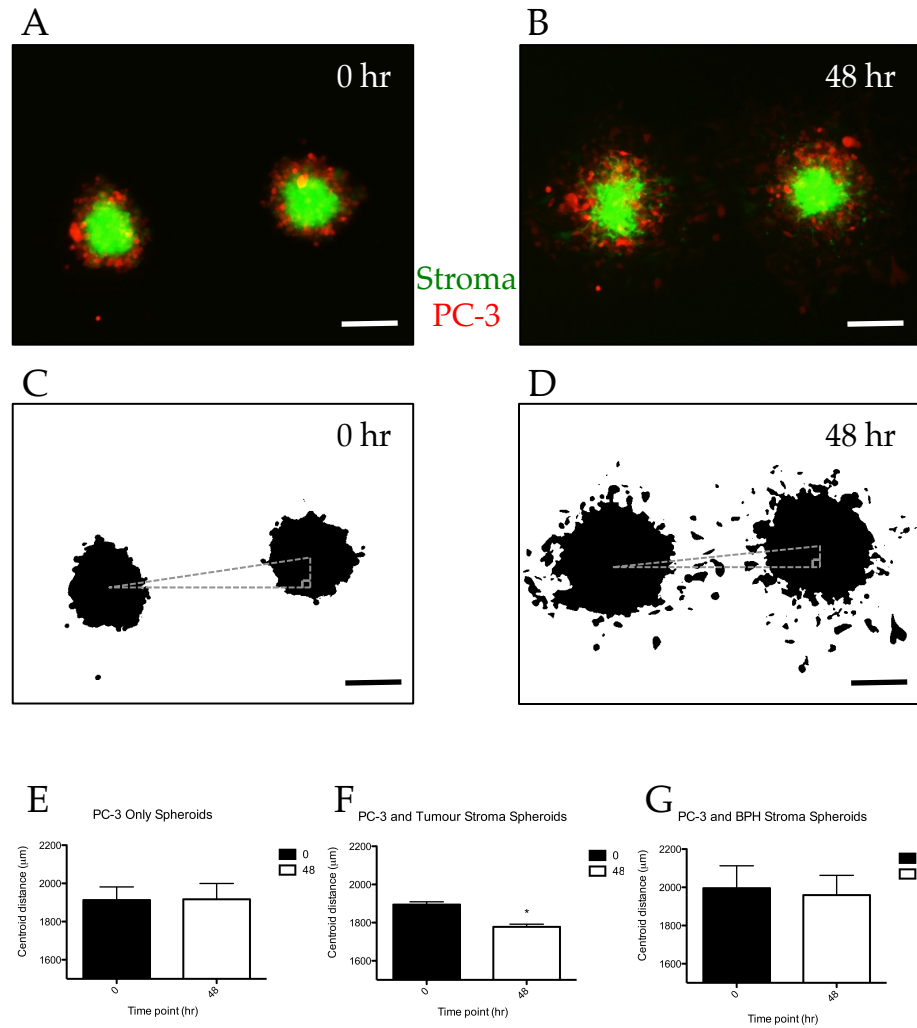
Figure 3.8 Representative results from the 24-well plate format of the spheroid growth, migration, and invasion assay. (A) Epifluorescence image of a pair of spheroids containing PC-3 cells (red) and tumour stromal cells (green) at the beginning of the experiment (0 hr). (B) The same two spheroids imaged 2 days later (48 hr). (C) Binary image of the fluorescent image in (A) in to order to analyse the spheroid area, perimeter, and centroid position. Dashed grey right-angled triangles depicts how the distance between the 2 centroids was calculated. (D) Binary image of (B). (E&F) Imaging data reveals that PC-3 only spheroids show no movement toward one another whereas spheroids containing both PC-3 and tumours stromal cell do. (G) When PC-3 cells are mixed together with BPH stroma in to spheroids, no migration is seen. Bar represent mean±SEM,*p<0.01 (paired t test)

Chapter 4

Investigation of the Molecular

Mechanisms of Stroma Induced

Migration

4.1   Introduction

4.1.1   Characterising stroma in tumours

The Gleason grading system is used to grade the severity and level of prostate cancer progression. Low grade tumours up to Gleason grade 4 have an increase in stromal content relative to normal prostate and an increase in the volume of stroma between the glands. However, there is no cancer cell infiltration into the stromal compartment. Above grade 4, glands lose the supporting stroma and cancer cells exclude and outgrow the stroma to form a continuous mass – the tumour (Yanagisawa et al. 2008). The cancer associated stroma surrounding the tumour mass continues to expand be it at a lower rate than the transformed epithelium. At higher disease grades the stroma-epithelial boundary is breached and cancer cells infiltrate the surrounding stroma, an event thought to be the first mechanistic step in tumour metastasis (Stark et al. 2009).

The interaction of the stroma with epithelial cells during prostate development is critical for both normal gland formation and for prostate cancer development (Cunha et al. 1987). Stromal derived growth factors, including those from the fibroblastic growth factor (FGF) protein family, have been shown to promote EMT and cancer progression during high grade cancer in mouse models (Abate-Shen & Shen 2007). Stromal FGF10 expression, and expression of other FGFs in prostate cancer, promotes androgen receptor (AR) up regulation through FGF receptor-1 (FGFR1)

signaling (Abate-Shen & Shen 2007). FGF10 is however only expressed at very low levels in human prostate cancer (Ropiquet et al. 2000) leading to the concept that other FGFs may signal through FGFR1 particularly FGF7 or FGF22.

The more pronounced the alteration to the prostate tumour microenvironment, including loss of smooth muscle cells, an increase in fibroblasts, myofibroblasts, and collagen deposition is directly associated with a poorer outcome (Yanagisawa et al. 2007). The tumour microenvironment is characterised by immune cell accumulation and infiltration including macrophages, lymphocytes and mast cells (Kärjä et al. 2005; Lissbrant et al. 2000; Fleischmann et al. 2009). This immune infiltrate has been observed to form highly organised tertiary lymphoid structures, the development of which is determined by cytokines such as lymphotoxin and TNF-α (Cupedo et al. 2004; Gräbner et al. 2009). The role of inflammation in the context of cell migration within tumours has not been investigated and in particular, the impact of inflammation on stromal mediated tumour cell migration is not well understood.

4.1.2   Tertiary lymphoid tissue

Tertiary lymphoid tissue (TLT) comprises tertiary lymphoid organs (TLOs). TLOs arise in ectopic areas (non-lymphoid sites) throughout the body at sites of chronic inflammation resulting from pathogenic infection, autoimmunity or tumour induced inflammation. These structures resemble secondary lymphoid organs, such as the lymph nodes, including such characteristics as organised B and T cell zones, follicular dendritic cells (FDC), fibroblastic reticular cells (FRC) and high endothelial vessels (HEV) in highly ordered structures (Shields et al. 2010). TLOs act to induce immune responses at the site of chronic inflammation by mediating efficient immune responses, whether TLOs lead to better or worse disease outcomes is unclear (Hjelmström 2001; Salomonsson et al. 2002). The high degree of organisation found within a TLO is dependent on activated lymphocytes being present (Cupedo et al. 2004). It was shown that TLO induction and organisation was dependent on Lymphotoxin (LT) and further cytokines including TNF-α have been proven to be required to organise lymphoid like architecture (Cupedo et al. 2004; Gräbner et al. 2009; Koning & Mebius 2012).

Stromal cells provide the structural basis for both secondary and tertiary lymphoid tissues through providing microenvironments where leukocytes can migrate and interact permitting development of high affinity adaptive immune response through the production of chemokines and cytokines. LN stroma contains HEVs, lymphatic endothelial cells (LECs) and mesenchymal cell networks (Koning & Mebius 2012). In lymph nodes these multiple distinct stromal cells are found in different zones. These include FRCs that support the T cells zone, marginal reticular cells (MRC) found in the subcapsular zone, B cell stroma and mature FDCs found in B cell follicles (Bajénoff et al. 2007). All of these cells are derived from localised mesenchymal progenitor cells. MRCs are characterised by the expression of the adhesion molecules VCAM-1 and ICAM-1 which are the first markers to be upregulated during lymphoid tissue formation initiated by lymphoid tissue inducer (LTi) cells (Cupedo et al. 2009). In a process involving LTβ receptor signaling mesenchymal precursor cells differentiate into mature lymphoid tissue organiser (LTo) cells which up-regulate VCAM-1, ICAM-1 and chemokine expression. Through selective recruitment and retention LTi cells accumulate in the nascent anlagen driving the development and maturation of the organ and ultimately give rise to MRCs found in adult lymph nodes (Vondenhoff et al. 2009). LN stromal cells can be identified by the differential expression of podoplanin, the endothelial receptor CD31 and do not express the haematopoietic marker CD45 (Koning & Mebius 2012). Non-haemaopoietic cells that express podoplanin (GP38 in mouse, GP36 in human) are either lymphatic endothelium or mesenchymal-derived stromal cells. Podoplanin is highly upregulated during inflammation and has since been used as a marker of activated stroma (Roozendaal & Mebius 2011; Link et al. 2007).

4.1.3   TLOs in cancer

TLOs have been reported in lung cancer (Dieu-Nosjean et al. 2008), breast cancer (Coronella-Wood & Hersh 2003), ovarian cancer (Milne et al. 2009), and colorectal cancer (Suzuki et al. 2002). TLOs have been shown to be adjacent to tumours and can act as a site of anti-tumour adaptive immune responses (Pagès et al. 2010). In human lung tumours associated TLOs consisting of mature DC and T cell clusters as well as B cell follicles were

highly predictive for patient survival. It has been speculated that tumour associated TLT derived memory cells migrate to the draining LN to develop a central memory response against micro-metastases, hence prolonged survival (Dieu-Nosjean et al. 2008). TLOs that display a highly organised structure, with distinct T and B cell zones, have also been shown in colon cancer mucosa. Links to patient survival have yet to be determined but the presence of these ectopic structures may either have a role in sustaining the inflammatory environment surrounding the tumour or might be appearing as a result of chronic inflammation (Bergomas et al. 2011). TLOs associated with cancerous tissues demonstrate that T and B lymphocytes are being recruited and activated by antigens in the context of the tumour microenvironment. Although TLOs likely promote an adaptive immune response, it is not fully understood how a tumour can use cancer associated immune structures, cells and cytokines to its advantage. This could be important in understanding how tumour cells migrate and ultimately metastasise from the primary tumour site and particularly why TLT might be both beneficial yet correlate with a poor prognosis in some advanced cancers.

4.1.4   Murine Lewis Lung Carcinoma cells (LL/2)

The Lewis Lung carcinoma cell line (LL/2) was established in 1980 and is used as a syngeneic model of tumour formation in C57BL/6 wild type mice (Zupi et al. 1980). The cell line is hypotetraploid, tumourigenic and can undergo metastasis *in vivo* and as such has become a very well established model of tumour formation and spread (Duś et al. 1985). LL/2 cells have been used to study therapeutic administration efficacy of chemotherapy agents (Lai et al. 2009; Pan et al. 2012), mecahnisms of tumour cell growth, migration, and invasion of surrounding tissues as well as cancer metastasis (Heinke et al. 2012; Sipos et al. 2012; Kaluza et al. 2011).

4.2   Summary and Aims of this Chapter

Changes occur in stromal organisation and function with increased disease progression resulting in changes to stroma-epithelial crosstalk. Thus both cell types have a key role in on-going changes to the cancer microenvironment. During tumour formation, stromal cells change from a permissive role to a more instructive role promoting epithelial cell proliferation, migration and invasion of surrounding tissues in higher grade tumours. Therefore the stroma has an essential role in the metastasis process. However, how tumour stroma can influence tumour cell metastasis and the mechanism by which this occurs, is unknown. It is also little understood how the immediate immune environment, often occupied by multiple TLOs can impact on long term patient survival and short term cancer cell behaviour. Therefore, by utilising the 3-D tumour spheroid model in combination with gene expression analysis, and flow cytometry with *in vivo* murine tumour models, the aims of this chapter are:

1)   To investigate the role of cancer associated stroma in prostate cancer cell migration.
2)   To determine a molecular mechanism for this migration.
3)   To investigate the impact of inflammation on the migratory capacity of prostate cancer stroma and tumour cells.
4)   To determine a possible role for innate lymphoid cells and TLOs in tumour growth.

4.3　Results

4.3.1　High Gleason Grade stroma and tumour cells disrupt prostate architecture

Primary human BPH and high Gleason grade cancer tissue samples were sectioned and stained with DAPI (nuclear), anti-pan-cytokeratin (epithelial) and anti-collagen I (stroma). In BPH the glandular epithelial cell architecture is adjacent but separate to the prostate stroma (Figure 4.1A&C). Higher magnification imaging (Figure 4.1 C) shows the boundary between the epithelial cells (red) and collagen I staining in the stromal zone (green) showing complete separation of the epithelium and stromal cell compartments. In contrast high Gleason grade tumour architecture is disrupted with no glandular structures (Figure 4.1B&D). In higher grade tumours the cancerous epithelial cells are intermingled in the same space as the stromal cells (Figure 4.1 D). The cancer cells are phenotypically less differentiated and have a more uniform round morphology, as opposed to the hierarchy of oblong epithelial cells found in the glands in BPH tissue sections.

4.3.2　High Gleason Grade stroma but not BPH stroma elicits PC-3 cell migration

Early passage stroma cultured from patients exhibiting high Gleason Grade prostate cancer was formed in to 3-D spheroids with PC-3 cells as previously described. The same process was carried out for early passage stroma from BPH cultures. Confocal images of spheroids taken at the assay end point for both spheroid sets shows a strong difference in how the cells have migrated (Figure 4.2 A&B). High Gleason stromal cells migrated out of the spheroid in to the surrounding collagen matrix whereas BPH stromal cells remain within the spheroid. Interestingly, the same pattern is observed with the PC-3 cells in the mixed spheroids. PC-3 cells in spheroids containing high Gleason grade stroma migrated out of the spheroid in association with the accompanying stroma. However, PC-3 cells which are formed in spheroids with BPH stroma show no evidence of outward migration. To quantify the migration process, single stromal cells and single PC-3 cells were tracked in 3-D for each spheroid over 48 hours (Figure 4.2 C&D). A clear difference is seen in the migration of both cell types between the two spheroid sets. A significant increase in cell displacement over 48 hours is shown for PC-3 and

stromal cells in high Gleason spheroids compared to those in BPH spheroids (Figure 4.2 E).

4.3.3 The migratory capacity of high Gleason Grade stroma is lost over time in culture

The identical Gleason grade 9 tumour stromal cells used in section 4.3.2 were passaged sequentially through culture. At each passage, spheroids were formed which contained PC-3 cells mixed with tumour stromal cells from that passage at a ratio of 1:1. Confocal imaging data (Figure 4.3 A) is shown from tumour stromal cell passages 1, 4, and 7. The results clearly show a drop in cell migration for both cell types despite PC-3 cells being otherwise insensitive to prolonged *in vitro* cell culture. Spheroid growth and spread as measured by 2-D surface area from extended focus images was significantly reduced as early as stromal passage 4 (Figure 4.3 B&C).

4.3.4 Gene expression analysis of stroma

Tumour stroma from several donors were individually cultured through multiple passages over time. At early passage, where possible as early as passage 1, mRNA was extracted from stromal cell pellets. mRNA was then extracted at each passage over six successive passages.

Stroma Source	Passage Number
BPH	Passage 3
BPH	Passage 10
Gleason 6	Passage 1
Gleason 6	Passage 6
Gleason 8	Passage 1
Gleason 8	Passage 6
Gleason 9	Passage 1
Gleason 9	Passage 6

RNA quality was assessed on a BioAnalyser and samples were amplified and then Cy-3 labeled and hybridised with an Agilent Sure Print G3 Human GE 8x60k Microarray Chip (cat no. G4851A, Agilent Technologies) and analysed through a fully integrated Agilent platform. Raw data was normalised using Agilent analysis software (GeneSpring) providing robust multichip average (RMA) normalization to allow for meaningful comparisons across samples.

Figure 4.4 (A) shows the order in which the samples were loaded on to the chip which correlates to a full expression profile map, with clustering, analysed using TreeView (Figure 4.4 B). All early passage samples, with the exception of BPH, cluster closely with the same sample at later passage. It is unknown why the two samples from BPH did not fall in together but could relate to differential etiological causes of the BPH. Figure 4.4 (C) shows the expression profile of genes involved in matrix remodeling, migration and cancer metastasis across the early passage sample for BPH, mid-range Gleason Grade 6 tumour stroma, and higher Gleason Grade 8 tumour stroma. Although, perhaps counter intuitively, some major ECM remodeling proteins such as MMP1 and MMP3 are down-regulated in higher Gleason grade stroma in this analysis, the adhesion molecules VCAM-1 and ICAM-1 are strongly upregulated.

4.3.5 Flow cytometric analysis of cancer tumour stroma reveals a possible role for adhesion molecules and podoplanin

Tumour stromal cells from different individual human cancers were analysed for podoplanin (GP36), ICAM-1 and VCAM-1 expression. As a comparator the PC-3 cell line was also analysed. Briefly, all cells were collected at early passage (except the immortalised PC-3 cell line) and were washed and stained with antibodies specific for podoplanin, ICAM-1, and VCAM-1 and analysed by flow cytometry (Figure 4.5 A). At early passage all tumour stroma samples expressed high levels of these proteins, with some sample to sample variation (Figure 4.5 B). This is markedly different from PC-3 cells which show no expression of these stromal antigens. A direct correlation similar to that seen in lymphoid stroma was found between the expression of VCAM-1 and ICAM-1 (Figure 4.5 C). Stromal cells that were used in the experiments in section 4.3.3 during which a decline in migratory capacity was observed over time in culture, were correspondingly down regulating podoplanin, VCAM-1 and ICAM-1 expression during passage (Figure 4.5 D). Expression of all three markers, particularly VCAM-1, were high at early passage (green line Figure 4.5 D) and were reduced to almost background levels by late passage (blue lines in Figure 4.5 D).

4.3.6 Human, but not mouse xenograft tumour stroma resembles tertiary lymphoid tissue stroma

VCAM-1, ICAM-1 and Podoplanin are all molecules that are strongly expressed on stroma in both secondary and tertiary lymphoid tissues (TLT) (Honda et al. 2001; Peduto et al. 2009). TLT develops in a variety of different tissues in chronic infection including tuberculosis and influenza (Roozendaal & Mebius 2011) and in autoimmune diseases including atherosclerosis, Sjrogen's syndrome and multiple sclerosis (Gräbner et al. 2009). The lymphoid-like stroma associated with some tumours has been observed to be very similar to that of tertiary lymphoid stroma including expression of chemokines and recruitment of immune cells (Shields et al. 2010). Therefore, to determine the possible role for different adaptive and innate immune cells in tumour stroma composition we have used a xenograft model by which primary human prostate cancer tissues are grafted in to $\gamma c^{-/-}$ RAG2$^{-/-}$ mice which have no mature B and T lymphocytes, NK cells, nuocytes and highly reduced numbers of RORγ^+ innate lymphoid cells (ILCs). Once the tumour was established (~38 days) the mice were sacrificed and the tumours were recovered. The tumour was digested and dissociated in to single cells and human leukocyte antigen (HLA) negative host derived mouse cells were characterised by flow cytometry. These cells included infiltrating immune cells, stromal fibroblasts and endothelial cells. The non-epithelial host cells were found to contain a significant immune infiltrate with F4/80$^+$ macrophages (23%), CD11c$^+$ dendritic cells (1.3%) and GR1$^+$ neutrophils (4.9%), making up the majority of host cells. HLA$^-$ CD45$^-$ presumed mesenchymal cells were gated on and analysed for the expression of podoplanin, CD31, VCAM-1 and ICAM-1 to investigate stroma composition with 9% of the cells being CD31$^+$ endothelial cells and 30% mesenchymal stroma (Figure 4.6 C).

The mouse stroma, in contrast to primary human Gleason grade 8 stroma, showed very low levels or no detectable podoplanin, VCAM-1 and ICAM-1 expression (Figure 4.6 A). However, there is still evidence that the tumour is exposed to an inflammatory environment with a large CD45$^+$ F4/80$^+$ macrophage (Figure 4.6 B), dendritic cell and neutrophil infiltrate. Thus lymphocyte derived cytokines have a key role in driving tumour stromal cell inflammation. It is therefore not unsurprising that this type of mouse model

rarely gives rise to metastases when using the prostate cancer cell lines like PC-3, thus the requirement to use either *in vitro* models of human stromal cell activation or the use of syngenic tumour models to understand the molecular and cellular events driving tumour stroma activation in vivo.

4.3.7 Inflammatory cytokines rescue a lost High Gleason Grade Tumour Phenotype in stromal cells

During prolonged periods in culture *in vitro*, we have shown that prostate stromal cells lose their capacity to induce and support prostate cancer epithelial cell migration. This correlated with a loss in expression of podoplanin, VCAM-1, and ICAM-1. Our analysis of xenograft models showed that a large tumour component comprised CD45$^+$ F4/80$^+$ macrophages indicating that the tumour was still a potentially highly inflammatory environment, but failed to generate reactive lymphoid stromal like gene expression in tumours, implicating a specific role for lymphoid specific cytokines.

To investigate the effect of inflammatory conditions on human prostate cancer associated stroma we used an inflammatory cytokine mix consisting of tumour necrosis factor-alpha (TNF-α), lymphotoxin-beta (LT-β) and interleukin-4 (IL-4) as these are key lymphoid cytokines that could be delivered by infiltrating B and T cells and/or innate lymphoid cells and have previously been shown in the laboratory to induce tertiary lymphoid stroma (unpublished). These cytokines were added to stromal cells, which had reached passage 6 in culture, for a period of 72 hours. The cells were then analysed for podoplanin, VCAM-1 and ICAM-1 expression by flow cytometry. All three markers were significantly up-regulated thus high passage stroma responds to the inflammatory cytokine cocktail to take on the expression pattern observed in primary non-cultured stroma (Figure 4.7) with a tight correlation between the expression of adhesion molecules post treatment (Figure 4.7 B). Quantification across three independent experiments showed a significant increase in all three markers (Figure 4.7 C).

4.3.8 Treatment of late passage tumour stroma with inflammatory cytokines rescues the migratory phenotype of early passage tumour stroma

TNF-α, LT-β and IL-4 treated stromal cells that had been previously through 6 passages in culture and untreated control stroma were then formed in to

separate spheroids with PC-3 cells. Single stromal cells and single PC-3 cells were tracked in a 3-D migration assay through collagen showing a major change in stromal cell behaviour (Figure 4.8). Treating the stroma with inflammatory cytokines induced the stromal cells to migrate, permitting the secondary migration of PC-3 cells. Importantly in this experimental setup, PC-3 cells had never been in direct contact with the inflammatory cytokine cocktail thus the induction of cellular migration was dependent on reactivated stroma.

4.3.9   Syngeneic model using Lewis Lung Carcinoma cell line LL/2

To determine *in vivo* which cell types were required to activate stroma the syngenic LL/2 tumour cells were subcutaneously injected in to wild type and gene knockout backgrounds. All mice were on the C57BL/6 mouse background ($H2^b$), $RAG2^{-/-}$ mice with no T & B cells, $\gamma c^{-/-}$ $RAG2^{-/-}$ mice deficient in B, T and NK cells and have very limited numbers of ILCs, and $ROR\gamma t^{-/-}$ mice that lack $ROR\gamma t$ ILCs, T helper (Th) 17 and Th22 cells. Tumours were excised three weeks post-injection, trimmed of hair, skin, and fat and were weighed and measured. The tumours taken from $\gamma c^{-/-}$ $RAG2^{-/-}$ mice were significantly larger than those from all three other strains. This was true of their weight and also volume (Figure 4.9). Thus it is likely that natural killer cells have an active role in reducing tumour cell volume. Tumours were dissociated into single cell suspension with collagenase/dispase and stained for CD45 and the epithelial cell adhesion molecule (EpCAM). Double negative cells were gated from the digested tumour stroma population (Figure 4.10 A) and the cells analysed for expression of podoplanin and CD31 (Figure 4.10 B). Podoplanin quantification shows significantly less expression in the tumour stroma originating from $\gamma c^{-/-}$ $RAG2^{-/-}$ and $RAG2^{-/-}$ mice compared to B6 controls directly implicating a key role for T and B lymphocyte derived signals and cytokines in tumour stroma activation (Figure 4.10 C). To determine if this was dependent on Th17 or Th22 lymphocytes, podoplanin expression was analysed in $ROR\gamma^{-/-}$ mice, however a large level of variation was found between the samples making it impossible to draw any statistical conclusions and so would have to be repeated. Similarly the coordinated expression of VCAM-1 and ICAM-1 on $Rag2^{-/-}$, $\gamma c^{-/-}Rag2^{-/-}$ and $ROR\gamma^{-/-}$ tumour stroma was significantly reduced compared to C57BL/6 wild type control mice

consistent with T lymphocytes having a key role in activating stromal cells in the tumour microenvironment (Figure 4.10 D&E).

4.3.10 Cancer stem cells migrate rapidly in tumour spheroids

To determine the behaviour of CSCs in the *in vitro* spheroid microenvironments, tumour cells were isolated from high Gleason tumours based on the CSC phenotype $CD44^+/\alpha_2\beta_1^{high}/CD133^+$ (Collins et al. 2005). From six, 6cm dishes, up to 3,000 tumour stem cells were recovered, and stained with CellTracker dye and added to the hanging drop culture containing primary prostate tumour stroma and PC-3 cells as previously described. Analysis of CSCs showed they were highly migratory within the spheroids (Figure 4.11) A single CSC, highlighted by a white box in Figure 4.11 is shown spreading across the surface of the right hand spheroid during the first 12-18 hours. The cell then migrates to the left hand spheroid before migrating out in to the collagen matrix. Once within the matrix, the cell stalls before going through cell division on the second day. One of the daughter cells then migrates back toward the spheroids whilst the second daughter cell remains stationary within the matrix outside of the spheroids, consistent with stem cells having high migratory capacity compared with more differentiated cancer cells. CSCs were confirmed to be tumour initiated in soft agar colony formation assays as well as in *in vivo* tumourigenicity experiments by YCR (data not shown).

4.4   Discussion

Higher Gleason grade tumour but not BPH stromal cells will actively migrate through a 3-D *in vitro* collagen matrix. PC-3 cells will only migrate from the spheroid through the matrix in the presence of tumour and not BPH stroma. BPH is not an invasive or metastatic disease and instead is a hyper proliferative disease in both the stromal and epithelial prostatic compartments (Maitland 2008). Little evidence exists for the collective or single cell migration in BPH and there is no evidence for epithelial metastasis or breakdown of glandular integrity (Chang et al. 2012). In prostate cancer, particularly high Gleason grade tumours, metastasis occurs to peripheral sites including the bone, lymph nodes, and lungs. In advanced prostate cancer metastasis is found in the liver and brain (1-2%)(Abdulghani et al. 2008). Stroma from high Gleason grade human prostate tumours have previously been shown to migrate *in vitro* in 2-D culture, as well as some early 3-D Matrigel models (Hall et al. 2002). Here, for the first time, we have shown that in a collagen I rich matrix, only early passage high Gleason grade tumour stroma can elicit the prostate cancer cell migration *in vitro*. This behaviour is lost over time in culture and is not evident at all for BPH stroma. Loss in cell migration correlated with a loss in podoplanin, VCAM-1 and ICAM-1 expression. Whereas the role for podoplanin in stromal mediated cell migration is unknown, cell migration via adhesion molecule dependent processes has been extensively studied in other systems including leukocyte migration.

Initial findings from gene expression analysis on different tumour grades and BPH stromal cells showed higher adhesion molecule expression in higher grade tumours. Further conformation of this expression profile was done using antibodies specific for VCAM-1, ICAM-1 and podoplanin, a very similar expression pattern to that found in TLT. TLOs in tumours should drive vigorous anti-tumour immune responses but surprisingly TLOs in cancer have been linked to poor prognosis, which is contrary to their potential to generate high affinity immune responses as is observed in autoimmune disease (Kuerten et al. 2012; Pezzolato et al. 2012). As TLO formation requires chronic inflammation and localised influx of lymphocytes for their development, this might signify the presence of an unproductive immune response in the tumour which is driving a hyper inflammatory

tumour micro-environment through pro-inflammatory cytokine expression which induces TNF-α, LTβ and IL-4. We showed that after exposure of cultured tumour stroma to these three cytokines, cancer stroma which had lost the capacity to migrate is now able to elicit PC-3 migration and regains its high Gleason phenotype found in primary isolated cells. The reactive prostate cancer associated stroma resulting from exposure to an inflammatory environment may be the catalyst for local invasion and subsequent metastasis by cancer cells into surrounding tissues including draining lymphatics leading to lymph node metastasis. This process may involve invasive path generation (Scott et al. 2010) whereby the reactive stroma invades the surrounding tissue and matrix creating a path of least resistance for the cancer cells to follow.

Reactive tumour stroma was not observed in the murine xenograft models. Stroma recovered from tumours greater than one month after the subcutaneous injection of PC-3 cells, do not express podoplanin, VCAM-1 or ICAM-1 expression. Although we did not conclusively show why reactive tumour stroma does not develop, the absence of the adaptive immune system and absence of ILCs and NK cells in the $\gamma c^{-/-}$ RAG2$^{-/-}$ mice will lead to a failure of TLT formation and a lack of TNF-α, LTβ or IL-4 receptor signaling will occur in the stromal progenitor cells. A large F4/80$^+$ macrophage infiltrate could potentially produce IL-4, however there is no evidence that they can drive expression of lymphoid stromal specific gene signatures in tumour stromal cells *in vivo*. Thus the model of PC-3s injected in to immune deficient mice is not a robust model of human metastatic disease. Although PC-3 cells show some metastatic potential these experiments are done by transferring the cells intravenously into mice, thus the first step in the metastasis process is bypassed. The inherent nature of subcutaneous injection of a large population of cancer cells bypasses the normal formation of tumour microenvironments in the prostate. But perhaps the lack of a reactive stromal environment has a key role in the lack of progression of disease in this model. Thus the requirement to utilise models of prostate cancer that arise spontaneously in mice.

Using a syngeneic model of LL/2 cell carcinoma which is not rejected by the immune system it is possible to study the mechanisms driving tumour

stroma induction. LL/2 is an extremely aggressive lung cancer cell line from C57BL/6 mice which rapidly forms solid tumours after subcutaneous injection in syngeneic mice. The LL/2 model has been successfully used by immunologists analysing stroma in tumours and there has been good evidence that it can generate a reactive stroma that has a role in immune responses (Kraman et al. 2010). We found that podoplanin, VCAM-1 and ICAM-1 were rapidly induced on tumour stroma, consistent with B and T cell mediated reactive stroma induction. The failure of reactive stroma formation in the absence of B & T lymphocytes is consistent with a unique role for the adaptive immune response in stromal cell activation. In the future it will be interesting to determine which T or B cell populations are responsible for generating reactive stroma through using B cell (Ighm$^{-/-}$), $\alpha\beta$ T cell (TCR$\alpha^{-/-}$), $\gamma\delta$ T cell (TCR$\delta^{-/-}$), Th17/22, CD4 (class II$^{-/-}$) or CD8 T cells (β2M$^{-/-}$) mice.

Podoplanin is expressed by stromal cells, specialised epithelial cells, some macrophages and on lymphatic vessels and the increase in the numbers of podoplanin positive vessels in a tumour occurs as a result of lymphangiogenesis. This is used as a diagnostic marker in some tumour types (Swartz & Lund 2012). However, reports are conflicting as to whether this predicts a poor outcome (Pula et al. 2011; Kitano et al. 2010) or a favourable outcome for patients with cancer (Yamanashi et al. 2009). Whilst podoplanin can be found at the leading edge of some tumours and is expressed on some tumour cells (Kato et al. 2005), we found no evidence for the expression of podoplanin by PC-3 cells. Therefore any interaction between podoplanin and its ligand CLEC-2, may have role in stromal mediated tumour metastasis rather than direct effects on transformed epithelial cells. CLEC-2 in the immune system is highly expressed by dendritic cells and platelets and potentially neutrophils. Podoplanin is rapidly up regulated on mesenchymal stroma in secondary lymphoid tissues during infection and podoplanin has previously been shown to be up-regulated by CAFs (Kitano et al. 2010). Invasive lung carcinoma was associated with podoplanin expressing CAFs whereas fibroblasts within noninvasive disease were all negative (Kawase et al. 2008). In prostate tumour stroma, we found a clear association with podoplanin expressing stroma and higher Gleason grade, which in turn is associated with highly

migratory stromal cell behaviour. The loss of migratory capacity through culture correlates strongly with loss of podoplanin expression consistent with a requirement for podoplanin or the podoplanin gene expression profile in tumour cell migration and likely arises from loss of the stimulatory background. In the future it will be interesting to determine if co-culture of lymphocytes with stroma is sufficient to maintain phenotype or whether this requires an antigen specific response. This, combined with the lowered adhesion molecule expression by the stroma could be part of a mechanism that contributes to the migration, invasion and metastasis of prostate cancer cells. At this stage it is not possible to draw definitive conclusions for the role of podoplanin in this model. Podoplanin expression by the transformed stroma in this model and the fact that this tumour stroma elicits PC-3 invasion of the matrix, could suggest a role for podoplanin in marking activated tumour stroma.

Intercellular adhesion molecule-1 (ICAM-1) and vascular adhesion molecule-1 (VCAM-1) are both adhesion molecules involved in integrin binding and cell migration. When ICAM-1 binds to integrins on leukocytes they become attached to the vascular endothelium resulting in migration in to the interstitial space (Springer 1994). VLA-4 expressed on leukocytes interacts with VCAM-1 to promote migration and cell-cell interactions. VCAM-1 is expressed on activated vascular endothelium (Cybulsky et al. 1991) and binds to VLA-4 which is expressed on the surface of leukocytes (Alon et al. 1995). The process of cancer development, invasion, and metastasis involves cell migration and thus it is likely that some of the mechanisms used by the immune system may have a key role in tumour cell migration and interactions. Recent reports have linked podoplanin with a novel partner CD44 (the major hyaluronan receptor) which together promote directional cell migration in an epithelial mouse model of squamous carcinoma (Martín-Villar et al. 2010). But evidence is still contradictory as to it's association in human cancers and the role of podoplanin in cancer associated stroma remains unknown (Pula et al. 2011; Kitano et al. 2010; Chuang et al. 2009). Together this might lead to a model of tumour migration where VCAM-1, ICAM-1 and podoplanin have a role in regulating metastasis.

Putative prostate cancer stem cells as defined by CD44$^+$/$\alpha_2\beta_1^{\text{high}}$/CD133$^+$ and isolated from primary culture showed significant migration in our primary culture model and active cell division. The high level of $\alpha_2\beta_1$ integrin, also known as VLA-2, expressed by CSCs permits direct binding of collagen and the use of the fibrils along which to migrate. A process seen used by HT-1080s migrating through the same collagen *in vitro* matrix. $\alpha_2\beta_1$ expression has already been shown to promote collagen binding and cell migration in other cell types such as Th17 cells migrating to sites of inflammation (Boisvert et al. 2010). This was a direct contrast to PC-3 cells and more mature prostate cancer cell lines that must migrate in a collagen I independent process as they lack the integrin expression profile required to interact with the ECM and thus migration must depend on cellular interactions with stroma.
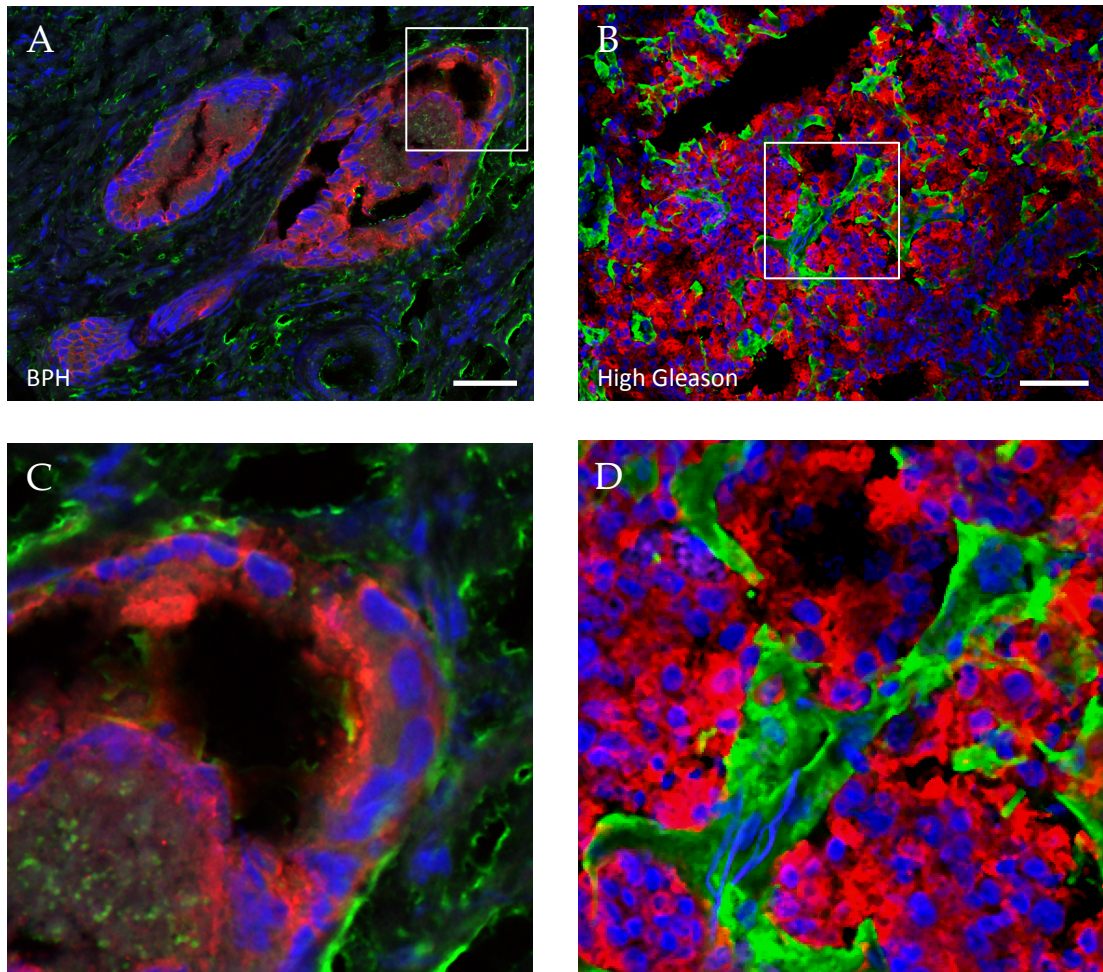
Figure 4.1 Normal prostate architecture is lost in high Gleason tumour tissue. (A) BPH tissue section stained for collagen I (green) to mark the stroma, pan-cytokeratin (red) to mark the epithelial cells, and DAPI (blue) for nuclei. The glandular structure of the tissue can clearly be seen. (B) Tumour tissue section stained with the same markers shows a loss of architecture, an overgrowth of epithelial cancer cells (red) and disorganised stroma (green). (C) zoomed image of (A) showing the clear boundary between the epithelia of the gland and the surrounding stroma. (D) zoomed in image of (B) highlighted the strong collagen I staining (green) of the stroma interspersed between the outgrowth of cancer cells (red). Bar: 50μm
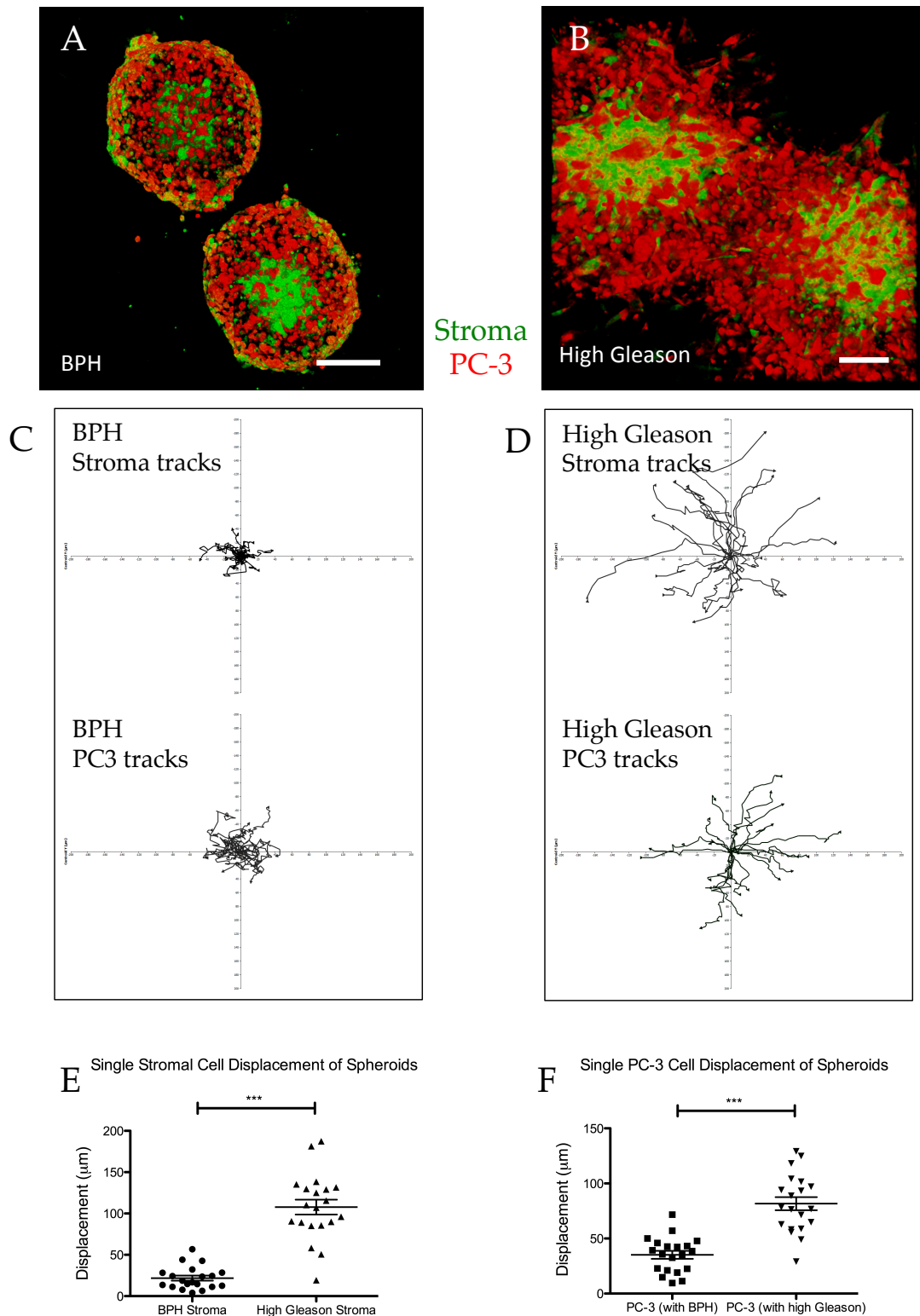
Figure 4.2 High Gleason stromal cells migrate further than BPH stroma and influence PC-3 migration in 3-D. (A) Pair of BPH stroma/PC-3 spheroids imaged after 48hr in 3-D culture in collagen. (B) second pair of spheroids containing tumour stroma. (C) quantification of BPH stromal and PC-3 cell migration over 48hr. (D) quantification of tumour stromal and PC-3 cell migration over 48hr. (E) Quantification of PC-3 cell displacement over 48 hours. (F) Quantification of single PC-3 cell displacement over 48hr. Bar: 71μm. Bar represents mean±SEM, ***p<0.0001 (t test)
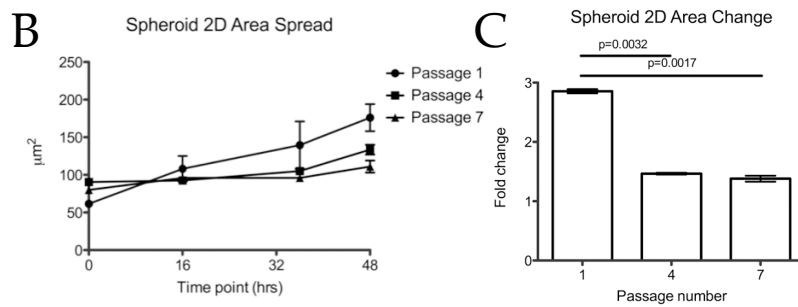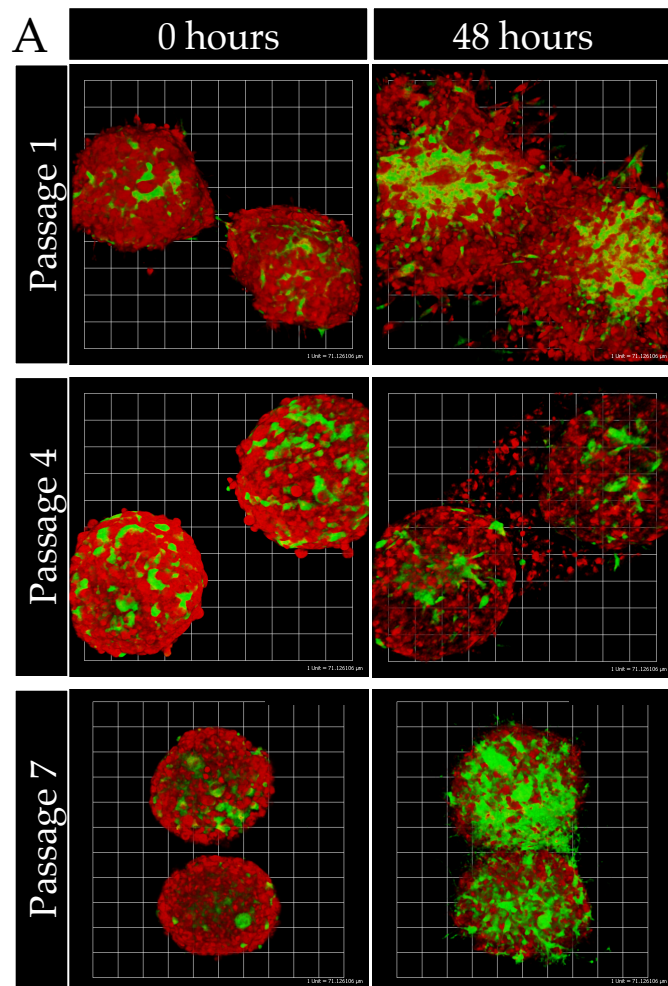
Figure 4.3 Migratory behaviour of stromal cells is lost over time in culture. (A) Comparison of spheroid growth and cell migration over 48 hours for spheroids containing PC-3 cells (red) and tumour stroma (green) at either passage 1, 4, or 7 over 48 hours. (B) 2-D spheroid area over time. (C) 2-D spheroid area change over 48 hours at different passage numbers. Scale unit for 3-D images: 71μm

Sample ID	Gleason Grade	Passage Number
1	6	1
2		6
3	8	1
4		6
5	BPH	3
6		10
7	9	1
8		6

A

B

3 4 5 1 2 6 7 8

C

Gene	BPH	Gleas 6	Gleas 8
MMP1			
MMP3			
MMP16			
MMP9			
PDPN			
MMP2			
MMP21			
MMP20			
IL4R			
MMP14			
MMP7			
MADCAM1			
MMP15			
SPARC			
MMP17			
MMP28			
MMP24			
CXCL12			
COL1A1			
MMP11			
VCAM1			
FN1			
ICAM1			

-3.0
-2.0
-1.0
0.0
1.0
2.0
3.0
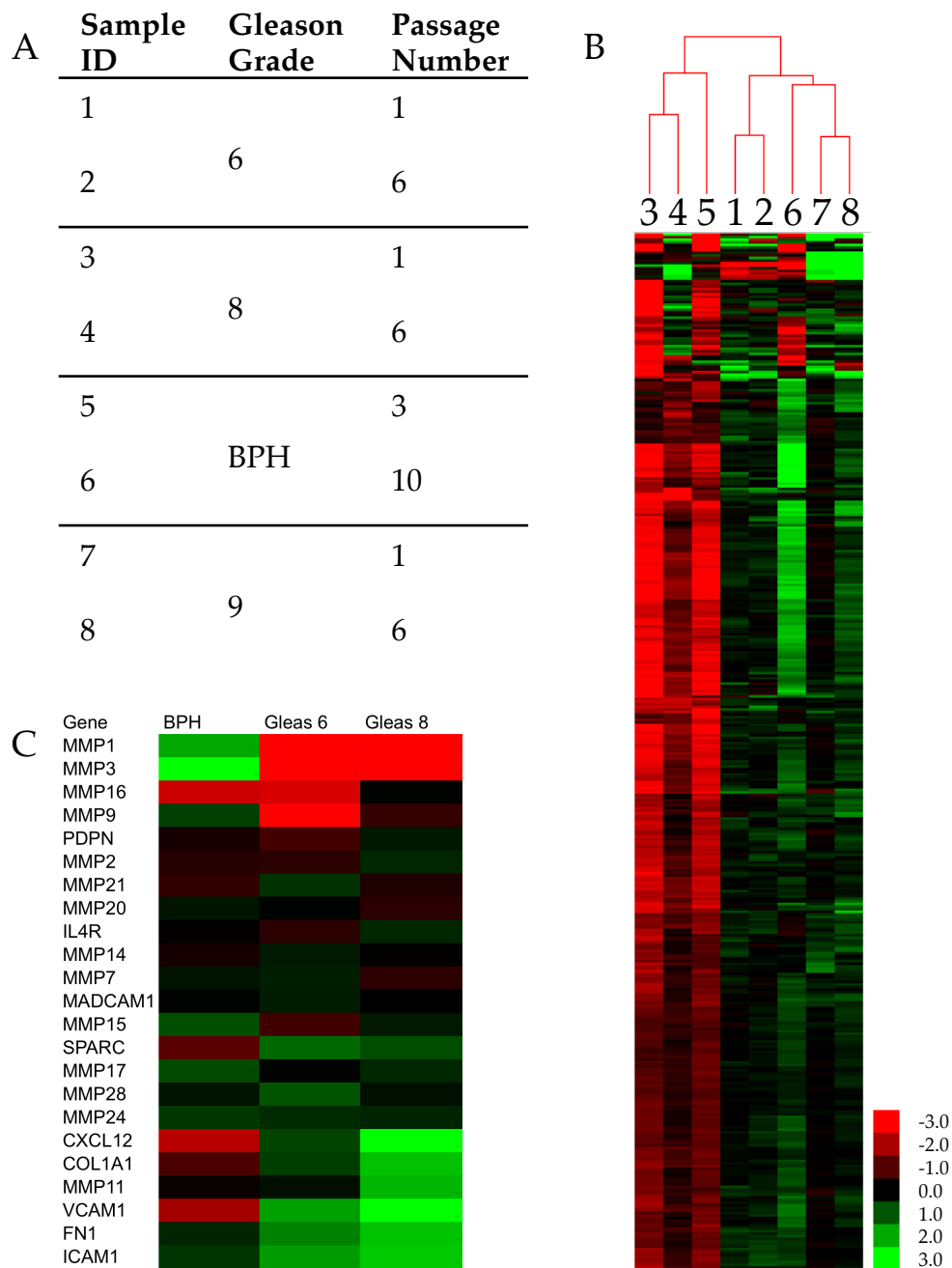
Figure 4.4 Gene expression analysis of a range of stromal cells over time in culture. (A) a table showing the collection of tumour stromal samples from Gleason 6, 8, and 9, and one from BPH ranging from early to late passage in culture. (B) Part of the full expression profile map, with clustering, analysed using Treeview. (C) a table of genes involved in matrix remodeling, migration and cancer metastasis showing the relative difference in expression between BPH, mid-range Gleason 6 and high Gleason 8.
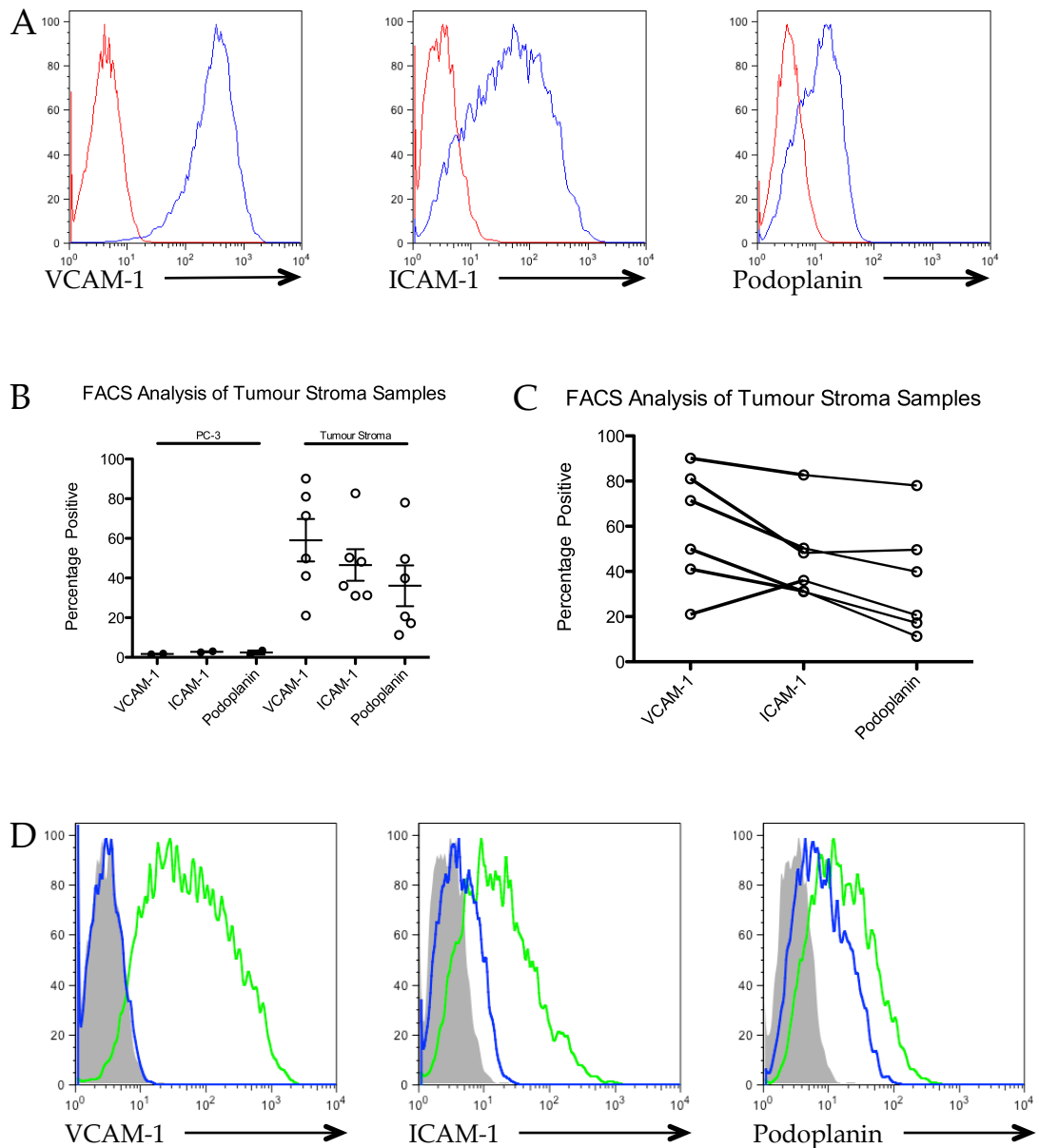
Figure 4.5 Prostate tumour stroma phenotypically resembles TLT. (A) Representative plot from one high Gleason tumour stroma sample showing the high level of VCAM-1, ICAM-1, and Podoplanin expression (blue line) against isotype controls (red line) (B) 6 tumour stroma samples were analysed and compared to the expression level of PC-3 cells which express very little of each marker. (C) a linked plot shows the potential link between the 3 proteins with high levels of VCAM-1 correlating with high levels of ICAM-1 and podoplanin. (D) Expression of VCAM-1, ICAM-1, and Podoplanin at passage 1 in culture (green line) compared to passage 6 in culture (blue line) against an isotype control (grey).
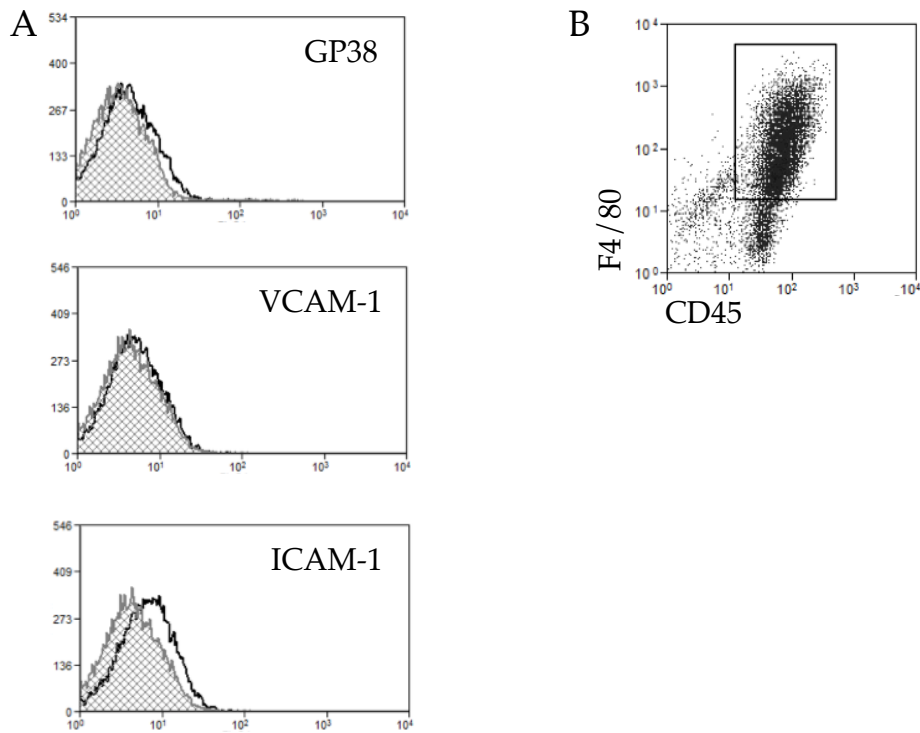
C Mouse tumour infiltrate.

Marker	Cell Type	Percentage	No. experiments
CD45+	Haematopoetic	45.4	5
CD31+	Endothelial	9	5
CD45- CD31-	Tumour Stroma	30	5

Haematopoetic cell analysis (CD45+).

Marker	Cell Type	Percentage	No. experiments
F4/80	Macrophages	51.5	4
CD11c	Dendritic Cells	3.15	2
GR1	Neutrophils	10.95	2

Analysis of tumour stroma (HLA- CD45- CD31-).

Marker	Cell Type	Percentage	No. experiments
VCAM	Vasculare Cell Adhesion Molecule	0	2
ICAM	Inter Cellular Adhesion Molecule	5.3	2

Figure 4.6 Analysis of mouse infiltrate in to human xenograft models. (A) representative plots of the expression of podoplanin (GP38), VCAM-1, and ICAM-1. Cells gated on CD45- CD31- expression. (B) The majority of CD45+ cells are F4/80+ as shown here. (C) Analysis of total mouse infiltrate, the hematopoietic population and tumour stroma.
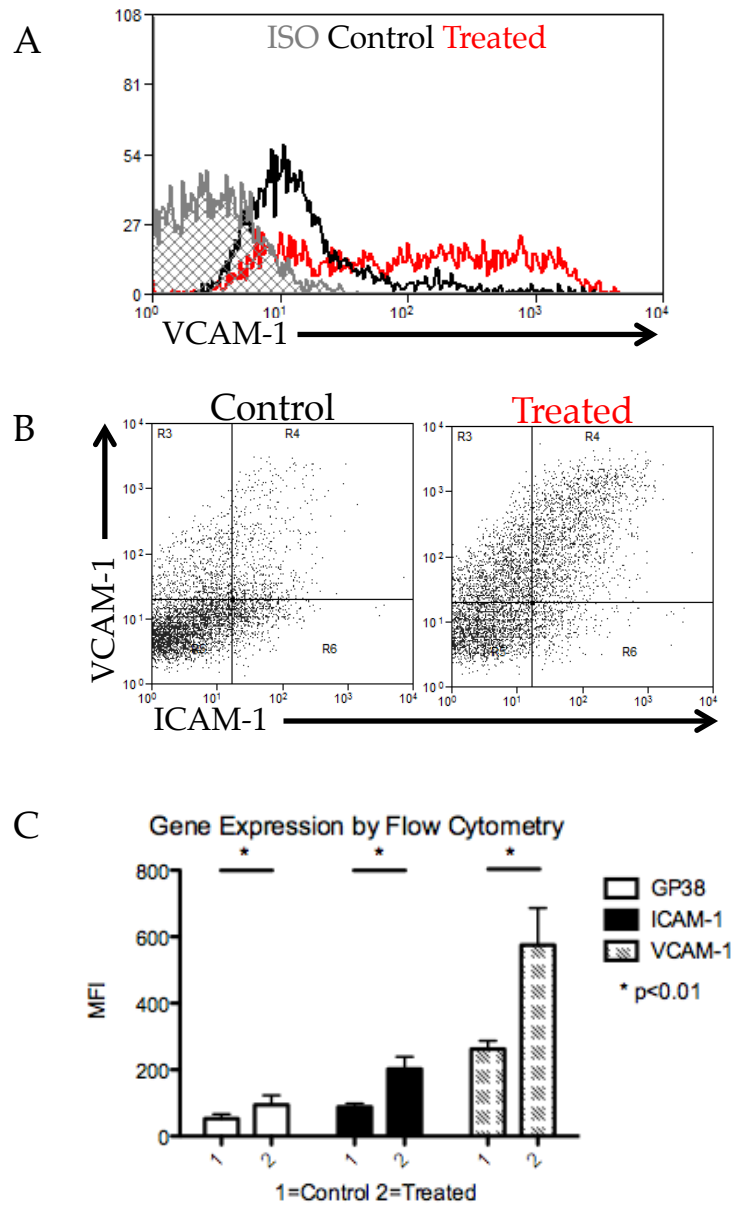
Figure 4.7 Inflammatory cytokines can rescue a high Gleason phenotype lost in passage through culture. (A) Representative histogram showing the level of VCAM-1 expression in non-treated, high passage, tumour stroma (Control – black line) against the same cells treated with an inflammatory cytokine cocktail (Treated – red line) compared to the isotype control (grey shaded). (B) Dot plots from the same experiment showing the raise in the level of expression of both VCAM-1 and ICAM-1 for the control and treated cells. (C) Quantification across 3 separate experiments of the expression levels of podoplanin, ICAM-1 and VCAM-1 for control and treated cells.
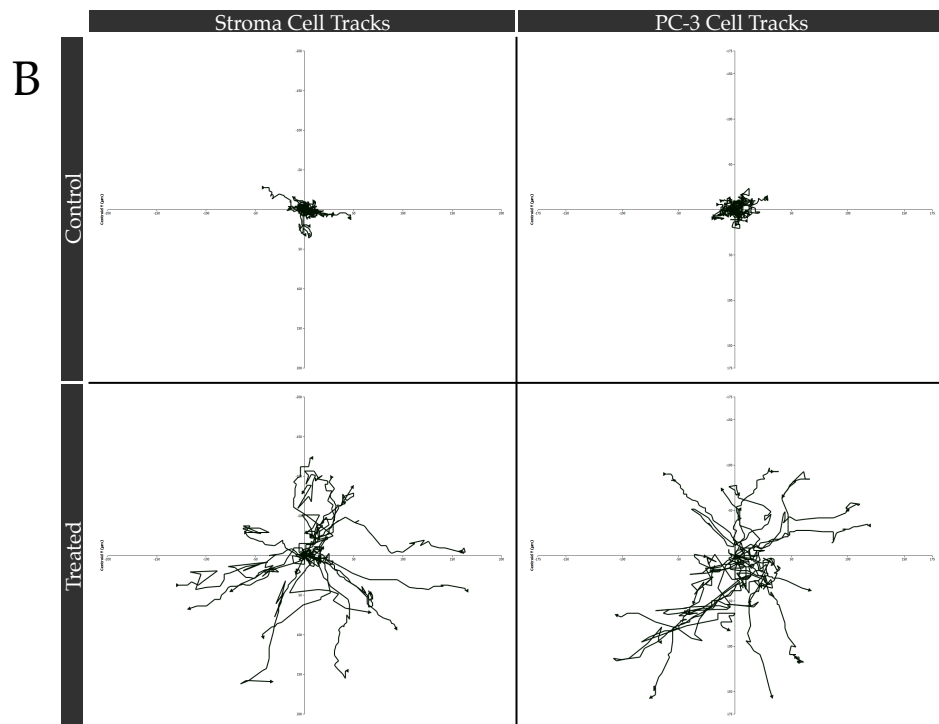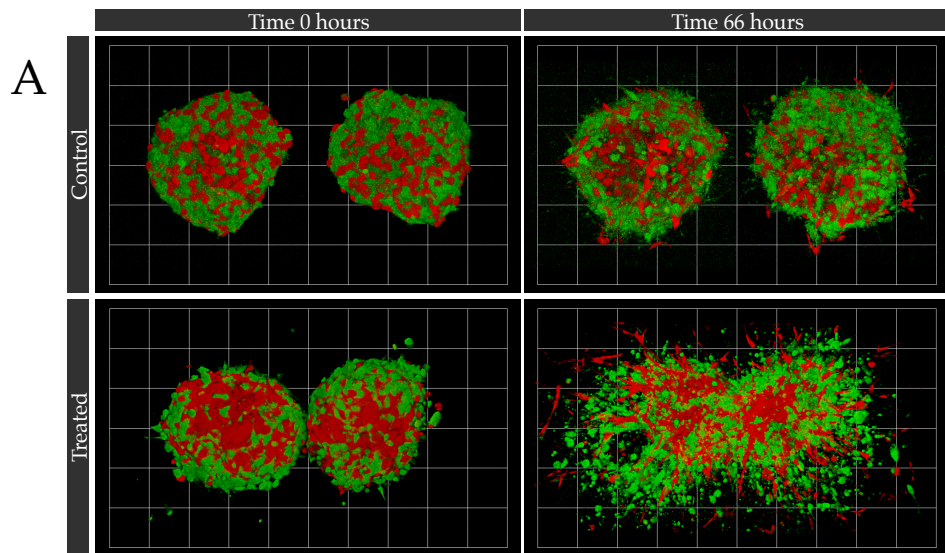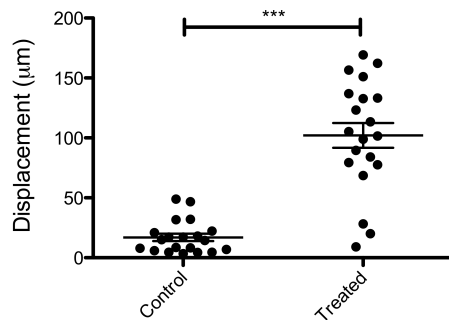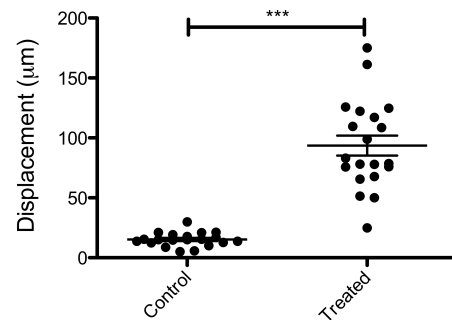
Figure 4.8 Inflammatory cytokines induced stromal cell migration and thus PC-3 migration. (A) Time-lapse imaging over 3 days for spheroids containing non-treated control vs treated stromal (red) both containing PC-3 cells (green). Scale unit: 64μm (B) Single cell tracking for stromal cells and PC-3 cells in control and treated spheroids. Quantification of cell displacement for stromal cells (C) and PC-3 cells (D) in control and treated spheroids. Bar represents mean±SEM, ***p<0.0001 (t test)

A   LL/2 Tumour Weight
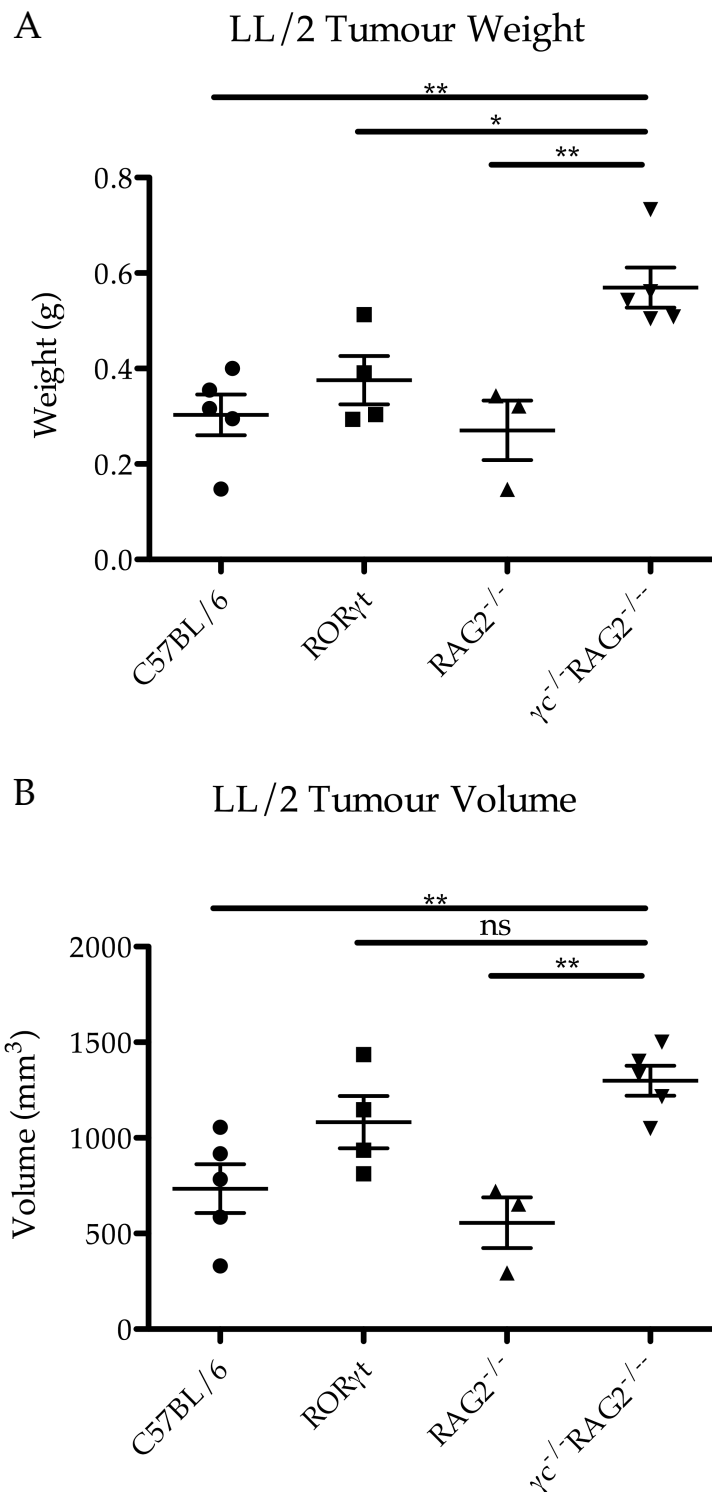
B   LL/2 Tumour Volume

Figure 4.9 Analysis of tumours resulting from subcutaneous injection of LL/2 cells in to mice from 4 different genetic backgrounds. Injections carried out by Dr Mark Coles (A) tumour weight and (B) tumour volume at 14 days. (n≥3); bars show means±SEM, ANOVA with post-hoc Tukey showed $\gamma c^{-/-}$ RAG2$^{-/-}$ to be significantly different to other mice groups. (ns not significant, * p<0.01, **p<0.001)
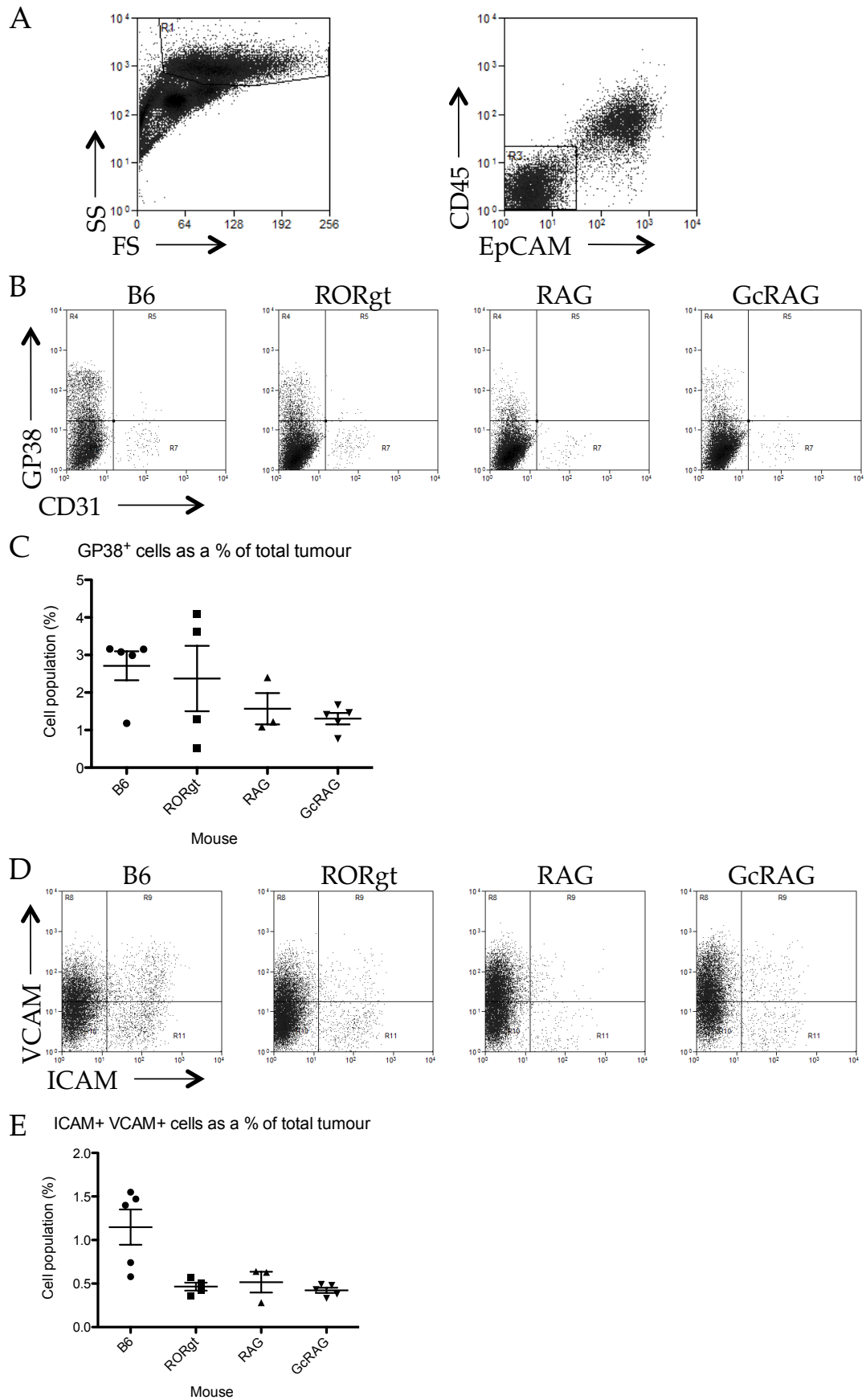
Figure 4.10 FACS analysis of LL/2 tumours. (A) Gating strategy to pull out the CD45- EpCAM- tumour stroma (B&C) the expression of podoplanin and CD31 across each mouse background (n≥3); bars show medians ± SE (D&E) the expression of VCAM-1 and ICAM-1 for each genetic background. (n≥3); Data was arsine transformed, bars show means±SEM, ANOVA with post-hoc Tukey (ns)
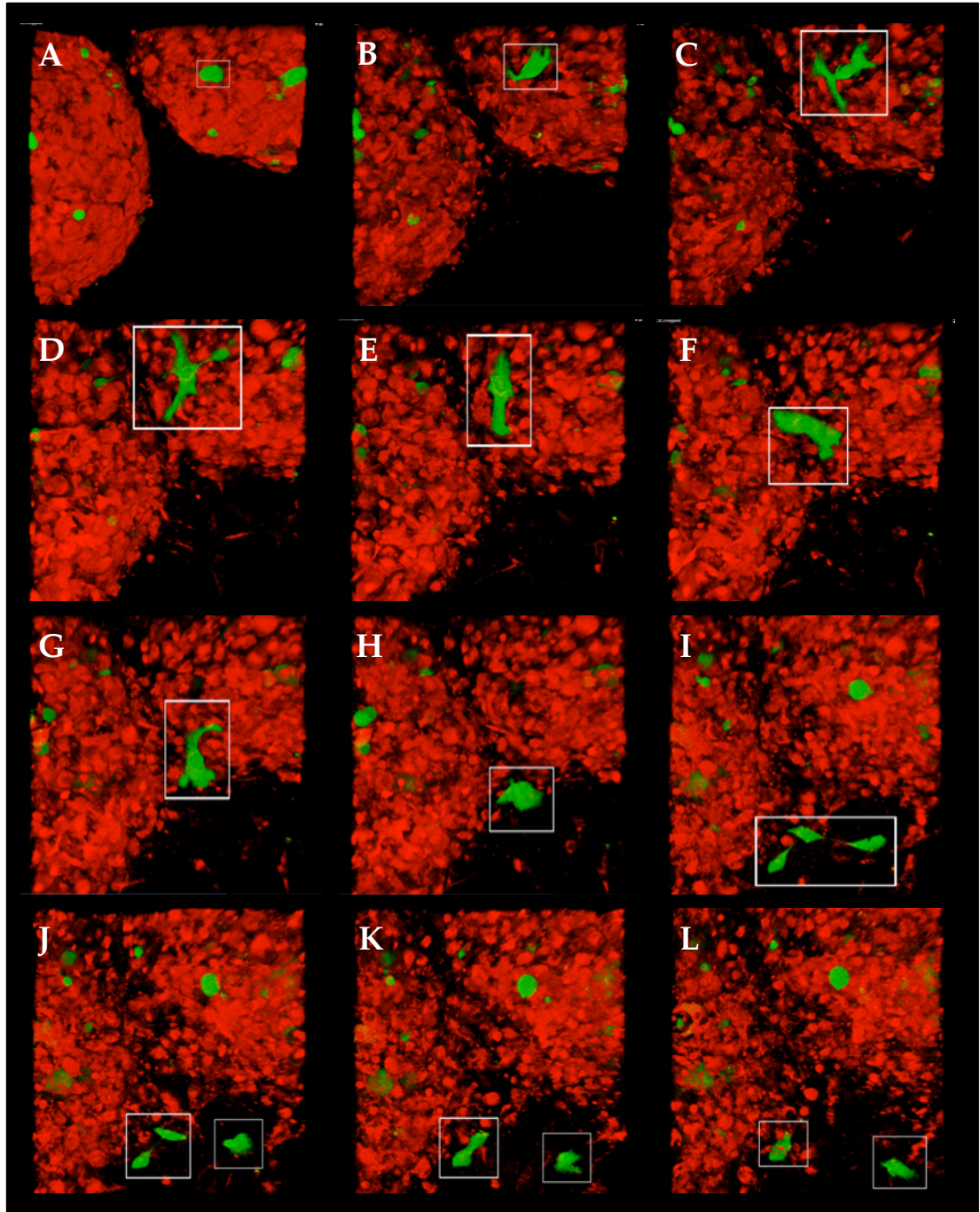
Figure 4.11 Primary human prostate cancer stem cells migrate in 3-D *in vitro* with tumour stroma/PC-3 spheroids. (A-L) Time-lapse imaging over 3 days of primary human prostate cancer stem cells (green) incorporated in to tumour stroma/PC-3 spheroids (red). Each image represents a 6 hour time point over 66 hours. A single CSC (white box in A) is tracked over time migrating out of the spheroid (B-H) before dividing (I-K) with one cell moving further in to the matrix and one cell rejoining the spheroid (L).

Chapter 5

A Role for SPARC and VLA-4 in

Prostate Cancer Cell Growth and

Migration in 3-D

5.1   Introduction

5.1.1   Vascular Cell Adhesion Molecule-1 (VCAM-1) – VLA-4 interactions

We have previously shown that VCAM-1 expression is regulated on tumour stroma. VCAM-1 is also expressed on activated vascular endothelium as a result of inflammatory signals including TNFα and IL-4 and has a key role in leukocyte extravasation into tissues (Cybulsky et al. 1991). VLA-4 (also known as integrin $\alpha_4\beta_1$) is the counter ligand for VCAM-1 that is expressed by leukocytes (Elices et al. 1990). Binding of VLA-4 to VCAM-1 results in the tethering of migratory leukocytes to the endothelial cells, permitting transmigration through the vascular endothelium and into the interstitial space of peripheral tissues (Alon et al. 1995).

Most of our understanding of the molecular and biophysical mechanism of VCAM-1-VLA-4 interactions has been carried out on leukocytes and understanding its role in the processes of tethering, adherence, and diapedesis. Using blocking monoclonal antibodies (mAb) to the α_4 integrin component of VLA-4, it has been shown that the migration and diapedesis of THP-1 cells is dependent on VLA-4-VCAM-1 interactions (Ronald et al. 2001). More recently Natalizumab (a humanized antibody against the α_4 integrin) has been developed as a therapeutic for Multiple Sclerosis (MS), preventing VCAM-1-VLA-4 mediated leukocyte migration into the peripheral nervous system. The antibody was developed as a therapeutic

after it was discovered that anti-α_4 antibodies prevented the accumulation of leukocytes in the central nervous system, and stopped the development of experimental autoimmune encephalomyelitis (EAE) in rats which has been used to model MS for several decades (Yednock et al. 1992). Two clinical trials in patients with MS resulted in an increase in the proportion of patients remaining relapse-free (76% and 67%) compared to patients in the placebo control group (53% and 46%) (Noseworthy & Kirkpatrick 2005). The Food and Drug Administration (FDA) approved Natalizumab for the treatment of patients with relapsing forms of MS in November 2004 (www.fda.gov). Although clinically highly effective, blocking VLA-4 using Natalizumab has lead to human polyomavirus mediated encephalitis in very small numbers of patients resulting from acute immunosuppression. Blocking both VLA-4 and VCAM-1 independently and together has been analysed in an experimental model of neuritis and found that in all three cases increased T cell apoptosis was observed indicating a potential alternative role for VCAM-1-VLA-4 interactions (Leussink et al. 2002).

Fibronectin, an alternative ligand for VLA-4, and VCAM-1 are both strongly expressed on bone marrow stroma. Analysis of hematopoietic progenitor cells adhesion to bone marrow stroma has shown a role for these interactions (Simmons et al. 1992). Additionally VLA-4 has been shown to mediate the attachment of myeloma cancer cells to bone marrow stroma, and was found to be the sole source of adhesion to VCAM-1 and fibronectin expressed by stromal cells (Sanz-Rodríguez et al. 1999; Sanz-Rodríguez et al. 2001). Analysis of human oral squamous cell carcinoma cell lines shows that 70% express VLA-4, and could interact with VCAM-1 on adjacent vascular endothelium (Song et al. 2012). Importantly, this study also showed that TNF-α expression from the tumour stimulated the expression of VCAM-1 on the endothelium resulting in tighter cell adhesion and fusion of the tumour to the endothelium. Treatment with anti-VCAM-1 or anti-VLA-4 blocking mAb, resulted in a significant decrease in cell adhesion and completely blocked fusion of tumour cells to the adjacent blood vasculature (Song et al. 2012; Leussink et al. 2002).

High expression of VCAM-1 correlates with the Gleason grade tumour stroma, and VCAM-1 high grade tumour stroma induces the migration of PC-3 cells thus it is possible that VCAM-1 has a significant role in tumour

cell migration. This could be through its transmembrane ligand VLA-4 or through an alternative ligand secreted protein, acidic and rich in cysteine (SPARC).

5.1.2   Secreted Protein, Acidic and Rich in Cysteine (SPARC)

SPARC, also known as osteonectin and BM-40, has been shown to have roles in cell repair, proliferation, and spreading (H. Sage, Decker, et al. 1989a; H. Sage, Vernon, et al. 1989b). SPARC expression has been linked to multiple different types of cancer including colorectal cancer (Porte et al. 1995), lung cancer (Bendik et al. 1998), human breast cancer (Gilles et al. 1998), and ovarian cancer (T. J. Brown et al. 1999). Although the mechanism of how SPARC functions is unknown, different cancers have implicated different potential mechanisms including a role in regulation of MMPs and tumour cell growth.

SPARC expression has been analysed in prostate cancer in comprehensive panels of primary tumours, metastatic foci, and prostate cancer cell lines. Analysis showed that high levels of SPARC mRNA and protein correlated with metastatic foci, and that although expression was detected in glandular epithelial cells of normal tissue, expression was higher in these foci and in some primary prostate cancer samples. Thus the differential expression of SPARC indicates it may have an important role in prostate cancer progression (R. Thomas et al. 2000). Presently, the role of SPARC in prostate cancer growth and metastasis is mechanistically unknown.

SPARC is a 40kD acidic glycoprotein, containing a cysteine-rich single polypeptide. The mature protein is glycosylated and SPARC predominantly, although not exclusively, acts as a secreted protein where it can bind collagen through a collagen-binding domain (Sasaki et al. 1998). SPARC was initially thought to be produced solely in bone and was identified as a chemoattractant found in bone conditioned media. Purified, SPARC was shown to promote DU-145 and PC-3 prostate cancer cell migration but not non-bone metastasising cell lines including B16-F10 mouse melanoma and HT-1080 fibrosarcoma. Specifically, SPARC induced an increase in the collagenase/gelatinase A protease MMP-2 activity in DU-145, PC-3 and also the breast cancer cell line MDA-MB-231. SPARC did not induce any change in MMP activity in B16-F10 and HT-1080 cells. Analysis of breast and

prostate cancer cell lines reactive to SPARC as shown by an increase in MMP-2 activity, in a Boyden chamber assay showed increased cancer cell invasiveness through a collagen IV matrix suggesting a role for SPARC induced MMP-2 activity in those cancer cells that exhibit bone metastasis (Jacob et al. 1999).

Genetic polymorphisms in SPARC have been identified including five common variations in the 3'-untranslated region (UTR) (Winder et al. 2012). These polymorphisms, including three single nucleotide polymorphisms (SNPs) found in the 3'UTR have been linked to bone density and bone mass (Delany et al. 2008). More recently SNPs located in the coding region of the SPARC gene have been significantly associated with cancer. An individual SNP in the 3'UTR has been strongly linked to a predisposition to gastric cancer recurrence (Winder et al. 2012) whereas another has been shown to be significantly associated with hepatocellular carcinoma (Segat et al. 2009).

It has been shown that SPARC can act to reduce metastasis and therefore act in a protective manner. Melanoma metastasis formation has been shown to reduce via a SPARC-dependent mechanism. Endothelial progenitor cells contribute to melanoma tumour growth and progression to a metastatic disease (D. Gao & Mittal 2009). However, more recent studies have shown that endothelial progenitor cells when preconditioned with tumour cell condition media, were able to physically interact with tumour cells, in a SPARC dependent manner (Defresne et al. 2011). The pre-conditioned endothelial progenitor cells, took on a defensive role and increased their phagocytic characteristics with the capacity to eliminate tumour cells. The overexpression of SPARC was observed in these cells after exposure to conditioned media, and subsequent experiments using recombinant human SPARC recapitulated the anti-tumour cell behaviour (Defresne et al. 2011). This is contrary to numerous studies that link SPARC overexpression in tumour cells to a pro-invasive role (H.-Y. Wang et al. 2012; Derosa et al. 2011; S. Thomas et al. 2011; Said et al. 2009). In addition, high levels of SPARC expression in colorectal cancer are associated with better disease outcome (Chew et al. 2011). The role of SPARC is highly contextual. SPARC expression in colorectal cancer is exclusive to stromal mesenchymal cells and not in tumour cells (Chew et al. 2011) whereas in prostate cancer expression is clearly seen in the tumour cells *in vivo* and in prostate cancer cells lines

(Said et al. 2009) where high levels of SPARC is associated with poor prognosis and increased metastatic disease.

SPARC, when overexpressed in a hepatocellular carcinoma cell line using adenovirus expression system, has no observed effect on cellular numbers and or cell cycle check point in 2-D cell culture (Atorrasagasti et al. 2010). However, when grown as spheroids in 3-D the SPARC overexpressing cells showed a clear reduction in the rate of proliferation, and mild increase in apoptosis, as compared to non-transfected controls (Atorrasagasti et al. 2010). *In vivo*, the human SPARC overexpressing human hepatocellular carcinoma cells failed to form tumours in an athymic mouse model and survival of tumour cells was decreased. The failure in tumour growth might originate from an observed increase in macrophage infiltration in to the tumour site (Atorrasagasti et al. 2010). Contrary to what was shown in hepatocellular carcinoma cells, overexpression of human SPARC in human melanoma cells promoted cell survival resulting from an increase in the degradation of tumour suppressor p53. Western blot analysis showed that SPARC activates Akt, leading to phosphorylation of MDM2 inactivating p53 (Fenouille et al. 2011).

To further study the role of SPARC in the development and function of normal tissues, mice with a homozygous null mutation in the SPARC gene (SP$^{-/-}$) mice were generated (Gilmour et al. 1998; Norose et al. 1998). These mice were shown to exhibit high levels of adiposity. The number of adipocytes as well as the cell size was significantly increased but not to the detriment of body weight compared to control mice. In this case SPARC was proposed to limit the accumulation of subcutaneous fat in mice primarily by regulating adipocyte size and number (Bradshaw et al. 2003). SP$^{-/-}$ mice also exhibit osteopenia – a loss in bone mineral density (Mansergh et al. 2007), early-onset cataractogenesis (Yan & E. H. Sage 1999) and accelerated wound healing (Bradshaw et al. 2002). Subsequently these mice were crossed with the TRAMP mouse model, surprisingly these mice developed tumours at a faster rate. This goes against the link between high levels of SPARC expression found in aggressive human tumours and the expression of SPARC in many human cancer cell lines (Said et al. 2009). Collectively these results indicate a limited role for SPARC in a primary TRAMP model of prostate cancer, but an overall complicated role in development and

tumourigenesis depending on cell type and microenvironment. Tumour growth in SP$^{-/-}$ mice using a mouse Lewis lung carcinoma is enhanced suggesting a role in tumourigenesis which is non-prostate specific. Thus the context of SPARC expression is critical to understand its function.

5.2   Summary and Aims of this Chapter

VCAM-1 and VLA-4 have a key role in leukocyte adhesion and migration, more recently a potential role for VCAM-1-VLA-4 interactions has been shown in sarcoma cell migration. However a role for both proteins in prostate cancer cell migration is unknown. A second ligand that binds to VCAM-1, SPARC, has been highlighted as having a possible role in prostate cancer (R. Thomas et al. 2000), thus we hypothesise that competition between membrane bound VLA-4 and secreted SPARC has a key role in regulating the adhesion/de-adhesion process of VCAM-1 mediated prostate cancer cell migration.

By utilising gene expression analysis, shRNA knockdown, 4-D imaging of spheroids and an *in vivo* xenograft mouse model the aims of this chapter are as follows:

1)   To investigate the levels of SPARC and VLA-4 expression, in BPH, across a range of primary prostate tumour samples and prostate cancer cell lines.
2)   To characterise the phenotype of PC-3 SPARC knockdowns.
3)   To investigate and determine the role of VCAM-1 ligands SPARC and VLA-4 in prostate cancer cell migration in 3D.
4)   To investigate the possible role of SPARC in human tumour development *in vivo*.

5.3 Methods

5.3.1 Immunofluorescence of SPARC protein expression

The PC-3 WT parent cell line and 3 different PC-3 SPARC knockdown clones (section 2.3.2) were seeded on to sterile 13mm circular coverslips in the bottom of a 24-well tissue culture plate. The cells were allowed to adhere overnight at 37°C with 5% CO_2 for 48 hours. All wells were then washed once with PBS and fixed with 4% PFA for 10 min.

Once washed twice more with PBS, the cells were stained with phalloidin, anti-SPARC antibody, and counterstained with DAPI to stain for f-actin, SPARC and DNA respectively.

After a second fixation step of 4% PFA for 10 min, the 13mm coverslips were mounted on to glass slides using ProLong Gold antifade reagent (Invitrogen) and imaged the following day, after an overnight incubation at 4°C, via confocal microscopy on an LSM 710 confocal microscope (Zeiss).

5.3.2 Subcutaneous injection of PC-3 cells in to γc$^{-/-}$ RAG2$^{-/-}$ mice

PC-3 wildtype cells resuspended in 3mg/ml collagen I at a cell density of 7×10^6 cells/ml. The same procedure was carried out for PC-3 SPARC knockdown cell line. A mix was also made consisting of both cell types at a ratio of 1:1 to give a total cell density of 7×10^6 cells/ml. Cells were mixed with collagen in order to recapitulate the *in vitro* microenvironment in which experiments leading up to this point had been carried out, to create a solid plug to stop cells escaping immediately post-injection, and to rule out any exogenous effects of other co-injection material such as Matrigel.

Five γc$^{-/-}$ Rag2$^{-/-}$ mice were subcutaneously injected for each group (15 mice in total) each receiving 5×10^5 cells in 100μl collagen and mice were sacrificed and tumours removed 5 weeks post injection. Tumours were cleaned of all hair, skin and fat, and then measured using calipers and weighed on a fine balance. Subcutaneous injections were carried out by Dr Mark Coles.

5.3.3 VCAM Fc binding

PC-3 cells in culture were first washed twice with Dulbecco's PBS, then collected by using a PBS-based non-enzymatic cell dissociation buffer

(Invitrogen), which allows for ligand binding studies via gentle cell dissociation. 1×10^5 PC-3 cells per sample were spun at 300 g and the supernatant discarded. The cell pellet was then resuspended in 100µl PBS supplemented with 0.05% BSA and the wash process repeated once more. VCAM Fc protein was reconstituted in PBS to a stock concentration of 100µg/ml. PC-3 cells were incubated in 100µl PBS containing VCAM Fc protein (final concentration of 20µg/ml) at 37°C for 30 minwith regular, gentle mixing. After a single wash with PBS supplemented with 0.05% BSA, cells were resuspended in anti-human IgG secondary antibody conjugated to PE at a concentration of 1:100. Cells were incubated for a further 30 min before being washed once and resuspended in 500µl PBS supplemented with 0.05% BSA. Cells were then analysed by flow cytometry.

5.4 Results

5.4.1 SPARC and VLA-4 expression in primary tumour cells

We have previously shown that VCAM-1 was expressed by primary human prostate tumour stroma (Chapter 4). Typically, high expression correlated with tumour stroma from higher Gleason grade tumours and from fresh, early passage cells. VCAM-1 expression was lost by the stromal cells over time in culture and lower levels of VCAM-1 expression were detected in tumour stroma originating from lower Gleason grade tumour and stroma from BPH samples. Therefore we analysed the expression of VCAM-1 ligands, α_4 and β_1 integrin subunits and SPARC by qRT-PCR in primary prostate cancer cells and prostate cancer cell lines. RNA was extracted from epithelial cells from a range of tumours as detailed below. cDNA was synthesised from this RNA and a qRT-PCR was carried out using primer pairs specific for α_4 integrin, SPARC, and GAPDH was used as an internal housekeeping control.

Analysis was carried out using the ABI software to ascertain Ct values from which the relative expression of the target genes was worked out. Analysis of SPARC expression shows expression levels correlate with Gleason grade tumour cells tested (Figure 5.1). Compared to two lower Gleason grade 6 tumours, expression of SPARC is approximately 15- to 20-fold greater. Relative to PC-3 cells which are known to express high levels of SPARC (S. Y. Wong et al. 2008) the expression in primary prostate tumour cells is up to 30-fold higher. One complication with this analysis was that these prostate tumour cells contain a non-homogeneous distribution of luminal, basal, and transit-amplifying epithelial cells between different samples.

The pattern of SPARC expression in primary cells originating from BPH tissue is less clear. All three samples showed relatively high levels of SPARC expression compared to the PC-3 control cells. The lowest being 10-fold greater expression than that found in PC-3 cells, and the highest being approximately 20-fold in two of the BPH cases.

Integrin α_4 expression does not, at this stage, appear to follow a clear pattern. The highest expression of α_4 integrin is exhibited by one of the Gleason grade 6 tumour samples (Figure 5.1 B), however a sample from a different patient

of the same Gleason grade shows very little expression. The same random expression of α_4 integrin is observed in the 3 BPH samples tested. However, consistently these samples express either the same, or lower levels of α_4 integrin compared to PC-3 cells. However what is unclear is how this correlates to the overall number of α_4 integrin expressing epithelial cells.

5.4.2 SPARC and VLA-4 expression in prostate cancer cell lines

The prostate cancer cell lines PC-3, LNCaP, and VCAP were all tested for the expression of SPARC and α_4 integrin by qRT-PCR. 5×10^5 cells were pelleted via centrifugation, washed once with PBS and lysed to extract RNA via an RNeasy kit (QIAGEN). cDNA was synthesised from this RNA and the expression of SPARC and α_4 integrin was analysed using gene specific primers.

The results of the qRT-PCR are shown in Figure 5.1 (C&D). Relative to PC-3 cells, the expression of SPARC in LNCaP and VCAP was undetectable. Again relative to PC-3s, the two other cell lines express very little VL-4 with expression undetected in LNCaP cells. Thus the percentage of PC-3 cells expressing VLA-4 was determined by dual antibody staining for both α_4 and β_1 integrin subunits analysed by flow cytometry (Figure 5.1 E). Interestingly although all PC3 cells expressed the β_1 integrin only a small percentage expressed α_4. The level of α_4 integrin staining is low showing a low level of expression on small percentage of cells. This was compared to T cells which in this case were used a positive control. T cells were isolated from leukocyte cones (NHS Blood and Transplant) using RoetteSep technology (Stem Cell Technologies), stained for α_4 integrin and analysed by flow cytometry. T cells are known to express VLA-4 (Alon et al. 1995; Muraro et al. 2000), and 60% of T cells were positive for α_4 integrin in this instance (Figure 5.1 F).

5.4.3 shRNA knockdown of SPARC in PC-3 cells

To further investigate the role of SPARC function in PC-3 cell migration, inducible shRNA constructs were sourced to knockdown human SPARC mRNA (Sigma-Aldrich) in PC-3 cells.

Plasmid DNA was introduced in to PC-3 cells as described in methods section 2.3.2 and bulk cultures of polyclonal transfected PC-3 cells as well as

single cell clones were cultured under selection until stable. Bulk cultures and single cells clones were analysed for SPARC mRNA knockdown with, and without, the addition of the inducible factor IPTG. Dioxine-free IPTG (Sigma-Aldrich) was added to the growth media of the cells at a final concentration of 1mM and 72 hours incubation was allowed for full induction of the shRNA as according to the manufacturers instructions. RNA was extracted from $0.5x10^6$ cells and SPARC mRNA levels were detected via qRT-PCR. The results are shown in Figure 5.2.

SPARC mRNA levels remained unchanged in the bulk cultures without the addition of IPTG. After 3 days of induction, levels of SPARC mRNA dropped by approximately 25% but with a large variability across triplicate cultures.

Of the 24 single cell clones, 6 survived long term culture under selection for sequential passages to increase numbers. Namely; PS1, PS3, PS5, PS10, PS14, and PS17. All 6 clones turned out to be markedly different in the expression levels of SPARC mRNA. Indeed some clones exhibited an increase in SPARC mRNA levels relative to the PC-3 wild type control, most notably PS10 whose levels rose as much as 20-fold without induction which decreased to a 10-fold rise after being induced by IPTG, again relative to the PC-3 wild type control. Of the 6 clones, PS5 exhibited the most efficient knockdown with levels of SPARC mRNA knockdown of 85% and 80% without and with induction respectively. This was consistent in subsequent tests and future cultures (Figure 5.2 D). Based on this, the PS5 clone was used as a non-inducible shRNA knockdown of SPARC mRNA levels in future experiments.

To further strengthen experiments, several more PC-3 SPARC knockdown clones were made using the same system and clones were selected for based on their efficiency of SPARC knockdown without the need for IPTG induction. This resulted in 2 further clones (PS1a and PS1b) that had close to 100% knockdown as shown in Figure 5.2 (D). These were treated as clones containing a non-inducible vector and so knockdown was assumed to be constitutive without the need to add IPTG.

5.4.4 PC-3 SPARC knockdown clones are markedly different to PC-3 WT parent cell line in morphology

Analysis using immunofluorescence of PC-3 cells deficient for SPARC expression showed clear differences in cellular morphology (Figure 5.3 A). Loss of SPARC protein affects both the cells shape and size. PC-3 cells are typically non-circular and mesenchymal in shape, and in the range of 30-60μm in length with evidence of focal adhesion sites that co-localise with SPARC (white arrows in Figure 5.3 A). A proportion of the SPARC knockdown cells are in excess of 250μm in diameter and have taken on a round, flat, and epithelial like morphology. Whilst the size of wild type cells remains homogeneous with close to 100% of the cells falling in the range of 30-60μm, there are clear differences in the size of the cells within the SPARC knockdown clones. The SPARC knockdown clones range from WT sizes of approximately 40μm up to cells as large as 250μm. However, from a shape morphology point of view, this is consistent, with all SPARC knockdown cells exhibiting a very uniform round cell shape. These cells exhibit high levels of cortical actin at the periphery of the cell (yellow arrow heads in Figure 5.3 A) which is not observed in WT controls.

The levels of SPARC protein expression was quantified using an anti-SPARC antibody (Figure 5.3 B). Whilst there is some staining on the knockdown cells, this is consistent with the shRNA knockdown not being 100% efficient. The overall levels of SPARC protein, as measured by anti-SPARC antibody staining and mean pixel fluorescence intensity across 3 independent fields of view, were significantly lower in the three PC-3 SPARC knockdown cell lines tested as compared with PC-3 WT cells.

5.4.5 Knocking down SPARC in PC-3 cells increases motility in 2D

PC-3 WT and SPARC knockdown cells were seeded on to a 3.5cm glass bottom dish and allowed to attach overnight in HAMS-F12 media. The following day the cells were imaged via bright field microscopy as described in methods section 2.14.4. Single cells were tracked from two or more independent experiments using the manual tracking plugin within the software package ImageJ.

PC-3 WT cells retained their original morphology (Figure 5.4 A-C) with wild-type cells appearing more mesenchymal in shape as opposed to the large

round phenotype of the SPARC knockdown cells. Analysis shows the SPARC knockdown cells move at a significantly faster velocity. PC-3 cells tended to move around one another in particular at times of cell division. However, PC-3 SPARC knockdown cells moved rapidly and often independent of any cell-cell contact.

5.4.6 Knocking down SPARC in PC-3 cells inhibits migration in 3-D in spheroids containing cancer tumour stroma

High Gleason grade, early passage tumour stroma was used in conjunction with PC-3 SPARC knockdown cells in a 3-D spheroid assay. As a control, spheroids were also made using the same tumour stroma, and PC-3 WT cells.

Both sets of spheroids were implanted in to collagen I gels and imaged via 2-photon microscopy. Representative images at 3 separate time points for both sets of spheroids are shown in Figure 5.5 (A&B). Imaging clearly shows that in both sets of spheroids, the stromal cells in green have migrated in to the collagen as previously observed. However, only control PC-3 cells migrated significantly into the collagen. The majority of PC-3 SPARC knockdown cells remain within the spheroid with very few migrating in to the matrix. Single cells were tracked and measurements are shown in Figure 5.5 (C). While the displacement of stromal cells remains unaffected in both spheroid sets, there is a significant reduction in the displacement of PC-3 cells with reduced levels of SPARC protein.

5.4.7 PC-3 SPARC knockdown cells fail to establish tumours *in vivo*

To investigate a possible role for SPARC *in vivo*, PC-3 wildtype (control) and PC-3 SPARC knockdown cells were introduced in $\gamma c^{-/-}$ Rag2$^{-/-}$ mice via subcutaneous injection in collagen either as a pure population or as a mixture with PC-3 WT cells.

Tumours were successfully recovered from 14 mice at the end of the experiment, leaving only one failing to establish (the mixed cells) which was then absent in subsequent analysis. Tumours were first cleaned of all hair, skin and fat, and then measured using calipers (Figure 5.6). The volume of the tumours resulting from the injection of PC-3 WT cells only, was significantly higher than that of the volume of the tumours consisting of PC-3 SPARC knockdown cells (p=0.035). The difference between wildtype and

the 50:50 mix of cells was not significant (p=0.07) but a strong difference was observed. Tumour weight, as expected, followed the same pattern when comparing PC-3 wildtype tumours to the SPARC knockdown tumours and to the mixed cell tumours. However, a statistically significant difference was not observed in either case (P=0.08 and 0.14 respectively).

5.4.8 PC-3 SPARC knockdown cells are in G2/M arrest but still proliferate *in vitro*

To determine if a defect in proliferation in the SPARC knockdown cells lead to failure or a delay in tumour growth, cell cycle analysis and a proliferation assays were carried out PC-3 wild type cells, and three PC-3 SPARC knockdown clones. In each case 1×10^6 cells were collected, and treated as in section 2.20 with offline cell cycle analysis carried out using FlowJo.

Analysis of control PC-3 cells (Figure 5.7 A) showed that 65% of cells were in G1, G0 or interphase, 16.1% of the population were in S-phase during which cells are replicating their DNA, and finally 18.3% were in G2/M phase, typical of a rapidly dividing tumour cell line.

In contrast, analysis of PC-3 SPARC knockdown clones show there is an increase in G2/M phase (40.2% of cells in G2/M) consistent with a block in cell cycle progression. Two other independent knock-down clones also show a G2/M blockade to a slightly lesser extent (data not shown).

In addition to cell cycle analysis, the comparative rate of proliferation was investigated to control cells. PC-3 WT tdTomato cells were mixed with non-fluorescent PC-3 SPARC knockdown cells and counted using AccuCheck Counting Beads (section 2.21). Cells were counted from 3 triplicate wells for each time point.

Figure 5.7 (D) shows that whilst still proliferating, the SPARC knockdown clone grew significantly slower than that of their wildtype counterparts. Sub culturing timings during culture was similar which could be accounted for by the size difference between the two cells types.

5.4.9   A sub-population of PC-3 cells bind VCAM-1

By utilising a VCAM Fc chimeric protein (R&D Systems) the possibility of VCAM-1 binding being instrumental in the migration of PC-3 cells was investigated. Based on previous results showing that VCAM-1 expression decreases over time in culture on stromal cells, which correlates with a loss in the ability to induce PC-3 migration, the hypothesis was the consideration that the binding of VCAM-1 by PC-3 cells was necessary for migration.

PC-3 WT and SPARC knockdown cells were analysed for their ability to bind VCAM Fc. Figure 5.8 (A) shows that there is an 11.8% PC-3 population that is binding VCAM Fc. This population is small but mirrors migration data gathered so far showing that some but not all PC-3 cells migrate in the model. PC-3 SPARC knockdown cells showed an increase in the levels of VCAM Fc binding to 21.8% in Figure 5.8 (B). Figure 5.8 (C) shows the significant increase in the level of VCAM Fc binding across three independent experiments.

To investigate if SPARC protein could outcompete the binding of VCAM-1 by other ligands, recombinant human SPARC (rhSPARC) was added to the staining cocktail alongside VCAM Fc protein at a concentration of $20\mu g/ml$. Figure 5.8 (D) shows a drop in VCAM Fc staining with the addition of rhSPARC to PC-3 WT cells. Although a smaller decrease is observed this is statistically significant (p=0.04) showing that rhSPARC is possibly binding to the VCAM Fc protein which in turn blocks this binding to ligands on the surface of PC-3 WT cells.

5.4.10 Recombinant human SPARC affects 2-D morphology and cellular migration in 3-D.

SPARC is a secreted protein. However, we and others have observed intracellular SPARC that could have potential roles in regulating cellular morphology consistent with the changes observed in cells with decreased amounts of SPARC protein. Therefore, the effect of exogenous rhSPARC was used to determine if it could modify cellular phenotype in 2-D and 3-D.

PC-3 SPARC knockdown cells were seeded on to glass coverslips and rhSPARC protein added ($30\mu g/ml$) as previously described (Wendt et al. 2010; Bradshaw et al. 1999). Analysis of cells for SPARC and f-actin

expression (Figure 5.9 A&B) shows that the morphology of PC-3 SPARC knockdown cells is partly restored to wild-type by the addition of rhSPARC to the media. Although the cell shape is still not as mesenchymal as control cells, the size of each cell has been reduced significantly to a size resembling that of wild-type cells according to cell diameter (Figure 5.9 C). Cells were measured within independent fields of view across 2 separate experiments.

PC-3 WT cells and PC-3 SPARC knockdown cells in 3-D spheroids with high Gleason, low passage stromal cells (green) were embedded in to collagen I matrices in the presence of 30μg/ml rhSPARC (Figure 5.9 E). While no significant changes in the migration of the stromal cells with and without the addition rhSPARC was observed, there is a slight increase in the mean average of the migration of PC-3 SPARC knockdown cells with the addition of rhSPARC compared to PC-3 SPARC knockdown cells without exogenous rhSPARC. However the result was statistically not significant (Figure 5.9 F).

5.4.11 Inhibiting VLA-4 using a blocking mAb

PC-3 WT cells were formed in to spheroids with high Gleason grade stroma as previously described. One set of spheroids were then embedded in to collagen I matrices and incubated in normal full growth media. A second set were embedded in separate collagen matrices and incubated in full growth media supplemented with 20μg/ml anti-human-VLA-4 blocking antibody (Elan Pharmaceuticals). Both sets of spheroids were imaged via two-photon microscopy for a period of 48 hours.

Images at the end of 48 hours are shown in Figure 5.10 showing spheroids in normal growth media (A) and in media supplemented with anti-VLA-4 antibody (B). Stromal cell (red) migration was unaffected by the presence of the antibody. However, there is a difference in the morphology and migration of PC-3 cells with and without anti-VLA-4 blocking antibody. The white arrows in Figure 5.10 (A) show the normal mesenchymal phenotype of PC-3 wildtype cells. The yellow arrows in Figure 5.10 (B) show that in the presence of the anti-VLA-4 blocking antibody, PC-3 cells have taken on more of a round phenotype. Cells were tracked and PC-3 cells in the presence of anti-VLA-4 blocking antibody exhibited significantly shorter displacements consistent with a role for VCAM-1 and its ligands, SPARC and VLA-4 in prostate cancer migration (Figure 5.10 C).

5.5   Discussion

The link between the expression of SPARC and the progression of prostate cancer to a metastatic disease has previously been observed (R. Thomas et al. 2000). There has also already been some work on the effect of exogenous SPARC purified from bone conditioned media, on the behaviour of cancer cells *in vitro* (Jacob et al. 1999). However, the mechanism by which SPARC works is little understood and the importance of its expression in human disease is unknown and controversial.

In this chapter we have shown that SPARC expression of primary epithelial cells is higher in higher Gleason grade tumours. It was also shown that SPARC expression is high in primary cells from BPH. Although it is uncertain why this difference is observed, BPH is a non-malignant pathological disorder which is mainly a stromal mediated disease. However, the epithelium is not normal. Whether or not SPARC expression in BPH is important is unknown as it is very challenging to obtain normal human prostate epithelium.

Of the prostate cancer cell lines analysed only PC-3 cells express SPARC at significant levels. These cell lines differ in many ways, PC-3 cells originate from an advanced androgen independent tumour with evidence of bone metastasis. In contrast LNCaP and VCAP cells both originate from metastatic lesions in lymph node and bone respectively and are androgen responsive whereas PC-3 cells are non-responsive to androgens (Rahim et al. 2011). However it is unclear if the relationship between androgen sensitivity and SPARC mediated migratory capacity is true. The difference in expression pattern is compounded by lack of VLA-4 expression by these cells. It is possible that LNCaP and VCAP cells can migrate by a VCAM-1 independent process. Interestingly, although LNCaP cells do not express VCAM-1, it can be induced to express the adhesion molecule under pro-inflammatory conditions *in vitro* (C. P. Wong et al. 2009). Whether expression of VCAM-1 on epithelial cells is important in tumour growth and migration is unknown.

Exogenous soluble human SPARC has been shown to promote the invasiveness of prostate cancer cell lines LNCaP, VCAP and PC-3 *in vivo* (N. Chen et al. 2007) and is consistent with the function of SPARC in prostate

cancer based on its believed function as a secreted protein. However, using shRNA knockdown of SPARC the strong phenotypic changes in PC-3s can only partially be rescued by the addition of soluble human SPARC. Moreover, SPARC effects the cell cycle in addition to migration behaviour and this itself might result from changes to cell adhesion and morphology, but intracellular SPARC might bind to and effect the function of key proteins in the cell. The addition of soluble rhSPARC to the 3-D spheroid only marginally improved PC-3 cell migration. This might result from soluble SPARC being present in the wrong place at the wrong point in time in the migration process as physiologically, SPARC is normally expressed strongly at focal adhesions. Alternatively most of the soluble SPARC may become immobilised on the collagen matrix on account of its collagen binding domain.

Interestingly , SPARC deficient PC-3 cells fail to efficiently establish tumours *in vivo*. Although cell cycle progression was affected by the knockdown of SPARC, tumour cells still proliferated *in vitro* albeit at a slower rate. The G2/M blockade was insufficient to inhibit the expansion of cells *in vitro* and is unlikely to account for the absence of tumours *in vivo*. Therefore, SPARC may have a key role in tumour initiation *in vivo*. Interestingly, Atorrasagasti et al showed the opposite in human hepatocellular carcinoma. They showed that the overexpression of SPARC completely prohibits the *in vivo* tumourigenicity of these cells (Atorrasagasti et al. 2010) adding more complexity to the possible role of SPARC.

Unlike in stroma independent 2-D cultures, SPARC deficient PC-3 cells do not migrate in 3-D. This could be related to VCAM-1 mediated adhesion and de-adhesion in stromal cell mediated migration. The results showing an increase in VCAM Fc binding by PC-3 cells deficient in SPARC could suggest a role for SPARC in regulating VCAM-1 bioavailability as previously described for monocyte transendothelial migration (Ronald et al. 2001). The addition of rhSPARC to wildtype PC-3 cells in a similar experiment showed the opposite effect – a drop in the levels of VCAM Fc binding to PC-3 cells. From these two experiments we can postulate that SPARC is acting as a secreted, or membrane bound ligand of VCAM-1 which blocks the binding of VCAM-1 by other ligands such as VLA-4. However, with the effects of

SPARC shRNA being seen *in vitro* in the absence of stromal cells, this is clearly not the only role for SPARC.

In 3-D, migration of PC-3 cells deficient in SPARC was not significantly altered by the addition of soluble rhSPARC, however a slight upward trend was observed. In order to migrate, cells have to not only adhere to each other/the matrix, but they also need to release in order to move off. With no expression of SPARC, perhaps the PC-3 cells are so tightly bound to the stromal cells and each other by VCAM-1/VLA-4 interactions that it is difficult for cells to migrate. By adding rhSPARC the binding of VCAM-1 maybe competed for allowing the release of VCAM-1 by VLA-4 and therefore directional migration may take over. However, Figure 5.5 does not necessarily show PC-3 cells tightly associated to the stromal cells and so this may not be the route that the addition of rhSPARC is taking. It would be interesting to assess the cell-cell levels of the two cell types and this ascertain whether there is a level of initial contact required between PC-3 cells and the stroma in order for migration to take place. This could be carried out by analysing time-lapse movies and quantifying the interactions in time.

This hypothesis was further investigated by using an anti-VLA-4 blocking antibody in the 3-D migration assay. The migration of PC-3 cells was not completely inhibited but it was significantly reduced. Blocking VLA-4 would block the interaction of VCAM-1 with VLA-4. The blocking antibody was added to the media so all VLA-4, both stromal and PC-3 in origin, would have been affected. With no VCAM-1/VLA-4 binding it is possible that there would be no, or little attachment of PC-3 cells. The normal SPARC levels courtesy of using wildtype PC-3 cells, would not have a role in this system because the outcompeting of VCAM-1 by SPARC would be made redundant by the absence of VLA-4 ligands to bind. Although relatively few PC-3 cells were shown to express a4 integrin by FACS, this correlates with the small proportion of PC-3 cells that were observed migrating out of spheroids cultured with stroma in 3-D. It is possible that this population of PC-3 cells might be the same cells that express α_4 and are therefore utilising the VCAM-1-VLA-4 interactions as a mean to migrate. However, further experiments would need to be carried out to explore this such as α_4 immunofluorescence studies of migrating PC-3 cells in 3-D.

5.6   Conclusions

SPARC has a key role in PC-3 cell behavior both in 2-D culture and in 3-D tumour spheroids. Reports to date have linked SPARC to metastasis with SPARC having a chemoattractant role, particularly with regard to metastases to the bone. This chapter has shown it has a clear role in cell shape control, the function of focal adhesions, cell cycle regulation and cell migration in both 2-D and 3-D environments.

There is a well established relationship between adhesion molecules and migration. Here, we show that VCAM-1 and two of its ligands VLA-4 and SPARC have a complicated role in tumour cell migration. This may well occur through controlling the attachment and detachment of PC-3 cells with stroma and the ECM to permit cell migration. This mechanism proposes a key role for the right balance of VCAM-1 adhesion via VLA-4, and the right level of SPARC to outcompete this binding at the focal adhesions to allow detachment and therefore forward migration. This is consistent with deficiencies or over expression of any of these proteins that may inhibit the metastasis process. A model for this hypothesis is presented in Chapter 6.
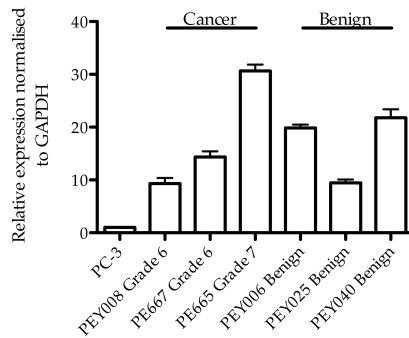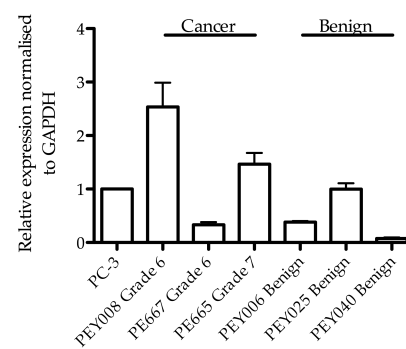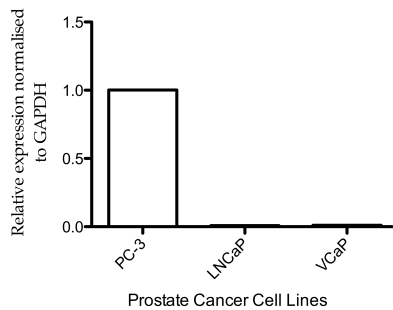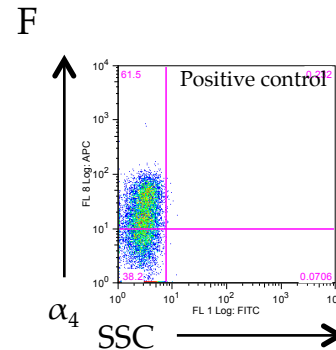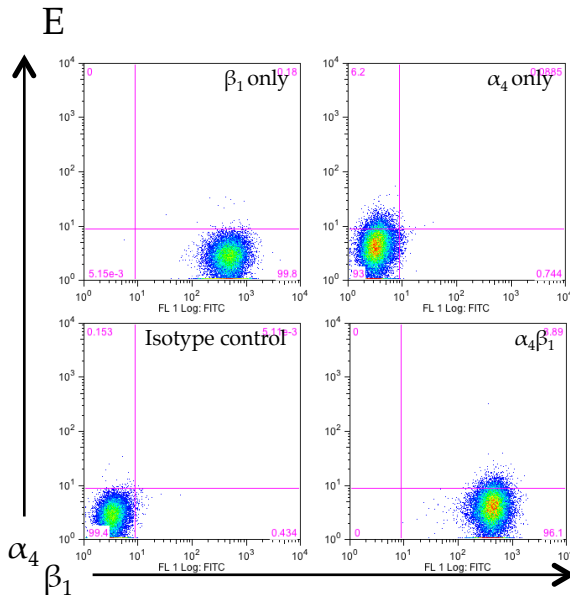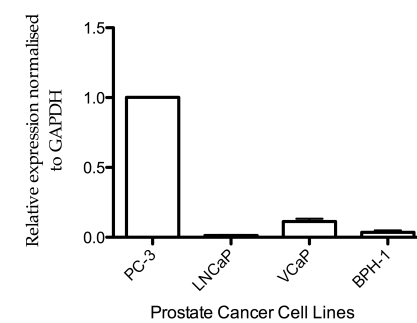
Figure 5.1 SPARC and α_4 integrin expression across a range of primary tumour cells and prostate cancer cell lines by qRT-PCR.(A) SPARC expression in primary tumour cells shows an increase in expression with increasing grade. BPH SPARC expression is relatively high across independent samples. (B) Primary cell α_4 integrin expression is less clear. (C) LNCaP or VCAP prostate cancer cell lines have little detectable SPARC expression. (D) α_4 integrin expression is very low in VCAPs and undetectable in LNCaP cell lines (E) Representative FACS dot plots showing levels of α_4 and β_1 integrin expression independently, as well combined expression of $\alpha_4\beta_1$ (VLA-4), against an isotype control. (F) T cells were used as a positive control of α_4 integrin expression.
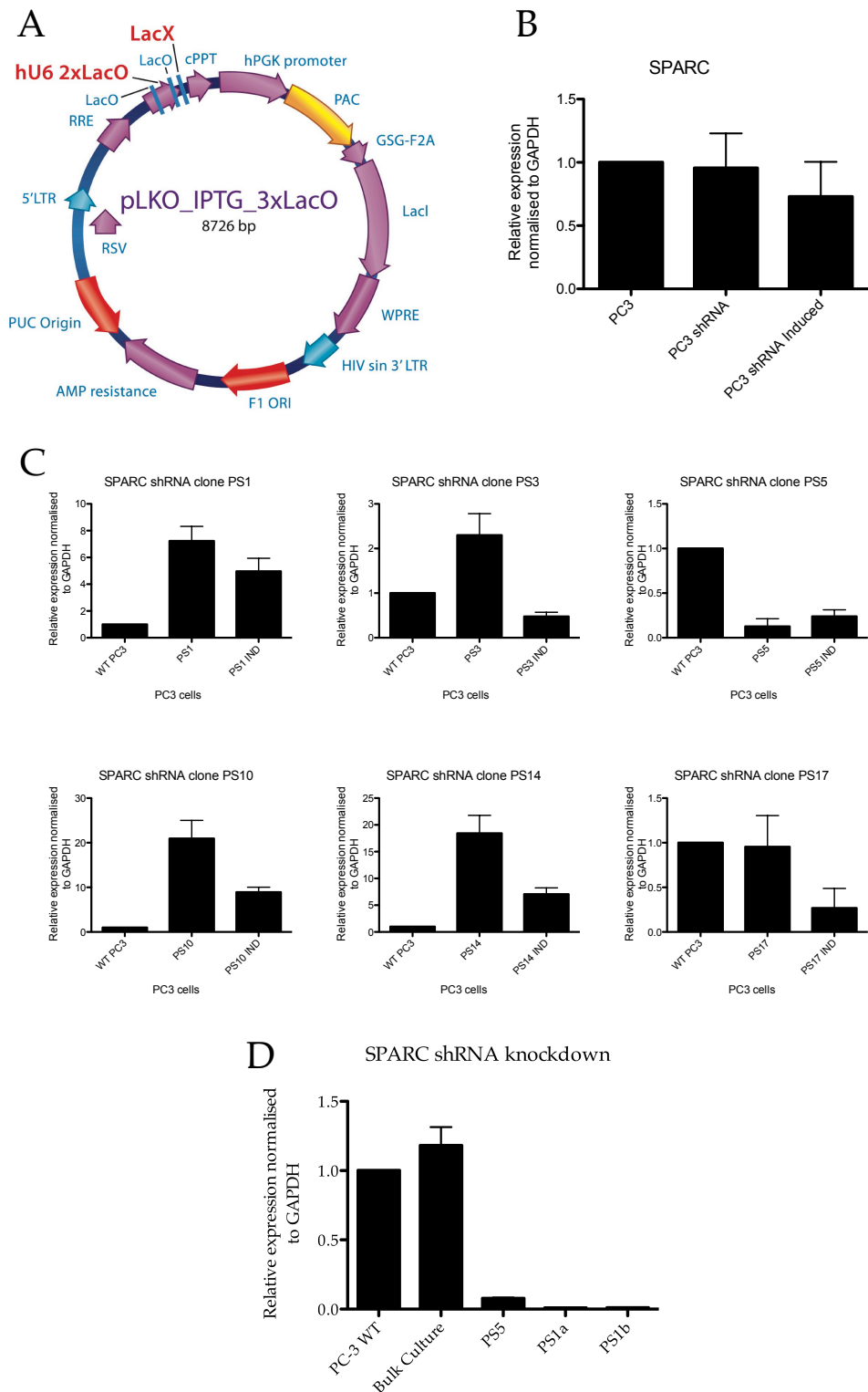
Figure 5.2 shRNA knockdown clones of PC-3 cells were successfully developed. (A) The pLKO inducible vector (Sigma) that was used to introduce SPARC shRNA. (B) Bulk cultures showed very little inducible knockdown of SPARC. (C) Single cell clones were made with varied degrees of knockdown of SPARC, with clone PS5 exhibited the most efficient knockdown of SPARC. (D) Further clones were made resulting in PS1a and PS1b which showed close to 99% knockdown of SPARC mRNA.
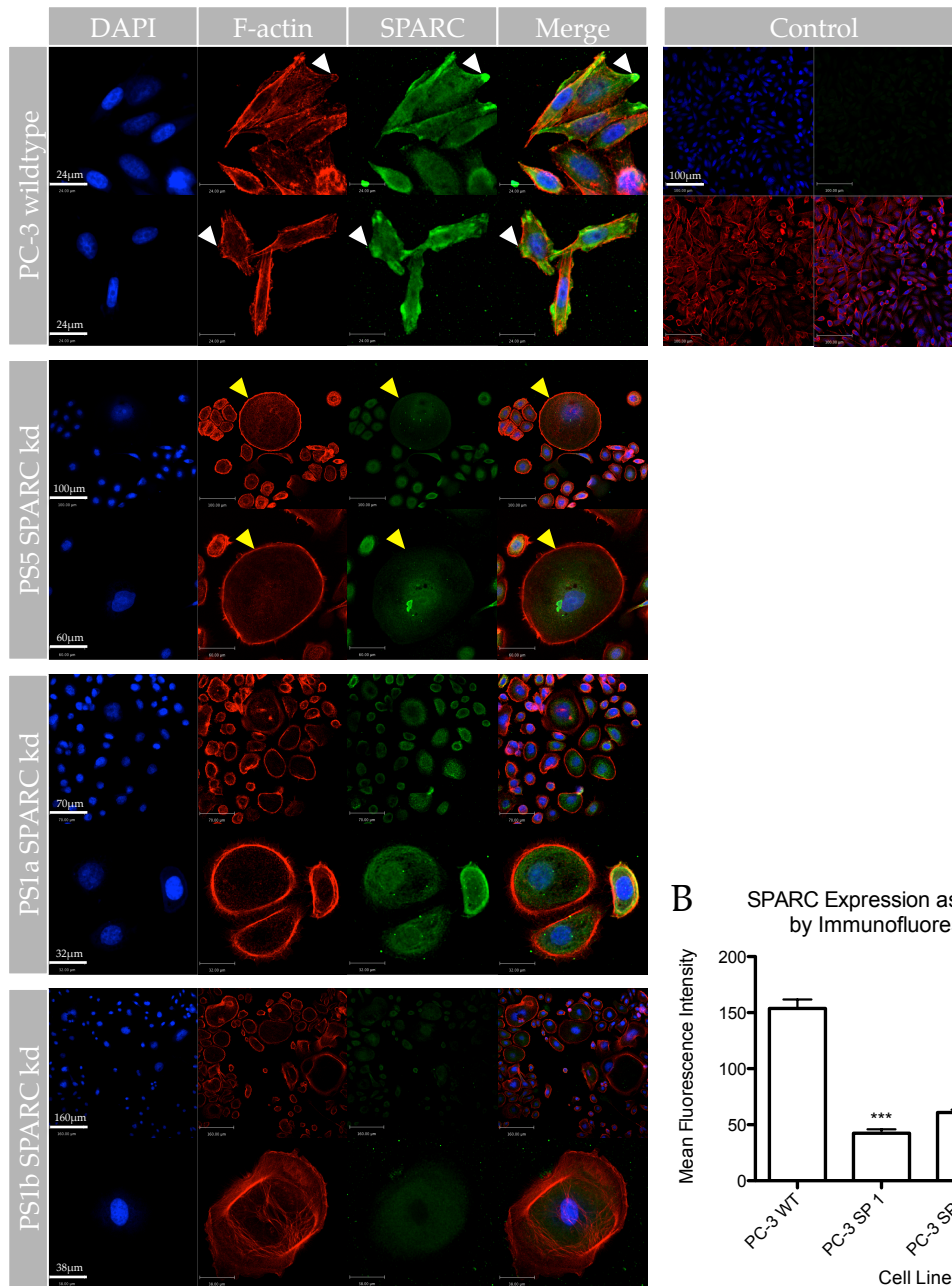
Figure 5.3 SPARC knockdown changes the morphology of PC-3 cells. (A) Panel shows staining for DAPI (blue), f-actin(red) and SPARC (green) for control PC-3 WT cells compared to the three knockdown clones. Control panel shows secondary antibody only staining control. (B) SPARC expression as measured by mean fluorescence intensity. Bars represent mean±SEM, ***p<0.001 (ANOVA with post-hoc Tukey)
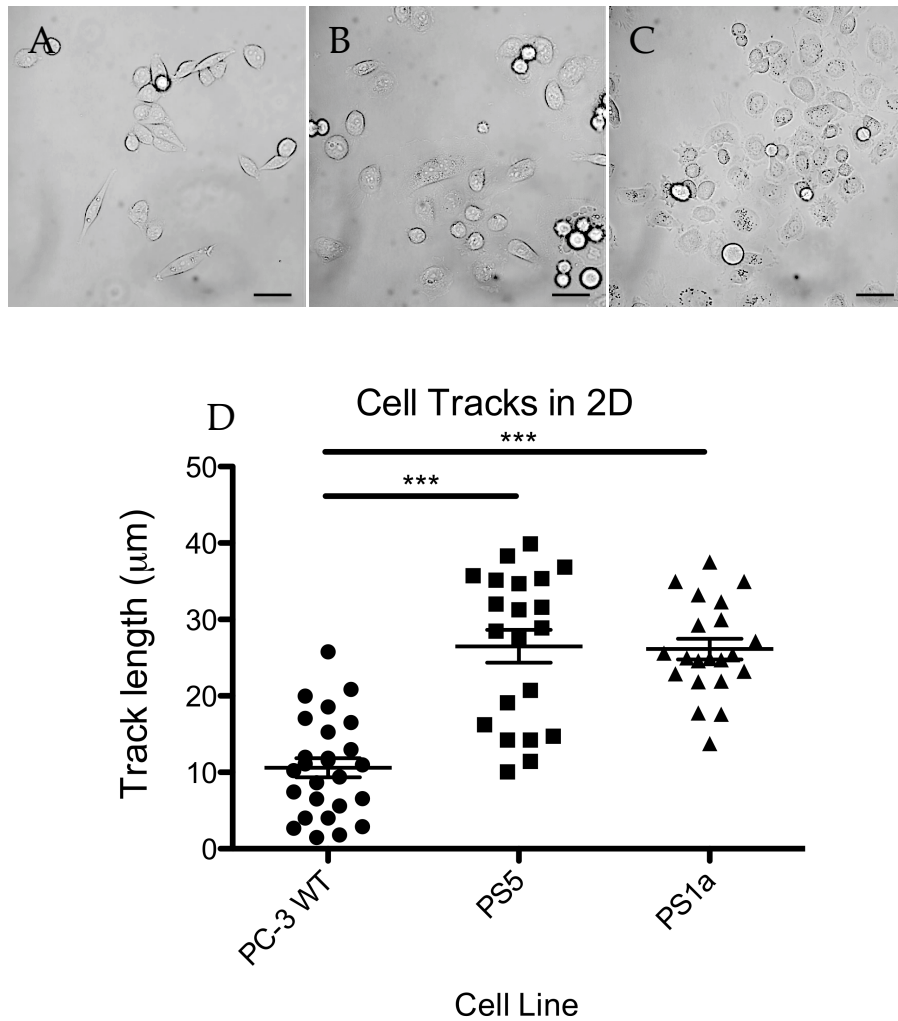
Figure 5.4 SPARC knockdown increases motility of PC-3 cells in 2-D. (A-C)) Representative image of cells (Bar:20µm) from (A) PC-3 WT cells, (B) SPARC shRNA knockdown clone PS5 and (C) PS1a. (D) Cells were tracked individually throughout the time-lapse video and the resulting tracks for both SPARC shRNA knockdown clones were significantly longer than the tracks for PC-3 WT cells. Bars represents mean±SEM, ***p<0.001 (ANOVA with post-hoc Tukey)
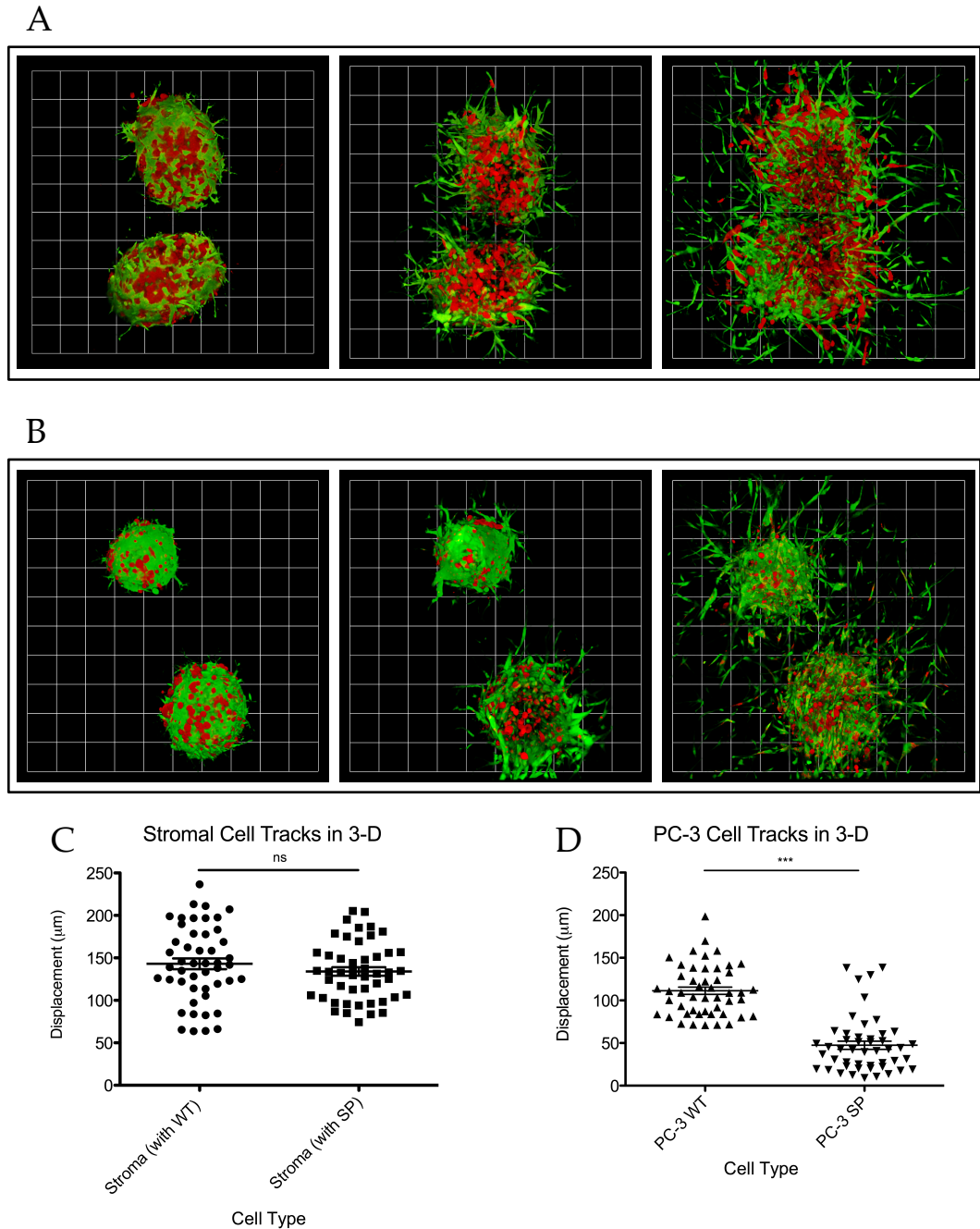
Figure 5.5 SPARC knockdown in PC-3 cells results in decreased migration in 3-D in spheroids containing high Gleason grade stroma. (A) PC-3 WT cells (red) migrate in to the matrix along with the stromal cells (green). Scale unit: 64μm. (B) PC-3 SPARC knockdown cells do not migrate in to the matrix, however the stromal cells exhibit normal migratory behaviour. Scale unit: 64μm. (C) Quantification of cell displacement reveals no difference in the migration of stromal cells in the presence of PC-3 WT or PC-3 SPARC knockdown cells, whereas there is a significant reduction in cell displacement and therefore cell migration, in PC-3 SPARC knockdown cells. Bars represent mean±SEM, ns=not significant, ***p<0.001 (Mann-Whitney).
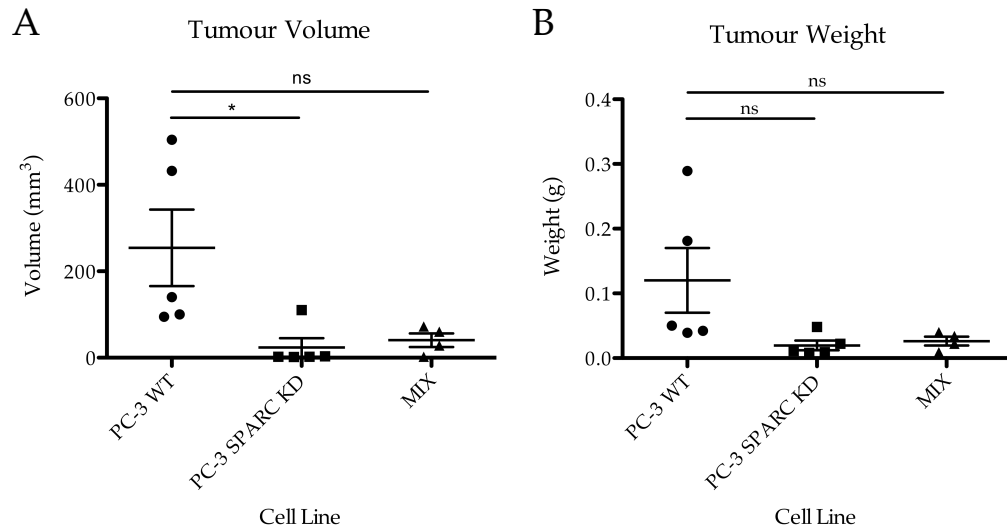
Figure 5.6 *In vivo* tumours of PC-3 SPARC knockdown cells fail to establish. (A) The final volume of tumours resulting from PC-3 SPARC knockdown cells, or a 50:50 mix of PC-3 SPARC knockdown cells and PC-3 WT cells, were both significantly smaller than the tumours resulting from 100% PC-3 WT cells. *p=0.025 (ANOVA with Tukey's post hoc test) (B) The same pattern is observed when measuring the tumours by weight. P=0.076 (ANOVA with Tukey's post hoc test) Bars represent mean±SEM.
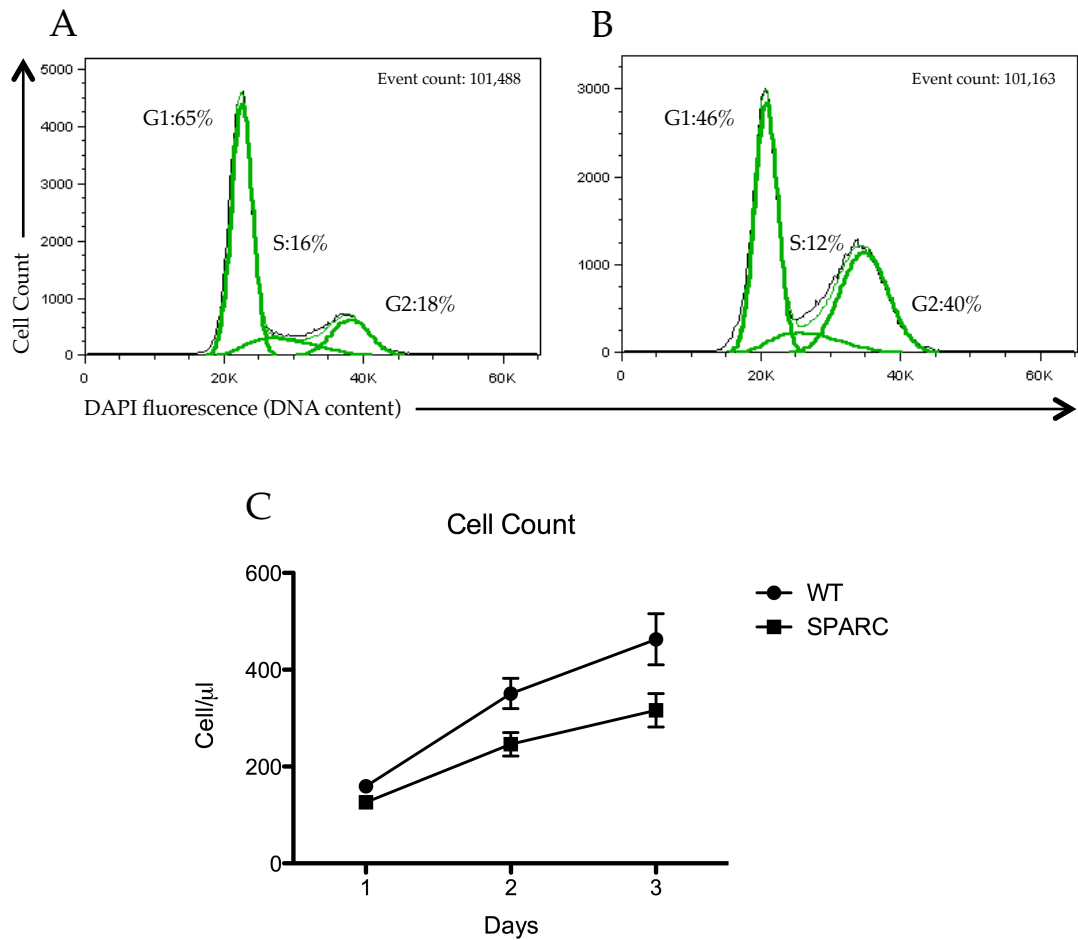
Figure 5.7 PC-3 SPARC knockdown cells are blocked at G2/M but still do proliferate. (A) The cell cycle profile of PC-3 WT cells shows a clear G1 phase for 65% of the population, with 16% and 18% of cells in S phase and G2/M phase respectively. (B) The cell cycle profile for PC-3 SPARC knockdown cells (clone PS5) shows a block at G2/M with 40% of cells now in G2/M, 12% in S phase and 46% in G1 phase. (C) PC-3 SPARC knockdown cells do still proliferate *in vitro* in tissue culture, however, this happens at a slower rate compared to PC-3 WT cells. Points represent mean±SEM, p=0.005 (Mann-Whitney).
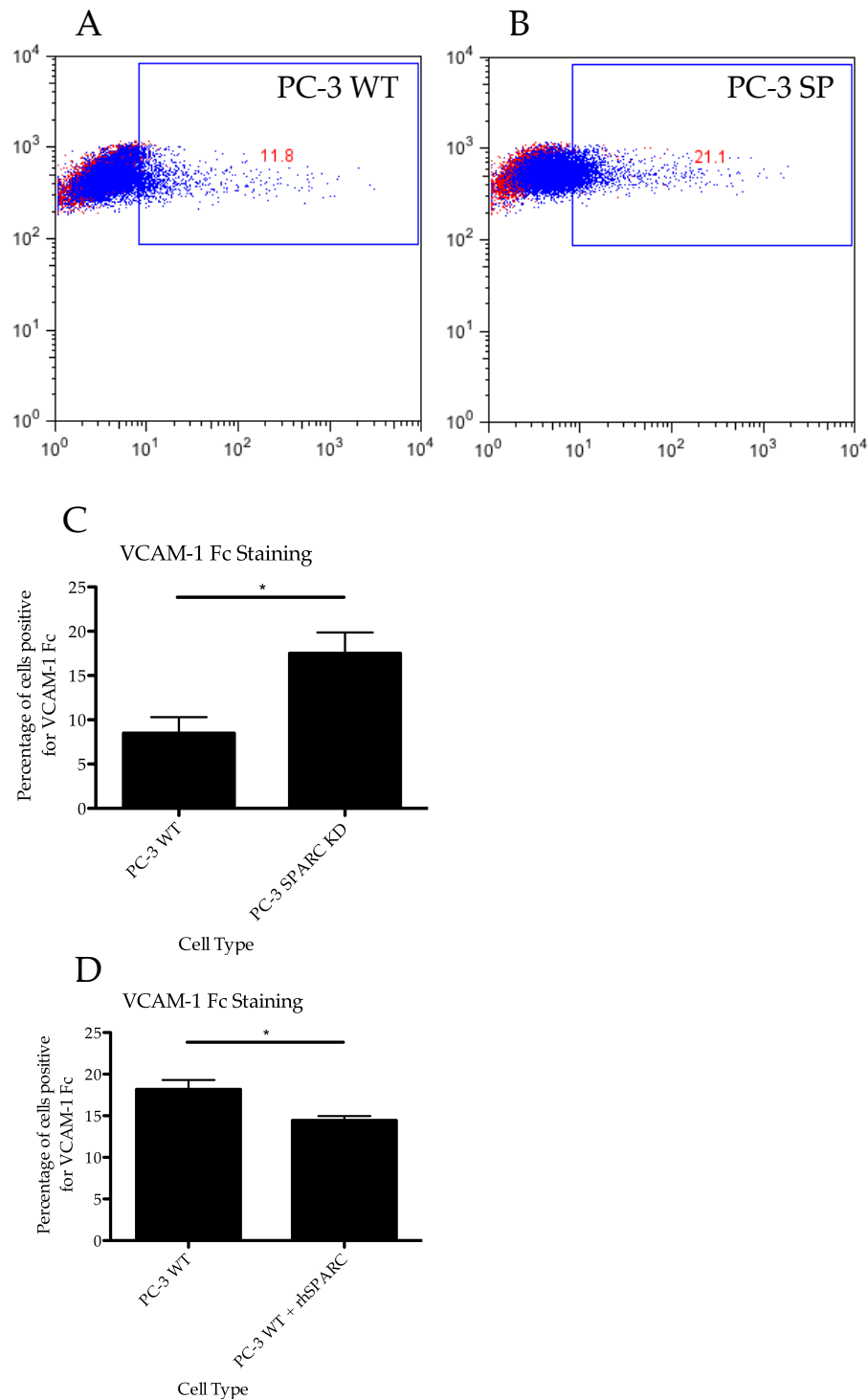
Figure 5.8 VCAM Fc binding of PC-3 WT cells is lower than that of PC-3 SPARC knockdown cells. Representative FACS dot plots showing that (A) 11.8% of PC-3 WT cells bind VCAM Fc protein compared to (B) 21.1% of PC-3 SPARC knockdown cells. Red shows secondary antibody staining control, blue shows VCAM Fc binding (C) Quantifying this over 3 independent experiments shows a significant raise in VCAM Fc binding for PC-3 SPARC knockdown cells. (D) The addition of rhSPARC does block to a lesser extent, the binding of VCAM Fc to wildtype PC-3 cells. Bar represents mean±SEM, *p<0.01 (t test).
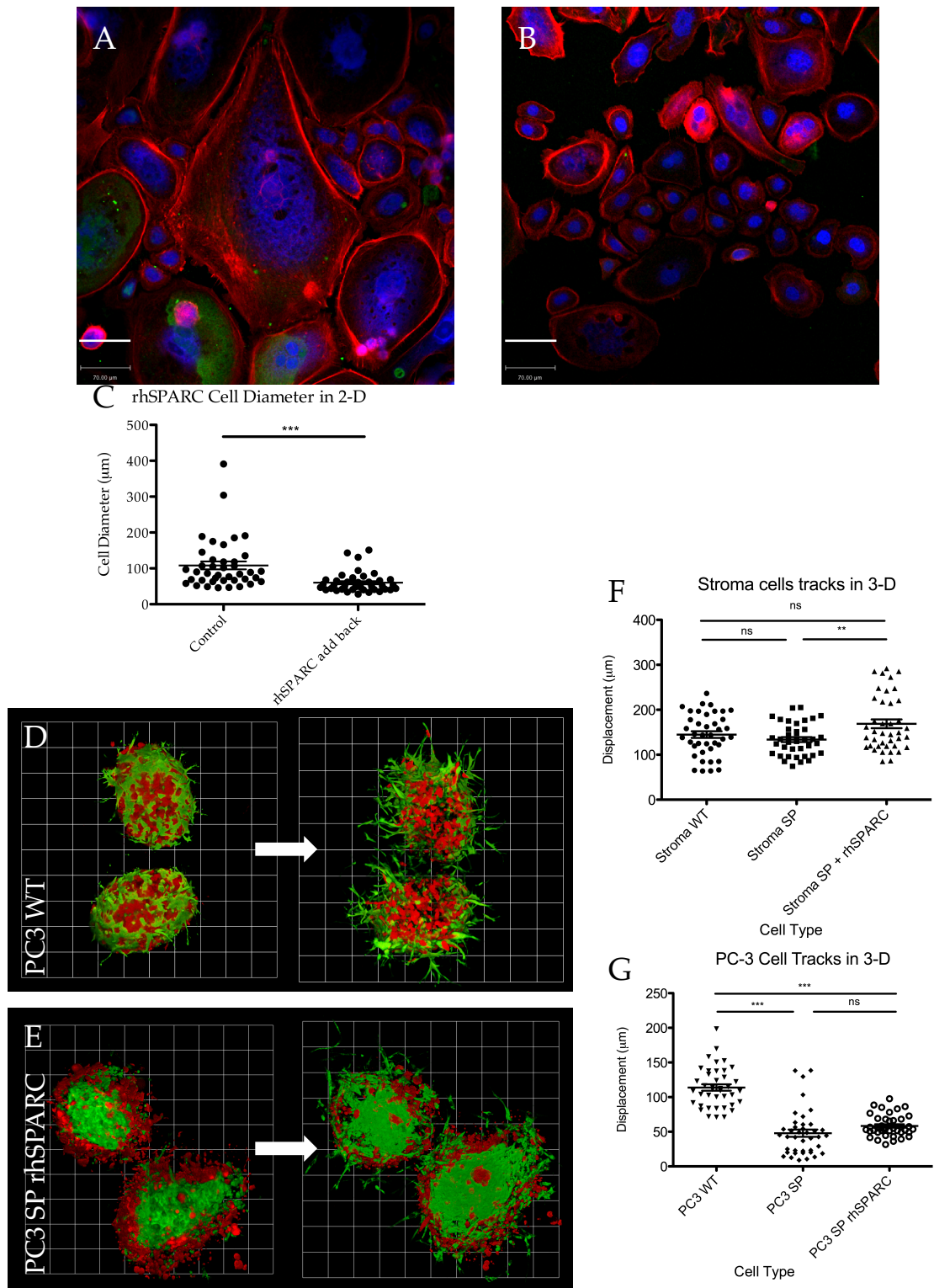
Figure 5.9 rhSPARC partially rescues phenotype of SPARC knockdown PC-3 cells in 2-D & 3-D. (A&B) 2-D IF of (A) PC-3 SPARC knockdown cells (B) PC-3 SPARC knockdown cells grown in the presence of rhSPARC. DAPI (blue) f-actin (red) SPARC (green). (C) Quantification shows a decrease in cell size in the presence of rhSPARC. Bar represents mean±SEM, *p<0.001 (Mann-Whitney). (D&E) 3-D images of spheroids. PC-3 (red) High Gleason stroma (green). (F&G) Quantification of cell displacement shows increased migration of stromal cells in the presence of rhSPARC, and a small but not significant increase in PC-3 SPARC knockdown cell migration in the presence of rhSPARC protein. **p=0.006, ***p<0.001 (ANOVA with Tukey;s post hoc test) (A&B) Bar:70µm (D&E) Scale unit: 64µm
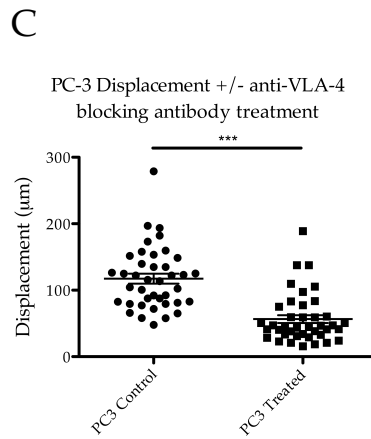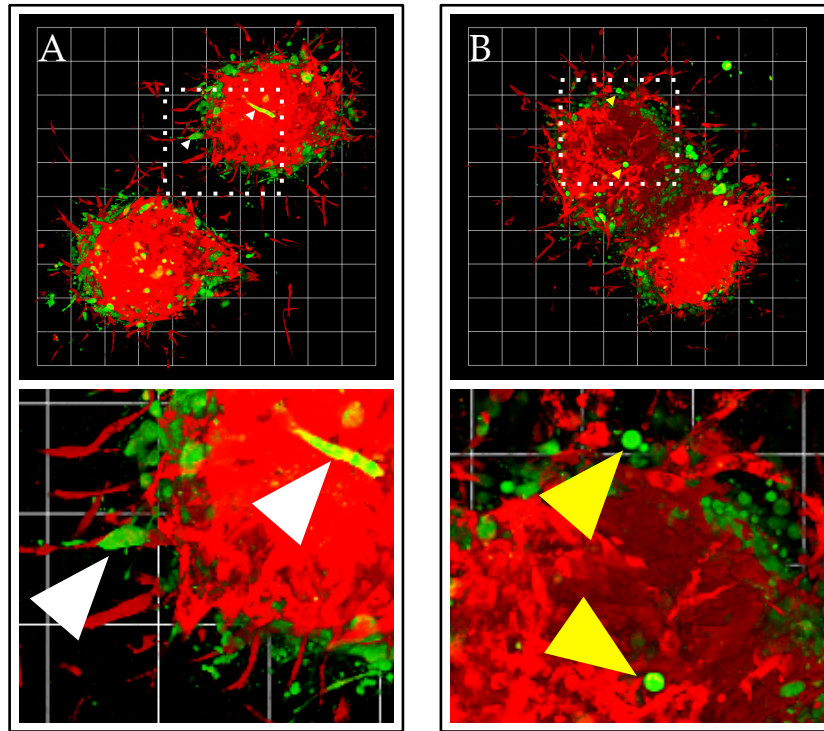
Figure 5.10 Blocking VLA-4 reduced the migration of PC-3 cells in 3-D. (A&B) 3-D imaging of spheroids containing high Gleason stroma (red) and PC-3 WT cells (green) at the end of time-lapse imaging at 48 hours. (A) Control spheroids in normal growth media compared to (B) spheroids in media containing anti-VLA-4 blocking antibody. (C) Quantification of cell displacement shows a significant reduction in cell migration over 48 hours. ***p<0.0001 (Mann-Whitney)

Chapter 6

Final discussion

Although mechanisms involved in cellular transformation and growth are well understood, the molecular and cellular basis leading to secondary metastasis, the major cause of mortality in cancer, is not well understood and is a major medical challenge. Tumour metastasis is a complex process that requires tumour cells to express molecules that permit invasion and migration from the tumour mass into surrounding tissues, lymphatic and blood vessels and subsequent colonisation of peripheral tissue to form secondary tumours (Larkin et al. 2012). A considerable amount of focus has been on changes that occur to tumour cells, including the expression of MMPs that are required for the metastasis process (Nalla et al. 2010; Müller et al. 2010). In this thesis we have focused on the role of stromal cells in the tumour microenvironment and mechanisms of stromal mediated transformed epithelial cell migration.

Role of stromal cells in epithelial cell migration: In vivo, prostate cancer tumour cells grow in a 3-D tumour microenvironment that contains both stroma (tumour fibroblasts, immune infiltrate and endothelial vessels) and normal and transformed epithelium, therefore to understand mechanisms of epithelial migration required development of a novel 3-D stroma-epithelial spheroid culture system that permitted real time imaging of tumour and stromal cell interactions and subsequent migration. Analysis of human prostate cancer cell migratory capacity *in vitro* showed that although migration in 2-D is not dependent on stroma, migration in 3-D is stromal cell dependent. PC-3 cells did not migrate in our 3-D culture model as single dispersed cells either alone, in the presence of a stromal cell monolayer or being cultured in stromal cell conditioned media. While MMP inhibitors increased the migration capacity of the HT-1080 fibrosarcoma cell line that could directly interact with collagen, it had no effect on PC-3 cell migration.

Using the 3-D spheroid tumour co-culture methodology we found that only primary human higher Gleason grade tumour stroma but not BPH stroma has the capacity to promote transformed epithelial cell migration. Additionally the capacity of tumour stroma to induce PC-3 cell migration diminishes over time in culture. Thus the induction of tumour cell migration requires cellular interactions with freshly isolated high Gleason grade stroma, consistent with a change occurring in stromal cells in tumour progression which is progressively lost when the cells are cultured *in vitro* in the absence of exogenous signals found in the tumour microenvironment.

Gene expression analysis of stromal cells by microarray, verified using qRT-PCR and antibody staining revealed a potential role for adhesion molecules VCAM-1 and ICAM-1 and the lymphatic endothelium marker podoplanin in stromal cell function in tumours. Specifically expression of these proteins on tumour stroma correlated with cancer progression. Tumour stroma that had been in culture for six or more passages lost both its migratory capacity and reverted to a BPH like stroma cell phenotype which was characterised by the expression of very low levels of VCAM-1, ICAM-1 and podoplanin. In the future, it would be important to build upon this and to generate a larger more comprehensive dataset of multiple tumours, across different patients and different tumour settings. This would, depending on outcome, strengthen the link between expression of VCAM-1, ICAM-1 and Podoplanin, and the ability of cancer stroma to promote tumour cell invasion.

Potential role of inflammation in prostate cancer cell metastasis: Primary human high Gleason grade tumour stroma has a similar gene expression profile to tertiary lymphoid tissue (TLT) associated with chronic infections and autoimmune disease (Cupedo et al. 2004). TLTs are specialised immunological tissues containing both stroma and leukocytes providing the microenvironment for efficient local adaptive immune responses in situ. Analysis of xenograft tumours showed that although inflammation occurred in the tumour microenvironment including the presence of F4/80^{+} macrophages, CD11c^{hi} dendritic cells and a GR1^{+} neutrophil infiltrate, stromal cells failed to express VCAM-1, ICAM-1 or podoplanin, hallmarks of primary human tumour stroma. To further understand the mechanisms driving expression of these TLT stromal gene expression patterns, C57BL/6

syngenic Lewis lung carcinoma cells were injected subcutaneously into mice with immune deficiencies. Analysis of stromal cells from these mice was consistent with a key role for T lymphocyte subsets in efficient stromal cell induction, consistent with a role for inflammatory cytokines in tumour stroma activation as is found in TLT formation. Primary human tumour stroma that had lost the expression of these adhesion markers could be reactivated by inflammatory cytokines. After 3 days in culture media containing TNF-α, LTβ and IL-4, expression of VCAM-1, ICAM-1 and podoplanin reached expression levels found in early passage high Gleason grade tumour stroma. The rescue of stromal cell gene expression was mirrored by the regain of function in promoting PC-3 cell migration in our 3-D model after stromal treatment with the cytokines.

Whilst we did not sequence the primary stromal cells or investigate the genetic normality, there was no evidence of abnormality or uncontrolled cell growth. There is also no evidence in the literature to suggest that mutations are found in the stroma in carcinomas. However, investigating the genetic makeup of tumour stroma could prove useful for further analyses of the effect of stroma on carcinomas at the genetic level if indeed there are any genetic changes.

SPARC, VLA-4 and VCAM-1; interactions driving prostate tumour cell migration: VCAM-1 has been shown to interact with two proteins that are expressed by PC-3 tumour cells, SPARC and VLA-4. VLA-4 is a heterodimer of the α_4 integrin combined with constitutively expressed β_1 integrin (Alon et al. 1995) and is only expressed on a small percentage of PC-3 cells. SPARC is a secreted protein that can bind both VCAM-1 and ECM and is highly linked to high Gleason grade prostate cancer (R. Thomas et al. 2000). Collagen binding domains exist in the structure of SPARC and once secreted, SPARC has been shown to bind the collagen components of the ECM. However, antibody staining revealed possible intracellular and membrane bound SPARC in PC-3 cells, specifically at putative focal adhesion points. SPARC is expressed by both stromal cells and epithelial cells in tumours leading to additional complexity within the 3-D tumour microenvironment, however it is unclear if stromal cell SPARC has any role in the epithelial cell migration.

To directly determine if VCAM-1 can interact with ligands on tumour cells, the capacity of soluble recombinant human VCAM Fc to bind to PC-3 cells was determined. Similarly with the previously shown expression of VLA-4, VCAM Fc bound only a small population of PC-3 cells. Consistent with a role for soluble SPARC inhibiting this process, an increase in binding was found in SPARC deficient PC-3 cells and a decrease in binding in the presence of exogenous SPARC, directly demonstrating SPARC's role in inhibiting VLA-4-VCAM-1 interactions. Thus the expression of these two ligands might have a role in controlling tumour cell interactions with stroma by regulating the adhesion and de-adhesion process involved in cellular migration.

To further determine the role of these two proteins we used gene knock-down, soluble protein and inhibitor antibodies. SPARC expression was knocked down in PC-3 cells using shRNA. PC-3 clones deficient for SPARC showed altered morphology with the cells taking on a large and rounded shape in 2-D and were spherical in 3-D in contrast to the more mesenchymal phenotype found in control PC-3 cells. Surprisingly despite the increase in PC-3 SPARC knock down cell line's migration in 2-D, in 3-D there was a complete inhibition of PC-3 cell migration, indicating an essential role for SPARC in 3-D tumour cell migration consistent with the elevated levels found in tumour cells. Therefore SPARC production by epithelial cells is required for their migration. The addition of recombinant human (rh) SPARC protein partially restored a wild type phenotype in 2-D and although not significantly, there was a small rescue in 3-D cell migration when growth media was supplemented with rhSPARC in the presence of tumour stroma. Although this did not completely rescue the phenotype this likely resulted from the high affinity binding of SPARC to collagen thus sequestering the majority of the protein in the ECM. To analyse the role of VLA-4 in PC-3 cell migration, an inhibitory antibody, anti-human α_4 (Elan Pharmaceutical), was added to the spheroids. Although no change in stromal cell migration was observed there was a significant change in the migratory potential of PC-3 cells. Additionally the PC-3 cells took on a more rounded phenotype similar to that observed in SPARC deficient clones. Thus both VLA-4 and SPARC have essential roles in PC-3 cell migration in 3-D co-culture tumour microenvironments but not in the 2-D stromal-free migration.

A new model for tumour cell migration: Utilising the 3-D spheroid model combined with gene expression analysis and functional assays we propose that prostate tumour cell invasion of ECM is dependent on the expression of the adhesion molecule VCAM-1 by tumour stroma. Thus we are proposing a new model for how transformed epithelial cells in prostate cancer migrate in the context of the tumour microenvironment. We propose the following model (Figure 6.1):

1) Epithelial cells interact with stroma.
2) Selective binding of VLA-4 to VCAM-1 leads to a specific adhesion.
3) Secretion of SPARC at focal adhesions mediates detachment of VLA-4.
4) New adhesions occurs inducing cell migration.

In this model VLA-4 and VCAM-1 is required for stromal cell mediated adhesion and SPARC competes for binding of VCAM-1 leading to localised de-adhesion. Furthermore that not only is the mesenchymal/lymphocytic gene VLA-4 required for migration, but that SPARC levels are also critical for the correct adhesion and detachment of transformed cells with cancer associated stroma in order to allow successful cell migration. A lack of SPARC leads to tight binding of VCAM-1 to VLA-4 thereby not allowing cell migration. Excess SPARC would inhibit the initial binding, therefore not allowing attachment in order to migrate. Thus tumours that express very high levels of SPARC may have limited capacity to metastasise are consistent with observations that although SPARC expression correlates well with tumour grade and metastasis, very high levels of SPARC expression correlate with a favorable outcome (Figure 6.2).

Does this process occur in vivo: Although we have shown a key role for expression of VCAM-1, VLA-4 and SPARC using an *in vitro* model of human prostate cancer it is entirely possible that the observations made *in vitro* do not correspond with what will occur *in vivo*. We have previously shown that xenogeneic tumour models are unlikely to provide a good model of tumour metastasis as the tumours do not contain reactive tumour stroma which *in vitro* is required for tumour cell migration. Thus we suggest the best models will be prostate tumours that spontaneously arise in mice selectively deficient for PTEN using the prostate specific probasin Cre (S. Wang et al. 2003; Kasper 2005). In these mice metastasis of developing tumours occurs to

secondary tissues within 12 weeks of age (Maddison et al. 2004). Using anti-VLA-4 we would predict that there would be a reduction in micro-metastases to the lung. SPARC^{-/-} TRAMP mice rapidly develop tumours at an accelerated rate (Brekken et al. 2003). This contradicts our data on the role of SPARC in human cell lines and the link between SPARC expression levels in aggressive prostate cancer and the expression of SPARC in many human cancer cell lines (Said et al. 2009). This might result from differences between the phenotype of epithelial cells in the TRAMP model (luminal transformation) compared to those found in human cancers (CSC/Basal) and cell lines. Thus it is possible SPARC has a very different role in luminal cells that lack expression of VLA-4 than it has in transformed CSCs and basal/transit amplifying cells that have a more mesenchymal like phenotype.

Understanding the cell biology of SPARC in tumours: Analysis of SPARC expression was consistent with selective secretion associated with putative focal adhesions based on cytoskeletal staining. To better understand the biology of the focal adhesion we propose that the use of high magnification confocal imaging combined with antibodies against paxillin and other focal adhesion proteins to both PC-3 cells cultured on plastic, and PC-3 cells co-cultured with stromal cells in monolayer cultures. We would like to expand these results combining TEM and SEM analysis of the focal adhesions with florescent imaging. SPARC clearly has other roles in PC-3 cells other than binding to VCAM-1. Loss of SPARC expression leads to changes in focal adhesions points that resemble a mesenchymal like phenotype and takes on an epithelial phenotype. Further characterisation of this process will provide additional insights into mechanisms of action. Focal adhesions are not readily detected *in vivo* because cells are embedded in a 3-D matrix so the role of focal adhesions *in vivo* are unknown, using the spheroid model it should be possible to image with sufficient resolution to start to understand the cell biology in 3-D culture systems. There is strong evidence that focal adhesion proteins, of which there are over 100, are important in tumour metastasis including focal adhesion kinase (FAK), paxillin and zyxin which are linked to metastatic potential *in vivo* (Fraley et al. 2010). Thus it is possible that the processes we observe *in vitro* are occurring within the tumour microenvironment *in vivo*. Through use of frozen sections of high Gleason grade tumours we believe it might be possible to determine if

SPARC expression is localised within primary tumour cells rather than a having uniform distribution.

Is there SPARC-VLA-4-VCAM-1 interactions in tumours: By utilising the same VLA-4 blocking antibody used in the 3-D migration studies, it would be possible to assess the binding of VCAM Fc by PC-3s in the absence of VLA-4. This experiment would strength the model for VCAM-1-VLA-4 dependent cell migration. Another way of investigating this process is to generate mice where floxed integrin α_4 (Itga4) is conditionally deleted using probasin-Cre and crossing the mice to PTEN$^{fl/fl}$ mice to generate mice where both genes can be simultaneously deleted in prostatic epithelium. Itga4 is required for normal embryo development and immune function thus this would provide a specific method to determine the role of VLA-4 in tumour metastasis to the lung and draining lymph node. SPARC has a clear role in cell shape control, focal adhesions, cell cycle regulation and cell migration. We have shown that SPARC has a complicated role in VCAM-1-VLA-4 mediated cell migration through possibly controlling adhesion and detachment between transformed epithelial cells and the associated stroma. There seems to be the need for the correct balance of VCAM-1 adhesion to VLA-4 and the right levels of competition for this interaction by SPARC in order for forward migration via cell attachment and detachment.

Is PC-3 cell migration a model cancer stem cell migration? We have shown that prostate CSCs are highly migratory in the spheroid model, rapidly migrating in a phenotype highly reminiscent of HT-1080 migration. Thus these cells which express high levels of SPARC may have unique potential to migrate. It is unclear if the highly migratory cells we observed in PC-3 cells upon stromal cell interactions represent a small population of stem-like cells within the PC-3 cell culture. At this stage we do not know if the migration of the stem cells was dependent on VCAM-1-VLA-4-SPARC interactions, or if primary CSCs can migrate in a stromal independent mechanism.

Understanding the dark and light of anti-tumour immune responses: Interestingly there is a direct link between the anti-tumour immune response and the formation of reactive stroma in advanced cancers. Activated stromal cells usually form into TLOs at sites of chronic infection and inflammation

stimulating high affinity immune response in the local site of persistent inflammation (Cupedo et al. 2004). Anti-tumour immune responses have been known to have a key role in controlling cancer growth and metastasis, consistent with our observations that in the absence of immune responses increased tumour volume in LL/2 tumours was observed. Recently it has been shown that in clinical studies in humans with very advanced stage tumours that monoclonal antibody therapies directed against the inhibitory receptors cytotoxic T lymphocyte-associated antigen 4 (CTLA-4) and programmed death 1 (PD-1) expressed by activated T cells can lead to spontaneous tumour clearance in 10-30% of the patients consistent with the an active but unproductive immune response on-going in the patients (Schneider et al. 2006; Brahmer et al. 2012; Danielli et al. 2012). The presence of TLOs in cancer has been associated with poor prognosis and as shown in this project, the effect of T cell mediated inflammation acts to induce stromal cell-dependent cancer epithelial cell migration. Thus the linkage between poor prognosis and TLOs containing activated stroma, in the absence of a productive immune response, means that inflammation perpetuates at the tumour site. This in turn drives stromal cell activation leading to an environment that permits tumour cell invasion of the stromal compartment and into secondary sites. Thus a proportion of patients with high grade prostate tumours might benefit from inhibiting VLA-4 function, reducing the risk of secondary prostate metastasis to the bone or lymph node. Anti-human α_4 integrin, Natalizumab (Tysabri), is a clinically approved treatment for the treatment of advanced multiple sclerosis thus in the future it might be possible to repurpose Natalizumab for the treatment of high Gleason grade tumours.

Role of mesenchyme in secondary metastasis: Metastatic prostate tumour cells commonly form secondary tumours in the bone and lymph nodes, both sites that contain lymphoid stromal cells (Josson et al. 2010). These cells provide not only the chemokines to drive tumour cell recruitment but also provide growth factors and adhesion molecules permitting tumour adhesion and colonisation including VCAM-1, ICAM-1, and podoplanin all found expressed in the reactive stroma of the parental tumour. Mesenchymal stromal cell lines including the bone marrow stromal cell (BMSC) line and mesenchymal stromal cells (MSCs) will allow for *in vitro* and *in vivo* studies

of stromal specific genes. In preliminary studies using adipose derived stem cells we have shown that treatment with the inflammatory cytokines not only drives expression of lymphoid expression profile but also induced the rapid migratory capacity in PC-3 cells. Using siRNA/shRNA and overexpression vectors, it will be possible to study the role of these genes in tumour growth and migration potentially through the selective targeting of gene expression in stromal cells.

Parallels to other epithelial tumours: Although all the data we have collected is specific for prostate stroma and epithelium we believe that other tumours may use similar mechanisms in their migration and metastasis. In order to investigate whether the results are specific to prostate cancer it will be interesting to investigate the properties of other tumour stroma and cancer cell lines/primary tumour cells from other organs including lung, breast of colon. This might including creating spheroids with breast cancer associated stroma coupled with MCF7 or MDA-MB-231 breast cancer cell lines for example.

Alternative targets for the therapy of metastatic disease: In this thesis we have focused on the VCAM-1 role in tumour cell migration. We found that both ICAM-1 and podoplanin expression strongly correlates with VCAM-1 in activated stromal cells. The role for podoplanin in tumours is complex as podoplanin expression has been linked to both poor and favourable outcomes in different types cancers. CLEC-2 has been shown to be an important ligand for podoplanin and has a role in dendritic cell migration on secondary lymphoid stroma (Acton et al. 2012). CD44 is a glycoprotein that can bind to both SPARC and podoplanin (Martín-Villar et al. 2010), and variants in CD44 (CD44v) has been correlated with progressive tumour stages in colorectal carcinomas (Wimmenauer et al. 1997). Podoplanin directly associates with CD44 on squamous stratified epithelial cells to drive directional tumour cell migration (Martín-Villar et al. 2010). Thus a complex interplay between gene expression on stroma and epithelium in prostate cancer through podoplanin, VCAM-1 and ICAM-1 with CD44, SPARC and VLA-4 may be key signals driving prostate tumour cell migration.

Conclusion

In summary, the data presented in this thesis reveals a key role for stroma mediated transformed cell migration, within an inflammatory environment created by TLT in activated stroma. Although perhaps contradictory at first, the presence of TLT in tumour stroma being poor for prognosis, the results shown here partly explain how the activation of an immune response in prostate cancer, can lead to a chronic T lymphocyte reaction. However, the tumour is unresponsive and indeed the large number of lymphocytes which provide high levels of inflammatory cytokines, causes the development of TLT in tumour stroma. Clinical trials with blocking antibodies, such as CTLA-4 which blocks T cell inhibitory signals allowing T cell activation, would not therefore work without TLT acting as a T cell source. However, assuming T cell activation once the inhibitory signals have been lifted, an increase in the level of inflammatory cytokines can occur, which as these results show can induce tumour cell migration and metastasis via a VCAM-1-VLA-4 dependent process possibly mediated by SPARC expression levels.
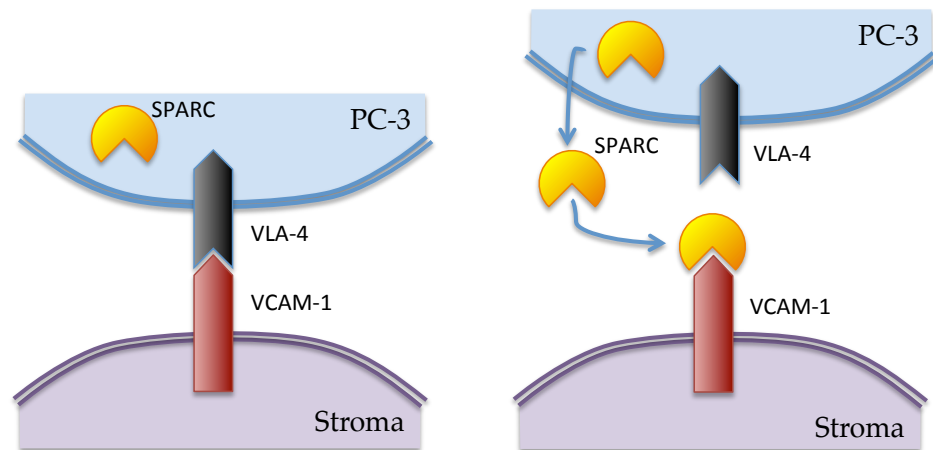
Figure 6.1 Prostate cancer epithelial cells have a complex interaction with the tumour stroma. VCAM-1 expressed by stromal cells binds VLA-4 on the surface of PC-3 cells leading to cell attachment. SPARC, expressed by the transformed cells, interferes with the interplay between VCAM-1 and VLA-4 by binding VCAM-1 thereby blocking VCAM-1-VLA-4 interaction which therefore allows detachment of both cells from each other leading to cell migration.
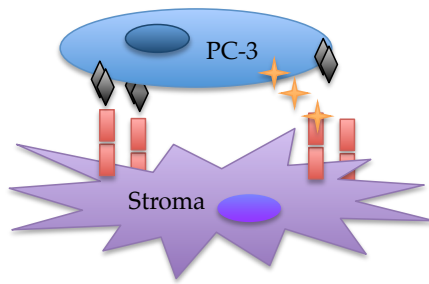
High Gleason Grade Tumour Stroma
Rapid tumour cell migration of $\beta 1^+$ tumour cells.
Membrane-bound VLA-4 induces attached SPARC secreted at focal points of adhesion.
Allows rapid attachment and detachment on stromal cells.
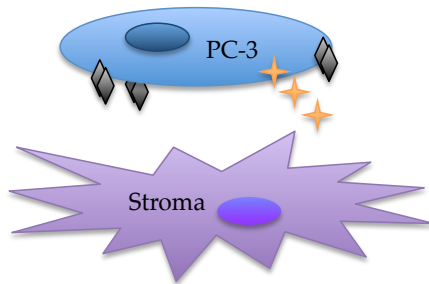
Low Gleason Grade Tumour Stroma
Low to no expression of VCAM-1 on stromal cells prohibits adherence between stroma and tumour cell.
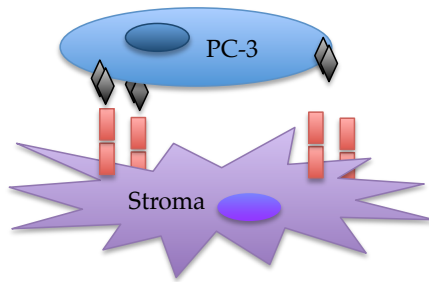
High Gleason Grade Tumour Stroma No SPARC
SPARC is not available to outcompete VLA-4 for VCAM-1 binding.
No detachment of cancer cells from stromal cells therefore no migration.
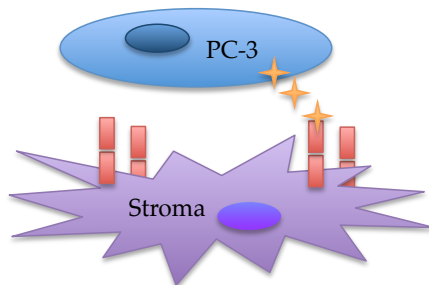
High Gleason Grade Tumour Stroma No VLA-4
Blocking VLA-4 prohibits binding of cancer cells to stromal VCAM-1 .
No attachment, SPARC made redundant, therefore no migration.

VCAM-1   VLA-4   SPARC

Figure 6.2 A proposed model for VCAM-1 – VLA-4 – SPARC interactions in tumour stroma mediated prostate cancer epithelial cell migration.

Abbreviations

1°	Primary
2°	Secondary
2-D	Two-dimensional
3-D	Three-dimensional
γc	Common gamma chain
μg	Microgram
μl	Microlitre
μm	Micrometer
μM	Micromolar
Ab	Antibody
AF	Alexafluor
APC	Antigen presenting cell
AR	Androgen receptor
ASPN	Asporin
bFGF	Basic fibroblast growth factor
Bio	Biotin
BM	Basement membrane
BPH	Benign prostatic hyperplasia
BSA	Bovine Serum Albumin
BSF	Biological Services Facility
C	Centigrade
CAF	Cancer associated fibroblast
CaP	Cancer of the prostate
CAV1	Caveolin-1
CCL/CXCL	Chemokine ligand
CCR/CXCR	Chemokine receptor
CD	Cluster of differentiation
cDNA	Complementary deoxyribonucleic acid
CFSE	Carboxyfluorescein diacetate, succinimidyl ester
CIC	Cancer initiating cell
CLEC-2	C-type lectin receptor-2
CMFDA	5-Chloromethylfluorescein Diacetate
CMTPX	$C_{42}H_{40}ClN_3O_4$
CMV	Cytomegalovirus
CO_2	Carbon dioxide

CSC	Cancer stem cell
CTLA-4	Cytotoxic T lymphocyte-associated antigen 4
CZ	Central zone
DAPI	4',6-diamidino-2-phenylindole
DC	Dendritic cell
DEPC	Diethylpyrocarbonate
dH_2O	Distilled water
DHT	Dihydrotestosterone
DMEM	Dulbecco's modified eagle medium
DMSO	Dimethyl sulfoxide
DNA	Deoxyribonucleic acid
DPBS	Dulbecco's phosphate buffered saline solution
DSB	Double stranded break
DTT	Dithiothreitol
EAE	Experimental autoimmune encephalomyelitis
ECM	Extracellular matrix
EDTA	Ethylenediamenetetraacetic acid
EHS	Engelbreth-Holm Swan
EMT	Epithelial-mesenchymal transition
EpCAM	Epithelial cell adhesion molecule
ERα	Estrogen receptor-alpha
ERβ	Estrogen receptor-beta
EtOH	Ethanol
FACS	Fluorescence activated cell sorting
FBS	Fetal bovine serum
FC	Flow cytometry
FCS	Fetal calf serum
FDA	Food and drugs administration
FDC	Follicular dendritic cell
FGF	Fibroblast growth factor
FITC	Fluorescein isothiocyanate
FL1-9	Fluorescence detectors
FLIM	Fluorescence lifetime imaging microscopy
FNBL1	Fibulin-1
FRC	Fibroblastic reticular cell
FSC	Forward scatter
g	Grams

g	g-force
GaAsP	Gallium arsenide phosphide
GFP	Green fluorescent protein
Gt	Goat
GP38	Glycoprotein 38 (mouse podoplanin)
GP36	Glycoprotein 36 (human podoplanin)
HAMS-F12	Hams nutrient mixture F12
H&E	Hematoxylin and eosin
HEV	High endothelial venule
HFF	Human foreskin fibroblast
HLA	Human leukocyte antigen
Hoechst 33342	2-(4-ethoxyphenyl)-5-(4-methyl-1-piperazinyl)-2,5-bi-lH-benzimidazole
Hu	Human
ICAM-1	Intercellular adhesion molecule-1
Ig	Immunoglobulin
IH	Immunohistochemistry
IL	Interleukin
ILC	Innate lymphoid cell
IPTG	Isopropyl β-D-1-thiogalactopyranoside
kD	Kilo Dalton
KO	Knock-out
KSFM	Keratinocyte serum-free medium
LB	Luria broth
LN	Lymph node
LN_2	Liquid nitrogen
LSM	Laser scanning microscopy
LT-α	Lymphotoxin alpha
LTi	Lymphoid tissue inducer
M	Molar
mAb	Monoclonal antibody
MACS	Magnetic cell sorting
MDM2	Murine double mutant 2
MEM	Minimal essential medium
MEF	Mouse embryonic fibroblast
MFI	Mean fluorescence intensity
mg	Milligram

MHC	Major histonecompatibility complex
min	Minutes
ml	Millilitre
mM	Millimolar
MMP	Matric metalloproteinase
MΦ	Macrophage
MP-LSM	Multiphoton laser scanning microscopy
mRNA	Messenger ribonucleic acid
ms	Millisecond
Ms	Mouse
NADH	Nicotinamide adenine dinucleotide (reduced)
NDD	Non-descanned detector
ng	Nanogram
NK	Natural killer cells
NOD	Nonobese diabetic
OCT	Optimal cutting temperature
PB	Pacific blue
PBS	Phosphate buffered saline
PCR	Polymerase chain reaction
PCS	Prostate cancer stem
PD-1	Programmed death 1
PDGF	Platelet derived growth factor
PDPN	Podoplanin
PE	Phycoertherin
PEI	Poly(ethylenimine)
PerCP	Peridinim chlorophyll protein
PFA	Paraformaldehyde
PKD1	Protein kinase D1
PSA	Prostate specific antigen
PZ	Peripheral zone
RAG1	Recombination activating gene 1
RAG2	Recombination activating gene 2
Rb	Rabbit
RIN	RNA integrity number
ROI	Region of interest
RT	Room temperature
RT-PCR	Real time-polymerase chain reaction

SCID	Severe combined immunodeficiency
secs	Seconds
SEM	Scanning electron microscopy
SHG	Second harmonic generation
shRNA	Short hairpin ribonucleic acid
SNP	Single nucleotide polymorphism
SPARC	Secreted protein acidic and rich in cysteine
SSc	Side scatter
SSC	Squamous cell carcinoma
TCR	T cell receptor
TEM	Transmission electron microscopy
TGF-β	Transforming growth factor beta
TLO	Tertiary lymphoid organ
TLT	Tertiary lymphoid tissue
TNF-α	Tumour necrosis factor alpha
TRAMP	Transgenic adenocarcinoma of the mouse prostate
TSP-1	Thrombospondin-1
TZ	Transition zone
UoY	University of York
UTR	Untranslated region
UV	Ultraviolet
v	Volt
VCAM-1	Vascular cell adhesion molecule-1
VEG-F	Vascular endothelial growth factor
VEGFR	Vascular endothelial growth factor receptor
VLA-4	Very late antigen-4
WT	Wild type
YO-PRO	YO-PRO®-1 Iodide $C_{24}H_{29}I_2N_3O$

Bibliography

Abate-Shen, C. & Shen, M.M., 2007. FGF signaling in prostate tumorigenesis--new insights into epithelial-stromal interactions. *Cancer cell*, 12(6), pp.495–497.

Abdulghani, J. et al., 2008. Stat3 promotes metastatic progression of prostate cancer. *The American journal of pathology*, 172(6), pp.1717–1728.

Abdulkadir, S.A. et al., 2002. Conditional loss of Nkx3.1 in adult mice induces prostatic intraepithelial neoplasia. *Molecular and cellular biology*, 22(5), pp.1495–1503.

Aboseif, S.R. et al., 1997. Effect of retinoic acid on prostatic development. *The Prostate*, 31(3), pp.161–167.

Acton, S.E. et al., 2012. Podoplanin-Rich Stromal Networks Induce Dendritic Cell Motility via Activation of the C-type Lectin Receptor CLEC-2. *Immunity*, 37(2), pp.276–289.

Adams, J.M. et al., 1985. The c-myc oncogene driven by immunoglobulin enhancers induces lymphoid malignancy in transgenic mice. *Nature*, 318(6046), pp.533–538.

Ahuja, D., Sáenz-Robles, M.T. & Pipas, J.M., 2005. SV40 large T antigen targets multiple cellular pathways to elicit cellular transformation. *Oncogene*, 24(52), pp.7729–7745.

Alimirah, F. et al., 2006. DU-145 and PC-3 human prostate cancer cell lines express androgen receptor: implications for the androgen receptor functions and regulation. *FEBS letters*, 580(9), pp.2294–2300.

Alon, R. et al., 1995. The integrin VLA-4 supports tethering and rolling in flow on VCAM-1. *The Journal of cell biology*, 128(6), pp.1243–1253.

Armstrong, P.B., Quigley, J.P. & Sidebottom, E., 1982. Transepithelial invasion and intramesenchymal infiltration of the chick embryo chorioallantois by tumor cell lines. *Cancer research*, 42(5), pp.1826–1837.

Aszódi, A. et al., 2006. What mouse mutants teach us about extracellular matrix function. *Annual review of cell and developmental biology*, 22, pp.591–621.

Atorrasagasti, C. et al., 2010. Overexpression of SPARC obliterates the in vivo tumorigenicity of human hepatocellular carcinoma cells. *International journal of cancer Journal international du cancer*, 126(11), pp.2726–2740.

Aumailley, M. et al., 2005. A simplified laminin nomenclature. *Matrix biology : journal of the International Society for Matrix Biology*, 24(5), pp.326–332.

Bajénoff, M. et al., 2007. Highways, byways and breadcrumbs: directing lymphocyte traffic in the lymph node. *Trends in immunology*, 28(8), pp.346–352.

Bakker, G.-J. et al., 2012. Fluorescence lifetime microscopy of tumor cell invasion, drug delivery, and cytotoxicity. *Methods in enzymology*, 504, pp.109–125.

Bartek, J., Hamerlik, P. & Lukas, J., 2010. On the origin of prostate fusion oncogenes. *Nature genetics*, 42(8), pp.647–648.

Beattie, L. et al., 2010. Dynamic imaging of experimental Leishmania donovani-induced hepatic granulomas detects Kupffer cell-restricted antigen presentation to antigen-specific CD8 T cells. *PLoS pathogens*, 6(3), p.e1000805.

Beattie, L. et al., 2011. Interferon regulatory factor 7 contributes to the control of Leishmania donovani in the mouse liver. *Infection and immunity*, 79(3), pp.1057–1066.

Becker, W., 2012. Fluorescence lifetime imaging - techniques and applications. *Journal of microscopy*, 247(2), pp.119–136.

Bendik, I., Schraml, P. & Ludwig, C.U., 1998. Characterization of MAST9/Hevin, a SPARC-like protein, that is down-regulated in non-small cell lung cancer. *Cancer research*, 58(4), pp.626–629.

Bergomas, F. et al., 2011. Tertiary Intratumor Lymphoid Tissue in Colo-Rectal Cancer. *Cancers*, 4, pp.1–10.

Berry, P.A., Maitland, N.J. & Collins, A.T., 2008. Androgen receptor signalling in prostate: effects of stromal factors on normal and cancer stem cells. *Molecular and cellular endocrinology*, 288(1-2), pp.30–37.

Bethel, C.R. & Bieberich, C.J., 2007. Loss of Nkx3.1 expression in the transgenic adenocarcinoma of mouse prostate model. *The Prostate*, 67(16), pp.1740–1750.

Bhowmick, N.A., Neilson, E.G. & Moses, H.L., 2004. Stromal fibroblasts in cancer initiation and progression. *Nature*, 432(7015), pp.332–337.

Bilozur, M.E. & Hay, E.D., 1988. Neural crest migration in 3D extracellular matrix utilizes laminin, fibronectin, or collagen. *Developmental biology*, 125(1), pp.19–33.

Bird, D.K. et al., 2005. Metabolic mapping of MCF10A human breast cells via multiphoton fluorescence lifetime imaging of the coenzyme NADH. *Cancer research*, 65(19), pp.8766–8773.

Birnie, R. et al., 2008. Gene expression profiling of human prostate cancer stem cells reveals a pro-inflammatory phenotype and the importance of extracellular matrix interactions. *Genome biology*, 9(5), p.R83.

Bissell, M.J. & Radisky, D., 2001. Putting tumours in context. *Nature reviews Cancer*, 1(1), pp.46–54.

Boisvert, M. et al., 2010. Alpha2beta1 integrin is the major collagen-binding integrin expressed on human Th17 cells. *European journal of immunology*, 40(10), pp.2710–2719.

Bollrath, J. & Greten, F., 2009. IKK/NF-kappaB and STAT3 pathways: central signalling hubs in inflammation-mediated tumour promotion and metastasis. *EMBO reports*.

Bonaccorsi, L. et al., 2000. Androgen receptor expression in prostate carcinoma cells suppresses alpha6beta4 integrin-mediated invasive phenotype. *Endocrinology*, 141(9), pp.3172–3182.

Bonkhoff, H. & Berges, R., 2009. The evolving role of oestrogens and their receptors in the development and progression of prostate cancer. *European urology*, 55(3), pp.533–542.

Bowen, C. et al., 2000. Loss of NKX3.1 expression in human prostate cancers correlates with tumor progression. *Cancer research*, 60(21), pp.6111–6115.

Bradshaw, A.D. et al., 1999. Primary mesenchymal cells isolated from SPARC-null mice exhibit altered morphology and rates of proliferation. *Molecular biology of the cell*, 10(5), pp.1569–1579.

Bradshaw, A.D. et al., 2003. SPARC-null mice exhibit increased adiposity without significant differences in overall body weight. *Proceedings of the National Academy of Sciences of the United States of America*, 100(10), pp.6045–6050.

Bradshaw, A.D., Reed, M.J. & Sage, E.H., 2002. SPARC-null mice exhibit accelerated cutaneous wound closure. *The journal of histochemistry and cytochemistry : official journal of the Histochemistry Society*, 50(1), pp.1–10.

Brahmer, J.R. et al., 2012. Safety and activity of anti-PD-L1 antibody in patients with advanced cancer. *The New England journal of medicine*, 366(26), pp.2455–2465.

Brekken, R.A. et al., 2003. Enhanced growth of tumors in SPARC null mice is associated with changes in the ECM. *The Journal of clinical investigation*, 111(4), pp.487–495.

Brinster, R.L. et al., 1984. Transgenic mice harboring SV40 T-antigen genes develop characteristic brain tumors. *Cell*, 37(2), pp.367–379.

Brown, T.J. et al., 1999. Activation of SPARC expression in reactive stroma associated with human epithelial ovarian cancer. *Gynecologic oncology*, 75(1), pp.25–33.

Campagnola, P.J. et al., 2002. Three-dimensional high-resolution second-harmonic generation imaging of endogenous structural proteins in biological tissues. *Biophysical journal*, 82(1 Pt 1), pp.493–508.

Cao, Q. et al., 2008. Repression of E-cadherin by the polycomb group protein EZH2 in cancer. *Oncogene*, 27(58), pp.7274–7284.

Carducci, M.A. & Jimeno, A., 2006. Targeting bone metastasis in prostate cancer with endothelin receptor antagonists. *Clinical cancer research : an official journal of the American Association for Cancer Research*, 12(20 Pt 2), pp.6296s–6300s.

Chang, R.T.M., Kirby, R. & Challacombe, B.J., 2012. Is there a link between BPH and prostate cancer? *The Practitioner*, 256(1750), pp.13–6– 2.

Chen, N. et al., 2007. A secreted isoform of ErbB3 promotes osteonectin expression in bone and enhances the invasiveness of prostate cancer cells. *Cancer research*, 67(14), pp.6544–6548.

Chen, Z. et al., 2005. Crucial role of p53-dependent cellular senescence in suppression of Pten-deficient tumorigenesis. *Nature*, 436(7051), pp.725–730.

Chew, A. et al., 2011. SPARC, FOXP3, CD8 and CD45 correlation with disease recurrence and long-term disease-free survival in colorectal cancer. *PloS one*, 6(7), p.e22047.

Chhabra, E.S. & Higgs, H.N., 2007. The many faces of actin: matching assembly factors with cellular structures. *Nature cell biology*, 9(10), pp.1110–1121.

Chlenski, A. et al., 2001. Androgen receptor expression in androgen-independent prostate cancer cell lines. *The Prostate*, 47(1), pp.66–75.

Chtanova, T. et al., 2008. Dynamics of neutrophil migration in lymph nodes during infection. *Immunity*, 29(3), pp.487–496.

Chuang, W.-Y. et al., 2009. Tumor cell expression of podoplanin correlates with nodal metastasis in esophageal squamous cell carcinoma. *Histology and histopathology*, 24(8), pp.1021–1027.

Collins, A.T. et al., 2005. Prospective identification of tumorigenic prostate cancer stem cells. *Cancer research*, 65(23), pp.10946–10951.

Colombel, M.C. & Buttyan, R., 1995. Hormonal control of apoptosis: the rat prostate gland as a model system. *Methods in cell biology*, 46, pp.369–385.

Conley-LaComb, M.K. et al., 2012. PTEN regulates PDGF ligand switch for β-PDGFR signaling in prostate cancer. *The American journal of pathology*, 180(3), pp.1017–1027.

Coronella-Wood, J.A. & Hersh, E.M., 2003. Naturally occurring B-cell responses to breast cancer. *Cancer immunology, immunotherapy : CII*, 52(12), pp.715–738.

Coussens, L.M., Fingleton, B. & Matrisian, L.M., 2002. Matrix metalloproteinase inhibitors and cancer: trials and tribulations. *Science (New York, NY)*, 295(5564), pp.2387–2392.

Cunha, G.R., 1994. Role of mesenchymal-epithelial interactions in normal and abnormal development of the mammary gland and prostate. *Cancer*, 74(3 Suppl), pp.1030–1044.

Cunha, G.R. et al., 1987. The endocrinology and developmental biology of the prostate. *Endocrine reviews*, 8(3), pp.338–362.

Cupedo, T. et al., 2009. Human fetal lymphoid tissue-inducer cells are interleukin 17-producing precursors to RORC+ CD127+ natural killer-like cells. *Nature immunology*, 10(1), pp.66–74.

Cupedo, T. et al., 2004. Induction of secondary and tertiary lymphoid structures in the skin. *Immunity*, 21(5), pp.655–667.

Cybulsky, M.I. et al., 1991. Alternative splicing of human VCAM-1 in activated vascular endothelium. *The American journal of pathology*, 138(4), pp.815–820.

Danielli, R. et al., 2012. Ipilimumab in pretreated patients with metastatic uveal melanoma: safety and clinical efficacy. *Cancer immunology, immunotherapy : CII*, 61(1), pp.41–48.

Davis, G.E. & Senger, D.R., 2005. Endothelial extracellular matrix: biosynthesis, remodeling, and functions during vascular morphogenesis and neovessel stabilization. *Circulation research*, 97(11), pp.1093–1107.

De Marzo, A.M. et al., 1999. Proliferative inflammatory atrophy of the prostate: implications for prostatic carcinogenesis. *The American journal of pathology*, 155(6), pp.1985–1992.

De Wever, O. & Mareel, M., 2003. Role of tissue stroma in cancer cell invasion. *The Journal of pathology*, 200(4), pp.429–447.

Decaestecker, C. et al., 2007. Can anti-migratory drugs be screened in vitro? A review of 2D and 3D assays for the quantitative analysis of cell migration. *Medicinal research reviews*, 27(2), pp.149–176.

Defresne, F. et al., 2011. Preconditioned endothelial progenitor cells reduce formation of melanoma metastases through SPARC-driven cell-cell interactions and endocytosis. *Cancer research*, 71(14), pp.4748–4757.

Delany, A.M. et al., 2008. Osteonectin/SPARC polymorphisms in Caucasian men with idiopathic osteoporosis. *Osteoporosis international : a journal established as result of cooperation between the European Foundation for Osteoporosis and the National Osteoporosis Foundation of the USA*, 19(7), pp.969–978.

Delongchamps, N.B. et al., 2008. Evaluation of prostatitis in autopsied prostates--is chronic inflammation more associated with benign prostatic hyperplasia or cancer? *The Journal of urology*, 179(5), pp.1736–1740.

Denk, W., Strickler, J.H. & Webb, W.W., 1990. Two-photon laser scanning fluorescence microscopy. *Science (New York, NY)*, 248(4951), pp.73–76.

Derosa, C.A. et al., 2011. Elevated osteonectin/SPARC expression in primary prostate cancer predicts metastatic progression. *Prostate cancer and prostatic diseases*.

Dewitt, D.D. et al., 2009. Collagen I-matrigel scaffolds for enhanced Schwann cell survival and control of three-dimensional cell morphology. *Tissue engineering. Part A*, 15(10), pp.2785–2793.

Di Lullo, G.A. et al., 2002. Mapping the ligand-binding sites and disease-associated mutations on the most abundant protein in the human, type I collagen. *The Journal of biological chemistry*, 277(6), pp.4223–4231.

Di Vizio, D. et al., 2009. An absence of stromal caveolin-1 is associated with advanced prostate cancer, metastatic disease and epithelial Akt activation. *Cell cycle (Georgetown, Tex)*, 8(15), pp.2420–2424.

Dieu-Nosjean, M.-C. et al., 2008. Long-term survival for patients with non-small-cell lung cancer with intratumoral lymphoid structures. *Journal of clinical oncology : official journal of the American Society of Clinical Oncology*, 26(27), pp.4410–4417.

Dillner, K. et al., 2003. Gene expression analysis of prostate hyperplasia in mice overexpressing the prolactin gene specifically in the prostate. *Endocrinology*, 144(11), pp.4955–4966.

Duś, D., Budzyński, W. & Radzikowski, C., 1985. LL2 cell line derived from transplantable murine Lewis lung carcinoma--maintenance in vitro and growth characteristics. *Archivum immunologiae et therapiae experimentalis*, 33(6), pp.817–823.

Elices, M.J. et al., 1990. VCAM-1 on activated endothelium interacts with the leukocyte integrin VLA-4 at a site distinct from the VLA-4/fibronectin binding site. *Cell*, 60(4), pp.577–584.

Evans, M.J. & Kaufman, M.H., 1981. Establishment in culture of pluripotential cells from mouse embryos. *Nature*, 292(5819), pp.154–156.

Fenouille, N. et al., 2011. SPARC functions as an anti-stress factor by inactivating p53 through Akt-mediated MDM2 phosphorylation to promote melanoma cell survival. *Oncogene*, 30(49), pp.4887–4900.

Finak, G. et al., 2008. Stromal gene expression predicts clinical outcome in breast cancer. *Nature medicine*, 14(5), pp.518–527.

Fleischmann, A. et al., 2009. Immunological microenvironment in prostate cancer: high mast cell densities are associated with favorable tumor characteristics and good prognosis. *The Prostate*, 69(9), pp.976–981.

Foster, K.E. et al., 2010. EphB-ephrin-B2 interactions are required for thymus migration during organogenesis. *Proceedings of the National Academy of Sciences of the United States of America*, 107(30), pp.13414–13419.

Fraley, S.I. et al., 2010. A distinctive role for focal adhesion proteins in three-dimensional cell motility. *Nature cell biology*, 12(6), pp.598–604.

Friedl, P., 2004. Prespecification and plasticity: shifting mechanisms of cell migration. *Current opinion in cell biology*, 16(1), pp.14–23.

Friedl, P. & Alexander, S., 2011. Cancer invasion and the microenvironment: plasticity and reciprocity. *Cell*, 147(5), pp.992–1009.

Friedl, P. & Gilmour, D., 2009. Collective cell migration in morphogenesis, regeneration and cancer. *Nature reviews Molecular cell biology*, 10(7), pp.445–457.

Friedl, P. et al., 1995. Migration of coordinated cell clusters in mesenchymal and epithelial cancer explants in vitro. *Cancer research*, 55(20), pp.4557–4560.

Friedl, P., Zänker, K.S. & Bröcker, E.B., 1998. Cell migration strategies in 3-D extracellular matrix: differences in morphology, cell matrix interactions, and integrin function. *Microscopy research and technique*, 43(5), pp.369–378.

Gaggioli, C. et al., 2007. Fibroblast-led collective invasion of carcinoma cells with differing roles for RhoGTPases in leading and following cells. *Nature cell biology*, 9(12), pp.1392–1400.

Galbraith, C.G., Yamada, K.M. & Galbraith, J.A., 2007. Polymerizing actin fibers position integrins primed to probe for adhesion sites. *Science (New York, NY)*, 315(5814), pp.992–995.

Gao, D. & Mittal, V., 2009. The role of bone-marrow-derived cells in tumor growth, metastasis initiation and progression. *Trends in molecular medicine*, 15(8), pp.333–343.

Gao, H. et al., 2006. Emergence of androgen independence at early stages of prostate cancer progression in Nkx3.1; Pten mice. *Cancer research*, 66(16), pp.7929–7933.

Geiger, T.R. & Peeper, D.S., 2009. Metastasis mechanisms. *Biochimica et biophysica acta*, 1796(2), pp.293–308.

Georgiou, E., 2000. Second and third optical harmonic generation in type I collagen, by nanosecond laser irradiation, over a broad spectral region. *Optics Communications*, 176(1-3), pp.253–260.

Germain, R.N., Robey, E.A. & Cahalan, M.D., 2012. A decade of imaging cellular motility and interaction dynamics in the immune system. *Science (New York, NY)*, 336(6089), pp.1676–1681.

Gilles, C. et al., 1998. SPARC/osteonectin induces matrix metalloproteinase 2 activation in human breast cancer cell lines. *Cancer research*, 58(23), pp.5529–5536.

Gilmour, D.T. et al., 1998. Mice deficient for the secreted glycoprotein SPARC/osteonectin/BM40 develop normally but show severe age-onset cataract formation and disruption of the lens. *The EMBO journal*, 17(7), pp.1860–1870.

Gingrich, J.R. et al., 1997. Androgen-independent prostate cancer progression in the TRAMP model. *Cancer research*, 57(21), pp.4687–4691.

Gingrich, J.R. et al., 1996. Metastatic prostate cancer in a transgenic mouse. *Cancer research*, 56(18), pp.4096–4102.

Gingrich, J.R. et al., 1999. Pathologic progression of autochthonous prostate cancer in the TRAMP model. *Prostate cancer and prostatic diseases*, 2(2), pp.70–75.

Gleason, D.F., 1966. Classification of prostatic carcinomas. *Cancer chemotherapy reports. Part 1*, 50(3), pp.125–128.

Gleason, D.F., 1992. Histologic grading of prostate cancer: a perspective. *Human pathology*, 23(3), pp.273–279.

Gräbner, R. et al., 2009. Lymphotoxin beta receptor signaling promotes tertiary lymphoid organogenesis in the aorta adventitia of aged ApoE-/-mice. *The Journal of experimental medicine*, 206(1), pp.233–248.

Greenberg, N.M. et al., 1995. Prostate cancer in a transgenic mouse. *Proceedings of the National Academy of Sciences of the United States of America*, 92(8), pp.3439–3443.

Greenberg, N.M. et al., 1994. The rat probasin gene promoter directs hormonally and developmentally regulated expression of a heterologous gene specifically to the prostate in transgenic mice. *Molecular endocrinology (Baltimore, Md.)*, 8(2), pp.230–239.

Gritsenko, P.G., Ilina, O. & Friedl, P., 2012. Interstitial guidance of cancer invasion. *The Journal of pathology*, 226(2), pp.185–199.

Grivennikov, S.I., Greten, F.R. & Karin, M., 2010. Immunity, Inflammation, and Cancer. *Cell*, 140, pp.883–899.

Guess, H.A. et al., 1990. Cumulative prevalence of prostatism matches the autopsy prevalence of benign prostatic hyperplasia. *The Prostate*, 17(3), pp.241–246.

Gunzer, M. et al., 2000. Migration of dendritic cells within 3-D collagen lattices is dependent on tissue origin, state of maturation, and matrix structure and is maintained by proinflammatory cytokines. *Journal of leukocyte biology*, 67(5), pp.622–629.

Haessler, U. et al., 2011. Dendritic cell chemotaxis in 3D under defined chemokine gradients reveals differential response to ligands CCL21 and CCL19. *Proceedings of the National Academy of Sciences of the United States of America*, 108(14), pp.5614–5619.

Hall, J.A. et al., 2002. Primary prostate stromal cells modulate the morphology and migration of primary prostate epithelial cells in type 1 collagen gels. *Cancer research*, 62(1), pp.58–62.

Hamill, K.J. et al., 2009. Laminin deposition in the extracellular matrix: a complex picture emerges. *Journal of cell science*, 122(Pt 24), pp.4409–4417.

Hanahan, D. & Weinberg, R.A., 2011. Hallmarks of cancer: the next generation. *Cell*, 144(5), pp.646–674.

Hanahan, D. & Weinberg, R.A., 2000. The hallmarks of cancer. *Cell*, 100(1), pp.57–70.

Härmä, V. et al., 2010. A comprehensive panel of three-dimensional models for studies of prostate cancer growth, invasion and drug responses. *PloS one*, 5(5), p.e10431.

Heer, R. et al., 2007. The role of androgen in determining differentiation and regulation of androgen receptor expression in the human prostatic epithelium transient amplifying population. *Journal of cellular physiology*, 212(3), pp.572–578.

Heinke, J. et al., 2012. Bone morphogenetic protein modulator BMPER is highly expressed in malignant tumors and controls invasive cell behavior. *Oncogene*, 31(24), pp.2919–2930.

Hildahl, J. et al., 2008. Involvement of growth hormone-insulin-like growth factor I system in cranial remodeling during halibut metamorphosis as indicated by tissue- and stage-specific receptor gene expression and the presence of growth hormone receptor protein. *Cell and tissue research*, 332(2), pp.211–225.

Hjelmström, P., 2001. Lymphoid neogenesis: de novo formation of lymphoid tissue in chronic inflammation through expression of homing chemokines. *Journal of leukocyte biology*, 69(3), pp.331–339.

Ho, C.K.M. & Habib, F.K., 2011. Estrogen and androgen signaling in the pathogenesis of BPH. *Nature reviews. Urology*, 8(1), pp.29–41.

Hoehn, W. et al., 1980. Human prostatic adenocarcinoma: some characteristics of a serially transplantable line in nude mice (PC 82). *The Prostate*, 1(1), pp.95–104.

Honda, K. et al., 2001. Molecular basis for hematopoietic/mesenchymal interaction during initiation of Peyer's patch organogenesis. *The Journal of experimental medicine*, 193(5), pp.621–630.

Hooper, S., Marshall, J.F. & Sahai, E., 2006. Tumor cell migration in three dimensions. *Methods in enzymology*, 406, pp.625–643.

Horoszewicz, J.S. et al., 1980. The LNCaP cell line--a new model for studies on human prostatic carcinoma. *Progress in clinical and biological research*, 37, pp.115–132.

Humphrey, P.A., 2004. Gleason grading and prognostic factors in carcinoma of the prostate. *Modern pathology : an official journal of the United States and Canadian Academy of Pathology, Inc*, 17(3), pp.292–306.

Humphries, J.D., Byron, A. & Humphries, M.J., 2006. Integrin ligands at a glance. *Journal of cell science*, 119(Pt 19), pp.3901–3903.

Jacob, K. et al., 1999. Osteonectin promotes prostate cancer cell migration and invasion: a possible mechanism for metastasis to bone. *Cancer research*, 59(17), pp.4453–4457.

Jaggi, M. et al., 2005. E-cadherin phosphorylation by protein kinase D1/protein kinase C{mu} is associated with altered cellular aggregation and motility in prostate cancer. *Cancer research*, 65(2), pp.483–492.

Jechlinger, M. et al., 2003. Expression profiling of epithelial plasticity in tumor progression. *Oncogene*, 22(46), pp.7155–7169.

Jeet, V., Russell, P.J. & Khatri, A., 2010. Modeling prostate cancer: a perspective on transgenic mouse models. *Cancer metastasis reviews*, 29(1), pp.123–142.

Josson, S. et al., 2010. Tumor-stroma co-evolution in prostate cancer progression and metastasis. *Seminars in cell & developmental biology*, 21(1), pp.26–32.

Junt, T. et al., 2007. Subcapsular sinus macrophages in lymph nodes clear lymph-borne viruses and present them to antiviral B cells. *Nature*, 450(7166), pp.110–114.

Kaighn, M.E. et al., 1979. Establishment and characterization of a human prostatic carcinoma cell line (PC-3). *Investigative urology*, 17(1), pp.16–23.

Kalluri, R., 2003. Basement membranes: structure, assembly and role in tumour angiogenesis. *Nature reviews Cancer*, 3(6), pp.422–433.

Kaluza, D. et al., 2011. Class IIb HDAC6 regulates endothelial cell migration and angiogenesis by deacetylation of cortactin. *The EMBO journal*, 30(20), pp.4142–4156.

Kaminski, A. et al., 2006. Tumour-stroma interactions between metastatic prostate cancer cells and fibroblasts. *International journal of molecular medicine*, 18(5), pp.941–950.

Kasper, S., 2005. Survey of genetically engineered mouse models for prostate cancer: analyzing the molecular basis of prostate cancer development, progression, and metastasis. *Journal of cellular biochemistry*, 94(2), pp.279–297.

Kato, Y. et al., 2005. Enhanced expression of Aggrus (T1alpha/podoplanin), a platelet-aggregation-inducing factor in lung squamous cell carcinoma. *Tumour biology : the journal of the International Society for Oncodevelopmental Biology and Medicine*, 26(4), pp.195–200.

Kawase, A. et al., 2008. Podoplanin expression by cancer associated fibroblasts predicts poor prognosis of lung adenocarcinoma. *International journal of cancer Journal international du cancer*, 123(5), pp.1053–1059.

Kärjä, V. et al., 2005. Tumour-infiltrating lymphocytes: A prognostic factor of PSA-free survival in patients with local prostate carcinoma treated by radical prostatectomy. *Anticancer research*, 25(6C), pp.4435–4438.

Keith, W.N. et al., 2007. Seeding drug discovery: integrating telomerase cancer biology and cellular senescence to uncover new therapeutic opportunities in targeting cancer stem cells. *Drug discovery today*, 12(15-16), pp.611–621.

Khoshnoodi, J., Pedchenko, V. & Hudson, B.G., 2008. Mammalian collagen IV. *Microscopy research and technique*, 71(5), pp.357–370.

Kingsley, L.A. et al., 2007. Molecular biology of bone metastasis. *Molecular cancer therapeutics*, 6(10), pp.2609–2617.

Kirfel, G. et al., 2004. Cell migration: mechanisms of rear detachment and the formation of migration tracks. *European journal of cell biology*, 83(11-12), pp.717–724.

Kitano, H. et al., 2010. Podoplanin expression in cancerous stroma induces lymphangiogenesis and predicts lymphatic spread and patient survival. *Archives of pathology & laboratory medicine*, 134(10), pp.1520–1527.

Klemke, M. et al., 2010. An MEK-cofilin signalling module controls migration of human T cells in 3D but not 2D environments. *The EMBO journal*, 29(17), pp.2915–2929.

Knoblich, J.A., 2008. Mechanisms of asymmetric stem cell division. *Cell*, 132(4), pp.583–597.

Koning, J.J. & Mebius, R.E., 2012. Interdependence of stromal and immune cells for lymph node function. *Trends in immunology*, 33(6), pp.264–270.

Kooistra, A. et al., 1995. Inhibition of prostatic epithelial cell proliferation by a factor secreted specifically by prostatic stromal cells. *The Prostate*, 26(3), pp.123–132.

Kopantzev, E.P. et al., 2010. Cellular and molecular phenotypes of proliferating stromal cells from human carcinomas. *British journal of cancer*, 102(10), pp.1533–1540.

Korff, T. & Augustin, H.G., 1998. Integration of endothelial cells in multicellular spheroids prevents apoptosis and induces differentiation. *The Journal of cell biology*, 143(5), pp.1341–1352.

Korpos, E. et al., 2010. Role of the extracellular matrix in lymphocyte migration. *Cell and tissue research*, 339(1), pp.47–57.

Kraman, M. et al., 2010. Suppression of antitumor immunity by stromal cells expressing fibroblast activation protein-alpha. *Science (New York, NY)*, 330(6005), pp.827–830.

Kramer, G. et al., 2002. Increased expression of lymphocyte-derived cytokines in benign hyperplastic prostate tissue, identification of the producing cell types, and effect of differentially expressed cytokines on stromal cell proliferation. *The Prostate*, 52(1), pp.43–58.

Kramer, G., Mitteregger, D. & Marberger, M., 2007. Is benign prostatic hyperplasia (BPH) an immune inflammatory disease? *European urology*, 51(5), pp.1202–1216.

Kraning-Rush, C.M. et al., 2011. The role of the cytoskeleton in cellular force generation in 2D and 3D environments. *Physical biology*, 8(1), p.015009.

Krieger, J.N., Ross, S.O. & Riley, D.E., 2002. Chronic prostatitis: epidemiology and role of infection. *Urology*, 60(6 Suppl), pp.8–12; discussion 13.

Kuerten, S. et al., 2012. Tertiary lymphoid organ development coincides with determinant spreading of the myelin-specific T cell response. *Acta neuropathologica*.

Kumar, S. & Weaver, V.M., 2009. Mechanics, malignancy, and metastasis: the force journey of a tumor cell. *Cancer metastasis reviews*, 28(1-2), pp.113–127.

Kundu, J.K. & Surh, Y.-J., 2008. Inflammation: gearing the journey to cancer. *Mutation research*, 659(1-2), pp.15–30.

Kusuma, N. et al., 2012. Integrin-dependent response to laminin-511 regulates breast tumor cell invasion and metastasis. *International journal of cancer Journal international du cancer*, 130(3), pp.555–566.

Kwak, C. et al., 2002. Thrombospondin-1, vascular endothelial growth factor expression and their relationship with p53 status in prostate cancer and benign prostatic hyperplasia. *BJU international*, 89(3), pp.303–309.

Kypta, R.M. & Waxman, J., 2012. Wnt/β-catenin signalling in prostate cancer. *Nature reviews. Urology*.

Lagacé, R. et al., 1985. Myofibroblastic stromal reaction in carcinoma of the breast: variations of collagenous matrix and structural glycoproteins. *Virchows Archiv. A, Pathological anatomy and histopathology*, 408(1), pp.49–59.

Lai, M.-D. et al., 2009. The effects of DNA formulation and administration route on cancer therapeutic efficacy with xenogenic EGFR DNA vaccine in a lung cancer animal model. *Genetic vaccines and therapy*, 7, p.2.

Laib, A.M. et al., 2009. Spheroid-based human endothelial cell microvessel formation in vivo. *Nature protocols*, 4(8), pp.1202–1215.

Lang, S.H. et al., 2001. Prostate epithelial cell lines form spheroids with evidence of glandular differentiation in three-dimensional Matrigel cultures. *British journal of cancer*, 85(4), pp.590–599.

Lang, S.H., Stower, M. & Maitland, N.J., 2000. In vitro modelling of epithelial and stromal interactions in non-malignant and malignant prostates. *British journal of cancer*, 82(4), pp.990–997.

Larkin, S.E.T. et al., 2012. Identification of markers of prostate cancer progression using candidate gene expression. *British journal of cancer*, 106(1), pp.157–165.

Lauffenburger, D.A. & Horwitz, A.F., 1996. Cell migration: a physically integrated molecular process. *Cell*, 84(3), pp.359–369.

Laurila, P. & Leivo, I., 1993. Basement membrane and interstitial matrix components form separate matrices in heterokaryons of PYS-2 cells and fibroblasts. *Journal of cell science*, 104 (Pt 1), pp.59–68.

Lawson, D.A. et al., 2010. Basal epithelial stem cells are efficient targets for prostate cancer initiation. *Proceedings of the National Academy of Sciences of the United States of America*, 107(6), pp.2610–2615.

Lämmermann, T. et al., 2008. Rapid leukocyte migration by integrin-independent flowing and squeezing. *Nature*, 453(7191), pp.51–55.

Leivo, I., 1983a. Basement membrane-like matrix of teratocarcinoma-derived endodermal cells: presence of laminin and heparan sulfate in the matrix at points of attachment to cells. *The journal of histochemistry and cytochemistry : official journal of the Histochemistry Society*, 31(1), pp.35–45.

Leivo, I., 1983b. Structure and composition of early basement membranes: studies with early embryos and teratocarcinoma cells. *Medical biology*, 61(1), pp.1–30.

Leussink, V.I. et al., 2002. Blockade of signaling via the very late antigen (VLA-4) and its counterligand vascular cell adhesion molecule-1 (VCAM-1) causes increased T cell apoptosis in experimental autoimmune neuritis. *Acta neuropathologica*, 103(2), pp.131–136.

Link, A. et al., 2007. Fibroblastic reticular cells in lymph nodes regulate the homeostasis of naive T cells. *Nature immunology*, 8(11), pp.1255–1265.

Lissbrant, I.F. et al., 2000. Tumor associated macrophages in human prostate cancer: relation to clinicopathological variables and survival. *International journal of oncology*, 17(3), pp.445–451.

Liu, X. et al., 2011. Two-photon fluorescence real-time imaging on the development of early mouse embryo by stages. *Journal of microscopy*, 241(2), pp.212–218.

Lohnes, D. et al., 1993. Function of retinoic acid receptor gamma in the mouse. *Cell*, 73(4), pp.643–658.

Lunt, S.J., Chaudary, N. & Hill, R.P., 2009. The tumor microenvironment and metastatic disease. *Clinical & experimental metastasis*, 26(1), pp.19–34.

Ma, Y.L. et al., 1997. Reconstruction of prostatic acinus-like structure from ventral and dorsolateral prostatic epithelial cells of the rat in three-dimensional collagen gel matrix culture. *The Journal of urology*, 157(3), pp.1025–1031.

Mackenzie, I.C., 2008. Cancer stem cells. *Annals of oncology : official journal of the European Society for Medical Oncology / ESMO*, 19 Suppl 5, pp.v40–3.

Maddison, L.A. et al., 2004. Conditional deletion of Rb causes early stage prostate cancer. *Cancer research*, 64(17), pp.6018–6025.

Madsen, C.D. & Sahai, E., 2010. Cancer dissemination--lessons from leukocytes. *Developmental cell*, 19(1), pp.13–26.

Maitland, N.J., 2008. Pathobiology of the human prostate. *Prostate Cancer*.

Maitland, N.J. & Collins, A., 2005. A tumour stem cell hypothesis for the origins of prostate cancer. *BJU international*, 96(9), pp.1219–1223.

Maitland, N.J. & Collins, A.T., 2008. Prostate cancer stem cells: a new target for therapy. *Journal of clinical oncology : official journal of the American Society of Clinical Oncology*, 26(17), pp.2862–2870.

Maitland, N.J. et al., 2011. Prostate cancer stem cells: do they have a basal or luminal phenotype? *Hormones & cancer*, 2(1), pp.47–61.

Mansergh, F.C. et al., 2007. Osteopenia in Sparc (osteonectin)-deficient mice: characterization of phenotypic determinants of femoral strength and changes in gene expression. *Physiological genomics*, 32(1), pp.64–73.

Marchiani, S. et al., 2010. Androgen-responsive and -unresponsive prostate cancer cell lines respond differently to stimuli inducing neuroendocrine differentiation. *International journal of andrology*, 33(6), pp.784–793.

Martin, P. et al., 2011. Prostate epithelial Pten/TP53 loss leads to transformation of multipotential progenitors and epithelial to mesenchymal transition. *The American journal of pathology*, 179(1), pp.422–435.

Martín-Villar, E. et al., 2010. Podoplanin associates with CD44 to promote directional cell migration. *Molecular biology of the cell*, 21(24), pp.4387–4399.

Mashino, K. et al., 2002. Expression of chemokine receptor CCR7 is associated with lymph node metastasis of gastric carcinoma. *Cancer research*, 62(10), pp.2937–2941.

Mayor, S., 2012. Latest UK figures show increase in prostate cancer diagnoses and falling death rate. *BMJ (Clinical research ed.)*, 344, p.e3252.

McCarthy, R.A. & Hay, E.D., 1991. Collagen I, laminin, and tenascin: ultrastructure and correlation with avian neural crest formation. *The International journal of developmental biology*, 35(4), pp.437–452.

McNeal, J.E. et al., 1988. Zonal distribution of prostatic adenocarcinoma. Correlation with histologic pattern and direction of spread. *The American journal of surgical pathology*, 12(12), pp.897–906.

Metzger, D. & Chambon, P., 2001. Site- and time-specific gene targeting in the mouse. *Methods (San Diego, Calif.)*, 24(1), pp.71–80.

Meyer, A.S. et al., 2012. 2D protrusion but not motility predicts growth factor-induced cancer cell migration in 3D collagen. *The Journal of cell biology*, 197(6), pp.721–729.

Milne, K. et al., 2009. Systematic analysis of immune infiltrates in high-grade serous ovarian cancer reveals CD20, FoxP3 and TIA-1 as positive prognostic factors. *PloS one*, 4(7), p.e6412.

Mishima, T. et al., 1998. Inhibition of tumor invasion and metastasis by calcium spirulan (Ca-SP), a novel sulfated polysaccharide derived from a blue-green alga, Spirulina platensis. *Clinical & experimental metastasis*, 16(6), pp.541–550.

Mitchell, S. et al., 2000. Phenotypic and genotypic characterization of commonly used human prostatic cell lines. *BJU international*, 85(7), pp.932–944.

Mosquera, J.-M. et al., 2007. Morphological features of TMPRSS2-ERG gene fusion prostate cancer. *The Journal of pathology*, 212(1), pp.91–101.

Mueller, M.M. & Fusenig, N.E., 2004. Friends or foes - bipolar effects of the tumour stroma in cancer. *Nature reviews Cancer*, 4(11), pp.839–849.

Muraro, P.A. et al., 2000. VLA-4/CD49d downregulated on primed T lymphocytes during interferon-beta therapy in multiple sclerosis. *Journal of neuroimmunology*, 111(1-2), pp.186–194.

Müller, M. et al., 2010. MMP19 is upregulated during melanoma progression and increases invasion of melanoma cells. *Modern pathology : an official journal of the United States and Canadian Academy of Pathology, Inc*, 23(4), pp.511–521.

Nagy, A., 2000. Cre recombinase: the universal reagent for genome tailoring. *Genesis (New York, N.Y. : 2000)*, 26(2), pp.99–109.

Nalla, A.K. et al., 2010. Targeting MMP-9, uPAR, and cathepsin B inhibits invasion, migration and activates apoptosis in prostate cancer cells. *Cancer gene therapy*, 17(9), pp.599–613.

Niu, Y. et al., 2008. Targeting the stromal androgen receptor in primary prostate tumors at earlier stages. *Proceedings of the National Academy of Sciences of the United States of America*, 105(34), pp.12188–12193.

Niu, Y.-N. & Xia, S.-J., 2009. Stroma-epithelium crosstalk in prostate cancer. *Asian journal of andrology*, 11(1), pp.28–35.

Norose, K. et al., 1998. SPARC deficiency leads to early-onset cataractogenesis. *Investigative ophthalmology & visual science*, 39(13), pp.2674–2680.

Noseworthy, J.H. & Kirkpatrick, P., 2005. Natalizumab. *Nature reviews. Drug discovery*, 4(2), pp.101–102.

O'Neill, G.M. et al., 2007. A new central scaffold for metastasis: parsing HEF1/Cas-L/NEDD9. *Cancer research*, 67(19), pp.8975–8979.

Ohnuki, Y. et al., 1980. Chromosomal analysis of human prostatic adenocarcinoma cell lines. *Cancer research*, 40(3), pp.524–534.

Oldridge, E.E. et al., 2011. Prostate cancer stem cells: Are they androgen-responsive? *Molecular and cellular endocrinology*.

Olumi, A.F. et al., 1999. Carcinoma-associated fibroblasts direct tumor progression of initiated human prostatic epithelium. *Cancer research*, 59(19), pp.5002–5011.

Orr, B. et al., 2011. Identification of stromally expressed molecules in the prostate by tag-profiling of cancer-associated fibroblasts, normal fibroblasts and fetal prostate. *Oncogene*.

Packard, B.Z. et al., 2009. Direct visualization of protease activity on cells migrating in three-dimensions. *Matrix biology : journal of the International Society for Matrix Biology*, 28(1), pp.3–10.

Pagès, F. et al., 2010. Immune infiltration in human tumors: a prognostic factor that should not be ignored. *Oncogene*, 29(8), pp.1093–1102.

Paku, S. et al., 2000. Organ-specificity of the extravasation process: an ultrastructural study. *Clinical & experimental metastasis*, 18(6), pp.481–492.

Palecek, S.P. et al., 1996. Integrin dynamics on the tail region of migrating fibroblasts. *Journal of cell science*, 109 (Pt 5), pp.941–952.

Pan, P. et al., 2012. Antitumor activity and immunomodulatory effects of the intraperitoneal administration of Kanglaite in vivo in Lewis lung carcinoma. *Journal of ethnopharmacology*.

Paoli, J., Smedh, M. & Ericson, M.B., 2009. Multiphoton laser scanning microscopy--a novel diagnostic method for superficial skin cancers. *Seminars in cutaneous medicine and surgery*, 28(3), pp.190–195.

Pavlaki, M. & Zucker, S., 2003. Matrix metalloproteinase inhibitors (MMPIs): the beginning of phase I or the termination of phase III clinical trials. *Cancer metastasis reviews*, 22(2-3), pp.177–203.

Peduto, L. et al., 2009. Inflammation recapitulates the ontogeny of lymphoid stromal cells. *Journal of immunology (Baltimore, Md : 1950)*, 182(9), pp.5789–5799.

Peehl, D.M., 2005. Primary cell cultures as models of prostate cancer development. *Endocrine-related cancer*, 12(1), pp.19–47.

Pezzolato, M. et al., 2012. Development of tertiary lymphoid structures in the kidneys of pigs with chronic leptospiral nephritis. *Veterinary immunology and immunopathology*, 145(1-2), pp.546–550.

Péterfia, B. et al., 2012. Syndecan-1 Enhances Proliferation, Migration and Metastasis of HT-1080 Cells in Cooperation with Syndecan-2. *PloS one*, 7(6), p.e39474.

Pongtippan, A. et al., 2004. Skene's gland adenocarcinoma resembling prostatic adenocarcinoma. *International journal of gynecological pathology : official journal of the International Society of Gynecological Pathologists*, 23(1), pp.71–74.

Porte, H. et al., 1995. Neoplastic progression of human colorectal cancer is associated with overexpression of the stromelysin-3 and BM-40/SPARC genes. *International journal of cancer Journal international du cancer*, 64(1), pp.70–75.

Potten, C.S. & Loeffler, M., 1990. Stem cells: attributes, cycles, spirals, pitfalls and uncertainties. Lessons for and from the crypt. *Development (Cambridge, England)*, 110(4), pp.1001–1020.

Pöschl, E. et al., 2004. Collagen IV is essential for basement membrane stability but dispensable for initiation of its assembly during early development. *Development (Cambridge, England)*, 131(7), pp.1619–1628.

Provenzano, P.P. et al., 2006. Collagen reorganization at the tumor-stromal interface facilitates local invasion. *BMC medicine*, 4(1), p.38.

Provenzano, P.P., Eliceiri, K.W. & Keely, P.J., 2009. Multiphoton microscopy and fluorescence lifetime imaging microscopy (FLIM) to monitor metastasis and the tumor microenvironment. *Clinical & experimental metastasis*, 26(4), pp.357–370.

Pula, B. et al., 2011. Podoplanin expression by cancer-associated fibroblasts predicts poor outcome in invasive ductal breast carcinoma. *Histopathology*, 59(6), pp.1249–1260.

Rahim, S. et al., 2011. YK-4-279 inhibits ERG and ETV1 mediated prostate cancer cell invasion. *PloS one*, 6(4), p.e19343.

Rakhra, K. et al., 2010. CD4(+) T cells contribute to the remodeling of the microenvironment required for sustained tumor regression upon oncogene inactivation. *Cancer cell*, 18(5), pp.485–498.

Randolph, G.J., Angeli, V. & Swartz, M.A., 2005. Dendritic-cell trafficking to lymph nodes through lymphatic vessels. *Nature reviews Immunology*, 5(8), pp.617–628.

Rasheed, S. et al., 1974. Characterization of a newly derived human sarcoma cell line (HT-1080). *Cancer*, 33(4), pp.1027–1033.

Rhee, S. et al., 2007. Microtubule function in fibroblast spreading is modulated according to the tension state of cell-matrix interactions. *Proceedings of the National Academy of Sciences of the United States of America*, 104(13), pp.5425–5430.

Richardson, G.D. et al., 2004. CD133, a novel marker for human prostatic epithelial stem cells. *Journal of cell science*, 117(Pt 16), pp.3539–3545.

Richter, F. et al., 2002. Immunohistochemical localization of the retinoic Acid receptors in human prostate. *Journal of andrology*, 23(6), pp.830–838.

Ridley, A.J. et al., 2003. Cell migration: integrating signals from front to back. *Science (New York, NY)*, 302(5651), pp.1704–1709.

Ronald, J.A. et al., 2001. Differential regulation of transendothelial migration of THP-1 cells by ICAM-1/LFA-1 and VCAM-1/VLA-4. *Journal of leukocyte biology*, 70(4), pp.601–609.

Roomi, M.W. et al., 2006. In vivo and in vitro antitumor effect of ascorbic acid, lysine, proline, arginine, and green tea extract on human fibrosarcoma cells HT-1080. *Medical oncology (Northwood, London, England)*, 23(1), pp.105–111.

Roozendaal, R. & Mebius, R.E., 2011. Stromal cell-immune cell interactions. *Annual review of immunology*, 29, pp.23–43.

Ropiquet, F. et al., 2000. FGF-10 is expressed at low levels in the human prostate. *The Prostate*, 44(4), pp.334–338.

Rosol, T.J. et al., 2003. Animal models of bone metastasis. *Cancer*, 97(3 Suppl), pp.748–757.

Rosol, T.J. et al., 2004. Animal models of bone metastasis. *Cancer treatment and research*, 118, pp.47–81.

Royuela, M. et al., 2001. Estrogen receptors alpha and beta in the normal, hyperplastic and carcinomatous human prostate. *The Journal of endocrinology*, 168(3), pp.447–454.

Rørth, P., 2009. Collective cell migration. *Annual review of cell and developmental biology*, 25, pp.407–429.

Sage, H., Decker, J., et al., 1989a. SPARC: a Ca2+-binding extracellular protein associated with endothelial cell injury and proliferation. *Journal of molecular and cellular cardiology*, 21 Suppl 1, pp.13–22.

Sage, H., Vernon, R.B., et al., 1989b. SPARC, a secreted protein associated with cellular proliferation, inhibits cell spreading in vitro and exhibits Ca+2-dependent binding to the extracellular matrix. *The Journal of cell biology*, 109(1), pp.341–356.

Sahai, E. et al., 2005. Simultaneous imaging of GFP, CFP and collagen in tumors in vivo using multiphoton microscopy. *BMC biotechnology*, 5, p.14.

Said, N. et al., 2009. The role of SPARC in the TRAMP model of prostate carcinogenesis and progression. *Oncogene*, 28(39), pp.3487–3498.

Salomonsson, S. et al., 2002. Expression of the B cell-attracting chemokine CXCL13 in the target organ and autoantibody production in ectopic lymphoid tissue in the chronic inflammatory disease Sjögren's syndrome. *Scandinavian journal of immunology*, 55(4), pp.336–342.

Sanz-Rodríguez, F. et al., 1999. Characterization of VLA-4-dependent myeloma cell adhesion to fibronectin and VCAM-1. *British journal of haematology*, 107(4), pp.825–834.

Sanz-Rodríguez, F., Hidalgo, A. & Teixidó, J., 2001. Chemokine stromal cell-derived factor-1alpha modulates VLA-4 integrin-mediated multiple myeloma cell adhesion to CS-1/fibronectin and VCAM-1. *Blood*, 97(2), pp.346–351.

Sasaki, T. et al., 1998. Crystal structure and mapping by site-directed mutagenesis of the collagen-binding epitope of an activated form of BM-40/SPARC/osteonectin. *The EMBO journal*, 17(6), pp.1625–1634.

Schmidt, S. & Friedl, P., 2010. Interstitial cell migration: integrin-dependent and alternative adhesion mechanisms. *Cell and tissue research*, 339(1), pp.83–92.

Schneider, H. et al., 2006. Reversal of the TCR stop signal by CTLA-4. *Science (New York, NY)*, 313(5795), pp.1972–1975.

Scott, R.W. et al., 2010. LIM kinases are required for invasive path generation by tumor and tumor-associated stromal cells. *The Journal of cell biology*, 191(1), pp.169–185.

Segat, L. et al., 2009. Secreted protein acidic and rich in cysteine (SPARC) gene polymorphism association with hepatocellular carcinoma in Italian patients. *Journal of gastroenterology and hepatology*, 24(12), pp.1840–1846.

Selivanova, G. & Ivaska, J., 2009. Integrins and mutant p53 on the road to metastasis. *Cell*, 139(7), pp.1220–1222.

Sen, A. et al., 2012. Paxillin mediates extranuclear and intranuclear signaling in prostate cancer proliferation. *The Journal of clinical investigation*, 122(7), pp.2469–2481.

Sen, A. et al., 2010. Paxillin regulates androgen- and epidermal growth factor-induced MAPK signaling and cell proliferation in prostate cancer cells. *The Journal of biological chemistry*, 285(37), pp.28787–28795.

Shannon, J.M. & Cunha, G.R., 1983. Autoradiographic localization of androgen binding in the developing mouse prostate. *The Prostate*, 4(4), pp.367–373.

Shao, Z.M., Nguyen, M. & Barsky, S.H., 2000. Human breast carcinoma desmoplasia is PDGF initiated. *Oncogene*, 19(38), pp.4337–4345.

Shapiro, E. et al., 1992. The relative proportion of stromal and epithelial hyperplasia is related to the development of symptomatic benign prostate hyperplasia. *The Journal of urology*, 147(5), pp.1293–1297.

Sharma, N.L., Shah, N.C. & Neal, D.E., 2009. Robotic-assisted laparoscopic prostatectomy. *British journal of cancer*, 101(9), pp.1491–1496.

Shields, J.D. et al., 2007. Autologous chemotaxis as a mechanism of tumor cell homing to lymphatics via interstitial flow and autocrine CCR7 signaling. *Cancer cell*, 11(6), pp.526–538.

Shields, J.D. et al., 2010. Induction of lymphoidlike stroma and immune escape by tumors that express the chemokine CCL21. *Science (New York, NY)*, 328(5979), pp.749–752.

Shulman, Z. & Alon, R., 2012. Real-time analysis of integrin-dependent transendothelial migration and integrin-independent interstitial motility of leukocytes. *Methods in molecular biology (Clifton, N.J.)*, 757, pp.31–45.

Shultz, L.D. et al., 2005. Human lymphoid and myeloid cell development in NOD/LtSz-scid IL2R gamma null mice engrafted with mobilized human hemopoietic stem cells. *Journal of immunology (Baltimore, Md : 1950)*, 174(10), pp.6477–6489.

Sieweke, M.H. et al., 1990. Mediation of wound-related Rous sarcoma virus tumorigenesis by TGF-beta. *Science (New York, NY)*, 248(4963), pp.1656–1660.

Signoretti, S. & Loda, M., 2007. Prostate stem cells: from development to cancer. *Seminars in cancer biology*, 17(3), pp.219–224.

Simmons, P.J. et al., 1992. Vascular cell adhesion molecule-1 expressed by bone marrow stromal cells mediates the binding of hematopoietic progenitor cells. *Blood*, 80(2), pp.388–395.

Sipos, E. et al., 2012. Proinflammatory adhesion molecules facilitate polychlorinated biphenyl-mediated enhancement of brain metastasis formation. *Toxicological sciences : an official journal of the Society of Toxicology*, 126(2), pp.362–371.

Skobe, M. & Fusenig, N.E., 1998. Tumorigenic conversion of immortal human keratinocytes through stromal cell activation. *Proceedings of the National Academy of Sciences of the United States of America*, 95(3), pp.1050–1055.

Slack, J.M., 2000. Stem cells in epithelial tissues. *Science (New York, NY)*, 287(5457), pp.1431–1433.

Slater, M., Barden, J.A. & Murphy, C.R., 2000. Changes in growth factor expression in the ageing prostate may disrupt epithelial-stromal homeostasis. *The Histochemical journal*, 32(6), pp.357–364.

Small, J.V., 2010. Dicing with dogma: de-branching the lamellipodium. *Trends in cell biology*, 20(11), pp.628–633.

Solozobova, V., Wyvekens, N. & Pruszak, J., 2012. Lessons from the embryonic neural stem cell niche for neural lineage differentiation of pluripotent stem cells. *Stem cell reviews*, 8(3), pp.813–829.

Song, K. et al., 2012. Tumor necrosis factor-α enhanced fusions between oral squamous cell carcinoma cells and endothelial cells via VCAM-1/VLA-4 pathway. *Experimental cell research*, 318(14), pp.1707–1715.

Sorokin, L., 2010. The impact of the extracellular matrix on inflammation. *Nature reviews Immunology*, 10(10), pp.712–723.

Springer, T.A., 1994. Traffic signals for lymphocyte recirculation and leukocyte emigration: the multistep paradigm. *Cell*, 76(2), pp.301–314.

Squirrell, J.M. et al., 1999. Long-term two-photon fluorescence imaging of mammalian embryos without compromising viability. *Nature biotechnology*, 17(8), pp.763–767.

Stark, J.R. et al., 2009. Gleason score and lethal prostate cancer: does 3 + 4 = 4 + 3? *Journal of clinical oncology : official journal of the American Society of Clinical Oncology*, 27(21), pp.3459–3464.

Stone, K.R. et al., 1978. Isolation of a human prostate carcinoma cell line (DU 145). *International journal of cancer Journal international du cancer*, 21(3), pp.274–281.

Sun, Y., Niu, J. & Huang, J., 2009. Neuroendocrine differentiation in prostate cancer. *American journal of translational research*, 1(2), pp.148–162.

Suzuki, A. et al., 2002. Mature dendritic cells make clusters with T cells in the invasive margin of colorectal carcinoma. *The Journal of pathology*, 196(1), pp.37–43.

Swartz, M.A. & Lund, A.W., 2012. Lymphatic and interstitial flow in the tumour microenvironment: linking mechanobiology with immunity. *Nature reviews Cancer*, 12(3), pp.210–219.

Syed, V. et al., 2008. Beta-catenin mediates alteration in cell proliferation, motility and invasion of prostate cancer cells by differential expression of E-cadherin and protein kinase D1. *Journal of cellular biochemistry*, 104(1), pp.82–95.

Tai, S. et al., 2011. PC3 is a cell line characteristic of prostatic small cell carcinoma. *The Prostate*, 71(15), pp.1668–1679.

Takahashi, K. et al., 2007. Induction of pluripotent stem cells from adult human fibroblasts by defined factors. *Cell*, 131(5), pp.861–872.

Tam, C. et al., 2011. 3D quantitative imaging of unprocessed live tissue reveals epithelial defense against bacterial adhesion and subsequent traversal requires MyD88. *PloS one*, 6(8), p.e24008.

Tan, W. et al., 2011. Tumour-infiltrating regulatory T cells stimulate mammary cancer metastasis through RANKL-RANK signalling. *Nature*, 470(7335), pp.548–553.

Tang, J. & Yang, J., 2009. Etiopathogenesis of benign prostatic hypeprlasia. *Indian journal of urology : IJU : journal of the Urological Society of India*, 25(3), pp.312–317.

Tang, S.-N. et al., 2010. The dietary bioflavonoid quercetin synergizes with epigallocathechin gallate (EGCG) to inhibit prostate cancer stem cell characteristics, invasion, migration and epithelial-mesenchymal transition. *Journal of molecular signaling*, 5, p.14.

Taylor, R.A., Toivanen, R. & Risbridger, G., 2010. Stem cells in prostate cancer - treating the root of the problem. *Endocrine-related cancer*.

Theodossiou, T.A. et al., 2006. Second Harmonic Generation Confocal Microscopy of Collagen Type I from Rat Tendon Cryosections. *Biophysical journal*, 91(12), pp.4665–4677.

Thiery, J.P., 2002. Epithelial-mesenchymal transitions in tumour progression. *Nature reviews Cancer*, 2(6), pp.442–454.

Thomas, R. et al., 2000. Differential expression of osteonectin/SPARC during human prostate cancer progression. *Clinical cancer research : an official journal of the American Association for Cancer Research*, 6(3), pp.1140–1149.

Thomas, S. et al., 2011. Development of Secreted Protein and Acidic and Rich in Cysteine (SPARC) Targeted Nanoparticles for the Prognostic Molecular Imaging of Metastatic Prostate Cancer. *Journal of nanomedicine & nanotechnology*, 2(112).

Thomson, A.A., 2008. Mesenchymal mechanisms in prostate organogenesis. *Differentiation; research in biological diversity*, 76(6), pp.587–598.

Timms, B.G., 2008. Prostate development: a historical perspective. *Differentiation; research in biological diversity*, 76(6), pp.565–577.

Timms, B.G. & Hofkamp, L.E., 2011. Prostate development and growth in benign prostatic hyperplasia. *Differentiation; research in biological diversity*, 82(4-5), pp.173–183.

Timpl, R. & Brown, J.C., 1996. Supramolecular assembly of basement membranes. *BioEssays : news and reviews in molecular, cellular and developmental biology*, 18(2), pp.123–132.

Tlsty, T.D., 2001. Stromal cells can contribute oncogenic signals. *Seminars in cancer biology*, 11(2), pp.97–104.

Tlsty, T.D. & Hein, P.W., 2001. Know thy neighbor: stromal cells can contribute oncogenic signals. *Current opinion in genetics & development*, 11(1), pp.54–59.

Tomić, T.T. et al., 2012. Castration resistant prostate cancer is associated with increased blood vessel stabilization and elevated levels of VEGF and Ang-2. *The Prostate*, 72(7), pp.705–712.

Tomlins, S.A. et al., 2005. Recurrent fusion of TMPRSS2 and ETS transcription factor genes in prostate cancer. *Science (New York, NY)*, 310(5748), pp.644–648.

Trimboli, A.J. et al., 2009. Pten in stromal fibroblasts suppresses mammary epithelial tumours. *Nature*, 461(7267), pp.1084–1091.

Tuxhorn, J.A. et al., 2002. Reactive stroma in human prostate cancer: induction of myofibroblast phenotype and extracellular matrix remodeling. *Clinical cancer research : an official journal of the American Association for Cancer Research*, 8(9), pp.2912–2923.

Valkenburg, K.C. & Williams, B.O., 2011. Mouse models of prostate cancer. *Prostate Cancer*, 2011, p.895238.

van Bokhoven, A. et al., 2003. Molecular characterization of human prostate carcinoma cell lines. *The Prostate*, 57(3), pp.205–225.

Vassilopoulos, A. et al., 2008. Identification and characterization of cancer initiating cells from BRCA1 related mammary tumors using markers for normal mammary stem cells. *International journal of biological sciences*, 4(3), pp.133–142.

Venkateswaran, V. et al., 2004. Antioxidants block prostate cancer in lady transgenic mice. *Cancer research*, 64(16), pp.5891–5896.

Vondenhoff, M.F. et al., 2009. LTbetaR signaling induces cytokine expression and up-regulates lymphangiogenic factors in lymph node anlagen. *Journal of immunology (Baltimore, Md : 1950)*, 182(9), pp.5439–5445.

Wang, H.-Y. et al., 2012. Secreted protein acidic and rich in cysteine (SPARC) is associated with nasopharyngeal carcinoma metastasis and poor prognosis. *Journal of translational medicine*, 10, p.27.

Wang, S. et al., 2003. Prostate-specific deletion of the murine Pten tumor suppressor gene leads to metastatic prostate cancer. *Cancer cell*, 4(3), pp.209–221.

Wang, W. et al., 2002. Single cell behavior in metastatic primary mammary tumors correlated with gene expression patterns revealed by molecular profiling. *Cancer research*, 62(21), pp.6278–6288.

Weeks, B.H. et al., 2001. Inducible expression of transforming growth factor beta1 in papillomas causes rapid metastasis. *Cancer research*, 61(20), pp.7435–7443.

Weidner, N. et al., 1993. Tumor angiogenesis correlates with metastasis in invasive prostate carcinoma. *The American journal of pathology*, 143(2), pp.401–409.

Weigelin, B., Bakker, G.-J. & Friedl, P., 2012. Intravital third harmonic generation microscopy of collective melanoma cell invasion: Principles of interface guidance and microvesicle dynamics. *IntraVital*, 1(1), pp.9–20.

Welch, D.R. & Rinker-Schaeffer, C.W., 1999. What defines a useful marker of metastasis in human cancer? *Journal of the National Cancer Institute*, 91(16), pp.1351–1353.

Wendt, M.K., Smith, J.A. & Schiemann, W.P., 2010. Transforming growth factor-β-induced epithelial-mesenchymal transition facilitates epidermal growth factor-dependent breast cancer progression. *Oncogene*, 29(49), pp.6485–6498.

Wicha, M.S., Liu, S. & Dontu, G., 2006. Cancer stem cells: an old idea--a paradigm shift. *Cancer research*, 66(4), pp.1883–90; discussion 1895–6.

Wight, T.N. & Potter-Perigo, S., 2011. The extracellular matrix: an active or passive player in fibrosis? *American journal of physiology. Gastrointestinal and liver physiology*, 301(6), pp.G950–5.

Williams, B.R. et al., 1978. Collagen fibril formation. Optimal in vitro conditions and preliminary kinetic results. *The Journal of biological chemistry*, 253(18), pp.6578–6585.

Wimmenauer, S. et al., 1997. Expression of CD44, ICAM-1 and N-CAM in colorectal cancer. Correlation with the tumor stage and the phenotypical characteristics of tumor-infiltrating lymphocytes. *Anticancer research*, 17(4A), pp.2395–2400.

Winder, T. et al., 2012. An individual coding polymorphism and the haplotype of the SPARC gene predict gastric cancer recurrence. *The pharmacogenomics journal*.

Winter, S.F., Cooper, A.B. & Greenberg, N.M., 2003. Models of metastatic prostate cancer: a transgenic perspective. *Prostate cancer and prostatic diseases*, 6(3), pp.204–211.

Wolf, K. et al., 2003. Amoeboid shape change and contact guidance: T-lymphocyte crawling through fibrillar collagen is independent of matrix remodeling by MMPs and other proteases. *Blood*, 102(9), pp.3262–3269.

Wolf, K. et al., 2007. Multi-step pericellular proteolysis controls the transition from individual to collective cancer cell invasion. *Nature cell biology*, 9(8), pp.893–904.

Wong, C.P., Bray, T.M. & Ho, E., 2009. Induction of proinflammatory response in prostate cancer epithelial cells by activated macrophages. *Cancer letters*, 276(1), pp.38–46.

Wong, S.Y. et al., 2008. Analyses of the role of endogenous SPARC in mouse models of prostate and breast cancer. *Clinical & experimental metastasis*, 25(2), pp.109–118.

Woodley, D.T. et al., 1991. Collagen telopeptides (cross-linking sites) play a role in collagen gel lattice contraction. *The Journal of investigative dermatology*, 97(3), pp.580–585.

Wu, X. et al., 2011. Differentiation of the ductal epithelium and smooth muscle in the prostate gland are regulated by the Notch/PTEN-dependent mechanism. *Developmental biology*, 356(2), pp.337–349.

Xie, T. & Li, L., 2007. Stem cells and their niche: an inseparable relationship. *Development (Cambridge, England)*, 134(11), pp.2001–2006.

Xu, K. et al., 2009. Regulation of androgen receptor transcriptional activity and specificity by RNF6-induced ubiquitination. *Cancer cell*, 15(4), pp.270–282.

Xu, T. et al., 2011. Prostate tumor cells with cancer progenitor properties have high telomerase activity and are rapidly killed by telomerase interference. *The Prostate*, 71(13), pp.1390–1400.

Xue, J. et al., 2009. NF-{kappa}B regulates thrombin-induced ICAM-1 gene expression in cooperation with NFAT by binding to the intronic NF-{kappa}B site in the ICAM-1 gene. *Physiological genomics*.

Yamanashi, T. et al., 2009. Podoplanin expression identified in stromal fibroblasts as a favorable prognostic marker in patients with colorectal carcinoma. *Oncology*, 77(1), pp.53–62.

Yamauchi, K. et al., 2012. Color-coded real-time subcellular fluorescence imaging of the interaction between cancer and host cells in live mice. *Anticancer research*, 32(1), pp.39–43.

Yan, Q. & Sage, E.H., 1999. SPARC, a matricellular glycoprotein with important biological functions. *The journal of histochemistry and cytochemistry : official journal of the Histochemistry Society*, 47(12), pp.1495–1506.

Yanagisawa, N. et al., 2008. Reprint of: Stromogenic prostatic carcinoma pattern (carcinomas with reactive stromal grade 3) in needle biopsies predicts biochemical recurrence-free survival in patients after radical prostatectomy. *Human pathology*, 39(2), pp.282–291.

Yanagisawa, N. et al., 2007. Stromogenic prostatic carcinoma pattern (carcinomas with reactive stromal grade 3) in needle biopsies predicts biochemical recurrence-free survival in patients after radical prostatectomy. *Human pathology*, 38(11), pp.1611–1620.

Yang, X. et al., 1997. KAI1, a putative marker for metastatic potential in human breast cancer. *Cancer letters*, 119(2), pp.149–155.

Yednock, T.A. et al., 1992. Prevention of experimental autoimmune encephalomyelitis by antibodies against alpha 4 beta 1 integrin. *Nature*, 356(6364), pp.63–66.

Yoshida, B.A. et al., 2000. Metastasis-suppressor genes: a review and perspective on an emerging field. *Journal of the National Cancer Institute,* 92(21), pp.1717–1730.

Yu, X. & Machesky, L.M., 2012. Cells assemble invadopodia-like structures and invade into matrigel in a matrix metalloprotease dependent manner in the circular invasion assay. *PloS one,* 7(2), p.e30605.

Zaman, M.H. et al., 2006. Migration of tumor cells in 3D matrices is governed by matrix stiffness along with cell-matrix adhesion and proteolysis. *Proceedings of the National Academy of Sciences of the United States of America,* 103(29), pp.10889–10894.

Zhang, X. et al., 2009. Thrombospondin-1 modulates vascular endothelial growth factor activity at the receptor level. *The FASEB journal : official publication of the Federation of American Societies for Experimental Biology,* 23(10), pp.3368–3376.

Zhong, J. et al., 2012. NEDD9 stabilizes focal adhesions, increases binding to the extra-cellular matrix and differentially effects 2D versus 3D cell migration. *PloS one,* 7(4), p.e35058.

Zupi, G., Mauro, F. & Sacchi, A., 1980. Cloning in vitro and in vivo of Lewis lung carcinoma: properties and characteristics. *The British journal of cancer. Supplement,* 4, pp.309–310.